Electron and Scanning Probe Microscopies

2008 Contractors' Meeting

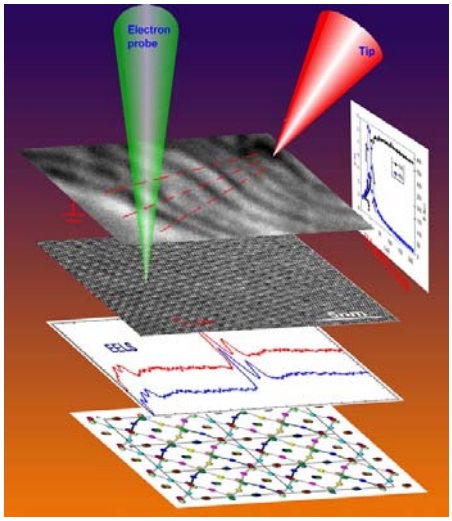

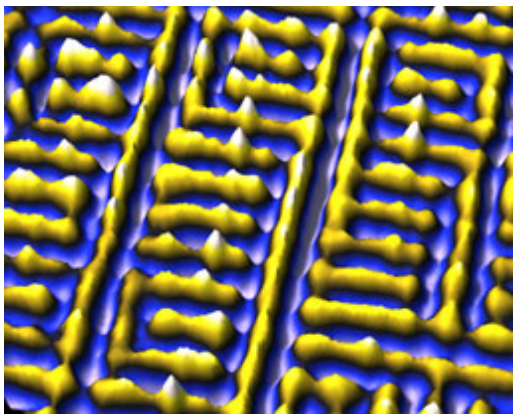

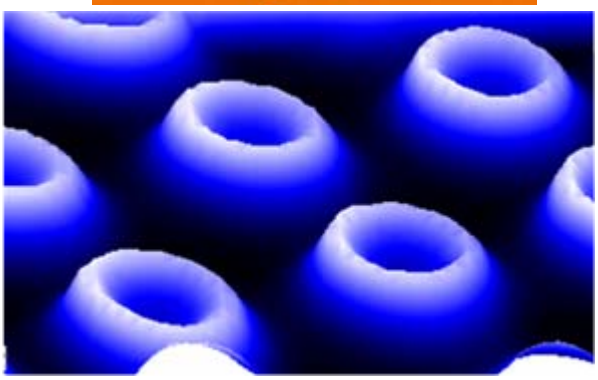

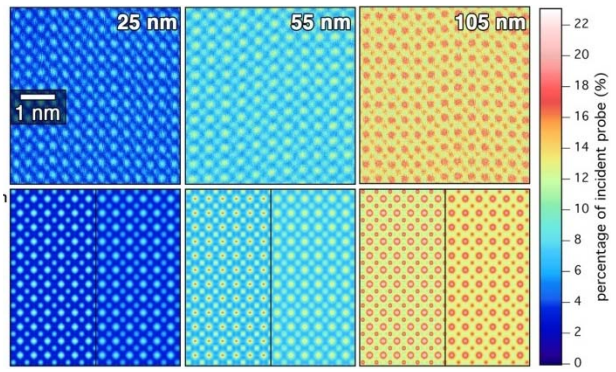

Airlie Conference Center
Warrenton, Virginia
October 26 - 29, 2008

Office of Basic Energy Sciences

Division of Materials Sciences and Engineering

Office of Science
U.S. DEPARTMENT OF ENERGY

On the Cover

Upper left: Schematic illustrating the way in which a combination of electron microscopy techniques were used to study the relationship between transport behavior and microstructure in strongly correlated electron systems such as $Pr_{1-x}Ca_xMnO_3$. An electron probe (green) was used to image and collect structural data while a scanning tunneling microscope tip (red) was used to apply current or an electric field to the sample. The first layered image of black lines shows polaron waves, which propagate during the application of the current. Fine dots in the second layer are the individual atom columns, while the periodic dot-clusters show the electron ordered state. The graph of electron energy loss spectroscopy reveals bonding-electron excitation. The bottom layer is a structural model of the crystal lattice. And the vertical graph shows the electric resistance (I-V curve) of the crystal when current is applied.
Courtesy: Yimei Zhu, Brookhaven National Laboratory

Upper right: Atomic resolution tunneling asymmetry scanning tunnel microscopy reveals electronic patterns centered along the Cu-O-Cu bonds (a_0 length) having $4a_0$ domains but without long-range order ('nanostripes') in underdoped cuprates. The emerging picture in this electronic cluster glass (ECG) region is partial hole localization. This electronic gridlock is broken at higher doping leading to superconductivity.
Courtesy: J.C. Davis, Cornell University and Brookhaven National Laboratory

Lower left: FMR image of the fundamental spin wave mode of a 2 micron permalloy dot. The image shows a cut through the fundamental FMR mode at a particular field. Three dimensional images of the mode (the spatial variation of the transverse magnetization) are obtained by combining slices obtained at several fields. The spatial resolution, given by the ratio of the spectral linewidth to the lateral field gradient, is approximately 200 nm.
Courtesy: Chris Hammel, Ohio State University.

Lower right: Experimental scanning transmission electron microscopy images of a SrTiO3 single crystal (top row) and theoretical images (bottom row). The Sr atomic columns are brightest and the Ti-O columns are second brightest. The right pane in the simulations accounts for spatial incoherence in the experiments. Note the unprecedented excellent agreement in high-resolution electron microscopy imaging.
Courtesy: Susanne Stemmer, University of California, Santa Barbara

This document was produced under contract number DE-AC05-06OR23100 between the U.S. Department of Energy and Oak Ridge Associated Universities.

Foreword

This volume summaries the scientific content of the 2008 Electron and Scanning Probe Microscopies (ESPM) Contractors' Meeting sponsored by the Division of Materials Sciences and Engineering (DMS&E) in the Office of Basic Energy Sciences (BES) of the U. S. Department of Energy (DOE). The meeting, held on October 26-29, 2008 at Airlie Conference Center, Warrenton, Virginia, is the second contractors' meeting in the ESPM area. It features ESPM research in materials sciences, and is broadly participated by PIs from several BES research program areas where appropriate and relevant.

Electron and Scanning Probe Microscopies formally became a BES core research activity (CRA) in July 2007, replacing the CRA previously known as Structure and Composition of Materials. Electron and scanning probe microscopy and spectroscopy are major tools for understanding the atomic, electronic, and magnetic structures and properties of materials, and are vital to the advancement of materials science, nanoscience and nanotechnology. The ESPM CRA supports research activities that advance the frontiers of materials sciences using ESPM and the development and improvement of novel microscopy and spectroscopy techniques to enable new scientific discoveries. Our first contractors' meeting, in October 2006, focused on the Surface and Interface Science at the Atomic Scale (SISAS) research theme that highlighted the atomic-scale microscopy and spectroscopy studies of surfaces and interfaces in combination with theory. The 2008 meeting is organized around the following research topics, as reflected in the agenda, to better facilitate in-depth scientific discussions: magnetic and multiferroic materials, electronic and superconducting materials, interfaces and grain boundaries, surfaces, structure determination, and nanostructured materials.

The purpose of this Contractors' Meeting is to bring together researchers funded by BES in this important research area, to facilitate the exchange of new results and research highlights, to foster new ideas and collaborations among the participants, and to identify needs of the research community. The meeting will also help DMS&E in assessing the state of the program, charting future directions and identifying programmatic needs.

It is my great pleasure to thank all the participants for their active contributions and for their willingness to share their ideas and latest research results. The dedicated efforts of the Meeting Chairs, Chris Hammel and Amanda Petford-Long, towards organizing this meeting are genuinely appreciated. Thanks also go to Christie Ashton from DMS&E and to Sophia Kitts and staff from the Oak Ridge Institute of Science and Education for their outstanding work in taking care of all the logistical aspects of the meeting.

Jane G. Zhu
Program Manager, Electron and Scanning Probe Microscopies
Division of Materials Sciences and Engineering
Office of Basic Energy Sciences
U. S. Department of Energy
October 2008

Table of Contents

Research Summaries II: Electronic & Superconducting Materials

Electron and Scanning Probe Microscopies Contractors' Meeting

U.S. Department of Energy
Office of Basic Energy Sciences
October 26 – October 29, 2008
Chris Hammel and Amanda Petford-Long, *Meeting Chairs*

Sunday, October 26

3:00 – 6:00 pm	Arrival and Registration
5:00 – 6:00 pm	Reception (No Host)
6:00 – 7:00 pm	***** Dinner *****
7:00 – 7:30 pm	*Welcome* *Division and Program Updates* Helen Kerch Director (acting), Division of Materials Sciences and Engineering Jane Zhu Program Manager, Electron and Scanning Probe Microscopies
	Plenary Lectures Chairs: Chris Hammel and Amanda Petford-Long
7:30 – 8:15 pm	Ali Yazdani, Princeton University *Scanning Tunneling Microscopy & Spectroscopy of Correlated Electronic Systems: Challenges & Opportunities*
8:15 – 9:00 pm	Tom Kelly, Imago Scientific Instruments (Invited) *Atomic-Scale Tomography of Materials*

Monday, October 27

7:00 – 8:00 am	Breakfast
Session I	**Magnetic Materials** Chair: Amanda Petford-Long, Argonne National Laboratory
8:00 – 8:30 am	Chris Hammel, Ohio State University *Microscopic Imaging of Subsurface Magnetic Dynamics and Phenomena*

8:30 – 9:00 am	Yimei Zhu, Brookhaven National Laboratory *Understanding the Electronic and Magnetic Properties of Advanced Materials*
9:00 – 9:30 am	Marc De Graef, Carnegie Mellon University *Experimental Vector Field Tomography of Magnetic Objects*
9:30 – 10:00 am	Bernd Kabius, Argonne National Laboratory *Three-Dimensional Elemental Imaging of Oxide Heterostructures*
10:00 – 10:30 am	***** Break *****
Session II	**Electronic Materials I** Chair: Susanne Stemmer, University of California, Santa Barbara
10:30 – 11:00 am	Xiaoqing Pan, University of Michigan *Structure and Dynamics of Domains in Ferroelectric Nanostructures*
11:00 – 11.30 am	Rachel Goldman, University of Michigan *Determining the Origins of the Electronic States in Semiconductor Nanostructures*
11:30 – 12:10 pm	Poster presenters *Highlight to presentation in Poster Session I*
12:15 – 1:15 pm	***** Lunch *****
1:15 – 3:00 pm	**Time for Interaction and Discussions**
3:00 – 5:00 pm	**Poster Session I**
5:30 – 6:30 pm	***** Dinner *****
Session III	**Electronic Materials II** Chair: Chris Hammel, Ohio State University
6:30 – 7:00 pm	Raffi Budakian, Univ of Illinois, Urbana-Champaign *Investigating Magnetic Order in Mesoscopic Superconductors using Cantilever Torque Magnetometry*
7:00 – 7:30 pm	Austin Chang, University of Wisconsin, Madison *Characterization and Control of Interfacial Chemistry, Structure and Properties in Magnetic Tunnel Junctions*

7:30 – 8:00 pm	Séamus Davis, Cornell University and BNL *Atomic Scale Studies of Doped-Hole Distributions, Self Organized Electronic Nano-Domains, and Electron-Boson Coupling in High-Tc Cuprates*
8:00 – 8:30 pm	Bob Westervelt, Harvard University *Imaging Electron Flow in Graphene Nanodevices*
8:30 – 10:00 pm	***Interactions in Poster Room***

Tuesday, October 28

7:00 – 8:00 am	Breakfast
Session IV	**Interfaces and Grain Boundaries** Chair: Geoffrey Campbell, Lawrence Livermore National Laboratory
8:00 – 8:30 am	Nigel Browning, LLNL and University of California, Davis *Observing Materials Dynamics on the Fundamental Atomic Scale by Ultrafast In-Situ TEM*
8:30 – 9:00 am	Michael Weinert, University of Wisconsin, Milwaukee *Atomic and Electronic Structure of Polar Oxide Interfaces*
9:00 – 9:30 am	Dawn Bonnell, University of Pennsylvania *Local Electronic and Dielectric Properties at Nanosized Interfaces*
9:30 – 10:00 am	Ian Robertson, University of Illinois, Urbana-Champaign *Visualization and Quantification of Deformation Processes Controlling the Mechanical Response of Alloys in Aggressive Environments*
10:00 –10:30 am	***** Break *****
Session V	**Surface Interactions** Chair: Miquel Salmeron, Lawrence Berkeley National Laboratory
10:30 – 11:00 am	Renu Sharma, Arizona State University *In Situ Characterization of the Nanoscale Catalysts During Anodic Redox Process*
11:00 – 11.30 am	Peter Sutter, Brookhaven National Laboratory *Atomistic Transport Mechanisms in Reversible Complex Metal Hydrides*
11:30 – 12:10 pm	Poster presenters *Highlight to presentation in Poster Session II*

12:15 – 1:15 pm	***** Lunch *****
1:15 – 3:00 pm	**Time for Interaction and Discussions**
3:00 – 5:00 pm	**Poster Session II**
5:30 – 6:30 pm	***** Dinner *****
Session VI	**Structure Determination** Chair: John Spence, Arizona State University
6:30 – 7:00 pm	Nitash Balsara, Lawrence Berkeley National Laboratory *Development of Microcharacterization Tools for Soft Matter based on Advanced Electron Microscopy*
7:00 – 7:30 pm	Alex Zettl, Lawrence Berkeley National Laboratory *Electron and Scanned Probe Microscopy of sp^2-Bonded Nanostructures*
7:30 – 8:00 pm	Jim Zuo, University of Illinois, Urbana-Champaign *Quantitative Electron Nanocrystallography*
8:00 – 8:30 pm	Kevin McCarty, Sandia National Laboratories *Dynamic Surface Microscopy of Functional Materials*
8:30 – 10:00 pm	***Interactions in Poster Room***

Wednesday, October 29

7:00 – 8:00 am	Breakfast
Session VII	**Nanomaterials** Chair: Aharon Kapitulnik, Stanford Institute for Materials & Energy Sciences
8:00 – 8:30 am	Hari Manoharan, SIMES *Nanoscale Probes of Complex Materials with Atom Manipulation STM*
8:30 – 9:00 am	Uli Dahmen, Lawrence Berkeley National Laboratory *Structure and Phase Transformations of Nanophases Embedded in Solids*
9:00 – 9:30 am	M. Tringides, Ames Laboratory *Control of Nanostructure Growth at Low Temperature*
9:30 – 10:00 am	Rolf Koenenkamp, Portland State University *Electron Mapping on the Nanoscale*
10:00 – 10:30 am	***** Break *****

10:30 – 11:00 am	Stephen Pennycook, Oak Ridge National Laboratory *Seeing into the Nanoworld Using Aberration-Corrected STEM*
11:00 – 11.30 am	Chong-Yu Ruan, Michigan State University *Ultrafast Dynamics at Nano-Interfaces*
11:30 – 12:00 pm	Sergei Kalinin, Oak Ridge National Laboratory *Towards Atomistic Understanding of Kinetics and Thermodynamics of Phase Transitions and Energy Dissipation at a Single Defect Level by Scanning Probe Microscopy*
12:00 – 12:15 pm	Closing Remarks Chris Hammel and Amanda Petford-Long, Meeting Chairs Jane Zhu, Meeting Organizer
12:15 pm	***** Lunch ***** Open Discussions and Adjourn

POSTER SESSION I
Jefferson Room

Monday, October 27, 2008
3:00 – 5:00 pm and 8:30 – 10:00 pm

P-I.1 - Imaging of Buried Nanoscale Optically Active Materials
Ian Appelbaum, University of Delaware

P-I.2 - Complex Transient Events in Materials studied using Ultrafast Electron Probes and Terascale Simulations
Geoffrey Campbell, Lawrence Livermore National Laboratory

P-I.3 - Epitaxial Multifunctional Oxide Heterostructures
Venkat Chandrasekhar, Northwestern University

P-I.4 - Phase-Field Approach to Domain Structures and Switching Mechanisms of Epitaxial $BiFeO_3$ Thin Films
Long-Qing Chen, Pennsylvania State University

P-I.5 - Nucleation and growth of molecular layers of ice with STM
Konrad Thürmer and Norm C. Bartelt, Sandia National Laboratories, Livermore, CA

P-I.6 - Electronic Structure and Properties of Complex Ceramics and Their Microstructures
Wai-Yim Ching, University of Missouri, Kansas City

P-I.7 - Structure and Magnetic Properties of Lanthanide Nanocrystals
James Dickerson, Vanderbilt University

P-I.8 - The Virtual Scanning Tunneling Microscope
David Goldhaber-Gordon, Stanford University

P-I.9 - Toward the Realization of Room Temperature Ferromagnetic Semiconductors: A Spin-Polarized STM Study
Lian Li, University of Wisconsin, Milwaukee

P-I.10 - Atomic Structure and Function of Internal Interfaces
Doug Medlin, et al., Sandia National Laboratories, Livermore, Ca

P-I.11 - Strain Induced Atomic Surface Structure of Compound Semiconductor Alloys
Joanna Millunchick, University of Michigan

P-I.12 - Magnetic and Ferroelectric Domain Imaging of Oxide Heterostructures
Amanda Petford-Long/Seungbum Hong, Argonne National Laboratory

POSTER SESSION II
Jefferson Room

Tuesday, October 28, 2008
3:00 – 5:30 pm and 9:00 – 10:00 pm

P-II.1 - Computational Investigations of Solid-Liquid Interfaces
Mark Asta, University of California, Davis

P-II.2 - Towards the Development of Cluster-Based Materials
Kit Bowen, Johns Hopkins University

P-II.3 - Materials Properties at Interfaces in Nanostructured Materials: Fundamental Atomic Scale Issues
Nigel Browning, University of California, Davis

P-II.4 - Statics and Dynamics of Dimensionally and Spatially Constrained Ceramic Oxides
Vinayak Dravid, Northwestern University

P-II.5 - TEAM 0.5 - Performance and Early Applications
U. Dahmen, Lawrence Berkeley National Laboratory

P-II.6 - Discovering the Role of Grain Boundary Complexions in Materials
Martin Harmer, Lehigh University

P-II.7 - Singe Atom and Molecule Manipulation and its Application to Nanoscience and Nanotechnology
Saw-Wai Hla, Ohio University

P-II.8 - Grain Boundary Complexions and Transitions in Doped Silicon
Jian Luo, Clemson University

P-II.9 - Using Local Probes for the Study of Nano-Scale Phenomena in Complex Materials
Aharon Kapitulnik, Stanford Institute for Materials & Energy Sciences

P-II.10 - New Methods for Atomic Structure Determination of Materials
Lawrence Marks, Northwestern University

P-II.11 - Nanoscale Imaging of Electrostatic and Magnetic Fields
Martha McCartney, Arizona State University

P-II.12 - Electron Scattering from Surfaces
Dilano Saldin, University of Wisconsin Milwaukee

P-II.13 - Nanoscale periodicity in stripe-forming systems at high temperature: Au/W(110)
Norm C. Bartelt, François Léonard, Roland Stumpf, Kevin F. McCarty, and Juan de la Figuera, Sandia National Laboratories, Livermore, CA

Research Summaries I:

Magnetic and Multiferroic Materials

Epitaxial multifunctional oxide heterostructures

Venkat Chandrasekhar
Department of Physics and Astronomy
Northwestern University
2145 Sheridan Road
Evanston, IL 60208
v-chandrasekhar@northwestern.edu

Chang-Beom Eom
Department of Materials Science and Engineering
University of Wisconsin
1550 Engineering Drive
Madison, WI 53706
eom@engr.wisc.edu

Scope of Program

This experimental program is directed towards investigating how the microscopic characteristics of multifunctional epitaxial perovskite films affect their macroscopic properties, using variable temperature scanning probe techniques in combination with electrical, magnetic and ferroelectric measurements.

Recent Progress

Scanning Tunneling Microscopy and Spectroscopy on $La_{0.7}Sr_{0.3}MnO_3$: Evidence for a pseudogap

Despite almost five decades of research on the physical properties of manganites, the nature of the metal-insulator (MI) transition in heavily doped manganites is still an outstanding issue. The most widely accepted explanation says that intrinsic inhomogeneities in such systems lead to phase separation into conducting and insulating domains in the sample. Within this model, the system is at its metallic (ferromagnetic) ground state at very low temperature; at higher temperatures insulating (non-magnetic) regions are expected to emerge slowly. With such inhomogeneities, the interesting nature of the metal-insulator transition can be explained within a percolation transition model. Scanning tunneling microscopy (STM) and spectroscopy (STS) can be powerful tools in probing the electronic inhomogeneities. In the past some groups reported observation of electronic inhomogenieties in the conductance map of the surface of manganites by STM while some other groups reported that such inhomogeneities are not probed by STM. We have performed STM and STS on an epitaxial thin film of $La_{0.7}Sr_{0.3}MnO_3$ (LSMO) grown by pulsed laser deposition (PLD). The as-grown sample showed a granular surface. However, the annealed LSMO film showed nice atomic terraces of 0.4 nm height. We did not find direct signatures of electronic inhomogeneities in the

conductance map, but we have observed a pseudogap forming at low temperature *i.e.* in the metallic state of the film, an indication of the potential presence of localized polarons.

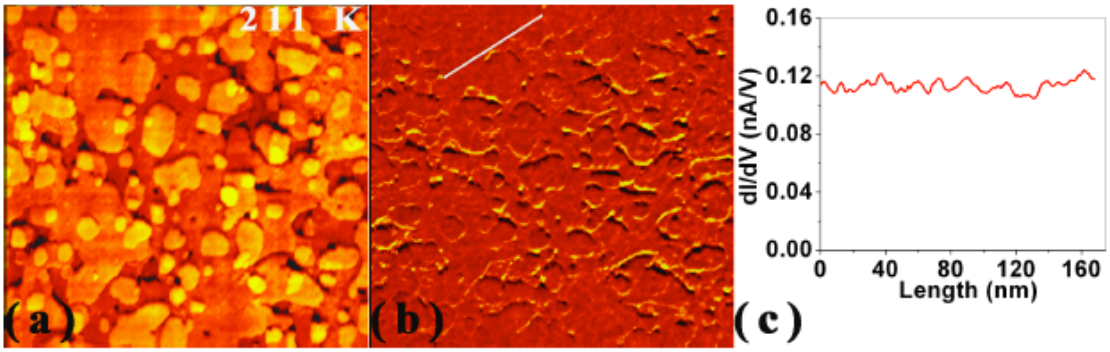

Figure 1. (a) Topographic and (b) corresponding conductance images of an annealed LSMO surface at 211 K. (c) shows a cut of the conductance map along the line shown in (b).

Figure 2. Averaged scanning tunneling spectra of the annealed LSMO sample at different temperatures, showing the emergence of a pseudogap at lower temperatures.

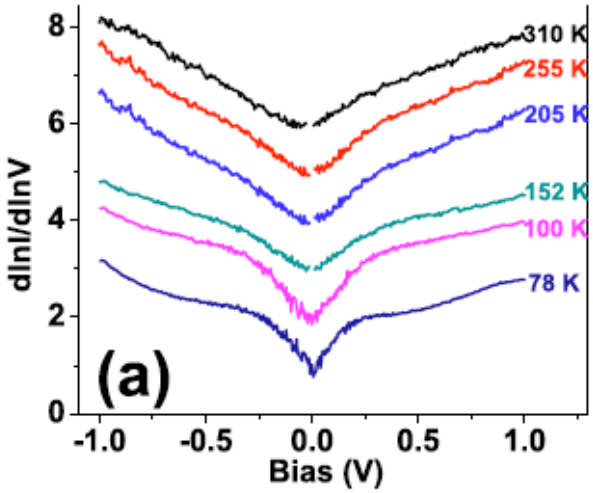

Publications

"Pseudogap Formation in the Metallic State of $La_{0.7}Sr_{0.3}MnO_3$ Thin Films," Udai Raj Singh, Anjan K. Gupta, Goutam Sheet, Venkat Chandrasekhar, H.W. Jang and C.B. Eom, submitted to Applied Physics Letters.

Future plans

We are currently working on three projects. The first is a continuation of the work discussed above. The STM work on the manganites has shown that STM may not be the best probe to study intrinsic inhomogeneities, as STM is only sensitive to the surface. We plan to use electrostatic force microscopy in combination with magnetic force microscopy to probe the "bulk" properties of the epitaxial manganite films.

The second project involves making artificial multiferroic structures using multilayered epitaxial complex oxide structures. The goal is the couple the ferromagnetism in a

manganite film to the ferroelectric order parameter in a ferroelectric perovskite film through strain coupling in order to be able to switch the magnetization of the ferromagnetic film by applying an electric field to the ferroelectric film. So far, we have fabricated magnetic cobalt ferrite (CFO) pillars with diameters down to 90 nm by electron beam lithography followed by ion milling (Figure 3). After ion milling, the sample is then coated with bismuth ferrite (BFO, a ferroelectric), and the BFO is planarized by ion milling at a glancing angle. Figure 4 shows a sample after planarization. As can be seen from the image, the problem is that the growth of the BFO after etching is not epitaxial. We plan to explore sol-gel techniques to grow these devices in the next few months.

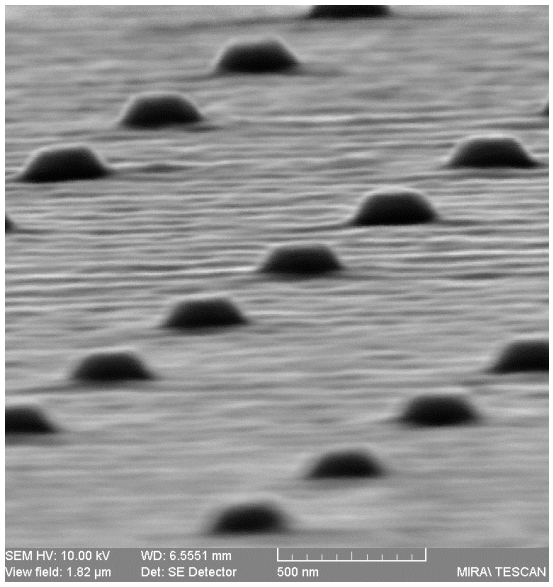

Figure 3. SEM of cobalt ferrite (CFO) pillars fabricated by electron beam lithography.

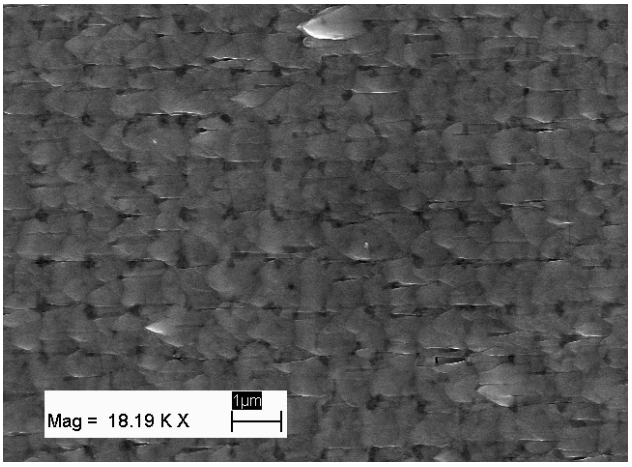

Figure 4. CFO pillars after planarization with bismuth ferrite (BFO).

The third project involves looking at spin polarized Andreev bound states at that are predicted to form at the interface between a ferromagnet and a *d*-wave superconductor by measuring the tunneling between LSMO and YBCO, using a STM or a conducting tip AFM.

Characterization and Control of Interfacial Chemistry, Structure, and Properties in Magnetic Tunnel Junctions

Y. Austin Chang (PI) and Paul Voyles (Co-PI since August 1, 2008), Dep't of MS&E, UW-Madison, 1509 University Ave, Madison, WI 53706, chang@engr.wisc.edu

Program Scope This grant, initiated on 08/01/99, was renewed on 08/01/05 to 07/31/08. Our objective since has been to engineer nanoscale magnetic multilayer structures via thermodynamic and kinetic considerations for a basic study of magnetic tunnel junctions (MTJs). The core of a MTJ consists of a thin insulating barrier (I), such as AlO_x, in between two ferromagnetic (FM) electrodes, i.e. (Co, Fe). The tunneling magnetoresistance (TMR) of a MTJ is governed by the properties of the electrodes, the tunneling barrier, and the interfaces between them. For an entire MTJ stack, there are other layers, such as buffer and antiferromagnetic (AFM) layers. The buffer layers have multiple functions to smoothing the interfaces and enhancing the texture or epitaxial nature of the critical central layers. The AFM layer such as IrMn is used to pin the magnetization direction of the adjacent FM layer by exchange bias. The pinned FM electrode is referred to as the top electrode in this abstract and the unpinned or free one as the bottom electrode.

Recent progress Our study during the past few years has focused on the effects of the crystal structure and strain state of the bottom electrode on the TMR of a MTJ. To isolate these effects, we developed junctions *with variable FM crystal structure and strain, but with constant FM composition, AlO_x tunnel barriers, and interface smoothness.* To achieve this goal, we developed a method using XPS to quickly determine the thickness of an ultra-thin tunnel barrier AlO_x obtained by oxidizing a thin Al precursor layer [06Yan, 06Yan1] and controlled the interfacial smoothness using selected buffers subject to appropriate annealing conditions. *Firstly, we showed experimentally a significant increase in the TMR when changing from a fcc to a bcc $Co_{87}Fe_{13}$ bottom electrode.* We attribute this structure-induced TMR enhancement to a higher *s*-electron spin polarization in the bcc structure. These results demonstrate the role of the crystal structure and the associated electronic structure of the FM electrodes on the spin dependent tunneling (SDT), independent of other differences in the MTJ structure which influence the TMR. *Secondly, we also showed that the strain of the lower epitaxial FM electrode affects the TMR of a MTJ*. The value of TMR increases with increasing strain of the electrode, suggesting that strain also increases the *s*-electron polarization of this electrode. *Thirdly, we obtained over 70% TMR in an AlO_x-based MTJs with the basic (Co, Fe) electrode [06Yan2] by annealing the bottom electrode to obtain a smooth surface.* Further improving of the bottom electrode using TiN as the buffer, 77% TMR was obtained [07Ji]. *Fourthly, we observed both normal and inverse TMRs in the extensively studied MTJ, $Co_{75}Fe_{25}/AlO_x/Co_{75}Fe_{25}$.* This result is unexpected since both interfaces are $Co_{75}Fe_{25}/AlO_x$, known to exhibit positive polarization [00Han]. Due to space limitation, we will presently only the results of the effect of crystal structure of the bottom electrode on the TMR of a MTJ and the observed positive and inverse TMR of a MTJ, *$Co_{75}Fe_{25}/AlO_x/Co_{75}Fe_{25}$.*

<u>Effect of crystal structure of the bottom electrode on the TMR of a MTJ</u> We prepared two MTJs: one having bcc-$Co_{75}Fe_{25}/AlO_x$/bcc-$Co_{87}Fe_{13}$(epitaxial) and the other bcc-$Co_{75}Fe_{25}/AlO_x$/fcc-$Co_{87}Fe_{13}$(epitaxial). The composition of the bottom electrode was selected knowing that bcc to fcc transition in thin-film (Co,Fe) alloys occurs at ≈ 13 at% Fe [97Woj]. The near degeneracy between these phases at ≈ 13 at%Fe enables us to use a Cu buffer to induce fcc-$Co_{87}Fe_{13}$ and a Cr buffer bcc-$Co_{87}Fe_{13}$. The wafers were annealed at 400°C for 1 hour after depositing 30nm Ag to improve the crystal quality/surface smoothness. Ag was used also as a cap layer for $Ir_{22}Mn_{78}$ which magnetically pinned the top electrode. Fig. 1(a) & (b) show four-circle XRD data confirming the different crystal structures of the $Co_{87}Fe_{13}$ bottom electrodes on the Cu and Cr buffers. For both samples, a Si (400) peak, an Ag (200) peak, and a third peak can be seen. Since the $Co_{87}Fe_{13}$ layer (15nm) is much thicker than the buffer (2nm), the third peak must come from

the $Co_{87}Fe_{13}$ layer. The third peaks in Fig. 1 (a) & (b) are at 51.9° and 66.0°, which correspond to diffractions from fcc-$Co_{87}Fe_{13}$ (200) (a=0.35 nm) and bcc-$Co_{87}Fe_{13}$ (200) (a=0.28 nm) respectively. To verify the symmetry of the crystal structure of the two epitaxial $Co_{87}Fe_{13}$ layers, the spectra of off-axis scans of samples with Cu and Cr buffer, either 54.74° or 45° off their [200] surface normal, were collected, as shown in Fig. 1 (c) & (d). Four Ag(111) and four Si(111) peaks (not shown) were observed in both samples. For the Cu-buffered sample with the off-axis angle of 54.74°, four fcc(111) peaks with a 2θ value of 44.15° were observed but there were no bcc(110) peaks (Fig. 1(c)). For the Cr-buffered sample, $Co_{87}Fe_{13}$ bcc(110) periodic peaks were observed, but no $Co_{87}Fe_{13}$ fcc(111) peaks (Fig. 1(d)). These results show the $Co_{87}Fe_{13}$ layers epitaxially grew along the [200] orientation into fcc and bcc structure in Cu- and Cr-buffered samples.

Since the interface roughness between the electrode and the tunnel barrier could have a big effect on the measured TMR [99Moo], the roughness must be controlled to be the same in all the MTJs. The argon pressure during film deposition was < 2 mTorr in order to improve the smoothness of

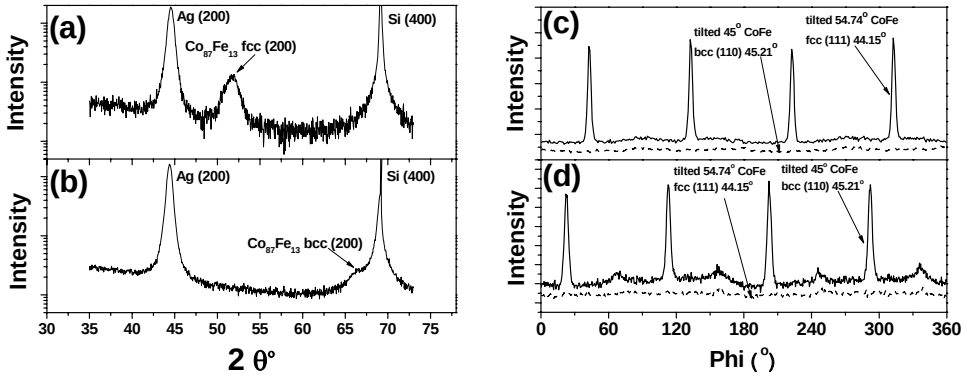

Fig. 1 XRD spectra for the bottom half of MTJs consisting of Si(100)/Ag(30 nm)/buffer(2 nm)/$Co_{87}Fe_{13}$(15 nm)/AlOx(1.6 nm). (a) and (b) are the normal θ-2θ spectra of samples with Cu and Cr buffer. (c) and (d) are the off-axis ϕ scans spectra of $Co_{87}Fe_{13}$ layers in samples with Cu and Cr buffer, respectively.

the multilayer. A piece of the bottom half junction was taken out of the chamber after the Al oxidation step for the AFM characterization. The 1 μm×1 μm AFM images of both samples are shown in Fig. 2. From Fig. 2, it can be seen that both interfaces of these samples are smooth with RMS roughness of ≈ 0.36nm and 0.40nm for Cu- and Cr-buffered samples. Considering that the Cu or Cr buffer layer was ≈ 2nm, these roughness values are comparable to reported values for (Co,Fe) surfaces. It is reasonable to conclude that significant difference of the transport properties obtained should not be caused by differences in interface roughness.

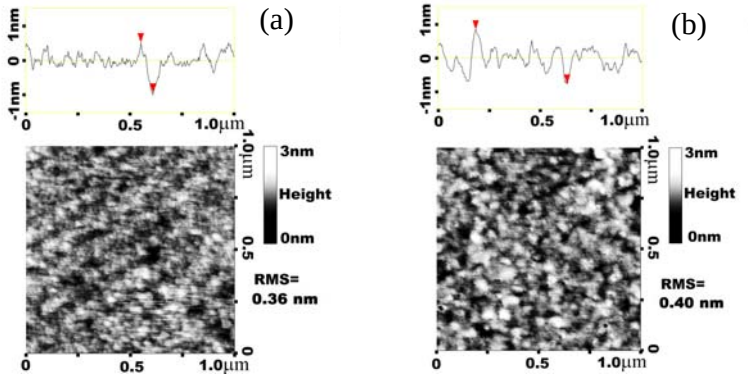

Fig. 2 AFM images (1μm × 1 μm) and section analysis of (a) Cu-buffered (b) Cr-buffered bottom electrodes.

Figure 3 shows the TMR curves of the two samples measured at room temperature. The TMR value of the Cr-buffered MTJ (bcc bottom electrode) reached 46.7% and that of the Cu-buffered MTJ (fcc bottom electrode) only reached 32.1%. The TMRs measured from several junctions for these two samples were 45 ± 3% and 31 ± 2%, respectively. The TMR value for the bcc electrode sample is about 1.4 times that for the fcc electrode sample. The results have been published [08Yan]. The values of the spin polarization for the Cu-buffered fcc- and Cr-buffered bcc-$Co_{87}Fe_{13}$ electrodes were extracted from the TMRs using Julliere's model [75Jul], are about 38% and 49%, respectively. We attribute the increase in the TMR values to a higher *s*-electron spin polarization for the bcc structure, which suggests that the bcc FM is the preferred structure for AlO_x based MTJ applications.

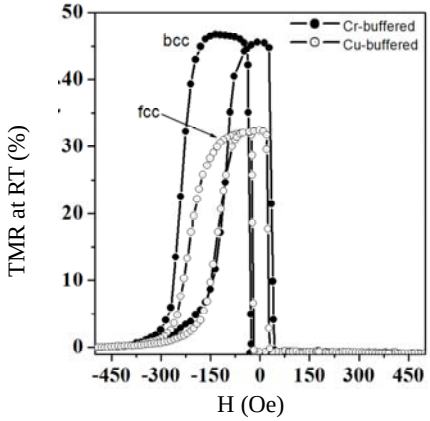

Fig. 3 Different TMR ratios at RT arising from the different FM crystal structures of the epitaxial bottom electrodes. The MTJs consists of Si(100)/Ag(30nm)/buffer(2nm)/$Co_{87}Fe_{13}$(15nm)/AlO_x (1.6nm)/$Co_{75}Fe_{25}$(4nm)/$Ir_{22}Mn_{78}$(18nm)/Ag(50 nm) and the buffer layers are Cu (open circles) or Cr (solid circles).

Inverse TMR obtained with a nominally symmetric MTJ, $Co_{75}Fe_{25}$ / AlO_x / $Co_{75}Fe_{25}$ We have observed both normal (+) and inverse (-) TMRs in the extensively studied MTJ, $Co_{75}Fe_{25}/AlO_x/Co_{75}Fe_{25}$. The TMR shown in Fig. 4(a) for the junction annealed at 230°C is positive, as expected, but the TMR shown in Fig. 4(b) annealed at 300°C are negative, which is unexpected. According to Julliere's model, when both electrodes are the same, the TMR of this junction should be positive. An inverse TMR results only when P_t and P_b have opposite signs with P_t and P_b being the spin polarization of the top and bottom electrode. Inverse TMR has been observed in asymmetrical MTJs with different electrodes, such as $Co/SrTiO_3/La_{0.7}Sr_{0.3}MnO_3$ [99Ter, 99Ter1] or in MTJs with composite tunnel barrier such as $NiFe/AlO_x/TaO_x/NiFe$ [99Sha]. That makes the inverse TMR we observed in this symmetric $Co_{75}Fe_{25}/AlOx/Co_{75}Fe_{25}$ junction striking, since both interfaces are $Co_{75}Fe_{25}/AlO_x$, known to exhibit positive polarization [00Han]. It is worth noting that the inversion occurs even at zero bias voltage, as shown in Fig. 4(d).

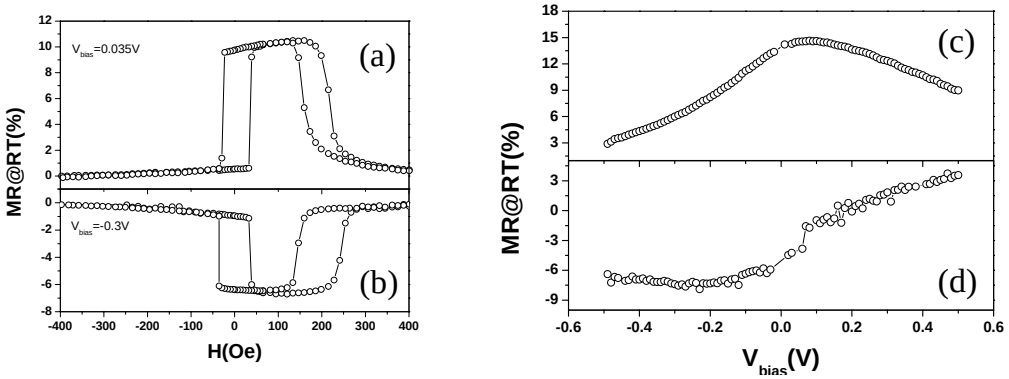

Fig. 4 TMR curves ((a)-(b)) and bias dependence curve ((c)-(d)) of samples annealed at 230°C ((a) and (c)) and 300°C

Future plans Our immediate plan focuses on (1) using aberration-corrected STEM and EELS to characterize the chemistry and structure of excess oxygen at the FM/AlOx interface in the junctions with inverse TMR and (2) to build a UHV deposition system. The inverse TMR in Fig. 4 suggests that this MTJ was not symmetric in terms of the chemistry at the FM/I/FM interfaces.

One plausible explanation is the formation of an oxide layer at the bottom FM/I interface annealed at 300°C, since the spin polarization of Fe3O4 is negative [05Par, 02Ded, 02Hu]. However, the over-oxidation of the bottom electrode has been common in fabricating MTJs, while the observation of the inverse TMR is rare, suggesting that a specific oxide (e.g., Fe3O4) forms only under certain conditions. We plan to use STEM to characterize the FM/I interface of the sample that exhibited inverse TMR. Our new deposition system is based on UHV chambers from Dr. E. George of ORNL. We expect to have better control over deposition conditions in the new system and to be able to fabricate junctions with epitaxial MgO tunnel barriers.

References

[75Jul] M. Julliere, Phys. Lett. **54A**, 225 (1975).
[97Woj] M. Wojcik, et al, Z. Phy B, 103, 5 (1997).
[99Moo] J. S. Moodera, J. Nassar, and G. Mathon, Annu Rev Mater Sci **29**, 81 (1999).
[99Ter] J. M. De Teresa et al, Science **286**, 507 (1999).
[99Ter1] J. M. De Teresa et al, Phys. Rev. Lett. **82**, 4288 (1999).
[99Sha] M. Sharma, S. X. Wang, J. H. Nickel, Phys. Rev. Lett. **82**, 616 (1999).
[00Han] X. F. Han et al, Appl. Phys. Lett. **77**, 283 (2000).
[02Ded] Y. S. Dedkov, J. Rüdiger, and G. Güntherodt, Phys. Rev. B **65**, 064417 (2002).
[02Hu] G. Hu and Y. Suzuki, Phys. Rev. Lett. **89**, 276601 (2000).
[05Par] C. Park et al, IEEE Trans. Magn. **41**, 2691 (2005).
[06Yan] J. J. Yang, et al, J. Electro. Mater. **35**, 2142 (2006).
[06Yan1] J. J. Yang, PhD Thesis, University of Wisconsin, Madison, WI, (2006).
[06Yan2] J. J. Yang, et al, Appl. Phys. Lett. 89, 202502 (2006).
[07Ji] C.-X. Ji, PhD Thesis, University of Wisconsin, Madison, WI, (2007).
[08Yan] J. J. Yang et al, Acata Mater., **56**, 1491-1495. (2008).

List of publications since 2006

1) Y. Yang, Y. A. Chang, J. Joshua. Yang, C.-X. Ji, P. F. Ladwig, F. Liu, B. B. Pant and A. E. Schultz, "Thermal stability of the interfaces between Co, Ni and Fe-based ferromagnets in contact with selected nitrides", J. Appl. Phys., 2006, 98, 053907/1- 053907/5.
2) C.-X. Ji, F. Ladwig, R. O. Ott, Y. Yang, J. J. Yang, Y. A. Chang, E. S. Linville, J. Cao and B. B. Pant, "Phase transformation behavior in", JOM, 2006, June, 52-57.
3) J. J. Yang, C.-X. Ji, X.-L. Ke, M. S. Rzchowski, and Y. A. Chang, "Over 70% TMR at room temperature for a CoFe and AlO_x based MTJ", Appl. Phys. Lett., 2006, 89, 202502/1-202502/3.
4) J. J. Yang, C.-X Ji, Y. Yang, Y. A. Chang, F. Liu, B. B. Pant, and A. E. Schultz, "Thickness determination of oxide film and its application in MTJs", J. Electro. Mater., 2006, 35, 2142-2146.
5) M.-L. Huang and Y. A. Chang, "Phase transformation in PdMn and PdPtMn thin films", JAP, 2006, 99, 023527/1-023527/4.
6) J. J. Yang, C.-X. Ji, Y. Yang, H. Xiang, Y. A. Chang, "Epitaxial growth and surface roughness control of ferromagnetic thin films on Si by sputter-deposition", J. of Electr. Mater., 2008, 37, 355-360.
7) J. J. Yang, A. K. Bengtson, C.-X. Ji, D. Morgan, and Y. A. Chang, "Crystal structure effect of ferromagnetic electrode on TMR", Acata Mater., 2008, 56, 1491-1495.
8) M.-L. Huang and Y. A. Chang, "Disorder-order phase transformation in sputter deposited Pd_3In thin films", J. Alloys Compounds, 2008, 455, 174-177.
9) J. J. Yang, A. K. Bengtson, C.-X. Ji, D. Morgan, and Y. A. Chang, "Origin of the dependence of TMR on the composition of $Co_{100-x}Fe_x$ electrodes in MTJs", JAP, 2008, 103, 056102-1 to-3.
10) C.-X Ji, J. J. Yang, F. Lu, M. S. Rzchowski, Y. A. Chang, "Growth and physical property of epitaxial Co70Fe30 thin film on Si substrate via TiN buffer", APL, 2008, 92, 022504-1 to -3.

Experimental Vector Field Electron Tomography of Magnetic Objects

Charudatta Phatak, and Marc De Graef (PI)
cd@cmu.edu, degraef@cmu.edu
Department of Materials Science and Engineering, Carnegie Mellon University,
Pittsburgh, PA 15213

Program Scope

The increasing complexity of today's materials systems must be accompanied by improvements in the methods used to study those materials. In this project (DOE# DE-FG02-01ER45893), we develop and apply tomographic reconstruction methods to the three-dimensional study of magnetic field distributions around nano-scale magnetic samples. The program consists primarily of an experimental component, supported by a strong modeling component. The modeling component is used to validate experimental observations, by using numerical simulations and analytical evaluation of error propagation. The experimental component makes use of a series of carefully selected samples, used in a series of increasingly more advanced electron microscopes and on a series of length scales.

The resulting 3D magnetic induction maps are to be compared with the results of extensive micromagnetic modeling. The program also further develops methods for the computation of magnetostatic interactions between nano-particles, based on the shape amplitude formalism (developed with prior DOE support).

There are two main program outcomes: an efficient, accurate tomographic reconstruction technique, including an experimental protocol, which can be used in contemporary microscopes to obtain 3D magnetic configurations; and 3D reconstructed magnetic configurations on a number of important magnetic material systems. The experimental and numerical techniques will also be made available to users at the DOE National User Facilities. The main impact of this program is the availability of a novel experimental technique to determine the three-dimensional magnetic induction and the magnetic vector potential in and around nano-scale magnetic objects.

The research is carried out by the P.I., Prof. Marc De Graef, and one graduate student, Charudatta Phatak. The work benefits from a strong collaboration with the group of Dr. Amanda Petford-Long at the Argonne National Laboratory.

Recent Progress

We have continued our theoretical efforts in the area of magnetostatic properties of and interactions between nanoscale objects. As before, this approach relies on the use of the *shape amplitude*, which is the Fourier transform of the object's indicator or shape function (a discontinuous function equal to 1 inside and 0 outside the object). The following list itemizes some of the most important findings of our work (citations are listed at the end of this abstract):

- Demagnetization factors of magnetized objects are often referred to in terms of a so-called *equivalent ellipsoid*, i.e., an ellipsoid with the same demagnetization factors as the object. All too often, one assumes that this ellipsoid has the same aspect ratio as the principal axes of the object. We have shown theoretically that this approach is incorrect, and we have proposed *a general method for the rigorous determination of the magnetostatically equivalent ellipsoid*. We have worked out explicit examples for discs, for cylinders with elliptical cross-section, and for prisms.

- We have determined the *phase diagram for a single-domain state magnetic nano-ring in terms of the material and shape parameters.* Our phase diagram compares favorably with micromagnetic simulations and electron holography results on actual magnetic nanorings.
- We have determined *an analytical expression for the local demagnetization factor for the ring-core flux gate geometry, based on a tangential magnetization model.* The ring-core flux gate is used as a sensor to measure small DC or low-frequency AC magnetic fields with 0.1 nT resolution. Our results are in good agreement with experimental measurements and indicate that the local demagnetization factor scales with the ratio of the cross-sectional area to the total area of the ring.
- We have created a *self-contained didactical derivation for the demagnetization factors of the general tri-axial ellipsoid.* While the demagnetization factors of the ellipsoid have been known since Maxwell's writings, there has not been a transparent derivation in the literature until now. We have derived the demag factors in terms of a two-parameter integral representation which makes use of the intrinsic symmetry of the ellipsoid, and we obtained expressions for the prolate and oblate spheroid in terms of well-known Gaussian hypergeometric functions.
- We have obtained a number of *analytical representations for the demag factors of cylindrical and elliptic rings as well as the dipolar coupling integral encoding magnetostatic interactions between a magnetized cylinder and a thin coating on its lateral surface,* a geometry of importance for high density magnetic memory applications.
- We have derived *general analytical expressions for the magnetostatic forces and torques (both mechanical and magnetic) between uniformly magnetized objects of arbitrary shape.* This result allows for the numerical computation of interaction forces and torques, while separating shape effects and dipolar coupling. This work will be useful for the simulation of the behavior of high-density magnetic nano-particle systems, such as ferro-fluids, in which the shape-shape interactions become important due to the close proximity of the particles.

In addition to the theoretical work summarized above, a significant portion of our work has focused on the application of tomographic reconstruction methods to the 3-D analysis of magnetic fields. We apply exit wave reconstruction methods and 3D scalar and vector field electron tomography algorithms developed during the previous portion of the program to determine the magnetic field distribution in and around magnetic materials at the nano-scale. As an example, consider the 3D structure of the core of a magnetic vortex in a circular disk, as shown schematically in Fig. 1. The vortex core is characterized by two parameters, the chirality and the polarity. Using numerical methods, we can compute the Fresnel through-focus images for this configuration for two tilt complete (i.e., 360°, one image every 5°) series around perpendicular tilt axes. From these images, we can reconstruct both the magnetic and electrostatic components of the electron wave phase shift, using the Transport-of-Intensity approach.

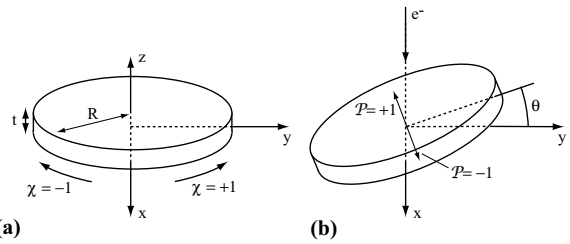

Figure 1: (a) Schematic of a circularly magnetized disk (radius R, thickness t) with positive ($\chi = +1$) or negative ($\chi = -1$) chirality. In (b), the disk is tilted around the x-axis by a counterclockwise positive angle θ. The vortex core polarity is either positive ($\mathcal{P} = +1$) or negative ($\mathcal{P} = -1$), as indicated. The electron beam travels along the negative z-direction; the x-direction points out of the plane of the drawing.

An example of such a phase reconstruction is shown in Fig. 2 for a Cobalt disk (32 nm radius, 11 nm thick, 1 T saturation induction) and for a 200 kV C_s-corrected microscope. The labels

"unflipped" and "flipped" refer to the orientation of the disk with respect to the incident electron beam. The subsequent tomography simulation employs a total of 144 through-focus series from which 72 magnetic phase shifts are extracted, which are then interpolated to a 2.5° tilt angle increment. This interpolation works well due to the smoothness of the magnetic phase shift.

Using the vector field tomography reconstruction formalism developed with prior DOE support, we can reconstruct both the magnetic vector potential $\mathbf{A}(\mathbf{r})$ and the magnetic induction $\mathbf{B}(\mathbf{r})$. Typical reconstructions are performed on an array of 256^3 voxels. For the magnetic induction, application of the vector slice theorem permits for the reconstruction of the B_x and B_y components; the condition $\nabla \cdot \mathbf{B} = 0$ is then used to obtain the third component B_z. For the magnetic vector potential, all three components A_x, A_y and A_z are simultaneously reconstructed. The combined knowledge of B_x and B_z allows for the simultaneous determination of vortex chirality and polarity. Fig. 3 shows the reconstructed magnetic induction near the center plane of the disk as a 3-D vector field.

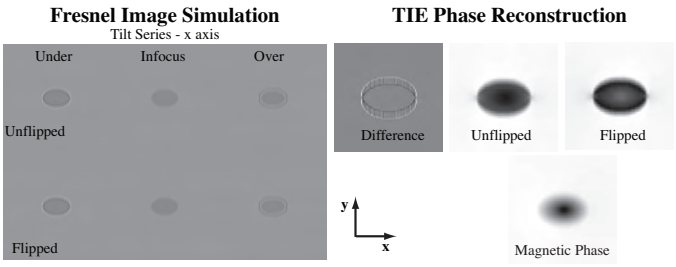

Figure 2: Example phase reconstruction for a circular disk with vortex core. On the left, two through-focus series are shown for the unflipped ($\theta = 50°$) and flipped ($\theta = 230°$) sample orientations. Each series is then used to solve for the total electron phase shift (upper right). The difference between unflipped and flipped shifts is the magnetic phase shift, shown on the lower right. [200 kV, $C_s = 0.05$ mm].

Note that the chirality and polarity of the core can be derived easily from this representation. Our numerical work shows that this method can be applied to a variety of sample geometries, including objects that contain magnetic domain walls. In fact, it should be possible to extract an accurate magnetization profile across a magnetic domain wall from the 3-D reconstructions.

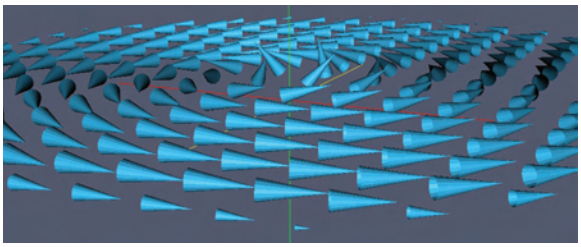

Figure 3: 3-D representation of the reconstructed magnetic induction near the center plane of the disk.

We have defined a number of error variables to quantify the deviations between the exact and the reconstructed magnetization states: the RMS deviation between the magnitude of the theoretical and reconstructed vectors, summed over all voxels inside or outside the object, and the distribution of angular errors between the sets of vectors, again inside and outside the object. It was found that the largest errors occur where the magnetization has the largest gradient, i.e., near the surfaces of the object.

Our analysis also shows that C_s correction is absolutely essential for the tomographic reconstructions to be accurate. In a typical Lorentz setup, the spherical aberration of the Lorentz pole piece is in the range of 5 to 10 meters, resulting in a theoretical spatial resolution (at Scherzer defocus) of about 2 nm. In reality, delocalization effects worsen the resolution, since Lorentz images are typically taken far out of focus, so that the actual spatial resolution is closer to 10 or 15 nm. C_s correction will improve the theoretical resolution to well below 1 nm, and will also virtually eliminate delocalization effects, so that the actual resolution becomes nearly an order of magnitude better than what is currently available. We are in the process of installing a new 300 kV FEI Titan microscope, equipped with an image aberration corrector and Lorentz pole piece. Early results indicate that correction of C_s from about 8 meters down to better than 1 mm should be feasible.

Future Plans

On the experimental side, we will begin by studying commercially available MFM tips and determine the 3D magnetic field configuration surrounding the tip. This will be followed by a series of experiments on patterned structures, in collaboration with Dr. Amanda Petford-Long (ANL). The material of the structures will be selected to have a large saturation induction, to generate a large magnetic phase shift; Co-Fe is a good candidate material. Initial observations will be directed towards vortex core structures and magnetic domain wall profiles. We will work also with Dr J.A. Liddle of the Center for Nanoscale Science and Technology (CNST) at NIST (Gaithersburg) to create a number of dedicated samples for VFET observations. These samples will be specifically designed to be used with a high tilt angle tomography holder, so as to avoid any problems with sample mounting. The fabrication method is a combination of electroplating and e-beam photolithography (line width $50 - 100$ nm) and can be used to fabricate 3-D shapes by creating layered structures. Among the shapes to be explored will be simple circular and ellipsoidal disks, a nano-scale horse-shoe magnet, and a solenoid coil with square cross-section.

The modeling effort will closely parallel and support the experimental work. While the basic theory of vector field electron tomography is now rather well established, it is not clear how sensitive the reconstruction is to the experimental parameters of Lorentz TEM observations. Since the phase is a relatively smooth function of position, we will study whether or not missing experimental data (missing wedge) can be extrapolated from the acquired data. We will compare the accuracy and speed of our algorithm with several other implementations, such as ART, SIRT, and the use of an interlaces sampling scheme. We will analyze the the propagation of errors in reconstruction sequence. Finally, all reconstructions will be compared with theoretical models of the magnetization state and field of a given particle geometry; the theoretical models will be derived using the shape amplitude formalism.

DOE Sponsored Publications in 2006-2008

- M. Beleggia, M. De Graef, and Y.T. Millev, "The equivalent ellipsoid of a magnetized shape," *J. Phys. D*, vol. 39, pp. 891–899, 2006.
- M. Beleggia, J.W. Lau, M.A. Schofield, Y. Zhu, S. Tandon, and M. De Graef, "Phase diagram for magnetic nano-rings," *J. Magn. Magn. Mat.*, vol. 301, pp. 131–146, 2006.
- M. De Graef and M. Beleggia, "The fluxgate ring-core demagnetization field," *J. Magn. Magn. Mat.*, vol. 305, pp. 403–409, 2006.
- M. Beleggia, M. De Graef, and Y.T. Millev, "Self-energy and demagnetization factors of the general ellipsoid: A self-contained alternative to the Maxwell-Stoner approach," *Phil. Mag.*, vol. 86, pp. 2451–2466, 2006.
- C. Phatak and M. De Graef, "Is a C_s corrector necessary for Lorentz vector field tomography?," *Microscopy Today*, vol. 15, pp. 24–27, 2007.
- C. Phatak, M. Beleggia, and M. De Graef, "Vector field tomography of magnetic materials: Theoretical development," *Ultramicroscopy*, vol. 108, pp. 503–513, 2008.
- M. Beleggia, D. Vokoun, and M. De Graef, "Demagnetization factors for cylindrical shells and related shapes," *J. Magn. Magn. Mat.*, 2008 (submitted).
- M. De Graef and M. Beleggia, "Magnetostatic shape-shape interaction forces and torques," *J. Magn. Magn. Mat.*, 2008 (submitted).

Structure and Magnetic Properties of Lanthanide Nanocrystals

James H. Dickerson
Department of Physics and Astronomy, Vanderbilt University
Station B #351807, 2301 Vanderbilt Place, Nashville, TN 37235-1807
james.h.dickerson@vanderbilt.edu

Program Scope:

The goal of this research is to determine how three nanocrystalline effects (size, proximity & boundary, and magnetic effects) may be interrelated in a class of ferromagnetic nanomaterials, lanthanide chalcogenide nanocrystals. This project will allow us to understand the fundamental characteristics that govern the physical phenomena within these cubic magnetic nanocrystals. Focusing on europium chalcogenides (EuX: X = O, S, Se, Te), exploring the relationship among nanocrystalline effects may give rise to an abundance of unexplored magnetic and magneto-optical phenomena. These properties could be exploited in applications ranging from nanostructured magnetic recording media to magneto-optical switches to bio-imaging reagents.

Recent Progress:

A. Synthesis of Sub-2.0 nm EuS Nanocrystals: The thermal decomposition of single molecular precursors has been proven to be an effective method to synthesize nanoscale metallic chalcogenides.[1] Finer control over these parameters can be obtained using different precursors and a refined thermolysis. Our technique to produce sub-2.0 nm EuS nanoparticles involves a thermolysis procedure of a synthesized single-source precursor, a method similar to that observed by others.[2-4] For the preparation of single source Eu precursor, we used a procedure similar to that reported for the synthesis of heteroligand lanthanide(III) diethyldithiocarbamate complexes with phenanthroline.[5-7] The decomposition procedure of the EuS nanoparticles was pursued via thermogravimetric analysis (TGA) and derivative thermogravimetric (DTG) analysis. A 1 mM methanolic solution of 1,10-phenanthroline was added under vigorous stirring to a 1 mM methanolic solution of $EuCl_2$. Thereafter, 2 mM of diethylammonium diethyldithiocarbamate were added into the reaction mixture, producing an orange precipitate. The orange EuS precursor crystals were isolated by centrifugation, washed twice with methanol and dried under vacuum. This work demonstrates that the synthesized resultant heteroligand complexes display high stability against hydrolysis, which tends to be the main obstacle for the successful fabrication of europium chalcogenides.[8-10]

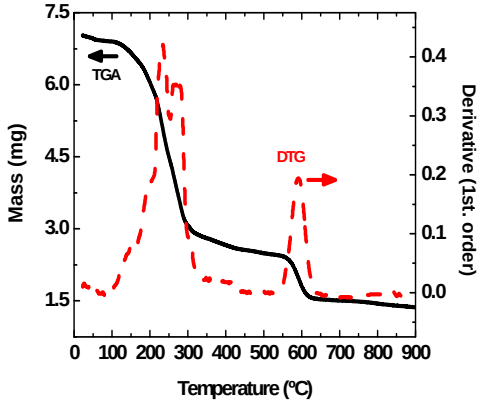

Fig. 1: TGA (solid line) and DTG (dashed line) analysis of the EuS precursor. [13]

For the synthesis of EuS nanoparticles, we transferred the precursor to a porcelain boat and inserted it into a horizontal tube furnace (Thermolyne #F21135, Barnstead International) for a time-sensitive mass reduction step. A steady stream of dry, ultrapure nitrogen prevented unintended hydrolysis or unintended devolution of the precursors. We heated the materials for approximately one hour at 700 °C. After this step, the resultant solid was cooled gradually to room temperature. Adjustments of decomposition temperature and time, and ramp-up/ramp-down time, yielded dispersed nanocrystalline particles with controllable size. This produces nanoparticles, which were dispersed in a variety of manners. For our studies, we have dispersed the EuS nanocrystalline powder in a variety of materials, including oleic acid solution, 2,2'-bipyridyl, and pyridyne (Alfa Aesar).

To assess the suitability of the precursor, prepared as described above for EuS nanoparticle synthesis, TGA was performed across a temperature range from 25 °C up to 900 °C at a heating rate of 10 °C min^{-1} under nitrogen atmosphere. The starting precursor mass for the analyses was 7 mg.

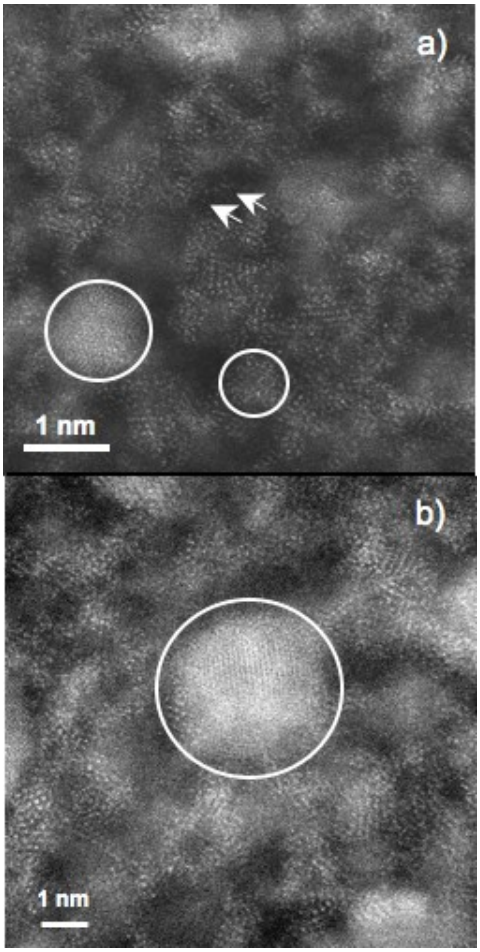

Fig. 2: Two HAADF images of EuS nanoparticles with bright intensities representing Eu atoms. (a) One (1.10 ± 0.20) nm nanoparticle neighboring one with a nominal diameter of (0.72 ± 0.13) nm. (b) A larger, (3.70 ± 0.67) nm nanoparticle. Each of the aforementioned nanoparticles is encircled to guide the eye. The positions of isolated single Eu atoms are indicated by arrows.[13]

The resulting TGA and DTG curves, which characterize the thermal decomposition of the precurosrs, are presented in **Figure 1**. The EuS precursor decomposes in two steps. The majority of the mass loss, approximately 50 %, occured in the 100 ºC to 350 ºC temperature region. This corresponds to pronounced peaks in the DTG curve at 200 ºC and 232 ºC, which indicates the rapid, vigorous decomposition of the single source precursor and the initial nucleation and growth of the EuS nanoparticles. Another smaller transition in the TGA designated a second stage in the decomposition process. This occurred in the 500 ºC to 625 ºC temperature range. The corresponding DTG curve displayed the maximum decomposition rate at 588 ºC with a mass loss of 12.5 % during this transition. It represented the decomposition of residual inorganic and organic compounds of the initial precursor material, yielding the final product at the end of decomposition: EuS NCs. The final residual mass was twenty-five percent of the original. At the high temperature of 700 ºC chosen for our synthesis, fast nucleation and growth of EuS is anticipated to facilitate ultrasmall particles.

B. Electron Microscopy of Sub-2.0nm EuS Nanocrystals: For our analysis of the size and structure of the nanomaterials, methanolic solutions of the EuS nanoparticles were dropcasted onto holey carbon films mounted on TEM specimen grids (Ted Pella, Inc.). High-angle annular dark-field (HAADF) Z-contrast scanning transmission electron microscopy (Z-STEM) images were acquired using an aberration-corrected VG Microscope HB603 U STEM, which was operated at 300 KeV.[11] Electron probe diameters were below 0.1 nm. Electron beam currents of less than 20 pA and dwell times of 32 µs/pixel were used.

Figure 2 shows two representative HAADF images of the EuS nanoparticles with bright image intensities representing Eu atoms. The chosen imaging conditions limit the visibility of sulfur and carbon atoms due to the large difference in the atomic numbers for Eu (Z=63), S (Z=16) and C (Z=6). The STEM analysis revelead highly crystalline face-centered cubic nanoparticles (encircled), the majority of which has dimensions well below 2 nm. For example, in **Figure 2a** two nanoparticles with nominal diameters of (1.10 ± 0.20) nm and (0.72 ± 0.13) nm are encircled. The detection of isolated Eu atoms dispersed on the carbon support film (marked by arrows) indicates atomic resolution and single atom sensitivity during the STEM experiments. In many areas of the sample, non-crystalline agglomerates of Eu atoms (likely in conjunction with sulfur atoms) were observed. More detailed investigations of the crystallinity of the EuS nanoparticles and their lattice plane spacings requires selected area electron diffraction experiments, which will be subject of future work. However, for the *quantum-confined*, sub-2.0 nm EuS nanomaterials, HAADF data provide both direct evidence for the size and crystallinity of the nanoparticles, and first indications of size-induced structural re-arrangements in individual particles.

A plot of the EuS nanoparticle size distribution is provided in **Figure 3a**. The abcissa label, circular diameter, refers to the diameter of a sphere characterized by the same area as covered by the

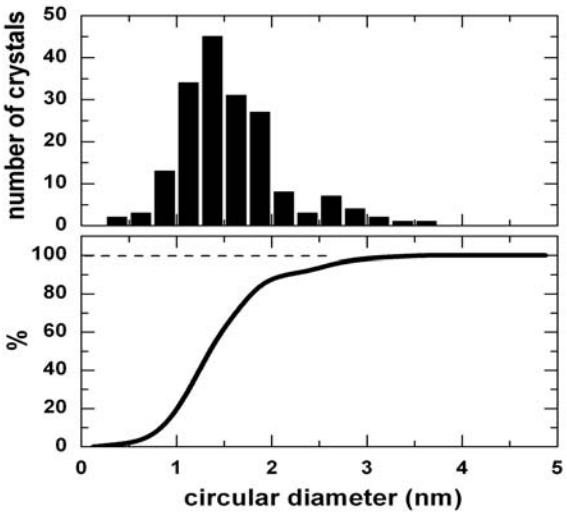

Fig. 3: a) Histogram of the EuS nanoparticle sizes prepared by thermolysis at 700 ºC as a function of circular diameter (see text). b) Percentage of the nanomaterials whose size are smaller than or equal to the corresponding circular diameter. [13]

individual particles. Thus, the diameter of the nanoparticles observed in the HAADF images were distributed in **Figure 3a** under the corresponding circular diameter. All reported circular diameters in **Figure 3** are subject to an uncertainty of 18 %. Approximately 45 % of the analyzed nanoparticles have circular diameters between 1.25 nm and 1.5 nm. Additional statistics, provided in **Figure 3b**, reveal that 88 % of the particles are characterized by diameters below 2.0 nm. Therefore, the predominance of the synthesized nanomaterials reside within the ultrasmall nanocrystal regime.

EuS nanoparticles with sub-2 nm sizes were synthesized by a thermolysis of a single source precursor —europium diethyldithiocarbamate complex with 1,10-phenanthroline. Favorable synthetic conditions for EuS nanomaterials with the sizes well below 2 nm were studied by TGA and DTA analysis and confirmed by imaging using aberration corrected STEM. We will continue our study of the relationship among the magnetic properties, the atomic arrangement, and the size of lanthanide chalcogenide nanomaterials.

C. Magnetic Characterization of 4nm and 14 nm EuS Nanocrystals: Magnetic measurements on larger EuS nanocrystals (4 nm and 14 nm) included the zero-field-cooled and field-cooled magnetic moment measurements as functions of temperature, and magnetization hysteresis loop measurements. The magnetization response of 14nm nanocrystal across a temperature range from 2 to 21K was measured. At 2 K, the counterclockwise hysteresis curve, typical for the ferromagnetic materials, was observed. Such a hysteresis yields a positive remanent magnetization (M_R). When the temperature increased, the hysteresis curve reversed direction, becoming clockwise. M_R studies performed on 4 nm EuS nanocrystals are comparable to previously reported measurements in which a reversal in M_R was observed as a function of temperature.[12] Investigation of magnetic properties for 14 nm EuS nanocrystals has shown a similar, yet unexpected, reversal phenomenon. M_R as a function of temperature for both 4nm and 14nm are displayed in **Figure 4**. The data confirmed the magnetization reversal phenomena for 4nm nanocrystals, but revealed similar physics in larger nanocrystals. We will study nanocrystals of size up to 20 nm, in which bulk-like traits dominate.

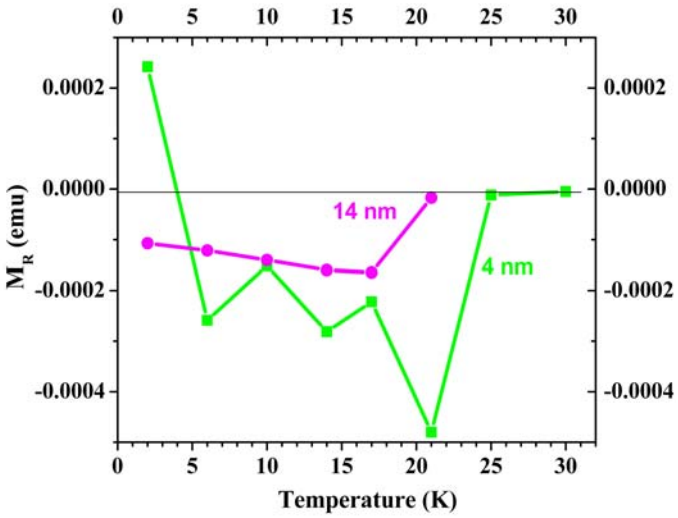

Fig 4: Remnant magnetization (M_R) versus temperature for 4 nm and 14 nm europium sulfide nanocrystals. For the majority of the temperatures, M_R is reversed.

Future Directions:

We have two intended trajectories of research for the upcoming twelve month period. The first activity involves the continued synthesis, magnetic and structural characterization of

our nanomaterials through high resolution electron microscopy (Z-STEM and HR-TEM), from sub-2.0 nm through 20 nm, to provide the first comprehensive study of the correlation between size, atomic arrangement, and magnetic characteristics. We already have evidence of the size dependence below approximately 10.0 nm; however, we wish to extend our studies up through 20 nm, which constitutes the approximate size at which bulk phenomena in EuS arises. This study will rely heavily on measuring the magnetic characteristics, such as M_R, the effective dipole moment, and the Curie temperature.

The second activity will be to synthesize and to characterize europium selenide nanocrystals, from sub-2.0 nm through 20 nm. Europium selenide (EuSe) possesses antiferromagnetic to ferrimagnetic to antiferromagnetic ordering transitions at 1.8 K, 2.8 K, and 4.6 K, respectively. Since we already have observed size-dependent augmentation of the remnant magnetizatoin in europium sulfide nanocrystals, we conjecture that we may be able to observe comparable changes, if not, the ability to ***tune*** the ferrimagnetic and antiferromagnetic characteristics of EuSe nanocrystals through size-dependent and temperature-dependent effects.

List of Publications Associated with the DOE Project:

Marcela L. Redígolo, Dmitry S. Koktysh, Klaus van Benthem, Sandra J. Rosenthal, and James H. Dickerson, ***Europium sulfide nanoparticles in the sub-2nm size regime***, submitted to Materials Chemistry and Physics, 2008.

Suseela Somarajan, Melissa A.Harrison, Sameer V.Mahajan, Chinessa T.Adkins, Eva Harth and James H. Dickerson, ***Electrophoretic Deposition of Star Polymer-Europium Chalcogenide Nanocomposite Films,*** imminent submission to Key Engineering Materials, 2008.

References:

1. M. A. Malik, P. O'Brien and M. Helliwell, *Journal of Materials Chemistry*, 2005, **15**, 1463-1467.
2. F. Zhao and S. Gao, *Journal of Materials Chemistry*, 2008, **18**, 949-953.
3. T. Mirkovic, M. A. Hines, P. S. Nair and G. D. Scholes, *Chemistry of Materials*, 2005, **17**, 3451-3456.
4. F. Zhao, H. L. Sun, S. Gao and G. Su, *Journal of Materials Chemistry*, 2005, **15**, 4209-4214.
5. R. A. Ivanov, I. E. Korsakov, N. P. Kuzmina and A. R. Kaul, *Mendeleev Communications*, 2000, 98-99A.
6. M. D. Regulacio, K. Bussmann, B. Lewis and S. L. Stoll, *Journal of the American Chemical Society*, 2006, **128**, 11173-11179.
7. M. D. Regulacio, N. Tomson and S. L. Stoll, *Chemistry of Materials*, 2005, **17**, 3114-3121.
8. D. J. Sellmyer, M. Yu and R. D. Kirby, *Nanostructured Materials*, 1999, **12**, 1021-1026.
9. D. J. Sellmyer, M. Yu, R. A. Thomas, Y. Liu and R. D. Kirby, *Physics of Low-Dimensional Structures*, 1998, **1-2**, 155-165.
10. S. H. Sun and C. B. Murray, *Journal of Applied Physics*, 1999, **85**, 4325-4330.
11. K. v. Benthem and S. J. Pennycook, *Electron Microscopy of Nanomaterials at very High Resolution*, Dekker, New York, 2008.
12. M. L. Redígolo, D. S. Koktysh, S. J. Rosenthal, J. H. Dickerson, Z. Gai, L. Gao and J. Shen, *Applied Physics Letters*, 2006, **89**.
13. M. L. Redígolo, Dmitry S. Koktysh, Klaus van Benthem, Sandra J. Rosenthal, and James H. Dickerson, ***Europium sulfide nanoparticles in the sub-2nm size regime***, submitted to Materials Chemistry and Physics, 2008.

Microscopic Imaging of Subsurface Magnetic Dynamics and Phenomena in Multicomponent Magnetic Materials

P. Chris Hammel*

Departments of Physics and Electrical and Computer Engineering, The Ohio State University

Introduction

Magnetic resonance force microscopy achieves very high resolution three-dimensional imaging capabilities of magnetic resonance imaging by taking advantage of very high sensitivity force detection. This enables non-contacting, microscopic studies and imaging of a broad range of materials. We have demonstrated scanned probe Ferromagnetic Resonance (FMR) imaging in ferromagnets where the the strong interactions between spins invalidates the assumptions underlying conventional magnetic resonance imaging. We present a new approach to localizing the resonant volume in an FMR measurement in ferromagnetic films. This capability is founded on the strong, nonuniform magnetic field of the micromagnetic probe tip. We present a model that accurately describes our local scanned probe FMR images obtained in patterned ferromagnetic films. By illuminating the mechanisms underlying localized FMR, this work provides the basis for submicron scanned probe FMR imaging of films and buried ferromagnetic elements. In addition to high sensitivity detection of FMR we are applying sensitive force detection to MFM imaging of paramagnetic spins in semiconductors:

- Demonstration of scanned probe ferromagnetic resonance (FMR) imaging of patterned ferromagnets using Magnetic Resonance Force Microscopy (MRFM)
- Observation of local FMR mode modification for localized FMR to enable spatially resolved imaging of ferromagnetic properties of samples
- Development of ultrasensitive Magnetic Force Microscopy (MFM) for imaging paramagnetic spin polarization in semiconductors

*email: hammel@mps.ohio-state.edu
Address: Room 2000 Physics Research Building,
191 W. Woodruff Ave.
The Ohio State University
Columbus, OH 43212

Program Scope

New magnetic materials and devices with unprecedented capabilities and levels of performance are now being created by tailoring the structure and composition of multicomponent materials at the nanometer scale. Some of the most important examples are systems incorporating and exploiting magnetism and ferromagnetic materials. The field of spin electronics offers a new generation of devices based on the interaction of the electronic spin with these materials. The present revolution in information processing is based on manipulation of electronic charge. Spin electronics envisions exploiting the spin degree of freedom of the electron either in concert with its charge, or by itself. This could offer significant new advantages including nonvolatile memory, increased speed and reduced power consumption relative to charge-based electronics and information processing. Spin based electronics offers the possibility of new capabilities extending from high density non-volatile solid state memory to spin-transistors to spin-based quantum computation and communication.

Major obstacles that must be overcome to achieve the vision of spin electronics include understanding and extending spin lifetimes, detecting spin magnetization in nanoscale structures and improved understanding of and control over spin transport across interfaces within these composite devices. It will be essential to have characterization and imaging tools with spatial resolution finer than device dimensions, sensitivity sufficient to detect very weak magnetic moments, and, very importantly, selective sensitivity to the *deeply buried interfaces* whose characteristics play a crucial role in determining the properties of these materials in order to address these challenges.

MRFM detection of Ferromagnetic Resonance (FMRFM) and Nuclear Magnetic Resonance (NMRFM) provides the basis for very high resolution imaging and studies of subsurface features of submicron layered magnetic constituents of spin-based electronics.

Magnetic Resonance Force Microscopy (MRFM) is a novel scanned probe technique based on mechanical

detection of magnetic resonance. At the heart of the technique is the compliant force sensing micromechanical element, typically a single crystalline cantilever, outfitted with a micromagnetic probe tip. This micromagnet generates a nonuniform magnetic field $\mathbf{H}_{\rm tip}$ the gradient of which $\nabla\mathbf{H}_{\rm tip}$ couples the cantilever to the magnetic moment $\mathbf{m}$ of the sample with the resulting force of probe-sample interaction given by

$$\mathbf{F} = (\mathbf{m}\cdot\nabla)\mathbf{H}_{\rm tip}.$$

This force displaces the compliant cantilever generating the measured signal. The MRFM mechanism of probe-sample coupling is much more effective than the inductive coupling mechanism between the magnetic moments under investigation and the detector coil used in conventional magnetic resonance experiment. MRFM sensitivity is further improved by application of standard *rf*/microwave magnetic resonance techniques to manipulate the sample magnetic moment $\mathbf{m}$ at the natural resonant frequency ω_c of the force sensing cantilever. As a result the response of the cantilever to an oscillating force of probe sample interaction F is amplified by the dynamic magnification (quality) factor Q of the cantilever which can be as high as 10^5. The excellent sensitivity of the MRFM has enabled detection of single electronic spin magnetic resonance [1, 2].

The generality of MRFM is a key strength: in principle, it is applicable to any signal detectable in a conventional magnetic resonance experiment (in contrast to many single spin detection techniques). MRFM detection has been demonstrated for Electron Spin Resonance (ESR), Nuclear Magnetic Resonance (NMR) and Ferromagnetic Resonance (FMR). The ultimate limit on MRFM sensitivity is imposed by the spontaneous thermally induced cantilever oscillations stemming from the contact of the cantilever with the surrounding thermal bath at temperature T, so the best MRFM sensitivity is achieved at low-temperatures; all the experiments presented here have been conducted at $T = 4$ K.

Scanned Probe FMR Imaging

We report on the discovery and understanding of a mechanism for local Ferromagnetic Resonance (FMR) imaging based on Magnetic Resonance Force Microscopy (MRFM). By combining experimental MRFM data (see Fig. 1), numerical micromagnetic modeling of locally excited FMR (see Fig. 2) and analytical calculations we have illuminated the mechanism for spatially resolved scanned probe FMR imaging. This capability is unique, in particular it is available in conventional FMR, and its development heralds a breakthrough spatially resolved techniques for characterization of magnetic systems.

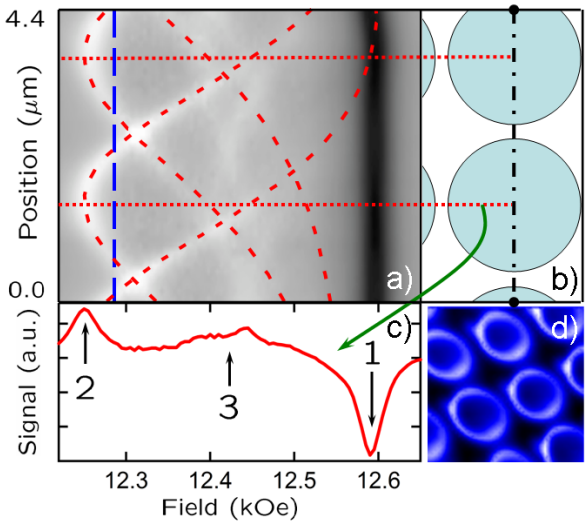

Figure 1: a) Field-position scan: FMR spectra recorded by sweeping the external magnetic field $H_{\rm ext}$ and spatially scanning the probe along the one-dimensional trajectory indicated by the dash-dotted line across the diagram of the dots in panel b). The red dashed curves in a) show the analytically calculated dependence of the TFR resonance field on probe position; these agree excellently with the experimental data. c) Spectrum extracted from image a) with the tip located over the center of the lower dot [see panel b)]. Numerical labels denote 1 - the ZFR mode, 2 and 3 - the TFR modes. d) Experimental fixed-field ($H_{\rm ext} = 12.28$ kOe) 2D image ($4.8\,\mu$m $\times$ $4.8\,\mu$m) of the spatial variation of the FMRFM signal.

The key to spatially localizing FMR excitation is the intense and spatially localized magnetic field of the MRFM probe magnet. This strong local magnetic field creates FMR conditions in this selected region which are significantly different than in the rest of the sample. This enables local excitation of FMR controlled which can be scanned throughout the sample. An example of such a spatially resolved excitation is shown in Fig. 2b and d which shows the spatial profile of the localized FMR mode excited in the spatial region directly beneath the MRFM probe magnet. In this particular case, the probe magnet is responsible for magnetic field oriented opposite to that of the externally applied field causing a region of the low total magnetic field beneath the probe. As a result the localized FMR mode is confined to that region.

This new understanding of the mechanism for spatially resolved FMR was experimentally verified in MRFM experiments on arrays of thin permalloy dots. These experiments have demonstrated two types of the excited FMR modes: the Zero Tip Field Resonance (ZFR) modes of the permalloy dots far from the probe magnet and therefore unaffected by the probe magnetic field and the Tip Field Resonance (TFR) modes which

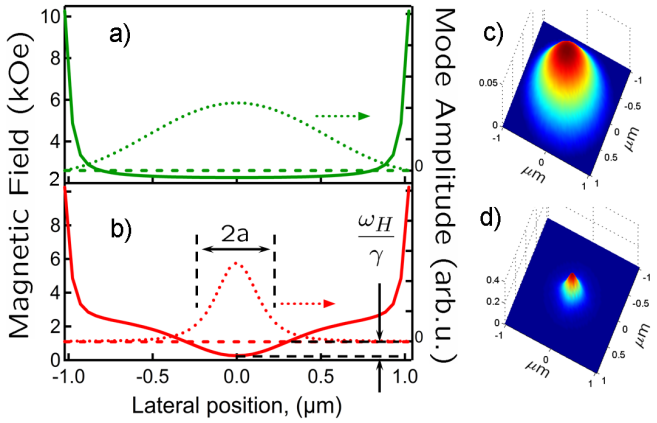

Figure 2: Numerically calculated spatial profile of $m_{\rm tr}$ for the first order FMR mode excited in a 2 μm diameter, 50 nm thick Py disk in a) a uniform external field and b) in the field of a 1 μm diameter spherical magnet located 250 nm above the center of the disk (probe magnetic moment *antiparallel* to $\mathbf{H}_{\rm ext}$. The mode is confined to the region of reduced field beneath the probe. c) and d) are the corresponding 2D maps of $m_{\rm tr}$.

are strongly affected by the nearby probe magnet. Examples of these are shown in Fig. 1c. Our understanding of spatially resolved FMR imaging in scanned probe experiments has also been confirmed by the excellent agreement between the experimentally recorded evolution of the TFR modes as a function of the spatial probe position (as shown in Fig. 1a) and the results of analytical modeling (dashed red lines in Fig. 1a). These results are described in detail in DOE Sponsored Reference 1.

High sensitivity low temperature MFM

Magnetic Force Microscopy (MFM) is a powerful and widely-used technique for characterizing magnetic systems. It is based on measuring the dipolar interaction between a micromagnetic probe mounted on a micromechanical cantilever [similar to that used in Atomic Force Microscopy (AFM)] and magnetic moments in the sample. While room temperature AFM/MFM microscopes are available commercially, these have insufficient sensitivity to detect spins injected into nonmagnetic samples. We have constructed a low temperature AFM/MFM optimized for this purpose; this is shown in Fig. 3. It consists of liquid He (T = 4.2 K) cryogenic dewar (Fig. 3a) containing a 3 T superconducting solenoid. The cryogenic insert (Fig. 3b) contains the custom designed AFM/MFM (Fig. 3c) based on a cryogenic three-axis piezo positioning mechanism (Attocube) for coarse approach and a PZT piezo tube for fine positioning and scanning. The instrument is equipped with a double laser fiber-optic interferometer the first of which is used for cantilever displacement detection and the second for measuring probe-sample separation.

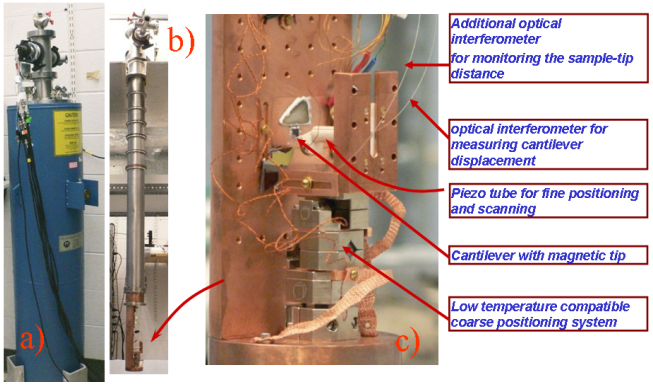

Figure 3: The low temperature AFM/MFM consists of liquid He (T = 4.2 K) cryogenic dewar a) containing a 3 T superconducting solenoid. The cryogenic insert b) carries a custom designed AFM/MFM c) based on a cryogenic three-axis piezo positioning mechanism (Attocube) for coarse approach and a PZT piezo tube for fine positioning and scanning. The instrument is equipped with a double laser fiber-optic interferometer the first of which is used for cantilever displacement detection and the second for measuring probe-sample separation.

In MFM the dipolar probe-sample interaction is detected by measuring the resulting shift of the resonant frequency of the cantilever ω_0. The cantilever is continuously driven at its ω_0 by a positive feedback, self-excitation circuit which we have implemented using a digital AN221E04 Field Programmable Analog Array (FPAA) manufactured by Anadigm (www.anadigm.com). The cantilever oscillation frequency $\omega_{\rm osc}$ is continuously matched to the loaded resonant frequency of the cantilever ω_0 regardless of changes of the probe-sample interaction. The cantilever oscillation frequency is demodulated and digitized using an algorithm we developed earlier with the support of the present DOE award; this approach is described in our earlier publication [3].

The frequency noise performance of our high sensitivity MFM based on frequency detection is shown in Fig. 4. The intensity of the cantilever frequency noise (in units of Hz/$\sqrt{\rm Hz}$) as a function of the demodulation bandwidth was measured at T = 4.55 K; the amplitude of cantilever oscillations was z_0 = 171 nm and the cantilever spring constant k = 0.25 N/m. The detection sensitivity in the demodulation bandwidth as wide as $\sim$ 10 Hz is dominated by the cantilever thermal noise and not by the sensitivity of the cantilever displacement

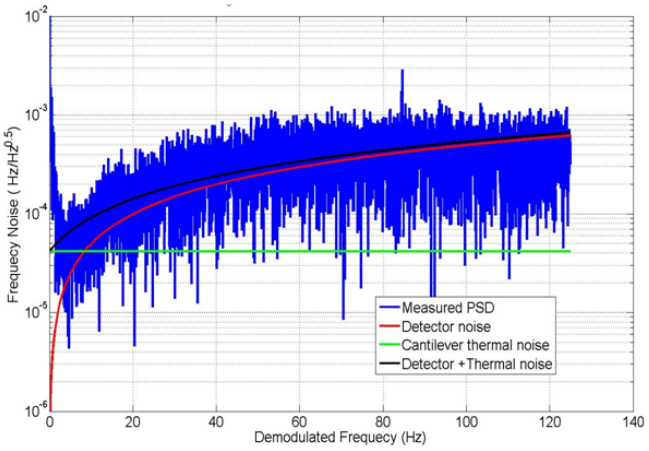

Figure 4: The frequency noise performance of the high sensitivity AFM/MFM setup. The intensity of the measured cantilever frequency noise (in units of $\mathrm{Hz}/\sqrt{\mathrm{Hz}}$) as a function of the demodulation bandwidth. The data was obtained at T = 4.55 K with a cantilever oscillation amplitude $z_0 = 171$ nm and cantilever spring constant $k = 0.25$ N/m. Detection sensitivity at low demodulation frequencies is dominated by cantilever thermal noise and not by cantilever displacement detection.

detector. The thermal noise floor was estimated to be 7.0×10^{-17} N/m. Thus we have demonstrated thermal noise limited cantilever frequency detection sensitivity—the ultimate performance test for any high-sensitivity detection scheme.

Future Plans

Future efforts will concentrate on the following avenues for application and development of FMRFM, sensitive MFM, and MRFM detected NMR:

- Application FMRFM imaging to important nanomagnetic samples such as GaMnAs
- Demonstration of dark-field FMR imaging using probe localization of FMR
- Demonstration of FMR imaging of buried ferromagnetic elements for study of ferromagnetic-normal metal interfaces
- Improved micromagnetic modeling of FMR in nonuniform magnetic fields and resulting FMRFM signals.
- Imaging of paramagnetic spin polarization in semiconductors
- Demonstration and application of MRFM/NMR for detection and study of Cu NMR at buried Co/Cu interfaces

DOE Sponsored Publications

[1] "Local Ferromagnetic Resonance Imaging with Magnetic Resonance Force Microscopy," Yu. Obukhov, D.V. Pelekhov, J. Kim, P. Banerjee, I. Martin, E. Nazaretski, R. Movshovich, S. An, T.J. Gramila, S. Batra, and P. C. Hammel, *Physical Review Letters* **100** 197601 (2008).

[2] "Probing arrays of circular magnetic microdots by ferromagnetic resonance," G.N. Kakazei, T. Mewes, P.E. Wigen, P.C. Hammel, A.N. Slavin, Yu. G. Pogorelov, M.D. Costa, V.O. Golub, K.Yu. Guslienko, and V. Novosad, *Journal Of Nanoscience And Nanotechnology* **8**, 2811–2826 (2008)

[3] "Spatial characterization of the magnetic field profile of a probe tip used in magnetic resonance force microscopy," E. Nazaretski, E.A. Akhadov, I. Martin, D.V. Pelekhov, P.C. Hammel and R. Movshovich, *Applied Physics Letters* **92**, 214104 (2008)

[4] "Detection of higher order modulation harmonics in magnetic resonance force microscopy," T. Mewes, C. K. A. Mewes, E. Nazaretski, J. Kim, K. C. Fong, Y. Obukhov, D. V. Pelekhov, P. E. Wigen, and P.C. Hammel, *J. Appl. Phys.* **102,** 033911 (2007).

[5] "Magnetic resonance force microscopy studies in a thin permalloy film," E. Nazaretski, J.D. Thompson, D.V. Pelekhov, T. Mewes, P.E. Wigen, J. Kim, M. Zalalutdinov, J.W. Baldwin, B. Houston, P.C. Hammel and R. Movshovich, *J. Magn. Magn. Mat.* **310,** E941 (2007).

[6] "Ferromagnetic resonance force microscopy on a thin permalloy film," E. Nazaretski, I. Martin, R. Movshovich, D.V. Pelekhov, P.C. Hammel, M. Zalalutdinov, J.W. Baldwin and B. Houston, *Appl. Phys. Lett.* **90,** 234105 (2007).

[7] "Temperature-dependent Magnetic Resonance Force Microscopy studies of a thin Permalloy film," E. Nazaretski, J.D. Thompson, R. Movshovich, M. Zalalutdinov, J.W. Baldwin, B. Houston, D.V. Pelekhov, P. Wigen, P.C. Hammel, and T. Mewes, *J. Appl. Phys.* **101,** 074905 (2007).

References

[1] D. Rugar, R. Budakian, H. J. Mamin, and B. W. Chui, Nature **430**, 329 (2004).

[2] P. C. Hammel, Nature **430**, 300 (2004).

[3] Y. Obukhov, K. C. Fong, D. Daughton, and P. C. Hammel, J. Appl. Phys. **101**, 034315 (2007).

Nanoscale Imaging of Electrostatic and Magnetic Fields

Martha R. McCartney and David J. Smith
molly.mccartney@asu.edu, david.smith@asu.edu
Department of Physics, Arizona State University, Tempe, AZ 85287

Program Scope

This research program involves the quantitative phase imaging of nanoscale electrostatic and magnetic fields using the technique of off-axis electron holography. One major focus of this research will emphasize the electrostatic potential profiles developed across undoped and doped heterojunctions and actual semiconductor devices, as well as piezoelectric fields in Group-III nitride semiconductors. We will compare the internal fields of nitride quantum wells for polar and non-polar growth directions to determine the effect on light-emitting properties. The influence of strain, dopants and *in situ* biasing on band offsets in for a limited group of Group-IV heterostructures and devices will also be assessed. A specially modified specimen holder purchased previously will be used to perform *in situ* biasing experiments during holographic imaging. Our second focus will relate to exchange-coupled nanostructures and antiferromagnetic oxides. Here, we plan to probe the nature of the coupling between the antiferromagnetic material and different ferromagnets. Changes in magnetic properties such as coercivity and reversal mechanisms attributable to reduced particle dimensions, in addition to differences arising from chemical reactions at the oxide/metal interfaces will be investigated.

Recent Progress

The primary objectives of this project have been to observe and to quantify nanoscale electrostatic and magnetic fields using off-axis electron holography. There have been two major areas of activity:

i) measurement of the 2D electrostatic potential distributions across complex semiconductor heterojunctions and devices; and

ii) investigation of the remanent states and magnetization reversal mechanisms in ferromagnetic nanostructures.

i) Electrostatic fields

Both wedge polishing and focused-ion-beam milling were used to prepare 2D Si p-n junctions and Si p-channel MOSFET samples for examination by electron holography. The effects of specimen preparation on the reproducibility of measurement of junction profiles were determined. The effect of the sample thickness and surface treatments on the junction measurements were also investigated.

Electron holography studies of several AlAs/GaAs structures, using samples prepared primarily by wedge polishing, enabled the mean inner potential (MIP) values and mean-free-path for inelastic scattering for both GaAs and AlAs to be determined. This information is essential for future studies of more complex III-V heterostructured devices.

Initial tests of a new specimen holder for *in situ* biasing were directed towards identifying methods suitable for providing contacts and enabling *in situ* biasing of samples with different geometries. These included the 2D Si p-n junction, and a 90-nm CMOS transistor device, as well as

field-emitting carbon nanotubes. In all cases, considerable progress was made in overcoming somewhat complex problems associated with specimen preparation since not only must the sample geometry be suitable for biasing in that it should be neither shorted nor open-circuit but it must also conform to all the demanding requirements for holographic imaging such as local thickness and proximity to the vacuum reference region.

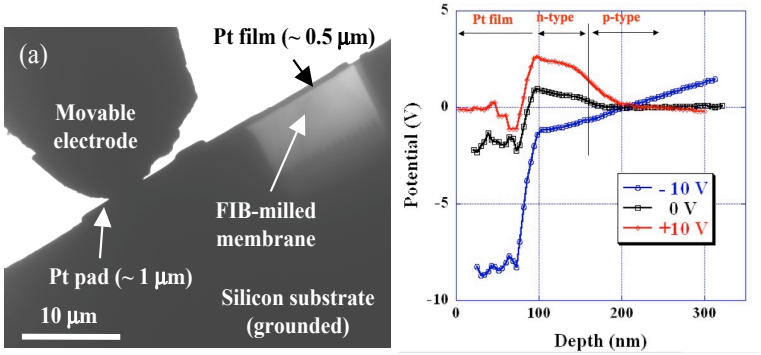

Figure 1 (left) TEM image showing FIB-prepared p-n junction sample ready for biasing experiment. Movable electrode is in contact with Pt layer extending over thin membrane region where holograms were acquired. (right) Line profiles across p-n junction at various applied voltages.

Figure 1 shows an example from a successful biasing experiment that was carried out on a 2D Si p-n junction. The line profiles shown in Figure 1(b) confirmed that the sample was successfully biased in both the forward and reverse directions. The large applied bias relative to the corresponding voltage response of the specimen reflected the fact that the sample geometry provided additional parallel paths for conduction of current during biasing. However, the response of the sample in the area used for holography examination behaved as expected, including the occurrence of increased depletion widths and "flat-banding" at negative bias.

ii) Magnetic fields

The phase imaging of nanoscale magnetic fields in this project has been directed primarily towards documenting the micromagnetic response of nanomagnets having a wide variety of different shapes. One major objective of these studies was to identify specific shapes that would achieve flux-closure states at remanence and also display rapid switching of chirality (i.e., clockwise (CW) or counterclockwise (CCW) flux directions) without the intermediate formation of a high-energy vortex core. Another goal was to establish any major differences in the remanent states and magnetization reversal behavior that were attributable to the introduction of shape asymmetry. The fabrication of the nanopatterned elements used for these studies was accomplished using electron-beam lithography and standard lift-off processes, while the substrates consisted of 50-nm-thick, self-supporting and electron-transparent, silicon-nitride membrane windows. The underlying support film caused loss of interference-fringe contrast but off-axis electron holography was still possible using the Lorentz lens configuration.

The initial experiments involved slotted Co nanorings having different combinations of ring sizes, ring widths, and slot angles. Single-vortex, double-vortex, and flux-closure states without any vortex were the most common remanent states observed. Magnetization reversal mechanisms were also determined by recording holograms at different stages during hysteresis cycles, and a robust and reliable software program was written to extract quantitative magnetization information from the corresponding phase images. **Figure 2** shows a typical set of reconstructed phase images as recorded in this case during cycling of a 30-nm-thick Co nanoring with outer/inner diameters of 300nm/50nm, and a slot angle of 120°. These studies of slotted Co nanorings confirmed that the shape anisotropy introduced by the slot could play a major role in determining the reproducibility of the remanent states.

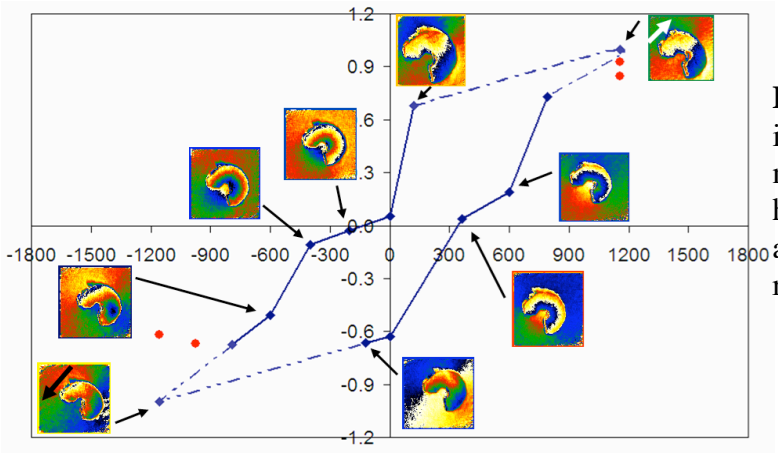

Figure 2 Reconstructed phase images of 30-nm-thick Co slotted nanoring element recorded during hysteresis cycle. In-plane field applied along diagonal from top right to bottom left.

Another set of experiments involving asymmetrical elements focused specifically on elements that were basically elliptically shaped. The remanent states of ellipses were compared with those for similar notched ellipses, while elliptical rings were compared with similar slotted elliptical rings. In the case of notched ellipses with the in-plane field directed along the long ellipse axis, double-vortex (DV) states were strongly predominant, which was contrary to what was observed for the perfect ellipses. It was also interesting that the DV states were often seemingly random combinations of CW/CW, CW/CCW, and CCW/CCW chiralities, with the relative fractions of each state relatively independent of the element dimensions or the direction of the applied field. Micromagnetic simulations are currently in progress to provide a better physical understanding of the various energy terms that must eventually determine the observed behavior of these elliptical elements, with the longer-term goal being to predictively control the final remanent state that is obtained.

Future Plans

Our holography studies of nanoscale electrostatic fields will primarily address the closely related topics of heterostructures and devices in Group-IV semiconductors and Group-III nitrides. Band bending across interfaces between dissimilar materials and the influence of strain, dopants and in situ biasing on electrostatic potential profiles in transistor device structures will be specifically targeted for close attention. We also plan to compare the fields associated with undoped and doped AlGaN, InGaN, and AlInGaN heterostructures grown on polar and non-polar substrates under identical conditions.

Our proposed studies of nanoscale magnetic fields will focus mainly on exchange-coupled nanomagnets and dilute magnetic semiconductors and oxides. Lorentz microscopy and micromagnetic simulations, as well as conventional microscopy and spectroscopy, will be used to provide complementary magnetic, structural and compositional information. Observations will be primarily made under field-free conditions using the Lorentz lens of our CM200 FEG-TEM, as shown already by the example in Figure 2, but small in-plane fields provided by tilting the sample with the objective lens slightly excited can be used to follow magnetization reversal processes.

References to publications of DOE sponsored research for period 2006-2008:

M.-G. Han, J. Li, Q. Xie, P. Fejes, J. Conner, B. Taylor, and M.R. McCartney, "Sample preparation for precise and quantitative electron holographic analysis of semiconductor devices", Micros. Microanal. 12 (2006) 295-301.

H. Wang, H. Hu, M.R. McCartney and D.J. Smith "Remanent states of nanoscale Co ferromagnets having different shapes", J. Magn. Magn. Mater. 303 (2006) 237-242.

H. Hu, H. Wang, M.R. McCartney, and D.J. Smith "Switching mechanisms and remanent states for nanoscale slotted Co circular elements studied by electron holography", Phys. Rev. B 73 (2006) 153401.

N. Agarwal, H. Wang, D.J. Smith, and M.R. McCartney, "Remanent states and magnetization reversal for nanopatterned Co elements", IEEE Trans. Magn. 42 (2006) 2414-2416.

M.-G. Han, P. Fejes, Q. Xie, S. Bagchi, B. Taylor, J. Conner, and M.R. McCartney, "Quantitative analysis of 2-D electrostatic potential distributions in 90-nm Si pMOSFETs using off-axis electron holography", IEEE Trans. Electron Devices 54 (2007) 3336-3341.

S. Chung, D.J. Smith, and M.R. McCartney, "Determination of the inelastic mean-free-path and mean inner potential for AlAs and GaAs using off-axis electron holography and convergent beam electron diffraction", Microsc. Microanal. 13 (2007) 329-335.

N. Agarwal, D.J. Smith, and M.R. McCartney, "Effect of shape on magnetic response for slotted Co nanorings using off-axis electron holography", J. Appl. Phys. 102 (2007) 023911: 1-7.

(invited review) M.R. McCartney and D.J. Smith, "Electron holography: phase imaging with nanometer resolution", Annu. Rev. Mater. Res. 37 (2007) 729-767.

M. R. McCartney, N. Agarwal, M-G. Han, H. Hu, H. Wang and D.J. Smith, "Nanoscale Imaging of Electrostatic and Magnetic Fields by Off-axis Electron Holography", Proceedings IMC16, Sapporo, Japan, (2007) pg 720.

M. G. Han, D. J. Smith and M. R. McCartney "In situ electron holographic analysis of biased Si n(+)-p junctions", Applied Physics Letters, **92**, 14, (2008) 143502.

N. Agarwal, K.Winn, D.J. Smith, and M.R. McCartney, "Effect of asymmetry on the remanent states of slotted Co elliptical nanostructures using Lorentz microscopy and off-axis electron holography", J. Magn. Magn. Mater. (2008) in press.

S. Chung, S.R. Johnson, Y.-H. Zhang, D.J. Smith, and M.R. McCartney, "Off-axis electron holographic mapping across AlGaAs/AlAs/GaAs heterostructures", J. Appl. Phys. (2008) in press.

K. He, D.J. Smith, M.R. McCartney, "Remanent states and magnetization reversal of nanopatterned spin valve elements using off-axis electron holography, J. Appl. Phys. (2008) in press.

Electron tomography and domain imaging of oxide heterostructures (FWPs 58931 and 58307)

A K Petford-Long, B Kabius, S Hong,
Materials Science Division, Argonne National Laboratory, 9700 S Cass Avenue, Argonne, IL 60439
Petford.long@anl.gov, kabius@anl.gov, hong@anl.gov

Program Scope

The goal of this program is to develop an understanding of the role that interface morphology and composition play in determining the functional properties and domain behavior of nanostructured oxide materials, with particular emphasis on magnetic, ferroelectric and multiferroic materials. We are addressing this issue via the use of advanced electron microscopy and scanning probe microscopy techniques. We are developing atomic-scale three-dimensional (3D) chemical imaging capabilities via the use of electron tomography combined with electron energy loss spectroscopy (EELS) and transmission electron microscopy (TEM). The aim is to reconstruct the chemical distribution in a single nanostructure or in arrays of nanostructures at high resolution. Our approach is based on analytical transmission electron microscopy techniques such as EELS and energy filtering TEM (EFTEM), which are being coupled with advances in data reconstruction to improve resolution, sensitivity and validity of data interpretation beyond what is currently available. We are using a range of techniques for imaging domain behavior in ferroic materials, including Lorentz TEM, electron holography, magnetic force microscopy and piezo-force microscopy.

Recent Progress

3D Elemental distribution of titanium oxide and carbon nanoparticles: Tomographic tilt series of TiO_2 particles were recorded in EFTEM mode, using the Ti M-edge at 36 eV. The 3D distribution of Ti in the nanoparticles was calculated using the simultaneous iterative reconstruction technique, with a spatial resolution of 3 nm, limited by the delocalization of the Ti-M EELS transition scattering process (Fig. 1). The resolution of the elemental maps is improved by using higher energy loss electrons, although this results in a lower signal-to-noise ratio: 3D reconstructions of carbon nanoparticles from tomographic series of EFTEM maps using the carbon K transition (284 eV) showed a resolution of ~0.9 nm.

Mapping chemical bonding in 2D: We used analysis of the near-edge fine structure of EELS transitions (ELNES) to investigate the interface chemistry between silicon and ultrananocrystalline diamond (UNCD). ELNES analysis of the carbon K edge allowed us to map the distribution of graphitic sp^2 and diamond-like sp^3 bonding in the UNCD adjacent to the UNCD/Si interface, and ELNES analysis of the Si L edge allowed elemental Si, SiC and SiO_2 to be distinguished. Regions showing carbon sp^3 bonding and Si-C bonding close to the interface were identified as nucleation sites for formation of UNCD.

Towards atomic resolution composition mapping in 2D: Achieving atomic scale resolution in elemental maps in 3D is important for understanding the chemical and physical properties at interfaces of complex oxides. Recently, the development of C_c correction enabled a step forward to atomic resolution energy EFTEM imaging which can be used to derive large area elemental maps. Fig. 2 shows line traces for La across an $LaCoO_3/(LaAlO_3)_{0.3}(Sr_2AlTaO_3)_{0.7}$ (LSAT) interface. The width across which the La-M edge intensity changes from its $LaCoO_3$ to its value in the LSAT value is >1 nm for the elemental map recorded with an uncorrected microscope while the C_c-corrected measurement gives an interface width of ~0.4 nm which is equivalent to the La atom separation in $LaCoO_3$. The resolution is limited by noise and we expect further resolution improvement by using higher beam currents and by minimizing sample drift.

3D imaging of magnetic tunnel junctions The 3D structure of a CoFe/MgO/CoFe magnetic tunnel junction (MTJ) was shown successfully using scanning TEM (STEM) tomography. Although the STEM images do not provide composition mapping, the STEM image contrast allows qualitative composition information to be obtained since the contrast is directly related to atomic number. The transport properties of this MTJ can be explained from the 3D shape of the barrier layer.

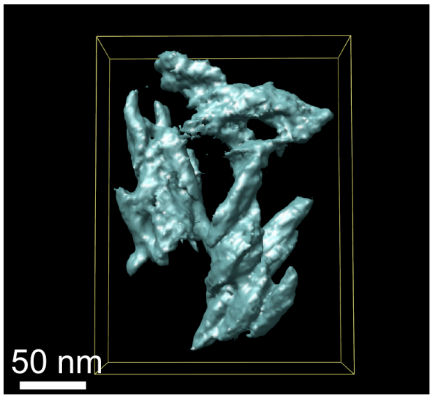

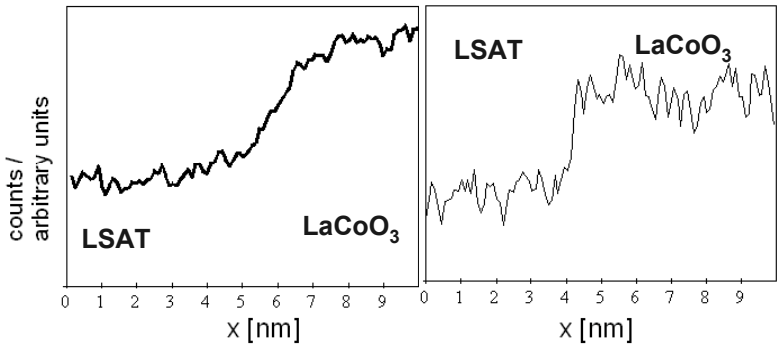

Fig. 1 3D reconstruction of TiO_2 nanoparticles obtained using EFTEM maps of the Ti distribution.

Fig. 2 Line scans of the La concentration across a ($LaCoO_3$)/LSAT interface for (a) uncorrected TEM and (b) C_c-corrected TEM. In (b) the La concentration changes within one unit cell (0.38 nm) at the interface.

Domain imaging in bismuth ferrite nanocapacitors: We have fabricated 500 nm diameter BFO capacitors using rf magnetron sputter deposition and focused ion beam lithography to investigate the dependence of domain configuration and behavior on nanocapacitor shape (square vs. circular). PFM images (Fig. 3) suggest that square capacitors have a mono-domain configuration whereas round ones exhibit a seven-domain configuration. We attribute the more symmetric and lower coercive field of round shape to the multi-domain state, which facilitates domain nucleation and growth. These findings have critical implications for the development of nanocapacitors for either energy harvesting ferroelectric solar cells or high-density non-volatile ferroelectric memories.

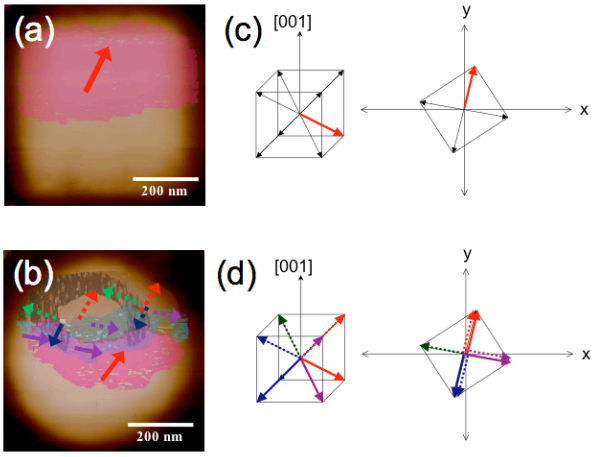

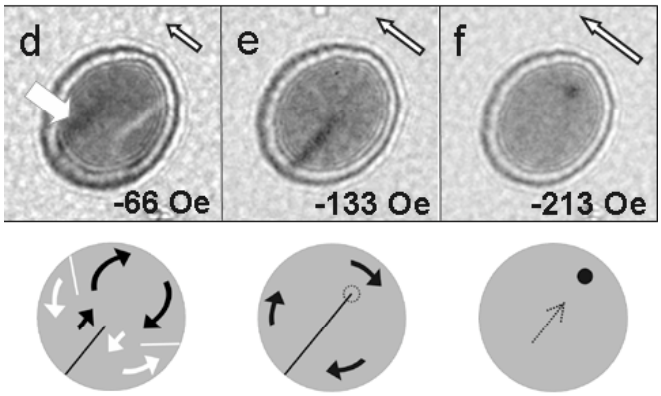

Fig. 3. Topographic images overlaid by domain images of (a) square and (b) circular BFO nanocapacitors extracted from PFM images. The crystallographic orientations of the domains are shown schematically in (c) square and (d) circular.

Fig. 4 LTEM images of magnetization reversal behavior in a $CoFe_{12nm}$ /$IrMn_{5nm}$ disk (diameter 1 µm). As field is reduced from saturation, domain walls nucleate which then collapse to form a vortex. Vortex motion is non-uniform as a result of varying energy surface across the disk.

Magnetization reversal behavior in exchange-biased magnetic disks We have combined in-situ LTEM studies of exchange-biased magnetic disks with micromagnetic simulations (collaboration with O

Heinonen, Seagate Technology) to determine the value of exchange bias in CoFe/IrMn and NiFe/IrMn disks set with exchange bias in a circular configuration, and also the way in which the exchange-bias influences the actual magnetization reversal mechanism, resulting in observation of a novel reversal mechanism, and of pinning of the vortex core by microstructural features and exchange bias variations (see Fig. 4). In collaboration with M De Graef and C D Phatak, Carnegie Mellon University, we have developed the first technique capable of determining the full magnetic structure (chirality AND polarity) of a magnetic vortex from a single measurement, namely a single LTEM image.

Future Directions

EFTEM tomography – extension to 3D The experimental procedures and algorithms established during this study will be used to extend elemental and chemical mapping from two to three dimensions.

3D analysis of oxide heterostructures We intend to extend our studies of oxide heterostructures to multiferroic tunnel junctions, which combine ferroelectric and ferromagnetic properties in a single heterostructure. We expect to observe novel phenomena as a result of the interplay of the magnetic and ferroelectric order parameters. For example control of the ferroelectric polarization as a result of an external magnetic field, via the magnetoelectric effect, or the generation of space charge at the barrier interfaces through application of an electric field, which would then strongly influence the spin-dependent tunneling. 2D elemental mapping has already been performed on ZrO_2/In_2O_3 heterostructures which will be extended this to 3D mapping on these materials and on structures such as $SrVO_3/SrTiO_3$. The interfaces are rough and, therefore the 2D study is limited in characterizing concentration gradients at the interfaces. The local chemistry will have a strong effect on proximity transport effects at the interface, and 3D EFTEM tomography is therefore essential in understanding the physical properties.

Further technique development In order to overcome the problems associated with increasing projected thickness for increasing tilt angles, which is encountered for standard TEM samples, we are developing cylindrical samples with the cylinder axis parallel to the tilt axis, which will be prepared using FIB. Combined with this new approach to sample fabrication, we intend to use a stage with full 360° rotation to avoid the "missing wedge" problem for 3D reconstruction, and enable a more complete data set. Experimental parameters have to be improved to minimize radiation damage, sample drift and experiment time for the tilt-series. This includes further improvement of sample preparation and further stage optimization in cooperation with Hummingbird Inc, for example to improve eucentricity. We have been using new software especially developed by FEI for our instrumentation. We will continue our efforts in adapting the freeware software IMOD and SerialEM for our specific hardware and in extending their capabilities to EFTEM image series combined with tilt series. In October 2008 the TEAM test column for the first Cc corrector will be installed at Argonne. This instrument has already proven that it offers a factor of four improvement in resolution in elemental maps, and further progress appears likely with improved signal-to-noise ratio. We are planning to use this instrument for 2D and 3D elemental mapping.

Vector tomography In collaboration with Prof Marc De Graef (Carnegie Mellon University) we are exploring methods for obtaining vector tomography maps that will enable the 3D magnetization structure of magnetic nanostructures to be determined and imaged. We plan to continue these novel experiments which can lead to a fuller understanding of the way in which the magnetic behavior of nanostructures is influenced by parameters such as thickness, shape and size.

Domain structure and dynamics in ferroelectric and ferromagnetic materials The grand challenge in ferroic nanostructures is to develop an understanding of their dynamic response. This includes the physics underlying reversal domain nucleation and domain wall velocity in ferroelectrics, and ferromagnetic magnetization reversal mechanisms in patterned oxide heterostructures. We are addressing this challenge through a combination of *in-situ* transmission electron microscopy (TEM) techniques and scanning probe microscopy techniques such as magnetic force microscopy (MFM) and piezo-force microscopy (PFM). For the PFM studies we intend to use the tip as the moving top electrode to characterize the size and

shape dependence of the switching and piezoelectric properties of patterned nanostructures. Imaging domain wall motion as a function of applied field, in a configuration in which we can also image the microstructure of the film, will allow us to measure domain wall velocities and to visualize effects such as pinning at defects. Our studies of the nanomagnetic behavior of arrays of patterned thin film oxide heterostructures is continuing and is being extended to artificial multiferroic heterostructures, including investigation of the effect of the ferroelectric field on magnetic phenomena and vice versa.

Aberration-corrected LTEM In an effort to increase the resolution that we can obtain using Lorentz TEM, we are installing a JEOL 2100F TEM equipped with a dedicated low-field objective lens. We intend to integrate a C_s-corrector custom built for this Lorentz lens which, together with phase imaging, should provide better resolution and quantification for magnetic field measurements. This is a collaborative project with JEOL and CEOS. The increased resolution will enable us to correlate the magnetization reversal behavior directly with the microstructure of magnetic nanostructures.

The submitted manuscript has been created by UChicago Argonne, LLC, Operator of Argonne National Laboratory ("Argonne"). Argonne, a U.S. Department of Energy Office of Science Laboratory, is operated under Contract No. DE-AC02-06CH11357

References to publications of DOE-sponsored research (2005–2008)

"Lorentz microscopy of elliptical magnetic rings", T J Bromwich, A K Petford-Long, FJ Castaño and CA Ross, *J. Appl. Phys.* **99**, 08H304 (2006).

"Remanent magnetic states and interactions in nano-pillars", T J Bromwich, T Kasama, R K K Chong, R E Dunin-Borkowski, A K Petford-Long, O Heinonen and C A Ross, *Nanotechnol.* **17**, 4367 (2006).

"Micromagnetic modelling of spin-wave dynamics in exchange-biased Permalloy disk", O Heinonen, D K Schreiber and A K Petford-Long, *Phys. Rev. B* **76**, 144407 (2007).

"In-situ structure and transport correlations in magnetic tunnel junctions", A.N. Chiaramonti, D K Schreiber, B. Kabius, W.F. Egelhoff Jr. and A.K. Petford-Long, *Microsc. And Microanal.* **13** (Suppl. 2), CD626 (2007)**.**

"Electric and magnetic phenomena studied by in-situ transmission electron microscopy", J Cumings, E Olsson, A K Petford-Long and Y Zhu, *Mat. Res. Bull*. **33(2),** 101–106 (2008).

"Transmission electron microscopy of multilayer thin films", A K Petford-Long and A N Chiaramonti, *Ann. Rev. Mater. Res*. **38**, 559–584 (2008).

"Magnetization reversal processes in epitaxial Co/Fe bilayers grown on MgO(001)", A Kohn, C Wang, A K Petford-Long, S G Wang and R C C Ward, *J. Appl. Phys*. **103**, 063918 (2008).

"In-situ TEM studies of local transport and structure in nanoscale multilayer films", A N Chiaramonti, L J Thompson, W F Egelhoff, B C Kabius and A K Petford-Long, *Ultramicrosc.* Doi:10.1016/ j.ultramic.2008.04.008 (2008).

"Three-dimensional atom probe investigation of boron distribution in CoFeB/MgO/CoFeB magnetic tunnel junctions", S Pinitsoontorn, A Cerezo, A K Petford-Long, D Mauri, L Folks and M J Carey, *Appl. Phys. Lett.* **93**, 071901 (2008).

"Characterization of Sensitivity and Resolution of Silicon Resistive Probe," J. Kim, J. Lee, I. Song, J. D. Lee, B.-G. Park, S. Hong, H. Ko, D.-K. Min, H. Park, C. Park, J. Jung, and H. Shin, *Jpn. J. Appl. Phys*. **47**, 1717-1722 (2008)

"Screen charge transfer by grounded tip on ferroelectric surfaces," Y. Kim, J. Kim, S. Bühlmann, S. Hong, Y. K. Kim, S.-H. Kim and K. No, *Phys. Stat. Sol. (RRL)* **2**(2), 74–76 (2008).

"Synthesis and characterization of smooth ultrananocrystalline diamond films via low pressure bias-enhanced nucleation and growth", Y C Chen, X Y Zhong, A R Konicek, D S Grierson, N H Tai, I N Lin, B Kabius, J M Hiller, A Sumant, R W Carpick, O Auciello, *Appl. Phys. Lett.* **92**, 133113 (2008).

"Effects of pretreatments on the growth mechanisms of ultra-nanocrystalline diamond films: A chemical bonding mapping approach", X Y Zhong, Y C Chen, N H Tai, I N Lin, J M Hiller, O Auciello and B Kabius, *Microsc. and Microanal.* **14** (Suppl. 2), CD1406, 2008.

Abstract for the Electron and Scanning Probe Microscopies Contractors Meeting 2008, Sponsored by the US Department of Energy, Office of Basic Energy Sciences, held at the Arlie Center, Warrenton, VA, October 26-29, 2008.

Program Title

Electron Density Determination, Bonding and Properties of Tetragonal Ferromagnetic Intermetallics

Program Duration

36 months (August 15/2008 to August /2011)

Principal Investigators

J.M.K. Wiezorek (PI),
Associate Professor,
Department of Mechanical Engineering and Materials Science,
University of Pittsburgh, Swanson School of Engineering,
848 Benedum Hall,
3700 O'Hara Street,
Pittsburgh, PA 15261, USA,
wiezorek@pitt.edu

O. Mryasov (Co-PI),
Senior Research Staff Member,
Seagate Technology LLC.;
1251 Waterfront Place
Pittsburgh, PA 15222;
Oleg.Mryasov@seagate.com

Program Scope and Definition

We synergistically combine quantitative experimentation by transmission electron microscopy (TEM), X-ray diffraction (XRD) and magnetometry with materials theory using first-principles calculations to study relationships between the electronic structure and intrinsic properties of the tetragonal ferromagnetic intermetallics FePd and FePt. We compare details of the 3d-4d (FePd) and 3d-5d (FePt) electron interactions and elucidate their role for properties of the respective ferromagnetic $L1_0$-ordered intermetallics FePd and FePt. We use the isostructural $L1_0$-phases of FePd and FePt as model systems for basic research of details of interactions of 3d (Fe) electrons with 4d (Pd) and 5d (Pt) electrons.

Key experiments use high-quality binary $L1_0$-FePd and $L1_0$-FePt crystals. We measure complete sets of structure factors (F_{hkl}) of the tetragonal ordered phases by the combination of quantitative convergent-beam electron diffraction (QCBED) using energy-filtered (EF) TEM and precision XRD. We also determine the anisotropic Debye-Waller factors (DWFs) for Fe, Pd and Pt in the chemically ordered $L1_0$-phases. This

experimentation will uniquely facilitate extraction of the electron density distribution with sufficient accuracy to study the nature of interatomic bonding in these chemically ordered model d-electron systems. We also use the high quality crystals for magnetometry and XRD to measure the temperature dependence of intrinsic magnetic and lattice properties. These latter experiments complement the electron density related diffraction experiments and provide additional experimental data sets suitable for comparison with and evaluation of prediction from theoretical work.

The theoretical component of this effort uses different first-principles computational methods and models (electronic and statistical) to calculate electron density, electronic structure characteristics and the temperature dependence of intrinsic properties (e.g. K_1, c/a, elastic Cij etc.) for direct comparison with our quantitative experiments. We use density functional theory (DFT), local density approximation (LDA), various beyond-LDA (e.g. LDA+U) and local spin density approximation (LSDA) methods, incorporating intra- and interatomic exchange between the 4d/5d (Pd/Pt) and 3d (Fe) electrons, including exchange splitting. We initially focus on the equiatomic composition $L1_0$-phases, providing a sound foundation for extension to study of composition effects in off-stoichiometric binaries Fe_xM_{1-x}, ~$0.42 \leq x \leq 0.55$ and M=Pd or Pt.

This effort advances the state of the art in quantitative electron beam and X-ray experimentation, provides new experimental data uniquely suited for the critically needed evaluation of competing computational models and enables development of improved, robust materials theory tools for reliable and ideally predictive studies of $L1_0$-*FePt and* $L1_0$-*FePd.*

Recent Progress and Future Plans

This is a new program, start date August 2008. There are not technical or scientific results to report at this time.

To date one graduate student (Mr. Xiahan Sang) and one post-doctor (Dr. Andreas Kulovits) have begun initiation of the research. They conduct literature research related to the XRD and CBED aspects of the program. Single crystal Si for the experimental calibration of diffraction instrumentation (both XRD and TEM) has been acquired.

Future Plans (next 12-18 months) include

- Evaluation and calibration of TEM instrumentation for QCBED and of XRD for Debye Waller factor and higher-order structure factor measurments using high purity Si.
- Testing of computation for F_{hkl}-refinement from QCBED using data for high purity Si.
- Preparation of Fe_xM_{1-x}, M=Pd/Pt, $0.42 \leq x \leq 0.55$, crystals.
- QCBED EF-TEM and XRD experiments with existing equiatomic $Fe_{0.5}M_{0.5}$, M=Pd/Pt.
- Strain field assisted ordering to obtain additional mono-domain $L1_0$-phase crystals.
- Theoretical calculations of elastic constants (Cij), F_{hkl}, DWF's and temperature dependence of properties for equiatomic $L1_0$-phases.

Understanding the Electronic and Magnetic Structure of Advanced Materials

Y. Zhu, M.A. Schofield, V.V. Volkov, L. Wu and J. Tao
zhu@bnl.gov, schofield@bnl.gov, volkov@bnl.gov, ljwu@bnl.gov and jtao@bnl.gov
Dept. of Condensed Matter Physics and Materials Science
Brookhaven National Laboratory, Upton, NY 11973

Program Scope

The focus of this program is to research nanoscale phenomena that control the functionality of technologically important materials having significant relevance to the DOE's energy mission. It includes two major areas of research: 1) electronic structure, structural defects and interfaces in strongly correlated electron systems; and 2) magnetic structure and nanoscale magnetism. Emphasis is on understanding structure-property relationships and the underlying mechanisms for the complex physical behaviors of various functional materials including high-temperature superconductors and thermoelectric materials. Advanced quantitative electron microscopy techniques, such as coherent electron diffraction, atomic imaging, electron spectroscopy, and phase retrieval methods are extended to study these materials. Experiments are closely coupled with structural modeling and theory. Although electron scattering and microscopy are the primary tools, complementary methods such as synchrotron x-ray and neutron scattering are also used.

Recent Progress

In the area of strongly correlated electron systems, we studied manganites that exhibit colossal electrical- and magneto-resistance effects (CR) as well as electronic phase inhomogeneities in order to further understand how the competing degrees of freedom in lattice-, charge-, orbital-, and spin-ordering dictate the material's functionality[1,2]. As a model system in these efforts, we systematically studied $Pr_{1-x}Ca_xMnO_3$ (PCMO, $0.32 \leq x \leq 0.5$) where substituting Ca with Pr elicits strong crystal distortion, i.e., a large tilt in the MnO_6 octahedra, due to the different ionicity of Pr and Ca. Controversy in correlating structure and property of the material stems from the fact that the crystal exhibits twinning and microscopic phase separation. Consequently, the crystal symmetry and space group was not determined unambiguously with neutron and x-ray experiments[3]. However, combining electron microscopy with in-situ tunneling microscopy (see figure) we, for the first time, measured local I-V characteristics of various ordered and disordered phases/states in the system[4]. This allowed us to understand the cooperative action of electrons and lattice, and the formation of a ferroelectric state that is characterized by polar displacements of the material's cations and anions. By directly applying a local $\sim 10^{10}$V/m electric field while observing the superstructure-associated charge/orbital ordering (CO-OO) phase, we were able to rule out the model Checkerboard-type CO-OO structure as well as a dielectric breakdown of the CO states for the insulator-metal transition, i.e., a "melting of the charged crystal" into a "charged liquid" at a switching field of 10^7V/m. Additionally, focusing on the change in crystal symmetry, we derived a structure model consisting of a Zener polaron CO-OO phase, and directly observed CR effects due to an electrically induced solid-liquid transition of the polarons (the combined motion of electrons associated with their lattice distortions). This established the connection between CR effects and multiferroic properties in the material, i.e., the coexistence of ferroelectric- and antiferromagnetic-ordering. In another example in the area of strongly correlated electron systems, our studies of La-doped PCMO was motivated by significant technological interest in the tunable La/Pr ratio in engineering transition from ferromagnetic (FM) to charge ordered (CO) phases[5]. Temperature-dependent measurements of dc resistivity and magnetization in $La_{0.625-y}Pr_yCa_{0.375}MnO_3$ ($0.275 \leq y \leq 0.375$) suggest there is incomplete growth of the FM metallic component upon cooling through the CO phase[6]. We observed the existence of mesoscale phase-separation (a few μm in domain size) over a wide range of temperatures, and found that the CO and FM phases are mutually exclusive on this length scale. Specifically, below 90K, CO and FM co-exist where the CO volume fraction increases with temperature while FM decreases. Above 160K, CO dominates and undergoes transition to a paramagnetic phase at 210K. Our integrated study using electron holography, Lorentz microscopy, electron diffraction and theoretical calculations reveal the existence of a strong demagnetization field in the FM domains that are strongly determined by the crystallographic twinning present

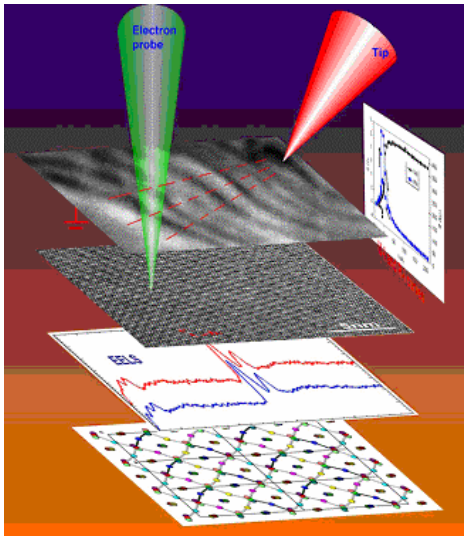

Experimental method: imaging probe (green) and the resistance measurement probe (red). The first layered image shows propagation of the polaron waves. The second layer shows individual atoms of the electron ordered state. The third layer displays electron spectra revealing bonding-electron excitation. The bottom layer is the resulting structural model, and the vertical graph shows the electrical resistance (I-V curve) of the crystal when current is applied.

in the material. Our results on these manganite systems have shed light on the CR effects in electric- and magnetic-fields which may impact the advancement of correlated electron-spin devices.

To address fundamental questions in nanomagnetism, such as the effects of long-range magnetostatic interactions in determining the magnetic and thermal responses in arrays of magnetic elements, we focused on studying the magnetodynamics of domain and vortex nucleation and evolution, their relation to structural defects, and magnetization reversal and switching behavior as a function of field and temperature in artificially patterned arrays of magnetic elements. We evaluated the energy landscape of specific systems for a given set of external parameters and found that magnetic elements below the single-domain critical size limit (showing a quasi-uniform magnetization topography) undergo a shape-induced magnetic phase transition. Below a critical combination of aspect ratios and distances, a system of three equilaterally-spaced magnetic disks change abruptly from an overall closure domain state, with zero net magnetization, to a dipolar ferromagnetic state with a net magnetization that depends on the interaction strength between the elements.

Future Planes

We will continue our study of the correlated behavior in manganites, especially the CR effects under various external fields (magnetic, electric, photoinduced, and strain). Developing a fundamental understanding of the mechanism of colossal photoinduced resistance is of great importance for advancing our knowledge of cooperative excitations in a strongly correlated electron system. In CO-OO PCMO, a photoinduced reduction of the electric resistivity of up to 8 orders of magnitude was observed[7], where some evidence suggests that a single absorbed photon can create collective excitations involving thousands of electrons. It is still unclear if the photoinduced metallic state exhibits magnetic ordering of the Mn spins, although a coherent form of excitations such as Jahn-Teller dynamics and orbital waves were observed[8]. We propose to explore photoinduced effects in PCMO. We recently designed a sample stage for the electron microscope with optical cables and mirrors that will enable us to shine light (visible light or tunable laser) on the sample (e.g., on electrically insulating polaron nanodomains) while taking transport measurement using a piezo-controlled system built into the microscope[4]. We will determine whether the photoinduced insulator-metal transition takes place via nucleation and growth of small domains, or by a homogeneous evolution of the high-conductance phase. Special emphasis will be put on exploring possible coherent polaron dynamics, as well as photoinduced remnant resistance in an applied dc electric field. The combination of local illumination, transport measurements, and cutting-edge analysis of the resulting lattice structure, electronic structure, and nanoscale phase separation can significantly improve our understanding of the transition mechanism and the nature of the resulting metal-like low conductivity phase.

Building on our recent work on thermoelectric materials that convert heat to electricity, of significant importance in answering national energy challenges, we will focus on structural defects that contribute to the low thermal conductivity in materials, such as Chalcogenide lead-based compounds, $AgPb_mSbTe_{2+m}$ (LAST-m, m=18). In our research thus far, we found Ag-Sb rich clusters (~3-4 unit-cell in size) embedded in a Pb-rich matrix, being consistent with the resonant peak related to the phonon density of state observed by our neutron scattering experiments. This points to the important role of nanoclusters in reducing thermal conductivity. In the misfit layered cobaltates $[Ca_2CoO_3]_{0.62}CoO_2$ we revealed a high hole concentration in the CoO_2 layer with remarkable in-plane lattice distortion in the CoO layer, and a significant charge transfer between the layers as

well. We will further identify the role of the mixture of "electro-crystal" (CoO_2 layers) and "phonon-glass" (CoO layers) that may contribute to its high thermoelectric power in the material. Additionally, we will determine the true structure and 4-D space group of the misfit layered cobaltates by combining electron diffraction and synchrotron x-ray techniques to determine the nature of the lattice displacement (static and dynamic) and its relation to charge- or spin-density waves. Our experimental observations will be compared with theory.

The authors would like thank some of our former members of the group, J. He, M. Beleggia, R. Klie, T. Asaka and Ch. Jooss for their contributions. The work was supported by the U.S. Department of Energy, Division of Materials Science, Office of Basic Energy Science, under Contracts No. DE-AC02-98CH10886.

References

[1] E. Dagotto, *Nanoscale phase separation and colossal megneto-resistance* . Solid-State Sciences, 2003 (Springer, Berlin).
[2] Y. Tokura, *Critical features of colossal magnetoresistive manganites. Reports on Progress in Physics*, 2006. **69,** p. 797.
[3] A. Daoud-Aladine, et al., *Phys. Rev. Lett*., **89**, 097205 (2002).
[4] Ch. Jooss et al, *Proc.Nat'l. Acad. Sci*, **104**, 13597 (2007).
[5] M.B. Salamon et al, *The physics of manganites: Structure and transport. Reviews of Modern Physics*, 2001. **73**, p. 583.
[6] M. Tokunaga, Y. Tokunaga, and T. Tamegai, *Phys. Rev. Lett*., **93**, 037203 (2004).
[7] V. Kiryukhin, et al., *Nature,* **386** 813 (1997).
[8] D. Polli et al., *Nature Materials,* **6** 643 (2007).

DOE Sponsored Publications in 2006-2008

2008

J. Carrasquilla-Alvarez, R. Castaneda, J. Garcia-Sucerquia, M.A. Schofield, M. Beleggia, Y. Zhu and G. Matteucci. "Retrieving the complex degree of coherence of electron beams", *Optik* **119** 127–133 (2008).
H. Chen et al., "Defect structures in B12As2 epitaxial layers grown on (0001) 6*H*-SiC", *J. Appl. Phys*. **103**, 123508 (2008).
H. Chen et al., "Single-crystalline B12As2 on *m*-plane (1100) 15*R*-SiC", *Appl. Phys. Lett*. **92**, 231917 (2008).
J. Cumings, E. Olsson, A.K. Petford-Long, and Y. Zhu, "Electric and Magnetic Phenomena Studied by In-Situ Transmission Electron Microscopy", *MRS Bulletin*, **33** 101-106 (2008).
J. He, J.C. Zheng, S. Chaudhuri, R.C. Budhani, and Y. Zhu, "Self-organization of epitaxial $La_{0.35}Pr_{0.275}Ca_{0.375}MnO_3$ manganite nanorods on NdGaO3 substrates", *J. Appl. Phys,* **103**, 064304 (2008).
C.L.Johnson, J.K.Bording, and Y.Zhu, "Structural inhomogeneity and twinning in $YBa_2Cu_3O_{7-\delta}$ superconductors: High-resolution transmission electron microscopy measurements", *Phys. Rev. B*, **71** (2008)
R.F. Klie, C. Johnson, and Y. Zhu, "Atomic-resolution STEM in the aberration-corrected JEOL JEM2200FS", invited article, *Microscopy & Microanalysis*, **14**, 104-112 (2008).
R.F. Klie, Y. Zhao, G. Yang, and Y. Zhu, "High-resolution Z-contrast imaging and EELS study of functional oxide materials", *Micron*, **39** 723–733 (2008).
Z.Li, J.Tao, X.Lu, Y.Zhu, and Y.Xia, "Facile Synthesis of Ultrathin Au Nanorods by Aging the AuCl(oleylamine) Complex with Amorphous Fe Nanoparticles in Chloroform", *Nano Lett*., in press
M. Malac, M. Beleggia, R. Egerton, Y. Zhu, "Imaging of radiation-sensitive samples in transmission electron microscopes equipped with Zernike phase plates", *Ultramicroscopy,* **108**, 126-140 (2008).
M.Malac, M.Beleggia, Y.Taniguchi, R.F.Egerton, and Y. Zhu, "Low-dose performance of parallel-beam nanodiffraction, *Ultramicroscopy* (2008), in press.
C. Phatak, M. Beleggia, M. De Graef, "Vector Field Electron Tomography of Materials: Theoretical Development", *Ultramicroscopy* **108** 503-513 (2008).
M. A. Schofield, M. Beleggia, and Y. Zhu, and G. Pozzi, "Characterization of JEOL 2100F Lorentz-TEM for low-magnification electron holography and magnetic imaging", *Ultramicroscopy*, **108** 625–634 (2008).
J.E. Villegas, K.D. Smith, L. Huang, Y. Zhu, R. Morales and I. K. Schuller, " Switchable collective pinning of flux quanta using magnetic vortex arrays: Experiments on square arrays of Co dots on thin superconducting films", *Phys. Rev. B* **77**, 134510 (2008)
V.V.Volkov, J.Wall, Y.Zhu, "Position-sensitive diffractive imaging in STEM by an automated chaining diffraction algorithm",*Ultramicroscopy* **108** 741–749 (2008).
K.E. Wagner, E. Morosan, Y. S. Hor, J. Tao, Y. Zhu, T. Sanders, T.M. McQueen, H.W. Zandbergen, A. J. Williams, D.V. West and R.J. Cava, "Tuning the Charge Density Wave and Superconductivity in Cu_xTaS_2", *Phys. Rev. B,* in press
H.Zhong, L.Huang, D.Wei, S.Wang, Y.Zhu and J.Yuan, "Experimental determination of ultra-sharp stray field distribution from a magnetic vortex core structure", *J. Magn. Magn. Mater*. in press.
Y. Zhu and J.Wall, "Aberration-corrected electron microscopes at Brookhaven National Laboratory", Book chapter in *Aberration-corrected Electron Microscopy*, A thematic volume of Advances in Imaging & Electron Physics, Ed., P.W.Hawkes, Elsevier/Academic Press, 2008

2007

M. Beleggia, M.A. Schofield, Y. Zhu, G. Pozzi. "Quantitative domain wall width measurement with coherent electrons". *J. Magn. Magn. Mater*. **310** 2696-2698 (2007).
S. Chaudhuri, R. C. Budhani, J. He and Y. Zhu, "Scaled frequency-dependent transport in the mesoscopically phase-separated colossal magnetoresistive manganite $La_{0.625-y}Pr_yCa_{0.375}MnO_3$", *Phys. Rev. B* **76** 132402 **(**2007).
G. Deptuch, A. Besson, P. Rehak, M. Szelezniak, J. Wall, M. Winter, and Y. Zhu, "Direct Electron Imaging in Electron Microscopy with Monolithic Active Pixel Sensors", *Ultramicroscopy* **107** (2007) 674–684.
Y. Ding and J. He, Domain structures and superdislocations of $La_{0.7}Ca_{0.3}MnO_3$ thin films grown on $SrTiO_3$ substrates, *J. Crystal Growth*, **306** 437 (2007).

W. Han, L.Wu, R. F. Klie, and Y. Zhu, "Enhanced optical absorption induced by dense nanocavities inside Titania Nanorods", *Adv. Mater*., **19**, 2525 (2007).
J. He, R.F. Klie, G.Logvenov, I Bozovic and Y. Zhu, "Microstructure and possible strain relaxation mechanisms of strained $La_2CuO_{4+\delta}$ thin films on $LaSrAlO_4$ and $SrTiO_3$ substrates", *J. Appl. Phys.* **101** (2007) 073906.
Ch. Jooss, L.Wu, T. Beetz, R. F. Klie, M. Beleggia, M. A. Schofield, S. Schramm, J. Hoffmann and Y. Zhu, "Polaron melting and ordering as key mechanisms for colossal resistance effects in manganites", *Proc.Nat'l. Acad. Sci*, **104**, 13597–13602 (2007).
R.F. Klie, J.C. Zheng, Y. Zhu, M. Varela, J. Wu and C. Leighton, "Direct measurement of the low temperature spin-state transition in $LaCoO_3$", *Phys. Rev. Lett.*, **99**, 047203 (2007).
J. W. Lau, R. D. McMichael, M. A. Schofield and Y. Zhu, "Correlation of edge roughness to nucleation field and nucleation field distribution in patterned Permalloy elements", *J. Appl. Phys*., **102**, 023916 (2007)
J. W. Lau, M. Beleggia and Y. Zhu, "Common reversal mechanisms and correlation between transient domain states and field sweep rate in patterned Permalloy structures", *J. Appl. Phys.*, **102**, 043906 (2007).
J.W. Lau, M.A. Schofield, Y. Zhu, "A straightforward specimen holder modification for remnant magnetic-field measurement in TEM", *Ultramicroscopy* **107** 396–400 (2007).
M. Malac, M. Beleggia, R. Egerton, Y. Zhu "Bright-field TEM imaging of single molecules: Dream or near future?", *Ultramicroscopy* **107** 40–49 (2007).
Q. Meng and Y. Zhu, "Structural modification of twin boundaries in $YBa_2Cu_3O_{6+\delta}$ oxides: Effects of oxygen concentration and temperature", *Phys. Rev. B*, **75**, 174501 (2007).
P. Moschkau, S. Schramm, J. Hoffmann, J. Fladerer, Ch. Jooss, L. Wu and Y. Zhu, " Electronic Phase Separation and the CMR Effect in $Pr_{1-x}Ca_xMnO_3$ Films on (001) vicinal $SrTiO_3$ Substrates", *Mater. Sci. & Eng.* B **144** (2007) 78–82
M. A. Schofield, M. Beleggia, J. W. Lau and Y. Zhu, "Characterization of the JEM2100F-LM TEM for electron holography and magnetic imaging", *JEOL News*, **42**, 1-7 (2007).
V. F. Solovyov, H. J. Wiesmann, L. Wu, Q. Li, L. D. Cooley, M. Suenaga, B. Maiorov and L. Civale, "High critical currents by isotropic magnetic-flux-pinning centres in a 3 μm-thick $YBa_2Cu_3O_7$ superconducting coated conductor", *Supercond. Sci. Technol.* **20** L20–L23 (2007).
Y. Sun, L. Zhang, H. Zhou, Y. Zhu, E. Sutter, Y. Ji, M. H. Rafailovich, and J. C. Sokolov, "Seedless and Templateless Synthesis of Rectangular Palladium Nanoparticles", *Chem. Mater*. **19**, 2065-2070 (2007).
G. Wang, Y. Ji, L. Zhang, Y. Zhu, P.-I. Gouma, and M. Dudley "Synthesis of Molybdenum Oxide Nanoplatelets during Crystallization of the Precursor Gel from Its Hybrid Nanocomposites", *Chem. Mater*., **19**, 979-981 (2007).
A.L. Willis, Z. Chen, J. He, Y. Zhu, N. J. Turro, and S.O'Brien "Metal Acetylacetonates as General Precursors for the Synthesis of Early TransitionMetal Oxide Nanomaterials", *J. of Nanomaterials,* **2007** 14858 (2007).
L. Wu, J. Zheng, and Y. Zhu, "A novel electron diffraction technique to accurately measure valence electron distribution and interfacial lattice displacement", Invited article, *J. of Chinese Electr on Microscopy Society*, **26**, 513-519 (2007).
L. Wu, R. F. Klie, Y. Zhu, Ch. Jooss, "Experimental Confirmation of Zener-polaron-type charge and orbital ordering in $Pr_{1-x}Ca_xMnO_3$", *Phy. Rev. B*, **76** 174210 (2007).
Y. Zhu, J. C. Zheng, L. Wu, A. I. Frenkel, J. Hanson, P. Northrup and W. Ku, "Nanoscale Disorder in $CaCu_3Ti_4O_{12}$: A New Route to the Enhanced Dielectric Response", *Phys. Rev. Lett.*, **99**, 037602 (2007).

2006
G. Pozzi, M. Beleggia, M. A. Schofield, and Y. Zhu, "Quantitative shadow technique for the investigation of magnetic domain wall widths", *Appl. Phys. Lett*., **88**, 152506 (2006).
M. Beleggia, M. De Graef and Y.T. Millev. "The equivalent ellipsoid of a magnetized shape". *J. Phys. D: Appl. Phys*. **39**, 891-899 (2006).
M. Beleggia, M. De Graef and Y.T. Millev. "Demagnetization factors of the general ellipsoid: An alternative to the Maxwell approach". *Philos. Mag*. **86**, 2451-2466 (2006).
M. Beleggia, J.W. Lau, M.A. Schofield, Y. Zhu, S. Tandon and M. De Graef. "Phase diagram for magnetic nano-rings". *J. Magn. Magn. Mater*. **301**, 131-146 (2006).
Z. Chen, L. Huang, J. He, Y. Zhu and S. O'Brien, "A New Nonhydrolytic Route to Synthesize Crystalline BaTiO3 Nanocrystals with Surface Capping Ligands", *J. of Mater. Res.,* **21** 3187-3195 (2006).
E. Cimpoiasu, E.Stern, R. Klie, R. A. Munden, G. Cheng, and M. A. Reed "The effect of Mg doping on GaN nanowires", *Nanotechnology* **17** 5735 (2006)
E. Cimpoiasu, R. Klie, R. A. Munden, G. Cheng, and M. A. Reed "Growth and properties of self-aligned MgO Nanowires,", *J. of Appl. Phys*. (in press)
W. Gao, M. Li, R.F. Klie, and E.I. Altman, Growth and Characterization of Model Oxide Catalysts, *J. Elect. Spectr*. **150** 136-149 (2006).
M. De Graef and M. Beleggia, "The fluxgate ring-core demagnetization field". *J. Magn. Magn. Mater*. **305**, 403-409 (2006).
D.A. Fischer, A.R. Moodenbaugh, Q. Li, G.D. Gu, Y. Zhu, J.W. Davenport, D.O. Welch and H. Su, "Soft x-ray absorption spectroscopy of the MgB_2 boron K-edge in an MgB_2/Mg composite", *Modern Phys. Lett. B* **20**, 1207-1216 (2006).
W. Gao, M. Li, R.F. Klie, and E.I. Altman, "Growth and Characterization of Model Oxide Catalysts," *J. Elect. Spectr.* **150**, 136-149 (2006)
W. Han, L. Wu, A. Stein, Y. Zhu, J. Misewich, and J. Warren, "Oxygen-Deficiency-Induced Superlattice Structures of Chromia Nanobelts", *Angew. Chem. Int. Ed*., **45**, 6554 –6558 (2006).
R. F. Klie, J. C. Zheng, Y. Zhu, A. J. Zambano and L. D. Cooley, "Electron energy-loss spectroscopy study of electron-doping in MgB_2", *Phys. Rev. B* **73** 014513 (2006).
I. Kuskovsky, Y. Gu, Y. Gong, H.F. Yan, J. Lau, I.C. Noyan, G.F. Neumark, O. Maksimov, X. Zhou, M.C. Tamargo, V.V.Volkov, Y. Zhu, and L. Wang, "Mechanism of Improved Doping in Semiconductors via Doped Nanostructures", *Phys. Rev. B* **73**, 195306-195311 (2006).
J. W. Lau, J. K. Bording, M. Beleggia, and Y. Zhu, " Energy barrier to magnetic vortex nucleation", *Appl. Phys. Lett.,* **88,** 012508 (2006).
M. G. Pozzi, M. Beleggia, M.A. Schofield, and Y. Zhu. "Quantitative Shadow technique for the investigation of magnetic domain wall widths". *Appl. Phys. Lett*. **88**, 152506-9 (2006).
M.Y. Sfeir, T. Beetz, F. Wang, L. Huang, X. M. Huang, M. Huang, J. Hone, S.O'Brien, J. A. Misewich, T.F. Heinz, L. Wu, Y. Zhu, L. E. Brus, "Optical Spectroscopy of Individual Single-Walled Carbon Nanotubes of Defined Chiral Structure", *Science*, **312,** 554-556 (2006).
Y. Sun, A. I. Frenkel, H. White, L. Zhang, Y. Zhu, H. Xu, J. C. Yang, T. Koga, V. Zaitsev, M.H. Rafailovich, and J. C. Sokolov, "Comparison of Decanethiolate Gold Nanoparticles Synthesized by One-Phase and Two-Phase Methods", *J. Phys. Chem. B*, **110**, 23022-23030, (2006).
Y. Sun, Anatoly I. Frenkel, R. Isseroff, C. Shonbrun, M. Forman, K. Shi, T. Koga, H. White, L. Zhang, Y. Zhu, M.H. Rafailovich, and J.C. Sokolov, "Characterization of palladium nanoparticles by using x-ray reflectibity, EXAFS and electron microscopy", *Langmuir*, **22**, 807-816 (2006).
E. Sutter, P. Sutter, and Y. Zhu, "Assembly and Interaction of Au/C Core-Shell Nanoparticles", *Surf. Sci*. **600**, 3654 (2006).
S. Xiao, J. Tang, T. Beetz, X. Guo, N. Tremblay, T. Siegrist, Y. Zhu, M. Steigerwald, and C. Nuckolls, "Transferring Self-Assembled, Nanoscale Cables into Electrical Devices", *J. Am. Chem. Soc*. **128**, 10700-10701 (2006).
J. Zheng, and Y. Zhu, "Searching for a higher superconducting transition temperature in strained MgB_2", *Phys. Rev. B*, **73**, 024509 (2006).

Research Summaries II:

Electronic & Superconducting Materials

Imaging of Buried Nanoscale Optically Active Materials

Ian Appelbaum
Department of Electrical and Computer Engineering, University of Delaware, Newark, DE 19716
appelbaum@ee.udel.edu

Program Scope:

Semiconductor heterostructure-based light-emitting diodes (LEDs) and solid-state lasers have benefited enormously from recent developments in materials science and nanotechnology. However, methods to characterize the carrier transport through (and the light emission from) these devices on the nanoscale at which they were designed are limited by the fact that the carrier recombination occurs in layers buried deep below the semiconductor surface. Hence, processes occurring in these layers are hidden from direct observation. The development and introduction of a successful technique to examine the carrier transport and photon emission in deeply buried optically-active layers will provide a means for materials science to unmask the detailed consequences of experimentally controllable growth parameters, such as quantum dot size statistics and orientation, and defect density and charge recombination pathways. This will lead to more efficient, brighter light emitting devices across a broader wavelength spectrum.[1]

Our project goal is to demonstrate and use Ballistic Electron Emission Luminescence microscopy to image the deeply-buried luminescent layer of semiconductor light-emitting devices with local hot electron injection from a Scanning Tunneling Microscope (STM) probe. Briefly, hot electrons are ballistically injected over a rectifying Schottky barrier into a n-i-p LED under bias. Electroluminescence from the optically active region directly below the injection point results from radiative recombination of these injected carriers. Microscopy is possible by raster-scanning the tip position. The electroluminescence mechanism has been demonstrated in solid-state devices using $Al/Al_2O_3/Al$ tunnel-junctions,[2] and in ambient conditions with the STM in spectroscopy mode on QW devices, without imaging.[3]

Recent Progress:

Because the STM tunneling current is only several nA, the ballistically-injected hot-electron current is small (1-100 pA). Therefore, the luminescence intensity is weak, and external collection efficiency is reduced by the large index of refraction mismatch between semiconductors and air. To most effectively use Ballistic Electron Emission Luminescence microscopy, we must efficiently collect as much emitted luminescence as possible with an integrated photodetector.[4]

In the past, we have used ultra-high-vacuum (UHV) metal wafer bonding to heterogeneously integrate full wafers, primarily for semiconductor spintronics

[1] E.F. Schubert and J.K. Kim, "Solid-State Light Sources Getting Smart", Science **308**, 1274, (2005)
[2] Ian Appelbaum et al., "Ballistic Electron Emission Luminescence", Appl. Phys. Lett. **82**, 4498 (2003).
[3] Ian Appelbaum et al., "Room-Temperature Ballistic Electron Emission Luminescence Spectroscopy with a Scanning Tunneling Microscope", Appl. Phys. Lett. **84**, 547 (2004)
[4] Ian Appelbaum et al., "Vertically Integrated Optics for Ballistic Electron Emission Luminescence Microscopy", Appl. Phys. Lett **86**, 063110 (2005)

applications where semiconductor-metal-semiconductor structures can be used for spin-polarized electron detection.[5] Our recent efforts on the present project have focused on using this unique fabrication technique to intimately incorporate semiconductor photodetectors with the electroluminescent hot-electron collector p-n structure to overcome the optical index mismatch problem in a materials-independent way.

We have started with a MBE-grown AlGaAs/GaAs quantum well p-n structure obtained from IntelliEpi and a Si p-n photodetector. Using only several nm of NiFe to maintain optical transparency, we bond these full 2" wafers in UHV using our custom wafer manipulator, shown below in various stages of operation *ex situ*.

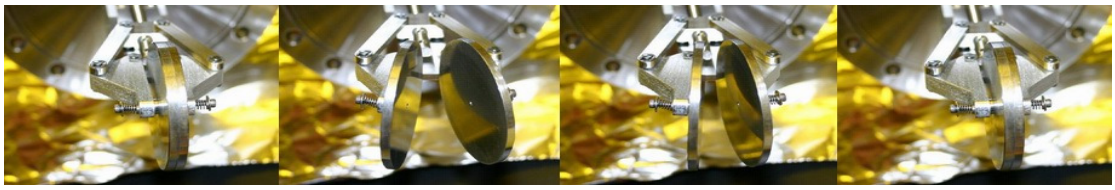

After this bonding, the handle wafer can be etch away to expose the n-type surface for forming hot-electron pass-filter Schottky barriers.

To verify proper injection and luminescence mechanisms, we first fabricate tunnel-junction devices which use $Al/Al_2O_3/Al$ evaporated (and shadow-mask patterned) structures. These devices are made from mesas defined by diamond-sawing through the bonded interface and result in arrays shown below, schematically in side-view (left) and in a micrograph in plan-view (right).

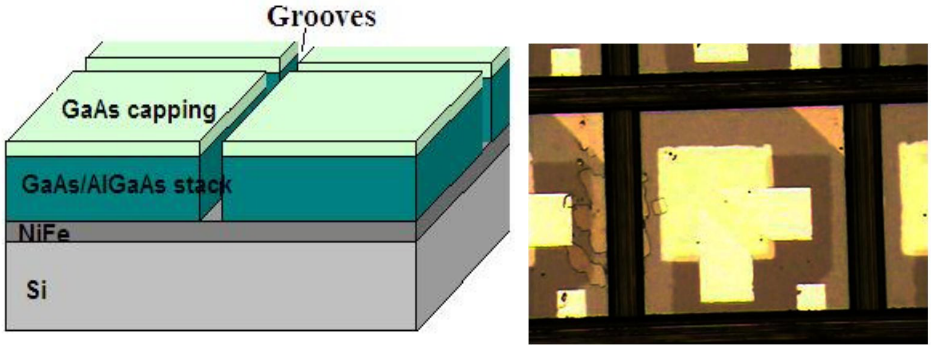

The resulting device band-diagram is shown below. The tunnel junction injects hot electrons from the emitter cathode on the left, once the emitter bias VE exceeds the injector Schottky barrier height. Under LED bias VC1, holes from the p+ region are given enough potential energy to recombine with injected electrons and emit bandgap luminescence at the GaAs QW. These photons are then absorbed in the Si p-n junction on the right, constituting our BEEL signal, photocurrent IC2.

[5] Ian Appelbaum, Biqin Huang, and Douwe J. Monsma, "Electronic measurement and control of spin transport in silicon", Nature **447**, 295 (2007)

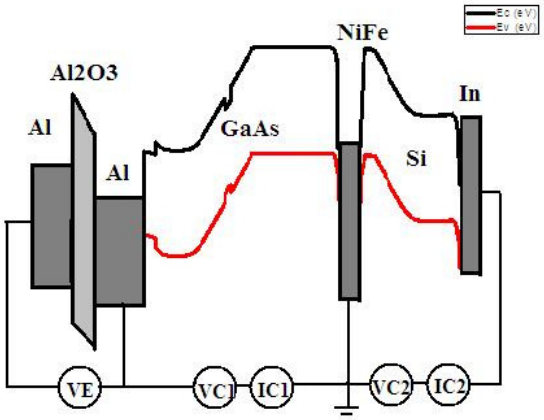

Future Plans:

Once we optimize the wafer-bonded photo-detector for maximum output current and firmly verify hot electron injection operation, we plan to begin measurements on LED structures where the luminescent layer has intentional spatial variation. These patterned and overgrown heterojunction samples will be obtained from MBE-growing collaborators and will utilize the InGaAs/GaAs materials system. After measurements using solid-state hot electron injectors in device mode to establish the presence of the expected transport, luminescence, and photon collection mechanisms, we will use the STM to determine the intrinsic lateral resolution of BEEL microscopy by comparing the obtained image with the pattern used before overgrowth. Beyond that, we will move to other materials systems, for instance to look for In segregation in InGaN LED structures.

Investigating Magnetic Order in Mesoscopic Superconductors Using Cantilever Torque Magnetometry

Raffi Budakian, Joonho Jang
budakian@illinois.edu
Frederick Seitz Materials Research Laboratory, University of Illinois at Urbana-Champaign, Urbana, IL 61801

Program Scope

Search for Chiral Domains and Fractional Vortices in Sr_2RuO_4

Following the initial μSR [1] and NMR [2] studies suggesting that Sr_2RuO_4 is a spin-triplet superconductor, there has been a great deal of interest to understand the nature of the order parameter [3-5]. Although Sr_2RuO_4 is similar in structure to the layered high-T_c cuprate superconductors, it is thought to possess chiral $p_x \pm ip_y$ pairing symmetry. The complex order parameter can give rise to a rich variety of new correlated states, such as domains having orbital order that possess a net magnetic moment and half-integer vortices with zero-energy modes. Fractional vortices, in particular, have attracted a great deal of attention as a potential candidate for topologically-protected quantum states for quantum computation.

Until now, fractional vortices have not been observed and there is differing experimental evidence as to the existence of chiral domains. The free energy required to stabilize fractional vortices or chiral domains could be minimized if the size of the sample is made sufficiently small. All measurements until now, however, have been made using macroscopic size samples. We are currently conducting experiments to measure the diamagnetic susceptibility of micron-size samples of Sr_2RuO_4 using cantilever torque magnetometry. One of the goals of these measurements is to look for magnetic domains which would directly result from the orbital ordering of the $\ell = 1$ superconducting condensate. The existence of domains with orbital order would strongly support the view that Sr_2RuO_4 possesses $p_x \pm ip_y$ symmetry.

Another goal of our measurements is to look for evidence of fractional vortices. It is believed that in order for fractional vortices to be energetically favorable, the *d*-vector must lie in the plane perpendicular to the *c*-axis. One way to achieve this orientation is by applying a field parallel to the *c*-axis. In our current measurements, we are testing these ideas by investigating the changes in magnetic moment of a single vortex as the magnitude and direction of the external field are varied.

Recent Progress

We believe that, by studying micron-size samples, it might be possible to measure the magnetic moment from single domains. The ultra-sensitive force detection techniques used in our group

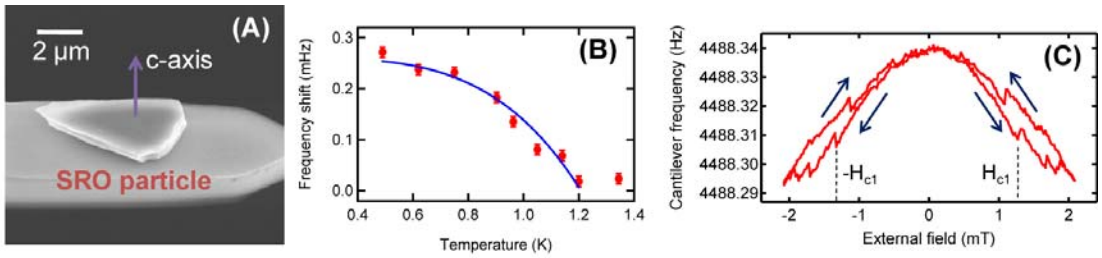

Figure 1: (A) SEM image of a micron-size Sr_2RuO_4 particle glued on a cantilever. (B) Cantilever frequency shift data proportional to diamagnetic susceptibility indicating T_c=1.2K. (C) Cantilever frequency vs. field applied along the c-axis of the particle. The quadratic region below 10 mT is the Meissner state of the superconductor. Individual jumps are consistent with single vortex entry.

are among the most sensitive means of measuring magnetic susceptibility. We have recently measured the diamagnetic susceptibility of a single 1.0 μm × 1.6 μm × 0.35 μm size Sr_2RuO_4 particle down to 0.4 K and are currently conducting experiments in search of chiral domains. In addition, we have observed jumps in the magnetic moment of the sample consistent with single vortex entry. Unlike macroscopic samples, the entry and arrangement of vortices is highly deterministic with respect to the external field applied to the sample. By cycling the field, we can sweep out all of the vortices in the sample and then repeat the field sweep to observe the same pattern of vortex entry events. This gives us a great deal of control in being able to make small changes to the direction of the applied field and study its effects on the magnetic moment of a given vortex entering the sample.

Future Plans

If fractional vortices are found, future experiments will be geared toward understanding the conditions, e.g. sample geometery and external field, required to stabilize the fractional vortex.

Superconductor-Mediated Cavity Cooling of a Micromechanical Resonator

Quantum mechanics is known to work without exception on the scale of subatomic particles, atoms and large molecules. As the number of atoms that make up a system increase, there is an open question as to whether or not quantum mechanics remains a complete theory [6-8]. In fact, quantum mechanics has never been tested beyond collections of atoms of order 10^2.

The focus of our research effort is to study quantum phenomena on the mesoscopic scale in high-frequency nanomechanical resonators. In order to observe quantum behavior, the resonator must be cooled to the ground state of its motion $T \sim \hbar\omega_c / k_B$. In recent years, there have been a number of experiments to cool the vibrational mode of an oscillator through direct feedback [9-11] and by coupling the oscillator to an external system, such as an optical cavity [12], single-

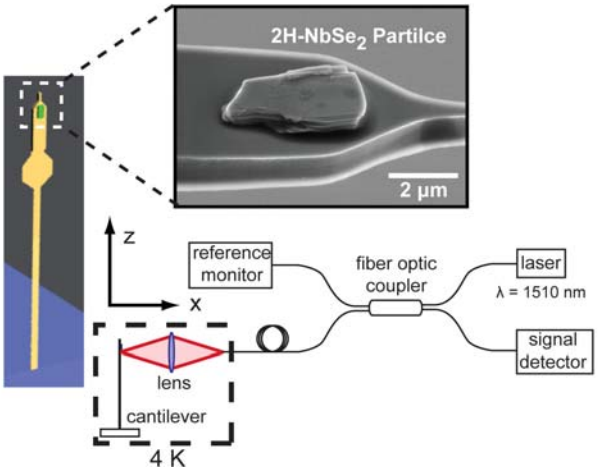

Figure 2: Image of cantilever used with $NbSe_2$ particle. The cantilever is placed is part of an optical cavity formed by the cleaved end of a single mode fiber and the reflective paddle.

electron transistor [13], and LC circuits [14], which can extract energy from the oscillator without introducing excess fluctuations, thereby cooling the vibrational mode.

From our torque magnetometry experiments, we have observed that when a micron-size superconductor is attached to the tip of a cantilever and placed inside an optical cavity, in the presence of an external magnetic field, the thermal fluctuations of the flexural mode can be greatly suppressed. Based on recent experimental data, we have developed the following model for this effect. A photon absorbed by the superconductor creates a large number of quasiparticles of order $\Delta/\hbar\omega_\gamma$, which in turn suppresses the diamagnetic susceptibility of the superconductor. Inside an optical cavity, the intensity of light is a function of the cantilever position. In the presence of a magnetic field, the position-dependent susceptibility generates a back-action on cantilever. The finite quasiparticle lifetime causes a phase lag between the cantilever motion and the change in susceptibility which modifies the damping rate of the cantilever. The damping rate can be controlled by changing the direction of the applied field and by varying the detuning of the optical cavity.

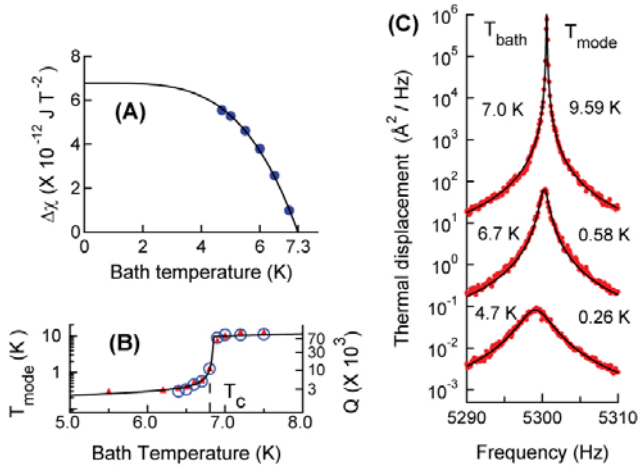

Figure 3: (A) Measurement of diamagnetic susceptibility for the particle shown in Fig. 2. (B) As the temperature of the bath is increased above T_c, the cooling effect turns off. (C) Using the fluctuation-dissipation theorem, the mode temperature can be obtained by integrating the thermal fluctuations. Data displayed in (B) was obtained by integrating the curves shown in (C).

Recent Progress

In recent experiments, we demonstrated the superconductor-mediated cooling phenomena using a 3μm×4μm×0.5μm piece of the anisotropic superconductor 2H-$NbSe_2$ attached to the tip of high-quality micromechanical resonator having a resonant frequency of 5.3 kHz and a quality factor of 6×10^4. With approximately 100 nW of optical power at λ=1.5 μm incident on the cantilever and an external field of 10 mT, the cantilev-

er was cooled by from 5 K down to 0.2 K.

Future Plans

Future experiments will attempt to cool a MHz frequency cantilever into the ground state. This will be accomplished by integrating the cantilevers into high-finesse optical cavities to enhance the cooling effect.

References

1. Luke, G. M. et al., Time-reversal symmetry breaking superconductivity in Sr2RuO4. *Nature* **394** (6693), 558 (1998).
2. Ishida, K. et al., Spin-triplet superconductivity in Sr2RuO4 identified by O-17 Knight shift. *Nature* **396** (6712), 658 (1998).
3. Kidwingira, F., Strand, J. D., Van Harlingen, D. J., and Maeno, Y., Dynamical superconducting order parameter domains in Sr2RuO4. *Science* **314** (5803), 1267 (2006).
4. Kirtley, J. R. et al., Upper limit on spontaneous supercurrents in Sr2RuO4. *Physical Review B* **76** (1), 8 (2007).
5. Xia, Jing et al., High resolution polar Kerr effect measurements of Sr2RuO4: evidence for broken time-reversal symmetry in the superconducting state. *Phys Rev Lett* **97** (16), 167002 (2006).
6. Ghirardi, G. C., Pearle, P., and Rimini, A., Markov-processes in Hilbert-space and continuous spontaneous localization of systems of identical particles. *Physical Review A* **42** (1), 78 (1990).
7. Leggett, A. J., Macroscopic quantum-systems and the quantum-theory of measurement. *Supplement of the Progress of Theoretical Physics*, 80 (1980).
8. Penrose, R., On gravity's role in quantum state reduction. *General Relativity and Gravitation* **28** (5), 581 (1996).
9. Cohadon, P. F., Heidmann, A., and Pinard, M., Cooling of a mirror by radiation pressure. *Physical Review Letters* **83** (16), 3174 (1999).
10. Kleckner, D. and Bouwmeester, D., Sub-kelvin optical cooling of a micromechanical resonator. *Nature* **444** (7115), 75 (2006).
11. Poggio, M., Degen, C. L., Mamin, H. J., and Rugar, D., Feedback cooling of a cantilever's fundamental mode below 5 mK. *Physical Review Letters* **99** (1) (2007).
12. Metzger, C. H. and Karrai, K., Cavity cooling of a microlever. *Nature* **432** (7020), 1002 (2004).
13. Naik, A. et al., Cooling a nanomechanical resonator with quantum back-action. *Nature* **443** (7108), 193 (2006).
14. Brown, K. R. et al., Passive cooling of a micromechanical oscillator with a resonant electric circuit. *Physical Review Letters* **99** (2007).

Structure and Dynamics of Domains in Ferroelectric Nanostructures

Long-Qing Chen, Department of Materials Science and Engineering, Penn State University, University Park, PA 16802; lqc3@psu.edu

Xiao-Qing Pan, Department of Materials Science and Engineering, University of Michigan, Ann Arbor, MI 48109; panx@umich.edu

Program Scope:

The main objective of the research program is to explore the fundamental understanding of structure, nucleation and dynamic evolution of ferroelectric domains in strained ferroelectric thin films and fabricated nanostructures by a close coupling of experimental observations (Pan) and mesoscale computational approaches (Chen). The experimental techniques used include high resolution transmission electron microscopy (HRTEM) and *in situ* transmission electron microscopy (TEM) using a novel scanning probe microscope (SPM)- TEM holder which allows the direct observation of nucleation and dynamic evolution of ferroelectric domains under applied electric fields. The domain structure evolution is modeled using the phase-field approach in combination with fundamental thermodynamic theories, electrostatics, and nano-/micro-mechanics. The PIs seek to elucidate the roles of homogeneous strains, electrical boundary conditions, defects and film thickness in the transition temperatures and domain nucleation and evolution of ferroelectric thin films. The nucleation and dynamic evolution of ferroelectric domains observed by *in-situ* TEM under applied external electric fields and during ferroelectric phase transitions will be quantitatively analyzed and directly compared with theoretical modeling and simulations.

Recent Progresses

During the first year of the research program, we have made several important progresses which are briefly described below.

- A double-tilt TEM holder with a built-in positionable Scanning Tunneling Microscopy (STM) probe, designed in collaboration with the Nanofactory Inc., has recently been installed in Professor Pan's laboratory at the University of Michigan. This holder is primarily for *in-situ* ferroelectric domain studies. It consists of several unique functions in comparison with the previous model of the Nanofactory's single-tilt STM holder: the double tilt of TEM specimen for imaging along different zone axes, electrical measurements using four point probes, and heating.
- A three-dimensional phase-field model was developed for studying domain structures in ferroelectric islands attached onto a substrate [1]. It simultaneously takes into account the long-range electric and elastic interactions, substrate constraint, as well as the stress relaxation caused by the surfaces of an island. The phase-field simulations demonstrated that the domain structures of ferroelectric islands could be dramatically different from those of continuous thin films due to the change of stress/strain state. The stress distribution inside islands is highly dependent on the aspect ratio of the islands. It provides us an effective way for engineering the domain structures of ferroelectric materials.

- Ferroelectric domain structures of $(001)_c$, $(101)_c$, and $(111)_c$ oriented epitaxial $BiFeO_3$ thin films were studied using the phase-field approach [2]. An example of a predicted domain structure is shown in Fig. 1 and compared to experimental observation. The effects of various types of substrate constraint on the domain morphologies were systematically analyzed. It is demonstrated that domain structures of $BiFeO_3$ thin films could be controlled by selecting proper film orientations and substrate constraint.

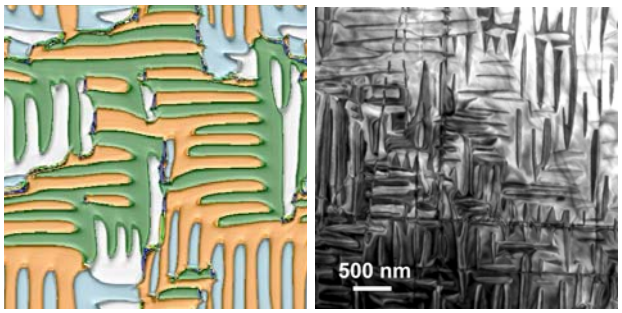

Fig. 1. An example of a $(001)_c$ film domain structure (top view) predicted from a phase-field simulation (left) and compared with a bright-field image (Ramesh)

- Role of boundary conditions in ferroelectric thin films was investigated in four $BiFeO_3$ thin films grown on (001) $SrTiO_3$ substrates with 4° miscut along the [100] direction. The films were fabricated by pulsed laser deposition. Fig. 1 shows the dark field diffraction contrast TEM images of 200 nm thick $BiFeO_3$ films consisting of different electric boundary conditions. Fig. 1(a) shows an array of 71° domain walls (71° twinning boundaries) observed in the $BiFeO_3$ film without electrode. It is seen that the domain walls are uniformly distributed with an average spacing similar to the film thickness, running perpendicular to the miscut [100] direction. Fig. 1(b) shows the domain structure of a $BiFeO_3$ film consisting of a 50 nm thick $SrRuO_3$ bottom electrode. The 71° domain walls are observed, but they are distributed inhomogeneously in the film. The average spacing of the domain walls is lower than that of the film without electrode. It should be noted that some small domains with triangular shapes bounded by two {101} boundaries (see the top right side of Fig. 1(b)) are frequently observed near the film surface,

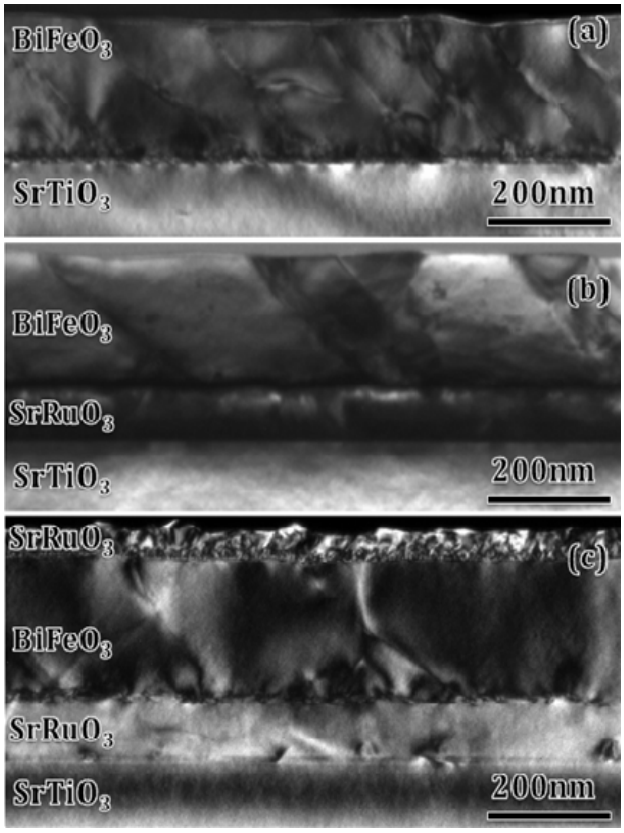

Fig. 2. Dark field TEM images showing the domain structures of $BiFeO_3$ films grown on (001) $SrTiO_3$ substrates with different electric boundary conditions: (a) without electrode, (b) with a bottom $SrRuO_3$ electrode, and (c) with both bottom and top $SrTuO_3$ electrodes. Note that the $SrTiO_3$ substrates consist of 4° miscut along the [100] direction.

which results in a higher density of domain walls in the free surface. The $BiFeO_3$ film consisting of both bottom and top electrodes shows a much lower density of domain walls, as shown in Fig. 2(c). Many areas in this film are free of domain walls. This may be caused by the charge compensation at the $BiFeO_3$ surface due to the existence of metallic $SrRuO_3$ electrodes. Phase-field simulations of domain structures in the (001) $BiFeO_3$ with 4° miscut towards [100] subject to different electric boundary conditions are currently underway to compare with experimental observations.

- We also studied the dependence of the domain structures of $BiFeO_3$ films grown on (001) $SrTiO_3$ substrates on the miscut angle of the substrate. It was found that the film grown on (001) $SrTiO_3$ with low miscut (< 1°) consists of the mixture of 71° and 109° domain walls (corresponding to {101} and {100} twinning boundaries) while the thick $BiFeO_3$ film grown on the (001) substrate with 4° miscut along the [110] direction, which consists of a 50 nm thick $SrRuO_3$bottom electrode, is completely free of domain walls, which results from the unique atomic structure at the substrate surface steps induced by miscut. These experimental observations are in agreement with our phase-field simulations of the domain structures in $BiFeO_3$ films with different miscut angles. We are currently studying the different switching behavior, including the domain nucleation and growth, using the phase-field simulations and experimental observations.
- In collaboration with Dr. S. Kalinin at Oak Ridge National Lab, we studied the domain stability, domain wall motion, and switching in multiferroic $BiFeO_3$ using combination of piezoresponse force spectroscopy, analytical theory, and phase-field simulations [3-4]. The critical parameters of the nucleating domain and the activation energy for nucleation are determined. We studied the role of atomic-scale defects and long-range elastic fields on nucleation bias lowering. Through a combination of phase-field modeling and scanning force microscopy of carefully controlled, we demonstrated the preference of domain nucleation at local defects such as twin boundaries.

Planned activities for next year

During the next year, our research will have two main focuses: (1) continue the studies of the effect of electric boundary conditions on the domain structures in $BiFeO_3$ thin films by both TEM and phase field theory, and (2) investigating the nucleation and switching behavior of $BiFeO_3$ and/or PZT films under applied electric field in TEM using our newly installed double-tilt STM holder. We will collaborate with Professor Eom at the University of Wisconsin to make stoichiometric $BiFeO_3$ and PZT films by the optimization of Bi concentration in sputtering targets. Furthermore, we will closely couple our TEM observations with the theoretical modeling and phase-field simulations.

References (Publications acknowledged the DOE grant)

1. J. X. Zhang, R. Wu, S. Choudhury, Y. L. Li, L. Q. Chen, S. Y. Hu, "Three-dimensional Phase-field Simulations of Domain Structures in Ferroelectric Islands", Applied Physics Letters, 2008. 92, 122906.
2. J. X. Zhang, Y. L. Li, S. Choudhury, L. Q. Chen, Y. H. Chu, F. Zavaliche, M. P. Cruz, R. Ramesh, and Q. X. Jia, *Computer simulation of ferroelectric domain structures in epitaxial $BiFeO_3$ thin films.* Journal of Applied Physics, 2008. **103**(9).

3. Stephen Jesse, Brian J. Rodriguez, Arthur P. Baddorf, I. Vrejoiu, D. Hesse, M. Alexe, Eugene A. Eliseev, Anna N. Morozovska, J. Zhang, S. Choudhury, L.Q. Chen, and Sergei V. Kalinin, "Direct Imaging of Spatial and Energy Distribution of Nucleation Centers in Ferroelectric Materials", Nature Materials, 2008. 7(3): p. 209-215.
4. S. V. Kalinin, B. J. Rodriguez, S. Jesse, Y. H. Chu, T. Zhao, R. Ramesh, S. Choudhury, L. Q. Chen, E. A. Eliseev, and A. N. Morozovska, *Intrinsic single-domain switching in ferroelectric materials on a nearly ideal surface.* Proceedings of the National Academy of Sciences of the United States of America, 2007. 104(51): p. 20204-20209.
5. (Review Article) L. Q. Chen, *Phase-field method of phase transitions/domain structures in ferroelectric thin films: A review.* Journal of the American Ceramic Society, 2008. **91**(6): p. 1835-1844.
6. (Review Article) D. G. Schlom, L. Q. Chen, X. Q. Pan, A. Schmehl, and M. A. Zurbuchen, *A Thin Film Approach to Engineering Functionality into Oxides.* Journal of the American Ceramic Society, 2008. **91**(8): p. 2429–2454.
7. Y.B. Chen, M.B. Katz, X.Q. Pan, C.M. Folkman, R.R. Das, and C.B. Eom, "Microstructure and strain relaxation of epitaxial $PrScO_3$ thin films grown on (001) $SrTiO_3$ substrates", *Applied Physics Letters*, **91**[3], 031902 (2007).
8. H. W. Jang, S. H. Beak, D. Ortiz, C. M. Folkman, R. R. Das, J. X. Zhang, S. Choudhury, L. Q. Chen, V. Vaithyanathan, D. G. Schlom, Y.B. Chen, X.Q. Pan, P. Shafer, Y. H. Chu, R. Ramesh, and C. B. Eom "Quasi-single crystal $BiFeO_3$ thin-film membranes " accepted in Physical Review Letters, 2008
9. M.D. Biegalski, S.T. Trolier-McKinstry, D.G. Schlom, D.D. Fong, J.A. Eastman, P.H. Fuoss, S.K. Streiffer, T. Heeg, J. Schubert, W. Tian, C. Nelson, X.Q. Pan, M.E. Hawley, M. Bernhagen, P. Reiche, and R. Uecker, "Critical thickness of high structural quality $SrTiO_3$ films grown on orthorhombic (101) $DyScO_3$", accepted in Journal of Applied Physics, 2008.
10. G. Sheng, J. X. Zhang, Y. L. Li, S. Choudhury,1 Q. X. Jia, Z. K. Liu, and L. Q. Chen, "Domain stability of PbTiO3 thin films under anisotropic misfit strains: phase-field simulations", accepted in Journal of Applied Physics, 2008.

Electron and Scanning Probe Microscopies

JC Séamus Davis, 622 Clark Hall, Cornell University, Ithaca NY.
jcdavis@ccmr.cornell.edu
Project Title: "ATOMIC SCALE STUDIES OF DOPED-HOLE DISTRIBUTIONS, SELF ORGANIZED ELECTRONIC NANO-DOMAINS, AND ELECTRON-BOSON COUPLING IN HIGH-T_C CUPRATES
DOE Award: DE-FG02-06ER46306 / Cornell University.

Recent Progress

Recent progress includes:

- d^2I/dV^2 **-Imaging for Electron-Boson-Interactions**

For conventional superconductors, tunnelling spectroscopy has established that pairing is mediated by bosonic modes (phonons); a peak in the second derivative of tunnel current d^2I/dV^2 corresponds to each phonon mode. For high-transition-temperature (high-T_c) superconductivity, however, no boson mediating electron pairing has been identified. With recent advances in d^2I/dV^2 spectroscopy using STM, it has become possible to study bosonic modes directly at the atomic scale. We reported d^2I/dV^2 imaging studies of the high-T_c superconductor $Bi_2Sr_2CaCu_2O_{8+\delta}$finding intense disorder of electron–boson interaction energies at the nanometer scale. Changing the density of holes has minimal effects on both the average mode energies and the modulations, indicating that the bosonic modes are unrelated to electronic or magnetic structure. Instead, the modes appear to be local lattice vibrations, because substitution of ^{18}O for ^{16}O throughout the material reduces the average mode energy by approximately 6 per cent—the expected effect of this isotope substitution on lattice vibration frequencies. The mode energies are spatially anticorrelated with the superconducting pairing-gap energies, suggesting an interplay between these lattice modes and the superconductivity. ***Nature 442***, 546 (2006*).*

Electronic Nematic of Glassy Nanodomains (Nanostripes)

Removing electrons from the CuO_2 plane of cuprates alters the electronic correlations sufficiently to produce high-temperature superconductivity. Associated with these changes are spectral weight transfers from the high energy states of the insulator to low energies. In theory, these should be detectable as an imbalance between the tunneling rate for electron injection and extraction—a tunneling asymmetry. We introduced atomic-resolution tunneling-asymmetry imaging, finding virtually identical phenomena in two lightly hole-doped cuprates: $Ca_{1.88}Na_{0.12}CuO_2Cl_2$ and $Bi_2Sr_2Dy_{0.2}Ca_{0.8}Cu_2O_{8+\square}$. Intense spatial variations in tunneling asymmetry occur primarily at the planar oxygen sites; their spatial arrangement forms a Cu-O-Cu bond centered electronic pattern with $4a_0$-wide unidirectional electronic domains. ***Science 315***, 1380 (2007).

• **Quasiparticle Interference in Ca2*x*Na*x*CuO2Cl2**.

The study of the material dependence of the *d*-wave superconducting gap (SG) can provide important insights into the mechanism of high-T_c superconductivity. However, because of the 'pseudogap' phenomenon, it is often unclear whether the energy gaps observed by spectroscopic techniques really represent the SG. Here, we used scanning tunnelling spectroscopy to image nearly optimally doped $Ca_{2-x}Na_xCuO_2Cl_2$(Na-

CCOC) with T_c=25–28 K. We observe the quasiparticle interference effect in this material, through which we obtain unambiguous information on the SG. Our analysis of quasiparticle interference in Na-CCOC reveals that the SG dispersion near the gap node is almost identical to that of $Bi_2Sr_2CaCu_2O_y$ (Bi2212) at the same doping level, despite the T_c of Bi2212 being three times higher than that of Na-CCOC. We also find that the SG in Na-CCOC is confined in narrower energy and momentum ranges than Bi2212.. ***Nature Physics 3***, 865 (2007).

• Pseudogap in Striped Cuprate Superconductors

We presented studies of the electronic structure of $La_{2-x}Ba_xCuO_4$, a system where the superconductivity is strongly suppressed as static spin and charge orders or "stripes" develop near the doping level of x = 1/8. Using angle-resolved photoemission and scanning tunneling microscopy, we detected an energy gap at the Fermi surface with magnitude consistent with d-wave symmetry and with linear density of states, vanishing only at four nodal points, even when superconductivity disappears at x = 1/8. Thus, the non-superconducting, striped state at x = 1/8 is consistent with a phase-incoherent d-wave superconductor whose Cooper pairs form spin-charge–ordered structures instead of becoming superconducting**.** ***Science 314***, 1914 (2006*).*

- **Impact on cuprate superconductivity of varying the inter-atomic distances within individual crystal unit-cells.**

Many theoretical models of high-temperature superconductivity focus only on the doping dependence of the CuO_2-plane electronic structure. However, such models are insufficient to explain the strong variations in superconducting critical temperature, T_c, among cuprates that have identical hole-density but are crystallographically different outside of the CuO_2 plane. A key challenge, therefore, has been to identify a predominant out-of-plane influence controlling the superconductivity, with much attention focusing on the distance d_A between the apical oxygen and the planar copper atom. We reported direct determination of how variations in inter atomic distances within individual crystalline unit cells affect the superconducting energy-gap maximum Δ of $Bi_2Sr_2CaCu_2O_{8+\delta}$. In this material, quasi-periodic variations of unit cell geometry occur in the form of a bulk crystalline "supermodulation." Within each supermodulation period, a $\approx 9 \pm 1\%$ cosinusoidal variation in local Δ that is anticorrelated with the associated d_A variations, occurs. We show that phenomenological consistency would exist between these effects and the random Δ variations found near dopant atoms if the primary effect of the interstitial dopant atom is to displace the apical oxygen so as to diminish d_A or tilt the CuO_5 pyramid. These data reveal the mechanism of a strong, nonrandom out-of-plane effect on cuprate superconductivity at atomic scale. ***PNAS* 105**:3203 (2008)

• Intrinsic Inelastic Scattering with approach of the Mott insulator in Bi2Sr2CaCu2O8+δ.

Coulomb interactions between the carriers may provide the mechanism for enhanced unconventional superconductivity in the copper oxides. However, they simultaneously cause inelastic quasiparticle scattering that can destroy it. Understanding the evolution of this balance with doping is crucial because it is responsible for the rapidly diminishing critical temperature as the hole-density p is reduced towards the Mott insulating state. We

used tunnelling spectroscopy to measure the $T \rightarrow 0$ spectrum of electronic excitations $N(E)$ over a wide range of p in superconducting $Bi_2Sr_2CaCu_2O_{8+\delta}$. We introduced a parameterization for $N(E)$ based on a particle–hole symmetric anisotropic energy gap $\Delta(k)=\Delta_1(\cos(k_x)-\cos(k_y))/2$ plus an inelastic scattering rate that varies linearly with energy $\Gamma_2(E)=\alpha E$. This form of $N(E)$ enables successful parameterization of differential tunnelling conductance spectra throughout much of the $Bi_2Sr_2CaCu_2O_{8+\delta}$ phase diagram. We find that Δ_1 values rise with falling p along the familiar trajectory of excitations to the 'pseudogap' energy, whereas the energy-dependent inelastic scattering rate $\Gamma_2(E)=\alpha E$ seems to be an intrinsic property of the electronic structure and rises steeply for $p<16\%$. Such diverging inelastic scattering may play a key role in suppression of superconductivity in the copper oxides as the Mott insulating state is approached.
Nature Physics 4, 319 (2008).

- **How Cooper pairs vanish approaching the Mott insulator in $Bi_2Sr_2CaCu_2O_{8+\delta}$**

The antiferromagnetic ground state of copper oxide Mott insulators is achieved by localizing an electron at each copper atom in real space (r-space). Removing a small fraction of these electrons (hole doping) transforms this system into a superconducting fluid of delocalized Cooper pairs in momentum space (k-space). During this transformation, two distinctive classes of electronic excitations appear. At high energies, the mysterious 'pseudogap' excitations are found, whereas, at lower energies, Bogoliubov quasi-particles—the excitations resulting from the breaking of Cooper pairs—should exist. To explore this transformation, and to identify the two excitation types, we imaged the electronic structure of $Bi_2Sr_2CaCu_2O_{8+\delta}$ in r-space and k-space simultaneously. We find that although the low-energy excitations are indeed Bogoliubov quasi-particles, they occupy only a restricted region of k-space that shrinks rapidly with diminishing hole density. Concomitantly, spectral weight is transferred to higher energy r-space states that lack the characteristics of excitations from delocalized Cooper pairs. Instead, these states break translational and rotational symmetries locally at the atomic scale in an energy-independent way. We demonstrated that these unusual r-space excitations are, in fact, the pseudogap states. Thus, as the Mott insulating state is approached by decreasing the hole-density, the delocalized Cooper pairs vanish from k-space, to be replaced by locally translational- and rotational-symmetry-breaking pseudogap states in r-space. ***Nature 454,*** 1072 (2008).

Publications

1. Interplay of electron-lattice interactions and superconductivity in $Bi_2Sr_2CaCu_2O_{8+\delta}$, Jinho Lee, K. Fujita, K. McElroy, J.A. Slezak, M. Wang, Y. Aiura, H. Bando, M. Ishikado, T. Masui, J. -X. Zhu, A. V. Balatsky, H. Eisaki, S. Uchida, and J. C. Davis, ***Nature 442***, 546 (2006*).*
2. Effects of Pairing Potential Scattering on Fourier-Transformed Inelastic Tunneling Spectra of High-T_c Cuprate Superconductors with Bosonic Modes , J.-X. Zhu, K. McElroy, Jinho Lee, T. P. Devereaux, Q. Si, J. C. Davis, and A. V. Balatsky, ***Phys. Rev. Lett. 97***, 177001 (2006).
3. The Ground State of Pseudogap in Cuprates: $La_{1.875}Ba_{0.125}CuO_4$, T. Valla, A. V. Fedorov, J. C. Davis , Jinho Lee, and G. D. Gu, ***Science 314***, 1914 (2006*).*

4. An intrinsic bond-centered electronic glass with disperse unidirectional domains in underdoped cuprates, Y. Kohsaka, C. Taylor, A. Schmidt, K. Fujita, C. Lupien, T. Hanguri, H. Eisaki, S. Uchida, H. Takagi and J. C. Davis, ***Science 315***, 1380 (2007).
5. Quasi-particle Interference and Superconducting Gap in $Ca_{2x}Na_xCuO_2Cl_2$, T. Hanaguri, Y. Kohsaka, J. C. Davis, C. Lupien, I. Yamada, M. Azuma, M. Takano, K. Ohishi & H. Takagi, ***Nature Physics 3***, 865 (2007).
6. Imaging the impact on cuprate superconductivity of varying the inter-atomic distances within individual crystal unit-cells J. A. Slezak, Jinho Lee, K. McElroy, K. Fujita, B. M. Andersen, P. Hirschfeld, M. Wang, H. Eisaki, S. Uchida, and J. C. Davis ***Proc Natl. Acad. Sci.*** **105**:3203 (2008)
7. Evolution of the electronic excitation spectrum with strongly diminishing hole-density in superconducting $Bi_2Sr_2CaCu_2O_{8+\delta}$, J. Alldredge, Jinho Lee, K. McElroy, M. Wang, K. Fujita, Y. Kohsaka, C. Taylor, H. Eisaki, S. Uchida, P.J. Hirschfeld and J.C. Davis , to appear ***Nature Physics 4,*** 319 (2008).
8. How Cooper pairs vanish approaching the Mott insulator in $Bi_2Sr_2CaCu_2O_{8+\delta}$, Y. Kohsaka, C. Taylor, P. Wahl, A. Schmidt, Jhinhwan Lee, K. Fujita, J. Alldredge, Jinho Lee, K. McElroy, H. Eisaki, S. Uchida, D.-H. Lee, & J.C. Davis, ***Nature 454,*** 1072 (2008).

The Virtual Scanning Tunneling Microscope

Principal Investigator: David Goldhaber-Gordon
McCullough Building Rm 346
476 Lomita Mall
Stanford, CA 94305
goldhaber-gordon@stanford.edu

Abstract: 2D electrons in a semiconductor heterostructure are an excellent model system for studying the behavior of correlated electrons in reduced dimensions. However, we have few experimental probes of the spatial organization of electrons in such 2D sheets. I will describe a new type of scanning probe: the virtual scanning tunneling microscope (VSTM). The concept of the VSTM starts from the premise that an STM would be a good tool for mapping out local electronic structure in a 2D electron system (2DES) in a semiconductor heterostructure, just as it is for mobile electrons and adatoms on surfaces. The only problem is that an STM cannot be brought close enough to the 2DES to obtain a measurable tunneling current at low bias. We need to find a way to bring a tunneling probe closer to the 2DES.

I propose to use as the tunneling probe a second 2DES between the surface and the 2DES whose electronic organization we wish to map (see figure). Simulations show that with proper heterostructure design a moderate voltage on a surface gate should enhance tunneling from probe to sample 2DES by more than a factor of 1000. If a scannable metal tip is used in place of a fixed gate on the surface, it will create a "virtual tip" within the heterostructure – a region of enhanced tunneling which can be scanned over the entire sample 2DE.

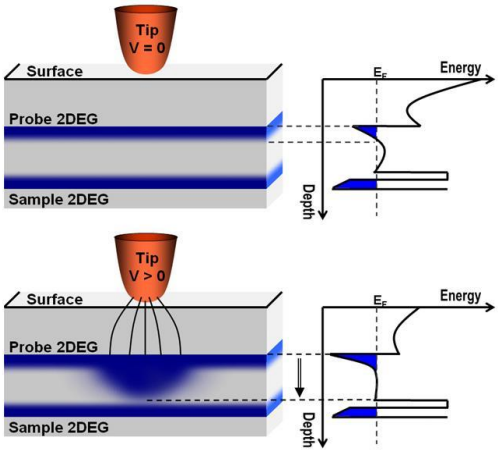

Sample schematic (left) and conduction band (right) showing how a positive bias on a scanned tip leads to induced local tunneling.

If the VSTM works, it will allow exploration of a broad range of predicted spatially-organized "stripe" and "bubble" states of 2D electrons. We will be able to extract not only spatial organization but also local spectroscopic information, just as with a conventional STM, but for structures that were formerly inaccessibly deep beneath the sample surface. I will discuss experimental progress toward this goal.

Determining the Origins of Electronic States in Semiconductor Nanostructures

Rachel S. Goldman[1] and Harley T. Johnson[2]
[1]Department of MSE, University of Michigan, Ann Arbor, MI 48109; rsgold@umich.edu
[2]Department of MechSE, University of Illinois, Urbana, IL 61801; htj@uiuc.edu

Program Scope

Determining the origins of atom-like electronic states in dimensionally-confined semiconductor structures is a classic problem in materials physics. Although advances in experimental probes and computational power have led to important breakthroughs, several critical fundamental questions regarding the effects of size, interface disorder, and point defects on the electronic states of semiconductor nanostructures remain unanswered. For example, how many atoms are needed in a nanostructure for it to cross over from behaving as an impurity state to a band of states? How do point defects alter the local electronic structure near embedded nanostructures? How does interface disorder contribute to the electronic states of a nanostructure? In this program, we are investigating these issues with a novel combination of state-of-the-art experiments and theory. Using a combination of plan-view and cross-sectional scanning tunneling microscopy, we will obtain 3D information about structure and electronic states associated with the nanostructures. The experimentally determined atomic positions will be used as input for real space order(N) moments-based tight-binding calculations. The computed local density of states will then be compared to spatially-resolved scanning tunneling spectroscopy (STS) data. Comparison between XSTM, STS, and tight-binding calculations is expected to elucidate the effects of nanostructure size, shape, strain, and interface disorder on the electronic band structure and confined states. Thus, this project is expected to reveal the origins of the atom-like electronic states in semiconductor nanostructures, as well as test the physical assumptions underlying the experimental and computational techniques.

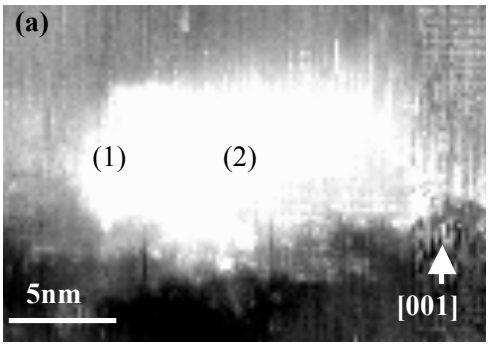

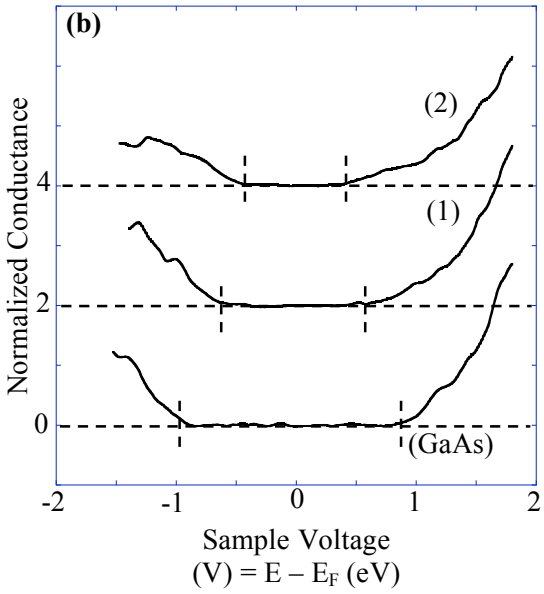

Fig. 1: (a) XSTM topographic image acquired at a sample bias of -2.0V. The gray-scale range displayed is 1 nm. Spatially resolved STS spectra from points (1) and (2) are plotted in (b) in comparison with a region of clean GaAs. The valence and conduction band edges are indicated by vertical dashed lines at negative and positive sample voltages, respectively.

Recent Progress and Future Plans

We have been working in four main areas: room temperature cross-sectional STM and STS of InAs/GaAs QDs, modeling using atomistic tight-binding and continuum electrostatic methods, room temperature plan-view STM and STS of InAs/GaAs QDs, and planning/preparing for low temperature STM and STS measurements. Each of these are described in detail below.

XSTM and STS of InAs/GaAs QDs and wetting layers

We have investigated the electronic states in individual (uncoupled) QDs and the surrounding wetting layers (WL) using a combination of XSTM and STS. XSTM images reveal uncoupled ellipse-shaped QDs with 18 ± 4 nm (9 ± 3 nm) major (minor) axes. Figure 1(a) shows an example XSTM image of a QD where the bright ellipse, with 16 nm (6nm) major (minor) axis, corresponds to the InAs QD in a GaAs matrix. In Fig. 1(b), the normalized conductance versus sample bias voltage is plotted for the edge and center of the QD shown in Fig. 1(a), in comparison with a region of clean GaAs. The GaAs spectrum, shown at the bottom of Fig. 1(b), displays well-defined band edges, with a bandgap of 1.45 eV, similar to that of bulk GaAs at room temperature. In Fig. 2(b), effective bandgaps of 1.09 eV (0.87 eV) are apparent at the QD edge (core) in plot 1 (2). Thus, a gradient in the effective bandgap is observed, with the effective bandgap decreasing laterally toward the QD core. In order to gain a more thorough understanding of the effective bandgap variation within QDs, it is necessary to measure the effective bandgap both laterally and in the growth direction.

Spatially-resolved STS spectra were collected from several ellipse-shaped QDs with 15 ± 5 nm major axes. The normalized conductance was then used to determine the energetic positions of the lowest electron and hole levels, and the resulting effective valence and conduction band edges as a function of lateral and vertical position within a QD are shown in Figs. 2(a) and 2(b). For comparison, the solid line shows the predicted bandgap variation for an undoped bulk-like $In_xGa_{1-x}As$ alloy. The $In_xGa_{1-x}As$ bandgap was calculated using values of x that were determined from XSTM measurements of [In] across similarly-sized QDs.[1] The lateral variations in the QD effective bandgap are shown in Fig. 2(a). In this case, the effective bandgap is narrowest at the QD center, possibly due to lateral variations in the well width and/or [In] in the QD.[2] Since lateral strain is predicted to increase the effective bandgap towards the QD core,[3] it is unlikely that strain is dominating the lateral effective bandgap variation. The vertical variations in the QD effective bandgap are shown in Fig. 2(b). Here, the effective bandgap is narrowest at the top of the QD, possibly due to [In] variations. Vertically, strain is predicted to increase the effective bandgap in the growth direction.[4] Therefore, it is unlikely that strain or vertical variations in the well width are dominating the effective bandgap variation in the growth direction, suggesting that [In] variations dominate the effective bandgap variations.

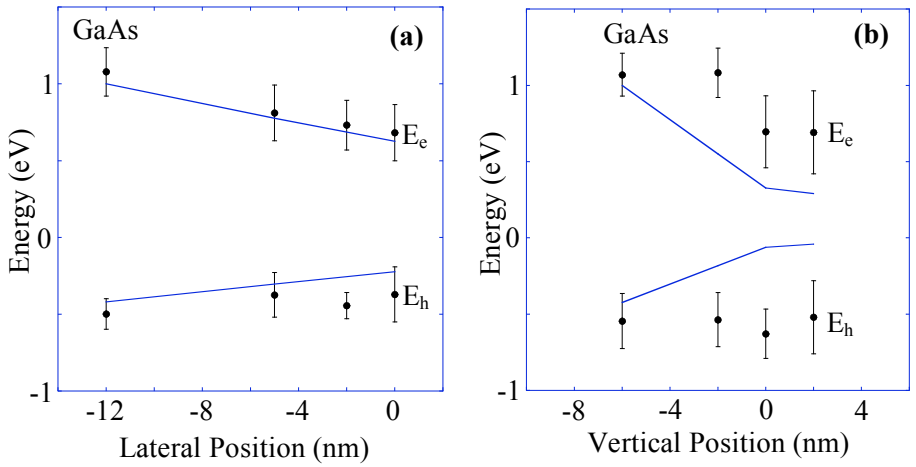

Fig. 2: Spatial variations in the lowest electron and hole energies in the GaAs and QD in the (a) horizontal and (b) vertical directions, with respect to the QD center. A calculated $In_xGa_{1-x}As$ confining potential with x=0.35, 0.65, and 0.6 at the QD edge, core, and top surface is indicated by the solid line.

We also examined the lateral and vertical variations in effective bandgap of the WL, as shown in Fig. 3. STS spectra were collected both laterally and vertically across WL InAs clusters. The normalized conductance was used to estimate the energetic positions of the effective valence and conduction bands, and the resulting effective bandgap variation as a

function of position within the WL laterally is shown in Fig. 3(a). In the plot, '0' marks the edge of a cluster of InAs. The effective bandgap decreases towards the center of the cluster, similar to the trend observed in the QDs. The vertical effective bandgap variation is plotted in Fig. 3(b). Vertically, there is limited variation in the WL effective bandgap, and the effective bandgap corresponds to $In_xGa_{1-x}As$, x=0.1±0.14. However, earlier XSTM investigations suggest that the [In] in the WL varies both vertically and laterally, due to In surface segregation and lateral In clustering.[5] For example, the fraction of group III sites occupied by In atoms has been reported to decrease from 30% to 10% over a vertical distance of 4nm within the WL. Thus, our observation of negligible vertical effective bandgap variation suggests that composition variations over a few nm length-scale have a negligible influence on the effective bandgap within the WL.

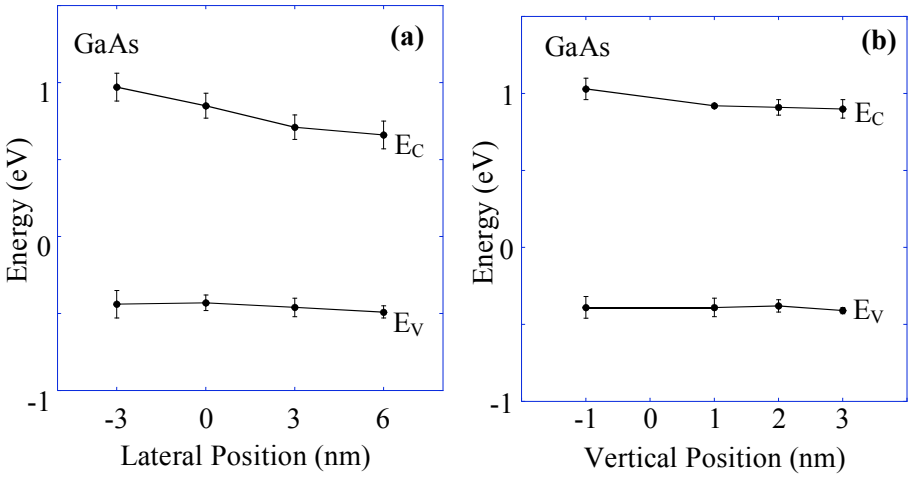

Fig. 3: Spatial variations the valence and conduction band edges in the WL (a) laterally and (a) vertically with respect to the WL edge.

Modeling: Moments-based order(N) tight binding and continuum electrostatic methods

The moments-based order(*N*) tight-binding method has been successfully demonstrated to study the effects of atomic scale defects and disorder on the local electronic structure in InAs/GaAs quantum dot systems.[6] The advantage of the method is that it can be used as a *computational* local atomic scale probe, and while an accurate $sp^3d^5s^*$ tight-binding parameterization is used, it is not necessary to directly diagonalize the Hamiltonian or resort to more expensive Green's function methods. Figure 4 shows the local density of states in various positions across an InAs/GaAs interface in a 3D nanostructure, where the atom positions were taken initially *directly from an XSTM image*.

Due to the proximity of the charged tip and the imaged surface, so-called tip-induced band bending often influences the measured apparent bandgaps. Preliminary

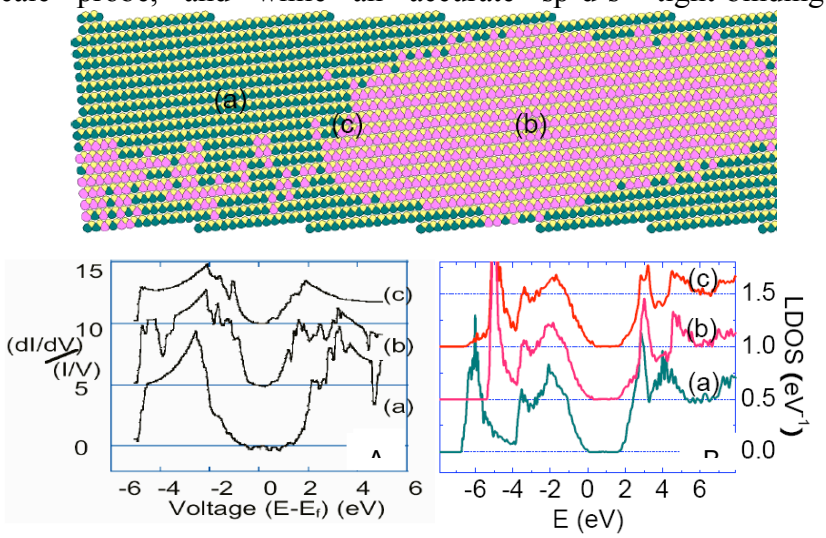

Fig. 4: Local densities of states computed by the tight-binding moments method (B, right) compared to measured dI/dV spectra (A, left). Atomic positions for the calculation are taken directly from the corresponding XSTM image. Pink indicates In atoms, green indicates Ga atoms, and yellow indicates As atoms. The local density of states shows features characteristic of the matrix (a), the quantum dot (b), and the interface (c). The figure shows a *direct comparison* between experiments and theory.

calculations of this tip-induced band-bending have been carried out recently using three-dimensional finite element analysis. A commercially available Poisson equation solver (COMSOL) has been used to simulate the potential drop from an idealized tip, across the gap, and into the dielectric substrate containing the cleaved quantum dot. The calculations reveal the strong sensitivity of the band-bending field on the tip-sample separation distance (ranging from about 0.5 eV at 3nm to 1 eV at 0.5nm), but the relative insensitivity of the effect to the different local alloy compositions in and around the quantum dot (less than 0.1eV difference in band-bending between the dot and the matrix at 0.5nm). In general, the band-bending shifts observed in the calculation, without accounting for quantum confinement effects, are in the tenths of an eV range of the observed experimental energy shifts, but final comparisons are still underway.

Plan-view STM and STS of InAs/GaAs quantum dots

We have also used plan-view STM and STS to examine QDs grown on a super-flat GaAs buffers.[7] As shown in Fig. 5 (left), these QDs have diameters ranging from 5 to 15 nm. In Fig. 5 (right), an example STS spectra acquired within a QD (blue line: E_g~1.3 eV), in comparison GaAs (black line: E_g ~1.8 eV). The QD effective E_g is much larger than the corresponding value for bulk InAs (~0.36 eV), suggesting the presence of confined states. Interestingly, most of the difference in effective bandgap between the QD and matrix is accommodated in the conduction band.

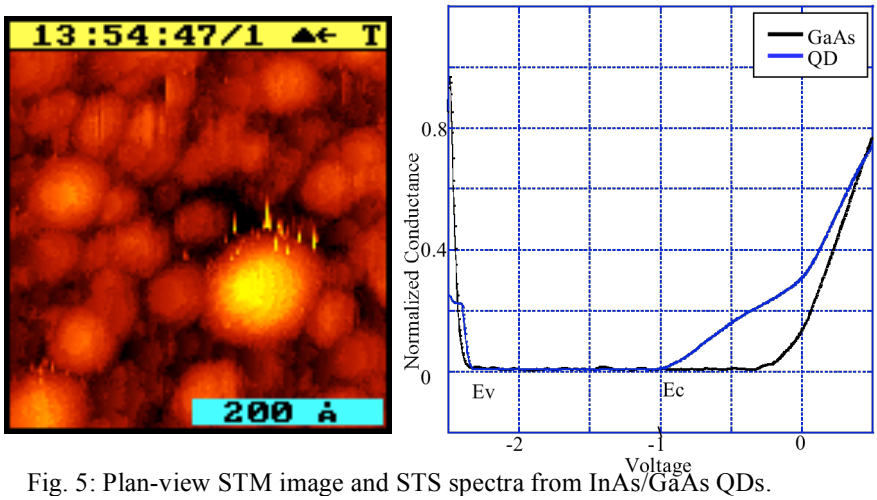

Fig. 5: Plan-view STM image and STS spectra from InAs/GaAs QDs.

Planning for low temperature experiments

Our XSTM and STS results to date are from room temperature experiments performed in the Goldman lab at U-Michigan. However, many of the confined states within quantum dots are expected to be separated by fractions of kT. Therefore, to improve the energy resolution of the spectra, it is necessary to perform XSTM and STS experiments at low temperatures. We have placed an order for an Omicron variable-temperature (VT) STM, to be housed in our lab at the University of Michigan, funded by the UM Provost's Office. Since we have previously used an Omicron VT-STM at Harvard University during Prof. Goldman's sabbatical (2005-2006 academic year), we have already designed an appropriate XSTM sample holder and cleaving approach. The new VT-STM is expected to be installed at U-Michigan by March, 2009.

References

[1] A. Lenz, R. Timm, H. Eisele, C. Hennig, S. K. Becker, R. L. Sellin, U. W. Pohl, D. Bimberg, and M. Dahne, *Appl. Phys. Lett.* 81, 5150 (2002).

[2] N. Liu, J. Tersoff, O. Baklenov, A. L. Holmes, Jr, and C. K. Shih, *Phys. Rev. Lett.* 84, 334 (2000).

[3] H. Shin, Y.-H. Yoo, and W. Lee, " *J. Phys. D: Appl. Phys.* 36, 2612 (2003).

[4] H. Shin, E. Yoon, Y.-H. Yoo, and W. Lee, *J. Phys. Soc. Jap.* 73, 3378 (2004).

[5] B. Lita, R. S. Goldman, J. D. Phillips, and P. K. Bhattacharya, *Appl. Phys. Lett.* 75, 2797 (1999).

[6] J.-Q. Lu, H. T. Johnson, V. D. Dasika, and R. S. Goldman, *Appl. Phys. Lett.* 88, 053109 (2006).

[7] W. Ye, S. Hanson, M. Reason, X. Weng, and R. S. Goldman, *J. Vac. Sci. Technol. B*, 23, 1736 (2005).

Toward the Realization of Room Temperature Ferromagnetic Semiconductors: A Spin-polarized STM Study

Lian Li
Physics Department, University of Wisconsin, Milwaukee, WI 53211
(lianli@uwm.edu)

Program Scope

Diluted ferromagnetic semiconductors (DMS) are a new class of semiconductors that exhibit long-range ferromagnetic ordering when alloyed with a few percent of a transition metal such as Mn [1]. They are being investigated for fabricating semiconductor spin devices that explore the use of electron *spin* to process information [2]. Using spin-polarized scanning tunneling microscopy and spectroscopy (SP-STM/STS), the goals of our program are to address two fundamental questions critical for the synthesis of a homogeneous room temperature DMS: 1) how are local magnetic moments created in semiconductors, and 2) how do these moments interact with each other to attain long range ferromagnetic ordering. During this budget period (2006-2008), we have made significant progress towards these objectives.

Since magnetism is typically associated with elements that have partially filled *d* and *f* shells, DMS can be created by doping semiconductors with transition metals. To this end, we have continued the investigation of the structural and magnetic properties of Mn/GaN system by SP-STM and STS using Fe coated W tip, and have demonstrated atomically resolved spin-dependent imaging on Mn_xGa_{1-x}/GaN(0001).

Magnetic moments can also be created by localized defect states in *s* and *p* shells materials, which could lead to ferromagnetism [3,4]. To explore this novel phenomenon, we have instigated an investigation on defect-induced magnetism in epitaxial graphene, a 2-dimensional sp^2 system ideal for SP-STM study. However, the existence of local magnetic moments alone does not necessarily result in ferromagnetic ordering; their interactions with the host also play an important role for the realization of room temperature ferromagnetism. In this part of research, we aim to address two critical issues: i) do these defect-induced moments couple ferromagnetically? and ii) is the coupling long-ranged in graphene?

Using a combination of SP-STM and first principles calculations, we are carrying out a systematic study of magnetism in epitaxial graphene, a material system that has shown great potential for applications in the next generation electronics [5]. We have determined the atomic structure of the 1st graphene layer grown on 6H-SiC(0001), a critical but controversial issue in the epitaxial growth of graphene. In addition, we have investigated the role of nitrogen in vacancy-induced magnetism in epitaxial graphene.

Recent Progress

1. Atomically resolved spin-dependent tunneling on Mn_xGa_{1-x}/GaN(0001)

In this work, we have investigated the growth of ultrathin Mn_xGa_{1-x} layers on the Ga-rich GaN(0001) pseudo-1x1 (denoted "1x1" hereafter) surface. The "1x1" surface is composed of more than two additional monolayers (ML) of Ga on top of the Ga-terminated GaN, typically found on films grown under Ga-rich conditions [6]. The presence of the Ga adlayer offers subsurface diffusion channels for lateral adatom transport during GaN MBE [7,8]. At 300K, the deposition of Mn onto this surface results in the growth of Mn_xGa_{1-x} layers. Using spin-polarized STM and first principles calculations, we found that at low Mn coverage, an antiferromagnetic $Mn_{0.11}Ga_{0.89}$ with a (3x3) surface reconstruction is formed. At higher Mn coverage, a $Mn_{3-x}Ga$ layer with an in-plane antiferromagnetic ordering is observed.

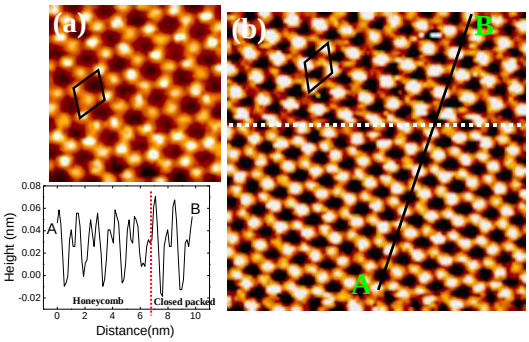

Fig. 1 (a) STM image of the (3x3) (V_s=-0.3 V, I_t=1.0 nA, 5 nm x 5 nm); (b) Honeycomb to closed packed as the bias changes from -0.5 V to -1.2 V at the dotted line (I_t=1.0 nA, 9.5 nm x 9.5 nm).

As shown in the STM images taken with a Fe coated W tip (Fig.1), the (3x3) exhibits a honeycomb structure for sample bias below -0.5 V, and a closed packed structure above. Based on first principles calculations, we determined that the difference in height (0.1 Å for -0.5 V and 0.3 Å for -1.2 V) between the neighboring bright and dark spots is due to the different spin states of the Mn, as explained in more details below.

Our calculations, shown in Fig. 2, suggest that the incorporation of Mn onto the "1x1" favors the formation of a covalently bonded bilayer structure by 0.55 eV/Mn. There is also a strong preference, by 0.41 eV/Mn, for the Ga adatom to be close to the substitutional Mn. More importantly, additional Mn atoms deposited on this newly formed Ga bilayer would also prefer (~0.05 eV/Mn) to be second nearest neighbors within the same plane, suggesting that the formation of a reconstruction is preferred rather than Mn clustering. Furthermore, the Mn atoms also favor antiferromagnetically coupling (by ~ 0.10 eV/Mn). We found that the smallest unit that can satisfy these conditions is a honeycomb structure with (3x3) periodicity (Fig. 2(b)), which is in excellent agreement with the STM observations.

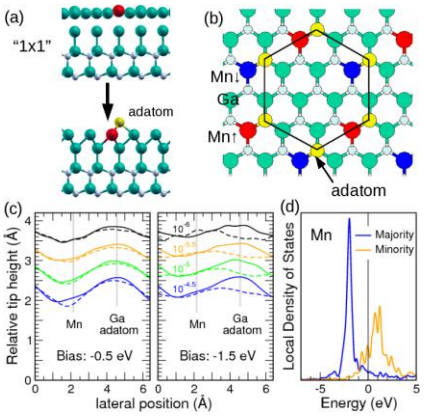

Fig. 2 (a)-(b) Ball-and-stick model showing the antiferromagnetic (3x3) ordering. (c) Calculated height difference between the spin-up and spin-down Ga-Mn, and (d) DOS for Mn.

The calculated densities of states (DOS) also provide direct insights into the bias-dependence of the images. In Fig. 2(c), the contours of constant density for two biases are plotted for the local majority (solid lines) and minority (dotted lines) states along a line through a Mn and its neighboring Ga adatom. The Ga is clearly the most prominent feature, but also observed is a distinct difference in height of the Mn atoms depending on their magnetic orientations: 0.1 Å for a bias of -0.5 eV and 0.3-0.4 Å for -

1.5 eV, in excellent agreement with the experimental data shown in Fig. 1. This difference is directly related to the Mn DOS, as shown in Fig. 2(d): the large peak in the majority DOS is not sampled for the smaller bias.

At Mn/Ga ratio of ~ 2-2.5, a $Mn_{3-x}Ga$ phase is observed (Fig. 3(a)). The growth mode is evidently layer-by-layer, where nevertheless the nucleation of second (and third) layer islands begins before the first (second) layer is completed. A close-up view of layers 1, 2, and the top islands (layer 3) marked by the crosses ("x") reveals no reconstruction. However, an alternating contrast between even and odd layers is observed, indicating an antiferromagnetic ordering for this phase. This can be more clearly seen in the dI/dV image (Fig. 3(b)). Layers 1, 2 and 3 alternate in contrast from dark to bright to dark, respectively, suggesting that the magnetization is also in-plane. These results clearly demonstrate our capabilities for spin-dependent imaging at the atomic scale.

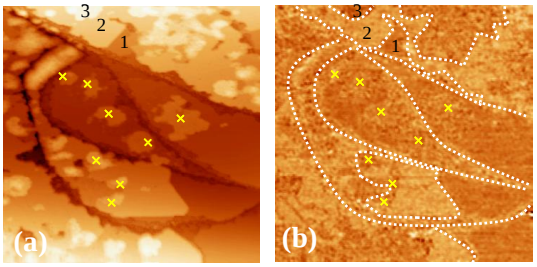

Fig. 3 (a) STM image of $Mn_{3-x}Ga$ (V_s= -1.3 V, I_t=1.0 nA, image size: 200 nm x 200 nm). (b) dI/dV image taken simultaneously using a Fe/W tip . Dotted lines highlight boundaries between different layers.

2. The effect of nitrogen on vacancy-induced magnetism in epitaxial graphene

In this part of research, we address two important issues in magnetism in graphene: 1) the nature of defect-induced local moments, and 2) the effect of adsorbates such as N on the magnetic ordering. The removal of one carbon atom from graphene creates the simplest defect: a vacancy, as shown in Fig. 4. As a result, localized states are created around the vacancy, leading to a magnetic moment of 0.84 μ_B. Furthermore, our calculations also show that the presence and precise position of a single N atom near a carbon vacancy in graphene can have profound effects on the spin configurations of the system. We found that the vacancy-induced magnetic moments can be controlled by the presence of nitrogen near the vacancy. In addition, the net magnetic moment varies with not only the presence of N, but also its relative distance from the vacancy. For example, in the center configuration in Fig. 4, where the N is positioned at the nearest site to the vacancy, no net magnetic moment is found. In configurations where the N atom and vacancy are further apart, as shown on the right in the figure, a localized magnetic moment is found, similar to that of the vacancy-only case, however with an enhanced net magnetic moment of 1.09 μ_B. These results indicate that the engineering of complexes of vacancy defects and impurities may provide a unique way to enhance the magnetism in graphene.

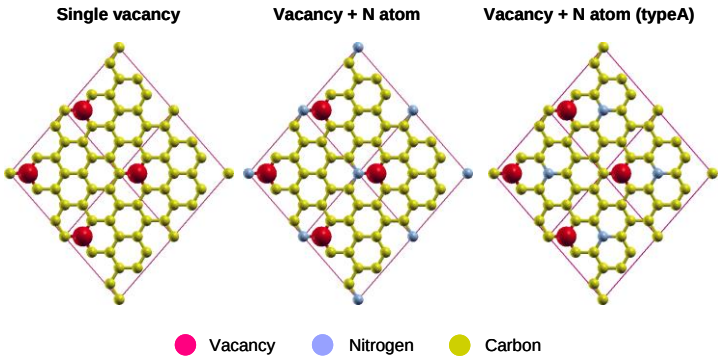

Fig. 4 Ball-and-stick model of the vacancy and N-vacancy complex in graphene.

Future Plans

Now that we have demonstrated atomic resolution in spin-polarized STM, we will continue with the work already in progress on the Mn(Cr)/graphene systems to determine the role of host electronic structure in mediating ferromagnetic coupling between transition metal dopants.

We will also continue to investigate the role of adsorbates other than nitrogen, e.g. hydrogen, in defect induced magnetism in epitaxial graphene using spin-polarized scanning tunneling spectroscopy and first principles calculations.

References

1. T. Dietl, H. Ohno, F. Matsukura, J. Cibert, and D. Ferrand, "Zener model description of ferromagnetism in zinc-blende magnetic semiconductor", Science **287**, 1019 (2000).
2. S. A. Wolf, D. D. Awschalom, R. A. Buhrman, J. M. Daughton, S. von Molnar, M. L. Roukes, A. Y. Chtchelkanova, and D. M. Treger, "Spintronics: A spin-based electronics vision for the future", Science **294**, 1488 (2001).
3. P. Esquinazi et al., "Induced magnetic ordering by proton irradiation in graphite", Phys. Rev. Lett. **91**, 227201 (2003).
4. L. Pisan, B. Montanari, and N. M. Harrison, "A defective graphene phase predicted to be a room temperature ferromagnetic semiconductor", New J. Phy. **10**, 033002 (2008).
5. A. K. Geim and A. H. MacDonald, "Graphene: Exploring carbon flatland", Phys. Today **60**, 35 (2007).
6. J. E. Northrup, J. Neugebauer, R. M. Feenstra, and A. R. Smith, "Structure of GaN(0001): The laterally contracted Ga bilayer model", Phys. Rev. B **61**, 9932 (2000).
7. J. Neugebauer, T. K. Zywietz, M. Scheffler, J. E. Northrup, H. Chen, R. M. Feenstra, "Adatom kinetics on and below the surface: The existence of a new diffusion channel", Phys. Rev. Lett. **90**, 056101 (2003).
8. "Atomistic view of the autosurfactant effect during GaN epitaxy", S. T. King, M. Weinert, and L. Li, Phys. Rev. Lett. **98**, 206106 (2007).

DOE Sponsored Publications in 2007-2008

1. "The effect of nitrogen on vacancy-induced magnetism in epitaxial graphene", S. H. Rhim, Y. Qi, G. F. Sun, M. Weinert, and L. Li (to be submitted).

2. "A spin-polarized STM study of Mn_xGa_{1-x} on GaN(0001)", Y. Qi, G. F. Sun, M. Weinert, and L. Li, Appl. Phys. Lett. (submitted).

3. "Electron standing waves on GaN(0001)-pseudo (1x1) surface: A FT-STM study at room temperature", G. F. Sun, Y. Qi, J. F. Jia, Q. K. Xue, M. Weinert , and L. Li, Phys. Rev. B (submitted).

4. "Incorporation of Ge on GaN(0001), Y. Qi, S. T. King, S. H. Cheng, M. Weinert, L. Li, Appl. Phys. Lett. **92**, 111918 (2008).

5. "Atomistic view of the autosurfactant effect during GaN epitaxy", S. T. King, M. Weinert, and L. Li, Phys. Rev. Lett. **98**, 206106 (2007).

Strain induced Atomic Surface Structure of Compound Semiconductor Alloys

Joanna Millunchick*, Jessica E. Bickel*, John C. Thomas* , Lee Sears *, Normand A. Modine+, Chris A. Pearson^, Anton VanDerVen*

joannamm@umich.edu, jebickel@umich.edu, johnct@umich.edu, leesears@umich.edu, namodin@sandia.gov, pear@umflint.edu, avdv@umich.edu,

*Department of Materials Science and Engineering, University of Michigan, Ann Arbor, MI 48105
+Sandia National Laboratories, Albuquerque, NM 87185
^ Department of Computer Science, Engineering Science and Physics, University of Michigan-Flint, Flint, MI 48502

Program Scope

The atomic surface structure of compound semiconductors plays an important role in the growth of alloyed thin films and devices, influencing both the macroscopic properties such as the compositional uniformity and the morphology of the grown material and microscopic atomic positions through ordering and surface segregation of individual species. Thus, understanding the surface structure is a vital step towards controlling the growth of electronic and optoelectronic devices made of III-V semiconductors where planar and compositionally abrupt interfaces are required to obtain optimal device properties. A great deal of work has been aimed at understanding binary compound semiconductors such as GaAs, InAs, and GaSb, however, less is known about the surface structure of ternary alloys such as InGaAs and GaAsSb.

This program is a combined experimental and theoretical effort that strives to examine and understand the surface structure of semiconductor alloys of InGaAs and GaAsSb. Experimentally, we study the atomic structure of both InGaAs and GaAsSb alloy surfaces. Specifically, we wish to determine the incorporation of the constituent species in the growing film, and the impact of the atomic surface structure on subsequent nanostructural evolution. Theoretically, we perform density functional theory (DFT) calculations and Monte Carlo (MC) simulations to explain some of the recent alloy surface experimental findings. Specifically, we wish to establish the details of the atomic surface structure. In both aspects of the work, we ultimately wish to understand growth mechanisms such as surface segregation in these strained alloy layers.

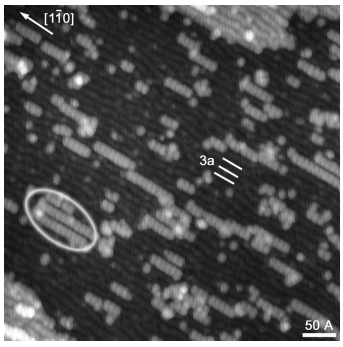

Figure 1: Filled state in vacuo 500 x 500 Å STM (-2.99 V, 100 pA) image of a h=40 ML $In_{0.81}Ga_{0.19}As$/InP film deposited at T=475°C, R=0.5 ML/s, F_{As4}=2.5 ML/s, and V/III flux ratio=5. (nx3) reconstructions are denoted by hash marks, and regions of β(2x4) domains are circled.

Recent Progress

Strain Induced Coexistence of Surface Reconstructions

Elastic strain in lattice mismatched films has an influence on the final atomic surface structure in III-V compound semiconductors. For example, thin films of $In_{0.81}Ga_{0.19}As$/InP, grown by molecular beam epitaxy and imaged by *in vacuo* scanning tunneling microscopy (STM), are observed to possess surfaces that consist of multiple reconstruction domains; small anisotropic regions of β2(2x4) in a matrix of a disordered (nx3) reconstruction, as shown in Fig. 1. The shape and size distribution of these domains shows that the coexistence of these reconstructions is thermodynamically stabilized by the

elastic relaxation between the reconstruction domains. Furthermore, the boundary energy between the domains is anisotropic, and varies with the growth temperature, indicating that the capacity for configurational or vibrational entropy along the $[1\bar{1}0]$ direction is higher than for the [110].

Elastic relaxation at step edges alters the atomic surface structure in GaAsSb films as well. STM of Sb-capped GaAs shows the coexistence of different surface reconstructions (Fig. 2a). The majority of the surface consists of an α2(2x4) reconstruction typically observed for GaAs(001) surfaces, while at step edges, an α(4x3) reconstruction, common for GaSb(001), is observed. DFT calculations show that the (4x3) reconstruction is stabilized when the lattice parameter is that of bulk GaSb (Fig. 2b). When the GaSb crystal is constrained to the GaAs lattice parameter (Fig. 2c), the stability of the different reconstructions changes dramatically. The lines shift relative to each other to the point that the (4x3) reconstruction is stable only over a very small Sb chemical potential (μ_{Sb}) range while the (2x4) is stable over most of experimentally achievable range. The shift in stability of the GaSb surface reconstructions at the GaSb and GaAs lattice parameters is experimentally demonstrated by the appearance of both the α2(2x4) and (4x3) reconstructions in the Sb/GaAs films, with the (4x3) appearing at step edges where elastic relaxation occurs, and the α2(2x4) appearing in areas where the lattice parameter is constrained, i.e., within large terraces or near the center of large 2D islands.

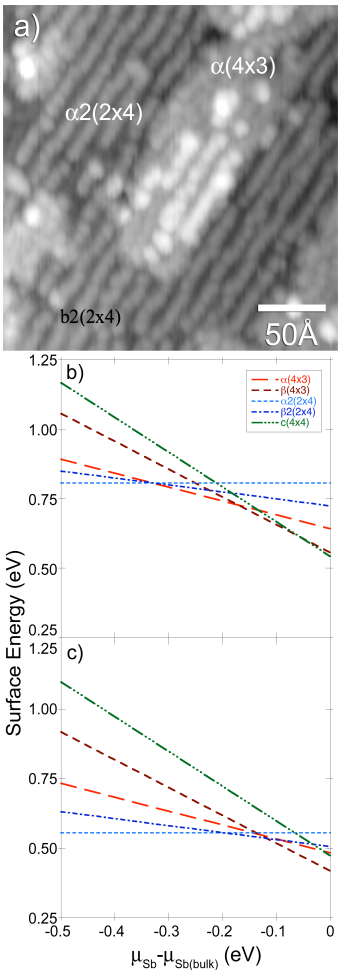

Figure 2: (a) STM of 0.8ML Sb/GaAs deposited at T=525°C at F_{Sb}=0.36ML/s. (b-c) Energy curves of various (2x4) and (4x3) reconstructions as a function of Sb chemical potential at the (b) GaSb and (c) GaAs lattice parameters

Atomic Mismatch and Configurational Entropy

In addition to atomic surface structure, disorder on the surface can contribute significantly to optoelectronic, thermodynamic, kinetic and interfacial properties of epitaxial thin films, especially at the nano-scale. In this work, the effect of finite temperature on the free energy of surface reconstructions is investigated in order to determine the role of entropy in affecting surface stoichiometry and atomic ordering. As a model system, we consider the a2(2x4) and b2(2x4) reconstructions on the (001) surface of In doped GaAs. A first principles model Hamiltonian is developed within the cluster expansion formalism and applied in equilibrium MC simulations to predict the equilibrium degree of long and short-rang order between surface dimers and segregated In ions. MC simulations show that the As chemical potential corresponding to the transition from the a2(2x4) reconstruction to b2(2x4) is very sensitive to the In chemical potential: high concentrations of segregated In ions (due to a high In chemical potential) stabilizes the a2(2x4) over the b2(2x4) as can be seen in the calculated phase diagram of Fig. 3. Indium segregation also plays an important role in modifying short and long-range between the surface dimers of the a2(2x4) reconstruction. On pure GaAs, surface dimers are more or less disordered at finite temperature, with the fraction of unit cells characterized by zig-zag dimer ordering comprising about 50% at both room temperature and typical growth temperatures. However, when indium is allowed to surface segregate, the fraction of zig-zag unit cells can approache 75% at room temperature, decreasing to 55% at typical growth temperatures. The enhanced dimer

ordering in the presence of surface segregated indium ions arises from a strong energetic coupling between As dimers and subsurface In ions. Due to its large size, surface segregated In ions preferentially order in a zig-zag arrangement to minimize misfit strain and this ordering in turn locks in a zig-zag ordering of the As surface dimers.

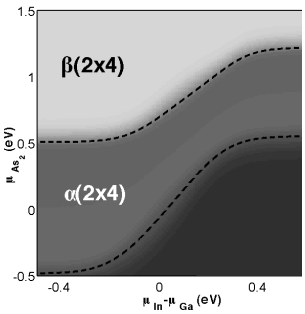

Figure 3: Reconstruction map of InGaAs surface at 460°C calculated from Monte Carlo simulation. Brightness indicates dimer coverage; the darkest region is an unphysical regime.

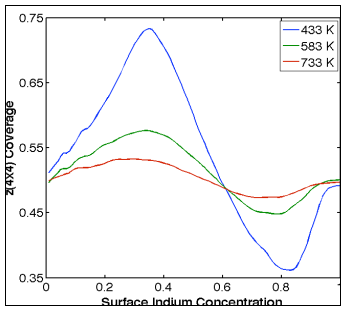

Figure 4: Fraction of unit cells exhibiting zig-zag ordering, at 50% dimer coverage (corresponding to a2(2x4)). Temperatures range from typical growth temperature (red) to slightly above imaging temperatures (blue).

Growth of alloy systems

Atomic surface structure alters the energy of the surface, and thus has an impact on subsequent film growth. InGaAs grown by molecular beam epitaxy and imaged via STM are observed to develop either islands or pits on the surface after some critical thickness, depending on the composition of the film. Figure 5 shows AFM images of a 16 monolayer (ML) thick $In_{0.27}Ga_{0.73}As$/GaAs film that has developed islands (Fig. 5a), and a 15 ML thick $In_{0.8}Ga_{0.2}As$/InP that has developed pits (Fig. 5b). Both films were grown under similar growth conditions and the same amount of lattice mismatch. The higher In content film has a lower surface energy, which drives pit rather than island formation. Once the pits form, their behavior as a function of growth conditions is similar to that of islanding. Namely, the critical thickness for pit formation decreases with increasing temperature, and the average size of the pits are inversely proportional to the growth rate. Once the pits develop, they act as preferential nucleation sites for 3D islands, which tend to form near β2(2x4) reconstructions (Fig. 6). The correlation between the (2x4) reconstruction and island nucleation suggests that the (2x4) reconstruction relieves some residual strain in the film.

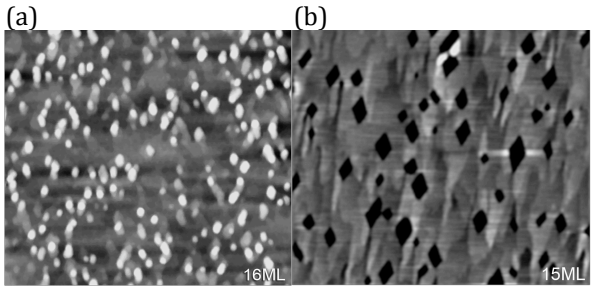

Figure 5: 1x1μm AFM images comparing the development of the surface morphology on the surface of (a) $In_{0.27}Ga_{0.73}As$ and (b) $In_{0.81}Ga_{0.19}As$ films grown at T=510°C, R=0.77 ML/s, and V/III flux ratio=4 for various thicknesses as noted. The height scale is 4 nm for (a) and 14 nm for (b).

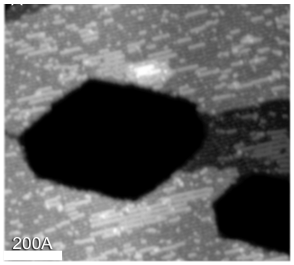

Figure 6: Filled state (-2.88 V, 100 pA) 500 x 500 Å STM images of a h=20ML $In_{0.81}Ga_{0.19}As$/InP film deposited at T=495°C, R=0.5 ML/s, F_{As4}=2.2 ML/s, and V/III flux ratio=4.

Future Work

One of the most important avenues to further understanding alloy surfaces is a fully cataloguing of the atomic structure of observed surface reconstructions. We have undertaken a new approach in this area whereby we computationally enumerate all symmetrically unique unit cells of a given size that adhere to the electron counting rule and a few basic structural requirements. We then employ DFT to test the stability of these candidate structures. We are currently applying this technique to uncovering the elusive (4x3) structure observed on InGaAs.

In addition to continuing the work described above, we are initiating new experiments and calculations to examine how atomic surface structure affects subsequent dislocation injection in highly mismatched films. Experimental results show that the Sb overpressure, which strongly affects the atomic surface structures, directly impacts the dislocations that form at the interface. In this work, we will use DFT to calculate the lowest energy dislocation in a GaSb/GaAs film and to examine the energy of this dislocation in proximity with various surface reconstructions.

Related Publications

1. J. Bickel, N. A. Modine, A. Van der Ven, Chris Pearson, J. Mirecki Millunchick, " Atomic size mismatch strain induced surface reconstructions," *Applied Physics Letters* **92** 062104 (2008)
2. J. Bickel, N. A. Modine, Chris Pearson, J. Mirecki Millunchick, " Elastically induced coexistence of surface reconstructions," *Physical Review B* **77** 125308 (2008)
3. L.E. Sears, J.M. Millunchick, C. Pearson, " The Coexistence of Surface Reconstruction Domains on Strained Heteroepitaxial Films," *Journal of Vacuum Science and Technology B (in press)*
4. J. Bickel, Chris Pearson, J. Mirecki Millunchick," Sb incorporation at GaAs(001)-(2x4) surfaces," submitted to Surface Science
5. L. E. Sears, A. Riposan, J. M. Millunchick, " Inverse Stranski Krastanov growth in InGaAs/InP," submitted to *Nano Letters*

Division of Materials Science and Engineering
Office of Basic Energy Science
US Department of Energy

1. DOE award # and name of the recipient (Institution)

DE-FG02-07ER46480
The Virginia Polytechnic Institute and State University

2. Project Title and name of the PIs

Correlation of bulk dielectric and piezoelectric properties to the local scale phase transformations, domain morphology, and crystal structure in modified $(Na,K)NbO_3$ nano-grain textured ceramics

Shashank Priya (PI) and Dwight Viehland (Co-PI)
304A Holden Hall, Materials Science and Engineering, Blacksburg, VA 24061.
Email: spriya@vt.edu; dviehlan@vt.edu

3. Program Scope

The objective of this research program is to discover the fundamental mechanisms and atomic level phenomenon's that can lead towards realization of giant piezoelectric response in lead free ferroelectrics. It will investigate the mechanisms controlling the piezoelectric response in lead free systems by systematically studying the local domain and crystal structure and their effect on properties. Textured nano-grain ceramics in the Li-modified $(Na,K)NbO_3$ system close to morphotrophic phase boundaries (MPBs) will be used as the representative lead free system. These compositions will be synthesized ranging from random to fully textured form to have complete set of samples required for microscopy and diffraction studies. Nanoscale domain structure and its ferroelectric response will be studied as a function of electric field, pressure and temperature to identify the phase transformational sequences in the MPB region and to determine the presence of (any) intermediate bridging phases. Another challenging issue confronted in this research program is to formulate the mechanism of domain engineering in the lead free materials. The crystal structure in the oriented single crystals will be investigated under varying electric field and temperature conditions to identify the lattice parameters, and domain distributions for various crystallographic directions.

4. Recent Progress

We began our investigations by determining the feasibility of finding monoclinic bridging phases in Pb-free systems. We have used x-ray diffraction and various microsctural probes. Initially, we choice to study crystals of the classic ferroelectric $BaTiO_3$ and to establish whether or not domain engineered states exist. We cooled the crystals under an electric field of

1kV/cm applied along the (001) direction to temperatures in the range of 260-300K. Mesh scans revealed the signatures of a monoclinic C structure. On removal of the field, this Mc phase in $BaTiO_3$ was found to be stable. These results clearly demonstrate the presence of a previously unknown phase in this classic perovskite system, which can only be obtained by domain engineering. It establishes the feasibility of finding low symmetry bridging phases in other Pb-free perovskite systems by a domain engineering approach. Investigations of domain engineered states by electron microscopy then showed the importance of domain miniaturization to nano-meter length scales, resulting in a structurally mixed state.

We concurrently performed studies on polymorphic phase transitions, structural changes and piezoelectric properties of $(K,Na,Li)NbO_3$ - $BaTiO_3$ [(1-x)KNLN-xBT] randomly oriented lead-free ceramics. Our results demonstrate that high piezoelectric properties are achieved in this system when the composition lies on a boundary between ferroelectric orthorhombic (O) and tetragonal (T) phases. By shifting the O-T boundary by substitutions, high piezoelectric properties can be obtained at desired temperatures following the relationship: $d_{33,RT}(pC/N)=306.21-1.02T_{O-T}(^oC)$, where d_{33} is the longitudinal piezoelectric constant and RT room temperature. Using Rietveld and powder diffraction analysis a correlation was established between the piezoelectric response, fraction of O and T phases, and KNN ratio for three different systems of $(Na,K)NbO_3$ – $BaTiO_3$ (KNN – BT), KNN – $LiNbO_3$ (LN) and KNLN – BT.

We have also modeled the sintering behavior of $(K, Na)NbO_3$ (KNN) based ceramics in the systems of KNN, $(K, Na, Li)NbO_3$ (KNLN) and KNLN-$xBaTiO_3$ (KNLN-BT). Our studies clearly show the evolution of microstructure in this system. Three stages of sintering were indentified using the time and temperature dependent scanning electron microscopy experiments. The first stage corresponds to re-arrangement of random shape particle to form stack of plate type particles. The second stage is characterized by rapid grain growth promoted by formation of liquid phase. The liquid phase formation was found to be related to Na_2O evaporation whose composition was identified to be "$0.995(K_{0.48}Na_{0.025}Li_{0.04})NbO_{2.7725}$-$0.005BaTiO_3$". Figure 1 shows the distribution of liquid phase in the KNLN matrix and corresponding EDS analysis. This is an important finding and shows the clear difference between the evolution of microstructure in Pb-based and Pb-free ceramics. In the final stage of sintering, densification slows and microstructural coarsening becomes the dominant process. It was clarified by Lifshitz, Slyozov, and Wagner (LSW) theory that diffusion-controlled coarsening was the dominant mechanism in KNN based ceramics. The volume fraction of liquid phase is an important parameter to obtain dense and uniform microstructure. In past, researchers have focused their attention on finding sintering aids for achieving higher density. However, our results show that just by controlling the formation of liquid phase we can achieve dense KNN-based ceramics. These pure and dense KNN ceramics offer the opportunity of comparative study with PZTs which can be easily densified.

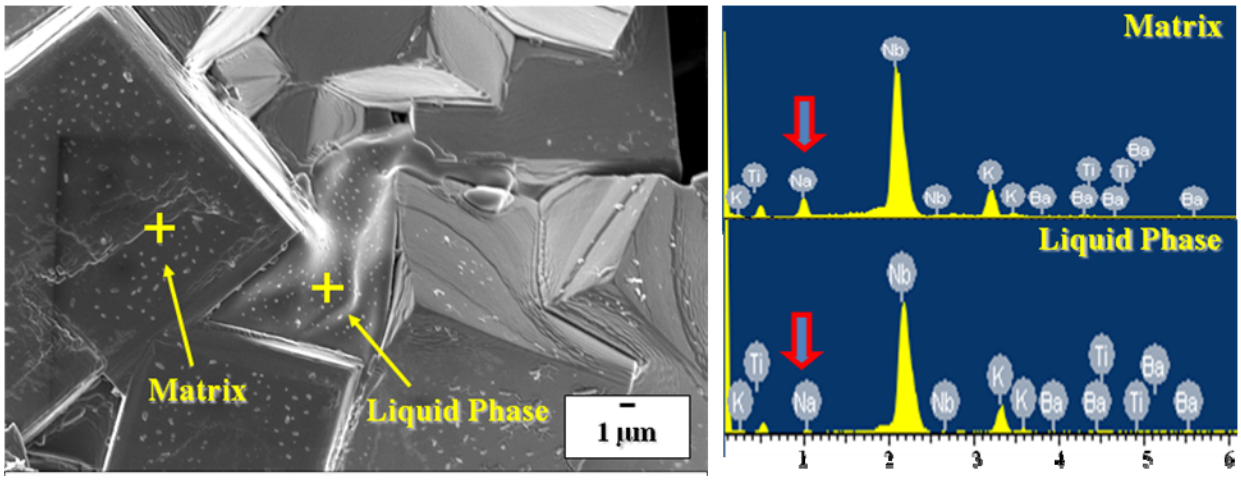

Figure 1: SEM image of the (1-x)KNLN-xBT (x=0.005) specimen sintered at 1150 ^{o}C for 0 min and EDS spectra taken from matrix and liquid phase.

In this presentation, we will show the data highlighting all these achievements. We will also cover some of the ongoing experiments which shed light on the nature of domain states in KNN ceramics.

5. Future Plans

We are presently beginning investigations of domain engineered states in $KNbO_3$ (KN) single crystals. We will determine whether low symmetry monoclinic structurally bridging phases exist in this end member of the KNN solid solution. We will compare the structural results to investigations of the domain stability by various microscopies. We will then expand this investigation to the KNN system, so that we can determine the relative importance of low symmetry phases in systems that have polymorphic phase boundaries. Studies of the symmetry of such domain engineered states is vital in order to determine the textures required in highly grain oriented ceramics that allow for access of intermediate structurally bridging states.

We have made some progress in achieving textured KNN ceramics as shown in Fig. 2. Please note the difference in grain size between Fig. 1 and 2. The textured grain sizes are in the range of ~10-20µm. We are now improving our synthesis process for seed crystals and their alignment in the matrix. The textured samples will be used for structural studies using reciprocal space mapping. We will also provide the samples to our colleagues for Raman spectroscopy which can deterministically elucidate the nature of domain states. We have also started to investigate the domain structures using HRTEM. The goal is to conduct the comparative study on domain structures in textured ceramics over various length scales for different electrical histories and orientations. The correlation between the structural observations and microscopic properties can then be tied by extracting the crystallographic data from the high resolution microscopy.

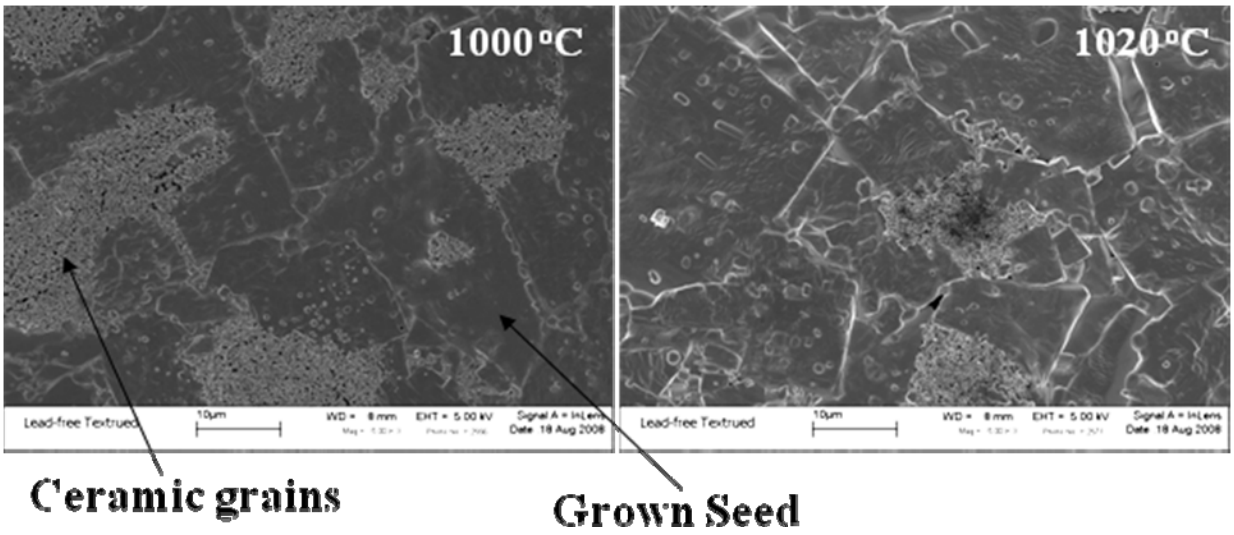

Figure 2: Microstructure of textured KNN ceramics at two different sintering temperatures.

6. References to publications of DOE sponsored research

1. "Domain-engineered monoclinic phases in the classic ferroelectric BaTiO3", H. Cao, C. DeVreugd, S. Priya, J.F. Li and D. Viehland, (in preparation).
2. C.-W. Ahn, S. Nahm, M. Karmarkar, D. Viehland, D.-H. Kang, K.-S. Bae and S. Priya, "Effect of CuO and MnO_2 on sintering temperature, microstructure, and piezoelectric properties of $0.95(K_{0.5}Na_{0.5})NbO_3$–$0.05BaTiO_3$ ceramics", Mater. Lett. 62, 3594-3596 (2008).
3. C. W. Ahn, M. Karmarkar, D. Viehland, D. H. Kang, K. S. Bae, S. Priya, "Low Temperature Sintering and Piezoelectric Properties of CuO-doped $(K_{0.5}Na_{0.5})NbO_3$ Ceramics" Ferroelectrics, (2008) (accepted).
4. C. W. Ahn, C. H. Choi, H. Y. Park, S. Nahm, S. Priya, "Dielectric and Piezoelectric Properties of $(1-x)(Na_{0.5}K_{0.5})NbO_3$-$xBaTiO_3$ Ceramics", J. Mat. Sci. (accepted).
5. C. –W. Ahn, C.-S. Park, D. Viehland, S. Nahm, D.-H. Kang, K.-S. Bae, and S. Priya "Correlation between Phase Transitions and Piezoelectric Properties in Lead-Free $(K,Na,Li)NbO_3$- $BaTiO_3$ Ceramics", Jpn. J. Appl. Phys. (submitted).

Microstructural Origins of the Dielectric Behavior of Ferroelectric Thin Films

Susanne Stemmer

stemmer@mrl.ucsb.edu

Materials Department, University of California, Santa Barbara, CA 93106-5050

Program Scope

The objective of the project is a comprehensive research program aimed at an atomic level understanding of the strongly modified properties of ferroelectric thin films. The project concentrates on interfaces and materials with known atomic arrangements and microstructures. These are obtained by controlled thin film growth experiments and by utilizing the unique capabilities of scanning transmission electron microscopy techniques, in particular high-angle annular dark-field (HAADF) imaging. We are working on establishing a quantitative understanding of HAADF image contrast to analyze defects in films and at interfaces. We are also investigating the stability of ferroelectric polarization in ultrathin films with metal electrodes and the influence of interface atomic structure on the transport properties across them.

Recent Progress

a) Epitaxial $SrTiO_3$ Tunnel Junctions

In the present project period we have focused on the properties of ultrathin ferroelectric thin films. We use $SrTiO_3$ as a model thin film because it is a prototype, incipient ferroelectric with the perovskite structure. Tunnel junctions need to be epitaxial, free of pinholes and other conduction paths and have smooth interfaces with the electrodes. The quality of the $Pt/SrTiO_3$ interface was characterized by transmission electron microscopy and the current transport studied as a function of temperature and bias field. Figure 1 shows cross-section HAADF-STEM images of the $Pt/SrTiO_3$ interface. Atomic resolution HAADF images confirmed the cube-on-cube epitaxy and an abrupt interface. At low voltages the junctions showed excellent insulting properties and temperature dependent, non-linear current-voltage characteristics (Fig. 1b). If junctions were biased to high fields (> 1.25 MV/cm) current hysteresis was observed.

b) Quantifying HAADF/STEM Image Contrast

Complete understanding of atomic resolution high-angle annular dark-field (Z-contrast) images requires quantitative agreement between simulations and experiments. In the present project period we have shown that intensity variations can be placed on an absolute scale by normalizing the measured image intensities to the incident beam. We showed that measurement of the incident beam intensity and the HAADF signal is possible using an annular dark field detector that has single electron sensitivity and an output voltage that is directly proportional to the electron flux averaged over time (intensity). This HAADF detector greatly facilitates quantitative measurements. Image simulations were carried out by our collaborators, Prof. Les Allen (U. Melbourne) and Dr. Scott Findlay (U. Tokyo).

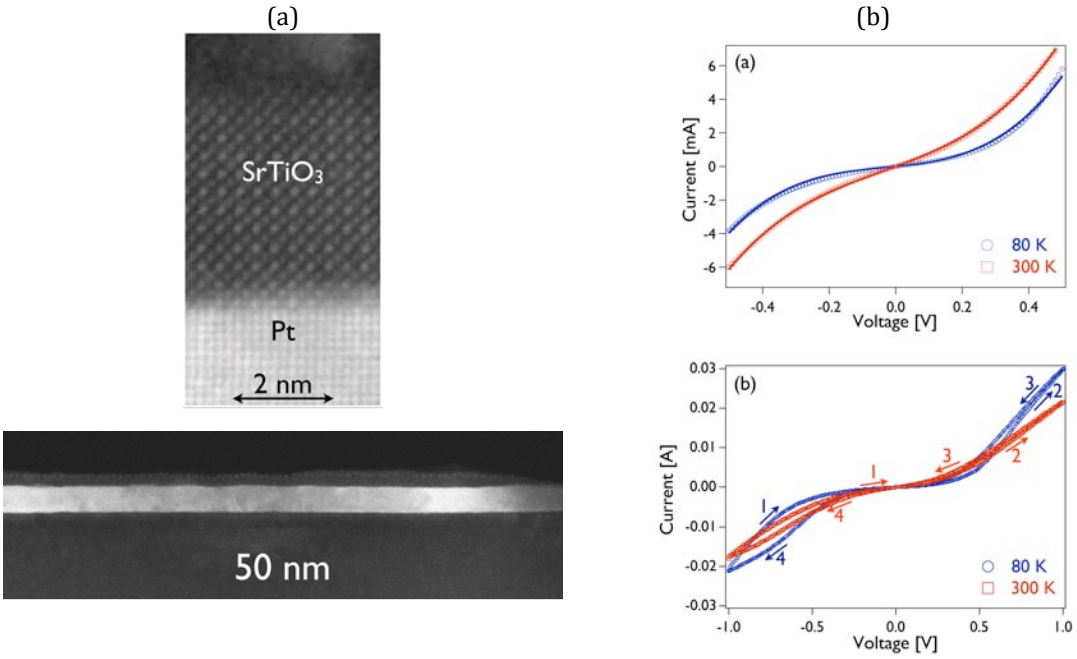

Figure 1: (a) Top: Cross-sectional HAADF image of the $Pt/SrTiO_3$ interface. Because of the strong atomic number contrast, the Pt appears very bright. Bottom: A high-resolution HAADF image of the $Pt/SrTiO_3$ interface along <100>. (b) Current-voltage characteristics (double-sweep) of $Pt/SrTiO_3$(4 nm)/Pt tunnel junction devices at 80 K and 300 K and bias voltages between – 0.5 V and + 0.5 V (a) and – 1 V to 1 V (b). The solid lines in (a) are fits to the Brinkman model. The tunnel current showed no dependence on the sweep direction in (a) and the data points for the two sweep directions overlap. The sweep direction (arrows) and sequence (numbers) are indicated in (b). The device area was $4\times4\mu m^2$.

Figure 2 shows fractional intensity images of a $SrTiO_3$ single crystal for regions of different thickness up to ~100 nm. Experimental images are compared directly with image simulations. Provided that spatial incoherence is taken into account in the simulations, almost perfect agreement is found between simulation and experiment.

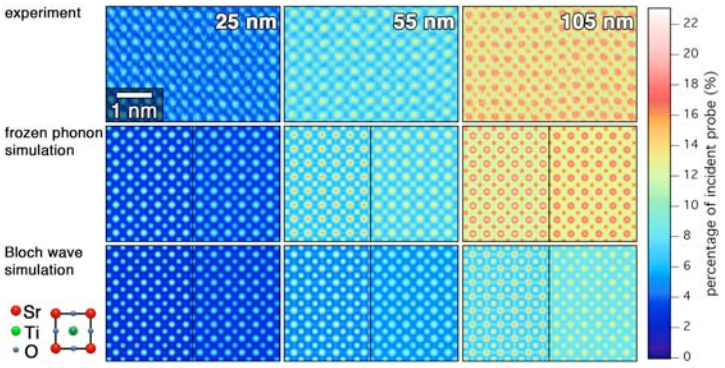

Figure 2: Top row: experimental HAADF images of $SrTiO_3$ along <100> with intensity variations normalized to the incident beam intensity (see color scale bar on the right). Regions of three different thicknesses are shown. The Sr columns are the brightest and the Ti-O columns are the second brightest features (see unit cell schematic on the left). Middle row: frozen phonon image simulations. Bottom row: Bloch wave image simulations. In each case, simulations are shown without (left pane) and with convolution with a 0.08 nm FWHM Gaussian (right pane).

Concerning the high-angle scattering physics, the results also showed that thermal scattering alone was sufficient to quantitatively predict the measured background. The agreement between theory and experiment is far better than for conventional HRTEM, where a large mismatch (a factor of around two to three) is usual. Multiple thermal scattering, easily incorporated in frozen phonon models, becomes important for thicker specimens.

We also developed a method to characterize the ADF detector and imaging system performance. The detector output is sufficiently linear for intensities ranging from the incident beam to image intensities corresponding to even the thinnest samples. Figure 3 shows the detector scintillator efficiency obtained by mapping the preamplifier output as a function of probe position across the detector surface. Variations in the efficiency are seen across the detector surface, in particular at low angles.

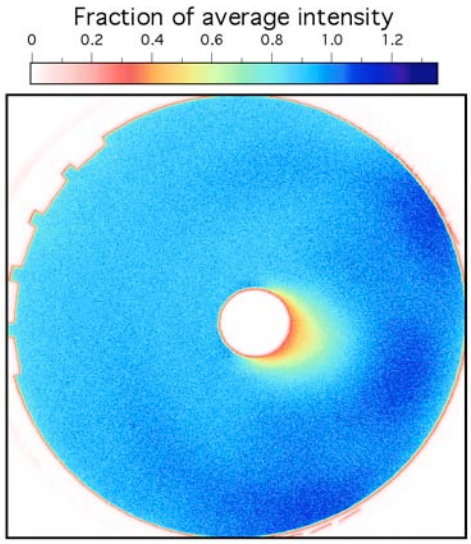

Figure 3: The ADF detector scintillator efficiency obtained by mapping the preamplifier output as a function of probe position across the detector surface. The output is plotted in terms of the fraction of an average output.

Future Plans

We plan to use the epitaxial Pt/$SrTiO_3$/Pt tunnel junctions for characterizing defects and phonon modes in ultrathin $SrTiO_3$ and related materials by inelastic tunneling spectroscopy (IETS). This will allow us to investigate how phonon modes change in ultrathin ferroelectric films with temperature and compare the behavior to bulk materials. We will next fabricate ferroelectric tunnel junctions using $BaTiO_3$. These experiments will show whether a switchable polarization can be sustained in the thickness regime that allows for direct tunneling. In HAADF/STEM, our future experiments will explore the agreement between simulations and experiments for samples containing higher atomic numbers. Furthermore, we will investigate the image contrast in low-angle ADF and compare with image simulations. The ultimate goal is to investigate whether a contrast mismatch exists at conditions closer to conventional HRTEM, where a large mismatch has been reported ("Stobbs-factor").

DOE Sponsored Publications in 2006 – 2008

[1] J. M. LeBeau, S. D. Findlay, L. J. Allen, S. Stemmer, *Quantitative atomic resolution scanning transmission electron microscopy*, Phys. Rev. Lett. **100**, 206101 (2008).

[2] J. M. LeBeau, S. Stemmer, *Experimental quantification of annular dark-field images in scanning transmission electron microscopy*, in press: Ultramicroscopy. http://dx.doi.org/10.1016/j.ultramic.2008.07.001

[3] S. D. Findlay, D. O. Klenov, S. Stemmer, L. J. Allen, *Atomic number contrast in high-angle annular dark field imaging of crystals*, Mater. Sci. & Technol. **24**, 660 (2008). [Invited Review Paper]

[4] D. S. Boesch, J. Son, J. M. LeBeau, J. Cagnon, S. Stemmer, Thickness Dependence of the Dielectric Properties of Epitaxial $SrTiO_3$ Films on (001)Pt/$SrTiO_3$, Appl. Phys. Expr., in press (2008).

[5] J. Son, J. Cagnon, D. S. Boesch, S. Stemmer, *Epitaxial $SrTiO_3$ tunnel barriers on Pt/MgO substrates*, Appl. Phys. Expr. **1**, 061603 (2008).

[6] N. H. Finstrom, J. Cagnon, S. Stemmer, *Properties of dielectric dead layers for $SrTiO_3$ thin films on Pt electrodes*, J. Appl. Phys. **101**, 034109 (2007).

[7] D. O. Klenov, S. D. Findlay, L. J. Allen, S. Stemmer, Influence of orientation on the contrast of high-angle annular dark-field images of silicon, Phys. Rev. B. **76**, 014111 (2007).

[8] D. O. Klenov, S. Stemmer, *Limitations in through-focus depth sectioning in non-aberration corrected high-angle annular dark-field imaging,* Jap. J. Appl. Phys. **45**, L602 (2006).

[9] D. O. Klenov, S. Stemmer, *Contributions to the Contrast in Experimental High-Angle Annular Dark-Field Images,* Ultramicroscopy **106**, 889 (2006).

[10] S. P. Keane, S. Schmidt, J. W. Lu, A. E. Romanov, S. Stemmer, *Phase transitions in textured $SrTiO_3$ thin films on epitaxial Pt electrodes*, J. Appl. Phys. **99**, 033521 (2006).

[11] S. Schmidt, D. O. Klenov, S. P. Keane, J. W. Lu, T. E. Mates, S. Stemmer, *Atomic Structure of (111) $SrTiO_3$/Pt Interfaces*, Appl. Phys. Lett. **88**, 131914 (2006).

Characterization of Impurity / Point Defect Complexes in Semiconductors by STEM

PI: Paul M. Voyles, Materials Science and Engineering, University of Wisconsin, Madison, 1509 University Avenue, Madison, WI 53706-1595; voyles@engr.wisc.edu

co-PIs: Dane Morgan, Materials Science and Engineering, University of Wisconsin, Madison, ddmorgan@wisc.edu; Hadis Morkoç, Electrical Engineering and Physics, Virginia Commonwealth University, hmorkoc@vcu.edu

Program Scope

Point defects in isolation and bound together in complexes play a substantial role in determining the properties of semiconductors, including carrier concentration and mobility. Electron microscopy has been an important tool for characterization of extended defects, but it has been used to characterize point defects inside crystals only recently [1-3]. This goal of this project is to leverage recent developments in high-stability, aberration-corrected scanning transmission electron microscopy (STEM) to measure concentrations of point defects and point defect complexes in semiconductors. High-angle annular dark-field *Z*-contrast STEM imaging will be used to detect substitutional and interstitial high-*Z* impurity atoms [1, 2], and low-angle annular dark-field strain contrast STEM imaging will be used to detect vacancies and the lattice relaxations surrounding defect complexes [3, 4]. The ability to co-locate component point defects spatially in a complex at atomic resolution is particularly important, and points the way to a new paradigm in point defect characterization: *count the defects one at a time, and know where they are with atomic resolution*.

Extracting this level of detail from STEM images will require new insight into the propagation of off-column STEM probes and their interaction with defect strain fields. We will address this problem using state-of-the-art multislice simulations from accurate *ab initio* defect model structures. We will also explore three-dimensional imaging by optical sectioning [5-7], which, while it is of limited effectiveness for extended structures [8], achieves useful vertical resolution for point objects [5-7]. Even limited depth resolution will help distinguish point defects bound together in complexes from isolated defects separated in depth.

In simulation, Morgan will use recent developments in alloy theory [9-14] to develop multiscale models of defect and defect complex thermokinetics. This approach incorporates calculations of the stability, diffusivity, and reaction kinetics of defects and complexes. Effective Hamiltonians will be used to efficiently search the space of possible defects to find complexes with large binding energy and favorable formation kinetics, and coarse grained rate equation models will predict the coupled concentrations of different defects as a function of a time, temperature, and chemical environment. Eventually, we hope to make quantitative comparisons of the populations of selected defects and complexes between simulations and STEM measurements. STEM data will serve as a constraint on the simulations, and the simulations will give insight into the populations of defects not detectable by STEM.

Morkoç will support the experimental effort with state-of-the-art molecular beam epitaxy growth of compound semiconductor thin films and with conventional electrical and optical measurements of defect levels and concentrations.

Future Plans

Imaging of Au interstitials in Si has recently been demonstrated [2]. The Z-contrast image of an isolated impurity samples the probe wave function at the depth of the impurity [15], so we will use Au interstitial images as experimental measurements of the off-column probe intensity. We will compare the distribution of those intensities to multislice simulations for impurities as a function of depth and sample thickness. Similar comparisons for $SrTiO_3$ lattice images have recently shown good quantitative agreement between experiment and simulation [16]. Images of Au_i will provide a new stringent test of the off-column propagation of the STEM probe.

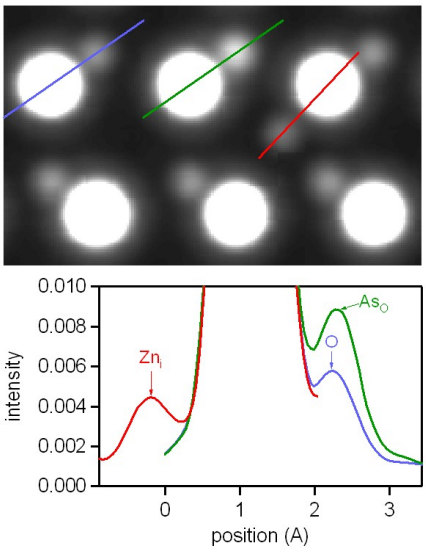

Figure 1: Frozen-phonon multislice simulation of Zn_i and As_O point defects in ZnO.

After the experiments on silicon, we will apply STEM imaging and materials simulation to the problem of developing *p*-type ZnO thin films. ZnO is a wide-gap semiconductor with significant potential for applications in optoelectronics in the blue to ultraviolet spectral region [17]. Like most wide-gap semiconductors, it has a strong tendency to carriers of one type, which for ZnO is *n*-type, due to intrinsic defects [17]. Straightforward substitutional acceptor doping of ZnO has proven ineffective [18-20], but recent work suggests that more complicated complexes involving impurity antisites, vacancies and large lattice relaxations may be reliable acceptors [21-25]. We will use our combination of imaging and simulation tools to understand the intrinsic and extrinsic defects and complexes in doped ZnO, with the goal of determining the limitations of current methods of *p*-type doping, and eventually engineering new doping schemes. Understanding impurities and defects in ZnO will significantly aid technologies based on this material and may illuminate the defect behavior of wide-gap semiconductors more generally.

Fig. 1 shows a multislice simulation of an aberration-corrected STEM image of As-doped ZnO in the $[11\bar{2}0]$ orientation. Both Zn_i and As_O defects show sufficient contrast to be detected in this image. Zn_i are likely to be mobile at room temperature, but may be sufficiently stable at low temperature to be imaged. As_O-centered defect complexes have been proposed as a source of *p*-type conductivity [25]. If some intrinsic point defects can be imaged, we will attempt to determine the nature of the intrinsic defect rendering most ZnO *n*-type.

The simulation effort will focus on ZnO. Building on his previous work on point defect thermokinetics in ZnO [26], Morgan will develop a three-stage thermokinetic model for defect evolution in ZnO. The first step is prediction of stable defect clusters using a cluster expansion representation of the interactions between point defects to aid a rapid search. The second step is predicting defect and cluster diffusivities using kinetic Monte Carlo simulation, and the third step is using a rate equation formalism to evolve defect populations over time, using energetics and diffusivities from previous stages as inputs.

References

[1] P. M. Voyles, D. A. Muller, J. L. Grazul, P. H. Citrin, and H. J. L. Gossmann, Nature **416**, 826 (2002).

[2] S.-H. Oh, K. v. Benthem, S. I. Molina, A. Y. Borisevich, W. Luo, P. Werner, N. D. Zakharov, D. Kumar, S. T. Pantelides, and S. J. Pennycook, Nano Lett. **8**, 1016 (2008).

[3] D. A. Muller, N. Nakagawa, A. Ohtomo, J. L. Grazul, and H. Y. Hwang, Nature **430**, 657 (2004).

[4] P. M. Voyles, D. J. Chadi, P. H. Citrin, D. A. Muller, J. L. Grazul, P. A. Northrup, and H. J. L. Gossmann, Phys. Rev. Lett. **91**, 125505 (2003).

[5] P. M. Voyles, Microchimica Acta **155**, 5 (2006).

[6] K. van Benthem, A. R. Lupini, M. Kim, H. S. Baik, S.-J. Doh, J.-H. Lee, M. P. Oxley, S. D. Findlay, L. J. Allen, J. T. Luck, and S. J. Pennycook, Appl. Phys. Lett. **87**, 034104 (2005).

[7] K. van Benthem, A. R. Lupini, M. P. Oxley, S. D. Findlay, L. J. Allen, and S. J. Pennycook, Ultramicroscopy **106**, 1062 (2006).

[8] D. A. Muller, V. Intaraprasonk, J. Xin, and P. Ercius, Microsc. Microanal. **13 (Suppl 2)**, 86 (2007).

[9] J. M. Sanchez, F. Ducastelle, and D. Gratias, Physica **128A**, 334 (1984).

[10] D. de Fontaine, in *Solid State Physics*, edited by H. Ehrenreich, and D. Turnbull (Academic Press, 1994), pp. 33.

[11] A. Zunger, in Statics and Dynamics of Alloy Phase Transformations, edited by P. E. A. Turchi, and A. GonisNew York, 1994), pp. 361.

[12] F. Zhou, G. Grigoryan, A. Keating, G. Ceder, S. Lustig, and D. Morgan, Phys. Rev. Lett. **95**, 148103 (2005).

[13] G. Grigoryan, F. Zhou, S. R. Lustig, G. Ceder, D. Morgan, and A. E. Keating, Plos Computational Biology **2**, 551 (2006).

[14] A. van de Walle, M. Asta, and G. Ceder, Calphad-Computer Coupling of Phase Diagrams and Thermochemistry **26**, 539 (2002).

[15] P. M. Voyles, D. A. Muller, and E. J. Kirkland, Microsc. Microanal. **10**, 291 (2004).

[16] J. M. LeBeau, S. D. Findlay, L. J. Allen, and S. Stemmer, Phys. Rev. Lett. **100**, 26101 (2008).

[17] Ü. Özgür, Y. I. Alivov, C. Liu, A. Teke, M. A. Reshchikov, S. Dogan, V. Avrutin, S.-J. Cho, and H. Morkoç, J. Appl. Phys. **98**, 041301 (2005).

[18] D. C. Look, and B. Claflin, Phys. Stat. Sol. B **241**, 624 (2004).

[19] M. G. Wardle, J. P. Goss, and P. R. Briddon, Phys. Rev. B **71**, 155205 (2005).

[20] S. J. Pearton, D. P. Norton, K. Ip, Y. W. Heo, and T. Steiner, J. Vac. Sci. Tech. B **22**, 932 (2004).

[21] V. Vaithianathan, B.-T. Lee, and S. S. Kim, Appl. Phys. Lett. **86**, 062101 (2005).

[22] F. X. Xiu, Z. Yang, L. J. Mandalapu, D. T. Zhao, and J. L. Liu, Appl. Phys. Lett. **87**, 152101 (2005).

[23] F. X. Xiu, Z. Yang, L. J. Mandalapu, D. T. Zhao, and J. L. Liu, Appl. Phys. Lett. **87**, 252102 (2005).

[24] W. Guo, A. Allenic, Y. B. Chen, X. Q. Pan, Y. Che, Z. D. Hu, and B. Liu, Appl. Phys. Lett. **90**, 242108 (2007).

[25] S. Limpijumnong, S. B. Zhang, S.-H. Wei, and C. H. Park, Phys. Rev. Lett. **92**, 155504 (2004).

[26] A. F. Kohan, G. Ceder, D. Morgan, and C. G. van de Walle, Phys. Rev. B **61**, 151019 (2000).

Imaging electron flow in graphene nanodevices

J. Berezovsky and R. M. Westervelt*
Harvard University

In recent years, there has been much interest in the physics and applications of graphene - a single atomic layer of graphite[1,2]. In this novel material, fascinating physics and intriguing technological possibilities are so plentiful that it seems to go beyond the metaphor of "low-hanging fruit" to the Newtonian level of sitting under the tree and letting the fruit hit you in the head. Among the interesting physical phenomena seen or predicted in graphene are unique quantum Hall behavior, unusual shot noise effects, and a host of outlandish effects hitherto considered to be in the domain of particle physics. However, graphene is not only interesting for its esoteric physics but also for its promising technological applications. Many phenomena - including high mobility, and remarkably, the quantum Hall effect - persist up to room temperature. Hurdles remain before graphene is found inside an ipod. Nevertheless, the material shows promise for high-mobility transistor-type devices, or perhaps even more exotic quantum technology.

A number of transport measurements have been performed on graphene nanostructures, and the results have been in fair agreement with theory. However, the analysis of these experiments typically assumes idealized conduction through the device. In reality, the current [1]flow is likely to be much more complex. Microscopic non-idealities can shape the flow of electrons into intricate branched patterns. To investigate how issues like local fluctuations in the background potential, sample edge roughness, or impurities affect the electrical transport, we plan to carry out a series of experiments employing a biased scanning tip to image the flow of electrons through graphene nanostructures.

Graphite is composed of stacked layers of carbon atoms in a

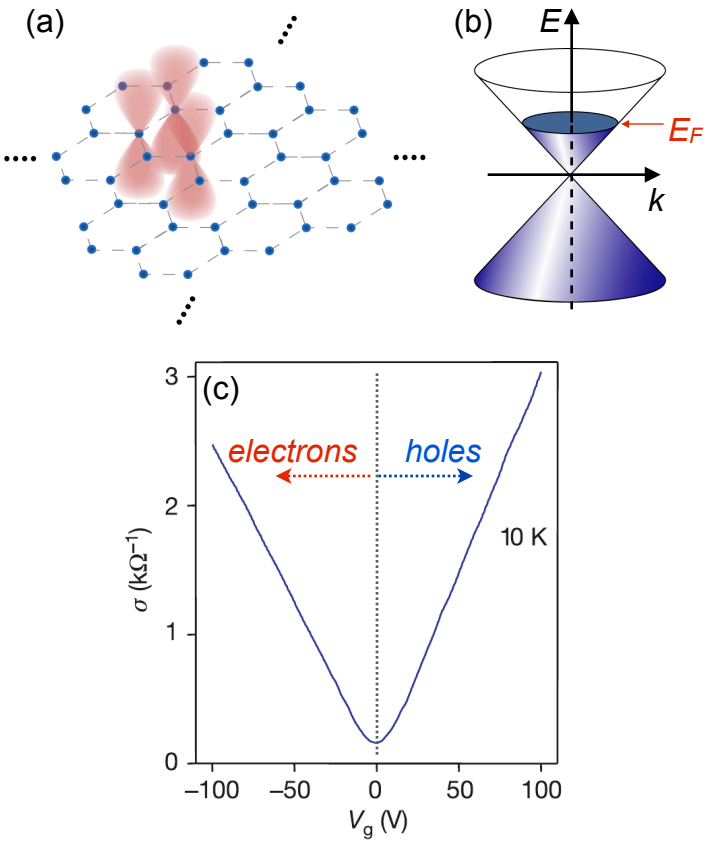

Figure 1. a) Schematic of the honeycomb lattice of carbon atoms comprising a sheet of graphene. Several *p*-orbitals are shown which give rise to a 2-dimensional layer of free charge. b) Band structure of graphene near the Dirac point. The Fermi energy, E_F, can be continuously tuned between the conduction and valence band by means of a gate voltage. c) Conductance of graphene as a function of gate voltage sweeping through the Dirac point (from K. S. Novoselov *et al.*, *Nature* **438**, 197 (2005)).

*Principal investigator. Mailing address: 29 Oxford St., Cambridge MA 02138.
Email: westervelt@physics.harvard.edu

honeycomb lattice. A single such layer is referred to as graphene. Figure 1a shows a schematic representation of this lattice. Also shown are several of the *p*-orbitals involved in π bonding, which lead to a delocalized two-dimensional sheet of charge carriers.

Graphene's unique band structure is responsible for many of its interesting phenomena. Unlike both metals and insulators, the filled valence band and empty conduction band meet at a point in *k*-space referred to as the Dirac point. For this reason, graphene can be thought of as a zero-gap semiconductor. Furthermore, the energy of electron and hole states near the Dirac point increase linearly with momentum, more like photons than electrons in conventional materials. As a result, the Hamiltonian describing these electrons looks just like the Dirac equation for relativistic particles but with an effective velocity much lower than the speed of light (~10^6 m/s). Figure 1b shows this linear band structure. Here, the Fermi energy is shown at some point above the Dirac point, which may be accomplished experimentally by applying a gate voltage. As the Fermi energy is swept upwards through the Dirac point, the conductivity of the material goes through a minimum as the density of holes goes to zero, and then increases again as the material becomes doped with electrons (Fig. 1c).

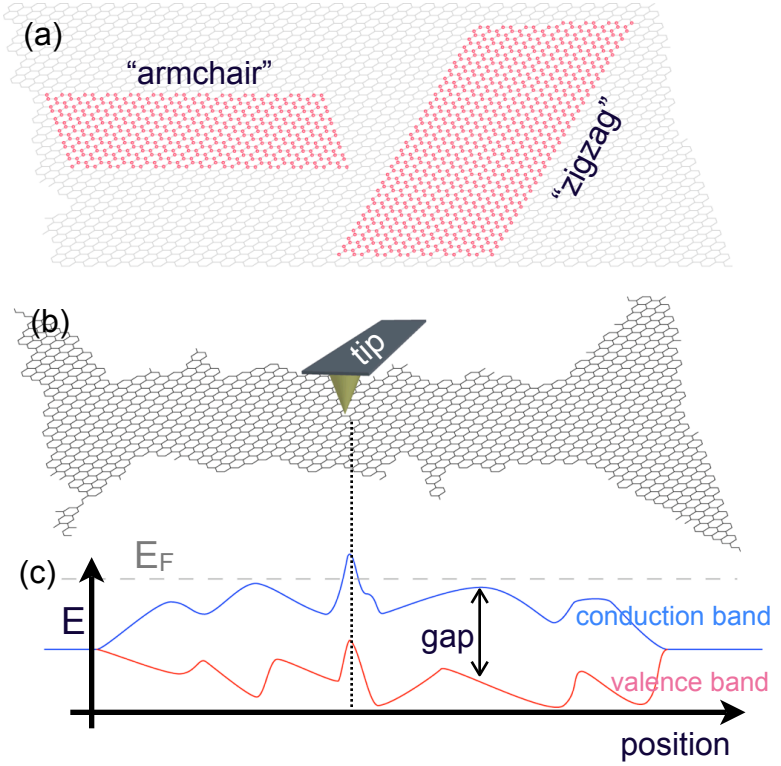

Figure 2. a) "Armchair" and "zigzag" graphene nanowires (red). b) Schematic of a disordered graphene nanowire (lattice spacing and tip size not to scale). c) Drawing of the conduction band minimum and valence band maximum along the length of a disordered nanowire. A biased tip may be used to map out spatial variations in the band gap and the background potential through changes in the nanowire conductance.

The gapless nature of graphene poses something of a challenge for potential applications. Transistors typically rely on the presence of a gap to turn conduction on and off. However by scaling down the devices, a gap can be induced to form. In graphene structures with widths less than about 50 nm, an appreciable gap opens up between the conduction and valence band due to quantum confinement of the carriers. Just as a carbon nanotube may be either metallic or semiconducting, a graphene nanowire (essentially an unrolled nanotube) may or may not have a gap depending on the orientation of the wire with respect to the crystal lattice. Theoretically, a perfect nanowire in the "armchair" orientation should have no gap, while a nanowire in the "zigzag" orientation should have a gap that depends on the wire width (Fig. 2a). In reality however, it is not known how to make a graphene nanowire with a perfectly regular arrangement of atoms at the edge. Figure 2b shows a more realistic nanowire (though not to scale). In such a

nanowire, one would expect the band gap to change depending on the local structure of the edges, as shown schematically in Fig. 2c. By scanning an electrically biased tip over graphene nanostructures, we plan to map out the variations in the conduction- and- valence band energies as a function of position, yielding information about the microscopic structure of the crystal as well as any underlying fluctuations in the potential.

We also plan to use scanning probe microscopy to image the flow of electrons through graphene devices. This type of measurement has been previously demonstrated in our group in a GaAs two-dimensional electron gas (2DEG)[3]. In those experiments, the biased tip depletes a small area of the 2DEG which backscatters electrons emanating from a quantum point contact. This backscattering is seen as a change in the device's conductance. By scanning the tip and measuring this conductance change, one obtains an image of the current flow through the device.

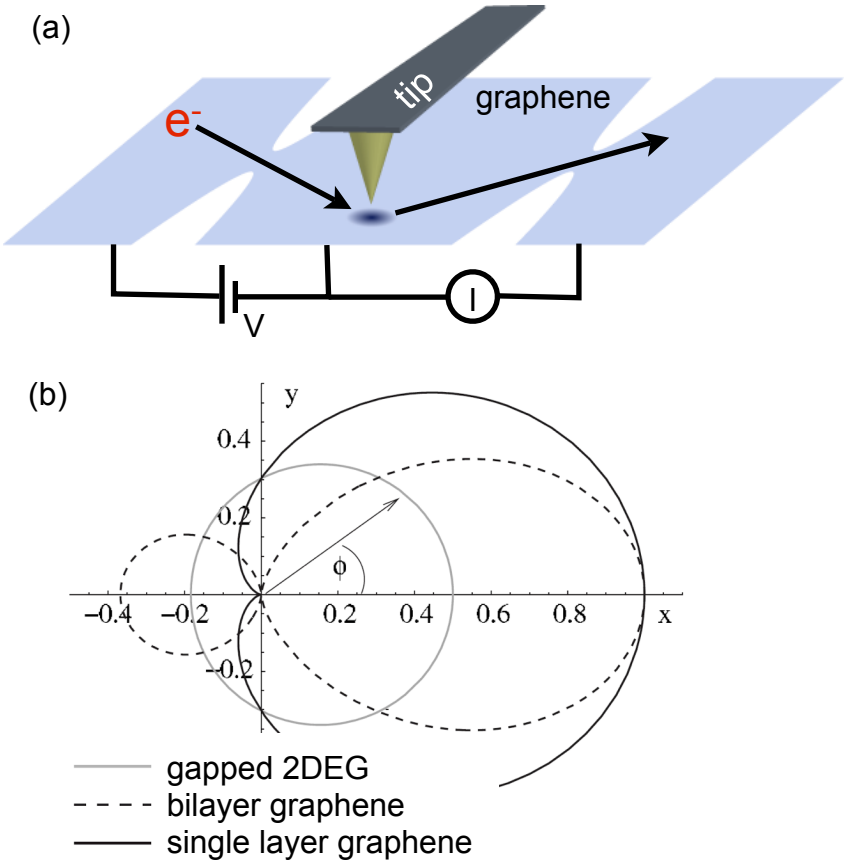

Figure 3. a) Experimental scheme for measuring electron flow in graphene (following the proposal by M. Braun *et al.*, *Phys. Rev. B* **77**, 115433 (2008)). Electrons emanating from a nanoconstriction scatter off of a local potential created by a charged tip, affecting the current flow through a second constriction. b) Calculated scattering cross section vs. scattering angle for single- and double-layer graphene (also from M. Braun *et al.*). The cross section for a regular semiconducting 2DEG is also shown.

We plan to perform an analogous measurement in a graphene structure. However, due to the unusual physical properties of graphene (specifically, Klein tunneling), electrons in graphene can not backscatter off of a potential barrier. The calculated scattering cross section for graphene is shown in Fig. 3b. Instead, we plan to use a structure with a pair of nanoconstrictions (Fig. 3a). Under an applied voltage, electrons will travel through the first constriction and scatter off of a local potential created by the biased tip. Electrons that scatter off the tip and through the second constriction will yield a change in the current through the second constriction. In this way, we will image the coherent flow of electrons, as well as obtain information about the scattering behavior of carriers in the device.

To date, we have succeeded in fabricating graphene nanostructures suitable for these imaging measurements. The graphene samples are prepared via the usual tape-assisted

micromechanical cleavage. Once a suitable piece of graphene has been identified using optical microscopy, electron beam lithography is used to create an alignment grid, and metal contacts to the graphene. A further e-beam step is then used to pattern an etch mask, and the excess graphene is removed with an oxygen plasma. Scanning electron microscopy is used to characterize the resulting devices (Fig. 4).

We are currently in the process of building two new low temperature, scanning probe microscopes. This new generation of systems will enable transport/ imaging measurements to be performed in vacuum down to Helium-3 temperatures (100s of mK), and at magnetic fields up to 7 T. Furthermore, the electronics for the system will be run by a customizable field-programmable gate array (FPGA) controller, allowing for fast feedback on the incoming data.

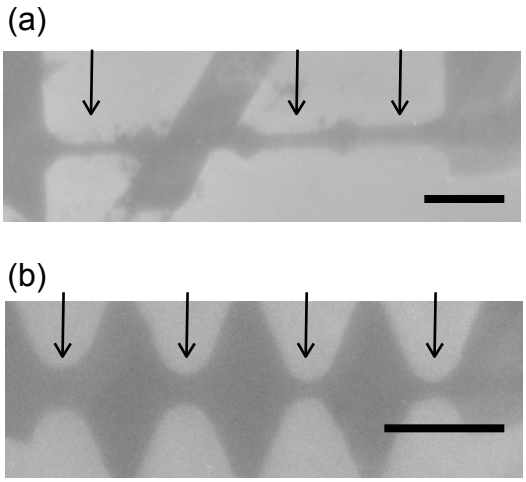

Figure 4. Scanning electron micrographs of preliminary graphene nanowire (b) and nanoconstriction (a) samples for imaging measurements. Scale bars = 500 nm.

Low temperature scanning microscopy measurements of transport in graphene nanostructures will increase our understanding of how electrons behave in actual devices. By understanding and controlling the edge effects in graphene nanowires, one could spatially engineer the band gap in a device allowing for metallic and semiconducting regions within a single piece of graphene. Furthermore, the imaging of coherent electron transport will yield information about quantum effects in graphene. These effects may provide unique possibilities for quantum technology. The field of graphene nanoelectronics is still in its infancy, but as we increase our understanding of the unique physics governing the material, it seems that this is a field with great potential for further scientific discovery, as well as a wide variety of applications.

1. A. K. Geim and K. S. Novoselov, *Nature Mat.* **6**, 183 (2007).
2. R. M. Westervelt, *Science* **320**, 327 (2008).
3. M.A. Topinka, R.M. Westervelt, E.J. Heller, *Physics Today* **56**, 12 (2003).

Probing Correlated Superconductors and their Phase Transitions on the Nanometer Scale

Ali Yazdani
Department of Physics
Princeton University
DOE-BES Supported Research Program

Program Scope:

Correlated electron systems have remarkable physical properties—ranging from unconventional high-temperature superconductivity to colossal magnetoresistance or large thermopower. Strong interactions between electrons and competition between various possible ground states are believed to be responsible for exotic behavior of correlated electronic materials. Among these materials, the nature of electronic states in hole-doped copper-oxide superconductors is one of the most intensely debated problems. Identifying the mechanism for superconductivity and understanding the usual correlated normal and the pseudogap states in these materials would have a major impact on research in condensed matter physics. Our program is focused on applying state-of-the-art scanning tunneling microscopy (STM) techniques to probe the nature of the electronic state in the cuprates on the nanometer scale and on studying their evolution across phase transitions between superconducting and non-superconducting states. Specifically, we have develop several new techniques, based on the scanning tunneling microscope (STM), to visualize the process of pair formation on the atomic scale [1] and to probe what controls the strength of pairing in these compounds with high precision.[2] In general the techniques we have developed, such as the ability to perform spectroscopy at a specific atomic site while varying temperature (from 4K up to over 100K), provide unique opportunities to examine phase transition phenomena in a heterogeneous material system. Our findings show that these experiments provide important clues to address fundamental questions in the physics of the cuprates—such as those essential to understanding the pseudogap state, the relevance of competing ordering phenomena for the cuprate phase diagram, or the role of various electron-boson coupling. Finally, to identify what aspect of our findings are unique to cuprates or generic to a randomly doped system, we will perform atomic scale studies of the newly discovered Cu-doped $TiSe_2$ superconducting system. In this layered material system, superconductivity emerges from a charge density wave (CDW) state by random doping of Cu in between $TiSe_2$ layers. Understanding the interplay between CDW and superconductivity and the role of random doping on the nanoscale will be a key outcome of studies with this new material system.

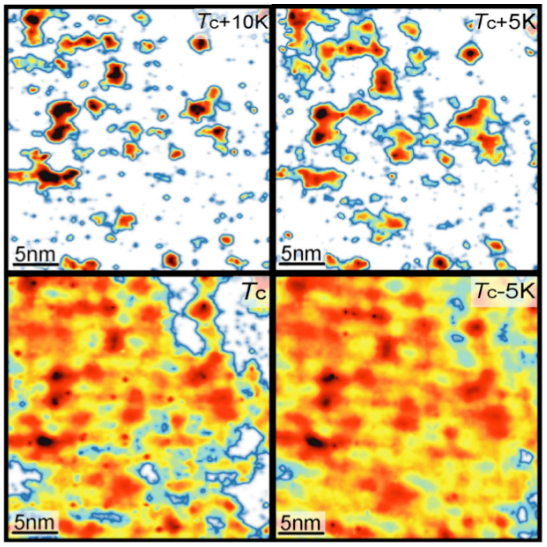

Using a specially-designed scanning tunneling microscope, we have mapped the strength of current-carrying electron pairs as they form in a ceramic high-temperature superconductor. From the top left, the images show the same 30 nm × 30 nm region of the material at successively lower temperatures spanning Tc, the temperature at which the entire sample exhibits superconductivity, . Red areas indicate the presence of superconducting pairs. Even at 10°C above T_c (top left image), the electron pairs still exist in localized regions.

Our experimental program is unique in that currently no other experimental group has the STM capabilities to perform high-resolution experiments on correlated electronic states across the wide range of temperatures we will study. The real space information we will obtain from our experiments will complement the scattering and ARPES studies on the $Bi_2Sr_2CaCu_2O_{8+\delta}$ system supported under the DOE-BES program. The experiments will be done in collaboration with Professor Robert Cava's group at Princeton, Dr. Genda Gu from Brookhaven National Laboratory, and Dr. Ando from the Central Research Institute of Electric Power Industry in Japan.

Recent Progress:

In the last two years our new experiments are providing evidence that pairing in these exotic superconductors occur above the bulk transition temperature and in nanoscale regions with sizes of 1-3nm. The high-temperature nucleation and proliferation of these nanoscale puddles have a strong connection to the temperature-doping phase diagram of these superconductors. Moreover, these variations of the pairing strength within the puddles can be examined to find microscopic clues of the mechanism of pairing. Specifically, we have found evidence that suggests that strong electronic correlation, as oppose coupling of electrons to bosons, is responsible for the pairing mechanism in the cuprates. Surprisingly, we have found that nanoscale measurements of electronic correlations in the normal state (at temperatures as high as twice T_c) can be used to predict the strength their pairing interaction at low temperatures. Overall, these measurements are providing important ways to examine the nanoscale nucleation of superconductivity in these exotic materials and its underlying mechanism.

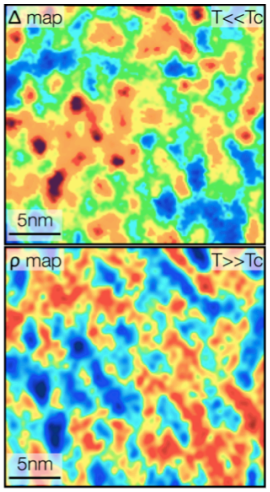

Using a specially-designed scanning tunneling microscope, we have tracked the properties of individual atoms of the copper -oxides from low temperatures (top panel, where the material is a superconductor) to high temperatures (bottom panel, where the material is not a superconductor). The color scale of the top panel indicates the strength of the attractive force between electrons in the superconducting phase with dark red indicating a strong force. The color scale of the bottom panel indicates the repulsion between electrons at high temperature where dark blue indicates strong repulsion. The two panels show the intimate relationship between the attractive pairing force at low temperature and the repulsion at high temperature.

References:

[1] K. K. Gomes, A. N. Pasupathy, A. Pushp, S. Ono, Y. Ando, and A. Yazdani, *Nature* **447**, 569 (2007).
[2] A. N. Pasupathy, A. Pushp, K. K. Gomes, C. V. Parker, J. S. Wen, Z. J. Xu, G. D. Gu, S. Ono, Y. Ando, and A. Yazdani, *Science* **320**, 196 (2008).

Research Summaries III:

Interfaces & Grain Boundaries

Computational Investigations of Solid-Liquid Interfaces

Mark Asta (PI)
Chemical Engineering & Materials Science Department, University of California, Davis
One Shields Ave., Davis, CA 95616
Email: mdasta@ucdavis.edu

Program Scope – In a wide variety of materials synthesis and processing contexts, atomistic processes at solid-liquid interfaces play a critical role governing defect formation, growth morphologies, and microstructural evolution. Accurate knowledge of solid-liquid interfacial structures, free energies, mobilities and non-equilibrium segregation coefficients are critical for predictive modeling of solidification phenomena, yet direct experimental measurements of these properties remains elusive in many cases. In this project first-principles calculations and atomistic simulations are integrated to derive detailed insights into the atomic-scale structural and dynamical properties of solid-liquid interfaces, and the relationship between these properties and the thermodynamic and kinetic parameters that impact the evolution of solidification structures at larger scales.

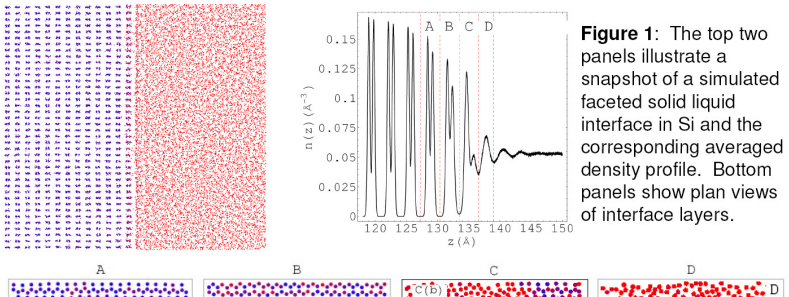

Figure 1: The top two panels illustrate a snapshot of a simulated faceted solid liquid interface in Si and the corresponding averaged density profile. Bottom panels show plan views of interface layers.

Recent Progress – Our recent research has involved two main thrusts. The first concerns the structural and dynamic properties of faceted solid-liquid interfaces. While crystal-melt interfaces in elemental metals and colloidal systems are typically molecularly rough, featuring highly isotropic interfacial free energies, solid-liquid interfaces between chemically dissimilar materials are generally much more anisotropic, and often feature one or more faceted orientations. Examples of faceted solid-liquid interfaces can be found in a wide variety of contexts, ranging from heterogeneous nucleation assisted by grain refiners in the casting of metal alloys, to semiconductor nanowire growth from liquid catalysts. While atomistic simulations have been extensively employed in studies of molecularly rough interfaces, far less effort has been devoted to faceted systems. Outstanding questions remain concerning the atomic interfacial structure, as well as the energetic and kinetic properties of steps and terrace nucleation processes that underlie their dynamics. Our recent efforts have involved development of molecular dynamics (MD) methods and analysis tools to characterize lateral short-range order at faceted crystal-melt interfaces (see Fig. 1), as well as the thermodynamic and kinetic properties of steps. These analysis techniques have provided a methodology to analyze fluctuations of clusters of the crystalline phase in liquid interfacial layers, from which step free energies and the thermodynamic properties underlying terrace nucleation kinetics have been derived. To date this work has

focused primarily on interfaces in Si, modeled with classical interatomic potentials. However, the analysis tools and simulation methodologies are far more general, and will be applied in the future to more chemically complex systems, as described below.

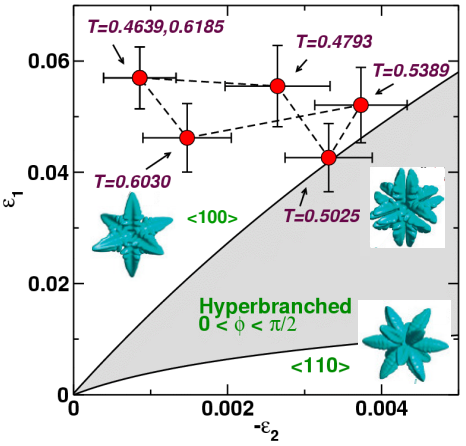

Figure 2: Red points show results of MD calculations for the composition dependence of 4-fold (ε_1) and 6-fold (ε_2) parameters characterizing the anisotropy of the solid-liquid interfacial free energy in a model fcc binary alloy. Addition of solute is found to lead to a destabilization of the <100> growth orientation. Simulated dendrites and calculated boundaries separating <100> and <110> growth orientations in are courtesy of collaborator A. Karma (Northeastern Univ.).

The second thrust concerns the effect of solute on both equilibrium and far-from equilibrium properties of crystal-melt interfaces in alloys. This work is primarily motivated within the context of the modeling of dendrite growth, the understanding of which is key to controlling solidification microstructures and associated mechanical properties of many cast and welded materials. Phase-field modeling, motivated by experimental investigations in Al and Mg alloys, demonstrate that solute-induced changes in the anisotropy of the crystal-melt interfacial energy (γ) can give rise to morphological transitions resulting from changes in the growth orientations of dendrite tips. These studies highlight a critical need to quantify composition dependencies of γ, in order to accurately model alloy solidification microstructures. Recent MD calculations of anisotropic crystal-melt interfacial free energies demonstrate unequivocally that composition-induced changes in γ anisotropies are large on the scale of the magnitudes required to induce observed changes in growth morphologies (see Fig. 2). The microscopic origins of the calculated composition dependencies have been analyzed within the framework of the Gibbs adsorption theorem, involving the first explicit calculations of solute adsorption coefficients for crystal-melt interfaces by Monte-Carlo (MC) methods. The results indicate that for the model system in Fig. 2 the temperature dependence of γ is dominated by excess entropy contributions.

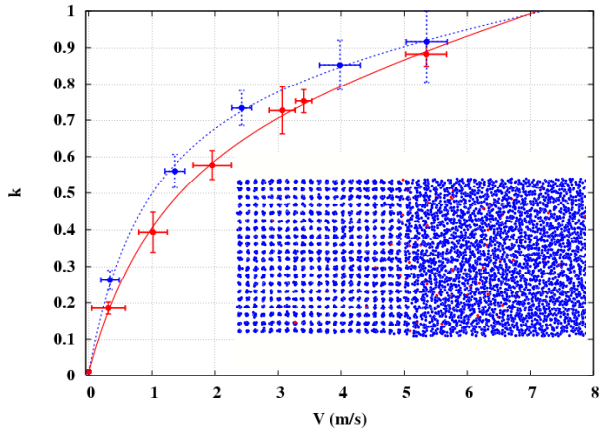

Figure 3: MD calculated partition coefficients (k) as a function of interface velocity (V). The inset is an interfacial region from an MD snapshot.

Under the non-equilibrium conditions characteristic of rapid solidification, solute effects on solidification microstructures arise also due to their influence on interface mobilities, and the closely-related phenomenon of solute trapping. We have recently developed a non-equilibrium MD methodology for the study of such properties. As shown in Fig. 3, the non-equilibrium partitioning

of solute between solid and liquid phases (*k*) as a function of interface velocity (*V*) has been calculated in a model fcc alloy system, considering two different interface orientations. The MD work is the first of its type to demonstrate anisotropic behavior in the *k(V)* relationship.

Future Work – Future work on faceted systems will involve two main directions. The first will be the development of methodologies for computing steps and nucleation barriers, with an ultimate goal of making direct contact with the measurements of such properties by U. Dahmen at NCEM using in-situ electron microscopy. The second involves the study of the structure of interfaces between liquid metals and chemically dissimilar (non-metallic) crystalline solids. Recent electron-microscopy and X-Ray scattering measurements have led to the observation of a wide variety of atomic-scale structures at such interfaces, the origins of which remain incompletely understood. Future work will aim to elucidate the microscopic forces underlying these measured structures. This will involve studies of liquid metals against hard walls with potentials of varying geometry to elucidate the role of substrate symmetry on interface structure, and will make use of the structural analysis tools for faceted solid-liquid interfaces described above. Ultimately, these simulations will be extended to incorporate "wall potentials" derived from first-principles simulations.

Future investigations into the nature of the coupling between solute composition, interfacial free energy anisotropies, and growth morphologies in alloy solidification will focus on the Al-Mg system, for which experimental observations at Ames have established dramatic changes in dendrite growth shapes induced by Mg additions to Al. Our work involves the development of an accurate classical interatomic potential for Al-Mg, in collaboration with M. Mendelev at Ames Laboratory, and J.J. Hoyt at McMaster University. The work also includes calculation of concentration dependent values of γ and associated crystalline anisotropies, the results of which will be analyzed through the Gibbs adsorption theorem employing MC methods described above. Future work on non-equilibrium properties of solid-liquid interfaces will involve further development of the methodologies described above, to compute interface mobilities as well as *k(V)* in alloys. This work will ultimately will target the study of Ni-based alloys where direct comparisons with experimental data is possible.

A new research direction involves the calculation of the interatomic forces underlying grain-boundary premelting phenomena in metals and alloys. This work, facilitated by collaborations through the Computational Materials Science Network (CMSN), focuses on the development of simulation methods for calculating short-ranged structural contributions to the disjoining potential which controls the width of a premelted layer at grain boundaries as a function of supersaturation or undercooling. This work is part of a larger CMSN collaborative effort aimed at modeling the mechanical properties of polycrystalline alloys at high temperatures, and phenomena such as hot-tearing associated with coalescence of solid-liquid interfaces in the late stages of solidification.

Finally, this research project has continued to maintain a focus on solid-solid as well as solid-liquid interfaces in cases where opportunities for direct comparisons with experimental measurements are possible. Our previous work on interfaces between precipitate and matrix phases in Al-Sc alloys is being extended in the study of highly

monodisperse core-shell precipitates in Al-Sc-Li alloys, which are the subject of detailed experimental investigations led by V. Radmilovic and U. Dahmen at NCEM. Our efforts involve the application of first-principles calculations to elucidate the energetic driving forces and kinetic mechanisms underlying the formation of the observed nanoscale precipitate microstructures, and their highly monodisperse size distributions.

Publications (2006-2008):

1. E. A. Marquis, M. Asta, D. N. Seidman and C. Woodward, "Composition Evolution of Nanoscale Al_3Sc Precipitates in an Al-Mg-Sc Alloy," *Acta Mater.* **54**, 119-130 (2006).
2. D. Y. Sun, M. I. Mendelev, C. A. Becker, K. Kudin, Tomorr Haxhimali, M. Asta, J. J. Hoyt, A. Karma and D. J. Srolovitz, "Crystal-Melt Interfacial Free Energies in HCP Metals: A Molecular Dynamics Study of Mg," *Phys. Rev. B* **73**, 024116 (2006).
3. Kuo-An Wu, A. Karma, J. J. Hoyt and M. Asta, "Ginzburg-Landau Theory of Crystalline Anisotropy for BCC-Liquid Interfaces," *Phys. Rev. B* **73**, 094101 (2006).
4. C. A. Becker, M. Asta, J. J. Hoyt and S. M. Foiles, "Equilibrium Adsorption at Crystal-Melt Interfaces in Lennard-Jones Alloys from Monte-Carlo Simulations," *J. Chem. Phys.* **124**, 164708 (2006).
5. J. J. Hoyt, M. Asta and D. Y. Sun, "Molecular Dynamics Simulations of the Crystal-Melt Interfacial Free Energy and Mobility in Mo and V," *Phil. Mag.* **86**, 3651-3664 (2006).
6. G. Ghosh, S. Delsante, G. Borzone, M. Asta and R. Ferro, "Phase Stability and Cohesive Properties of Ti-Zn Intermetallics: First-Principles Calculations and Experimental Results," *Acta Mater.* **54**, 4977-4997 (2006).
7. G. Ghosh, S. Vaynman, M. Asta and M. E. Fine, "Stability and Elastic Properties of $L1_2$-$(Al,Cu)_3(Ti,Zr)$ Phases: Ab Initio Calculations and Experiments," *Intermetallics* **15**, 44-54 (2007).
8. Z. G. Xia, D. Y. Sun, M. Asta and J. J. Hoyt, "Molecular Dynamics Calculations of the Crystal-Melt Interfacial Mobility for Hexagonal-Close-Packed Mg," *Phys. Rev. B* **75**, 012103 (2007).
9. C. A. Becker, D. Olmsted, M. Asta, J. J. Hoyt, and S. M. Foiles, "Atomistic Underpinnings for Orientation Selection in Alloy Dendritic Growth," *Phys. Rev. Lett.* **98**, 125701 (2007).
10. G. Ghosh, A. van de Walle and M. Asta, "First-Principles Phase Stability Calculations of Pseudobinary Alloys of $(Al,Zn)_3Ti$ with $L1_2$, $D0_{22}$ and $D0_{23}$ Structures," *J. Phase Equilibria and Diffusion* **28**, 9-22 (2007).
11. C. A. Becker, D. Buta, J. J. Hoyt and M. Asta, "Crystal-Melt Interface Stresses: Atomistic Simulation Calculations for a Lennard-Jones Alloy, Stillinger-Weber Si, and Embedded Atom Method Ni," *Phys. Rev. E* **75**, 061610 (2007).
12. D. Buta, M. Asta and J. J. Hoyt, "Kinetic Coefficient of Steps at the Si(111) Crystal-Melt Interface from Molecular Dynamics Simulations," *J. Chem. Phys.* **127**, 074703 (2007).
13. G. Ghosh, A. van de Walle, and M. Asta, "First-Principles Calculations of Structural and Energetic Properties of BCC, FCC and HCP Solid Solutions in the Al-TM (TM=Ti,Zr,Hf) Systems: A Comparison of Cluster Expansion and Supercell Methods," *Acta Mater.* (available on line).
14. D. Buta, M. Asta and J. J. Hoyt, "Structure and Dynamics of a Faceted Crystal-Melt Interface," *Phys. Rev. E* (in press).
15. M. I. Mendelev, M. J. Kramer, C. A. Becker and M. Asta, "Analysis of Semi-Empirical Interatomic Potentials Appropriate for Simulation of Crystalline and Liquid Al and Cu," *Phil. Mag.* (in press).

LOCAL ELECTRONIC AND DIELECTRIC PROPERTIES AT NANOSIZED INTERFACES

Dawn A. Bonnell
Department of Materials Science & Engineering
University of Pennsylvania
Philadelphia, PA 19104-6272

Program Scope

This project is aimed at understanding the functional properties of nano-sized interface. This project follows earlier work on SrTiO3 grain boundaries where it was shown that the properties in the vicinity of grain boundaries very considerably from that of the bulk. We showed that multiple transport mechanisms can operate simultaneously in this class of oxides (PRB 2004), that dielectric constants are suppressed by the local electric field near a grain boundary, and that vacancies in reduced samples are disordered in regions adjacent to grain boundaries (APL 2004), and that grain boundaries in SrTiO3 can induce ferroelectric ordering at low temperatures (PRL 2005). These results suggest that nano-sized interfaces will be influenced by similar phenomena.

In the current project the size dependence of metal-oxide interfaces is being explored. An idealized system of nano particles on SrTiO3 (100) is being used as a model. This requires that methods to quantify properties at specific local sites be developed and approaches to controlling interface structure be developed.

Recent Progress

Advances have occurred on 2 fronts: local property probes and nano-sized interface fabrication and control.

Recently we developed a number of multiple modulation SPM techniques that probe local electrical properties. The two questions addressed here are the origin of high spatial resolution in contact transport techniques and drift control of impedance on nanoparticles. A number of conductive tip scanning probes have recently demonstrated spatial resolution on the order of 1nm. This is surprising since the contact diameter in these cases is ~10nm. We used isolated defects in device grade HfO thin films as a model to test the limit of spatial resolution for this class of probes, Figure 1a and b. The reduction of the tip-surface interaction size from the contact diameter by a factor of 8–10 nm implies the operation of a field focusing mechanism. Two potential focusing effects are a localized phase transformation or an elastic strain induced conductivity increase. The stress distribution underneath the tip-sample junction is not uniform, with a region with half of the contact zone experiencing 50% greater stress than the nominal compressive load. Consequently, the load at the tip apex may be sufficiently large to induce changes in the substrate that will be restricted to a small volume under the tip. At moderately high loads a strain-induced reduction in band gap could occur. For the 10GPa load used here the result would be a decrease of 0.15 eV or about 10% of the Si band gap. Since tunneling current is a sensitive function of Eg this effect could be significant, and is also a function of

substrate dopant concentration. At higher pressures Si undergoes a phase transition from semiconducting diamond-like fcc to conductive tetragonal phase, and then to an insulating bcc phase upon release of pressure. We related the local pressure as a function of tip size and applied load to limits for increased current due to band gap effects and for a local phase transformation. Figure 1c shows a 'behavior diagram' for field focusing mechanisms. For the conditions used here, the phase transformation mechanism is most likely. The ultimate spatial resolution limit of this field focusing has not been determined but appears to be about 0.5nm at this point.

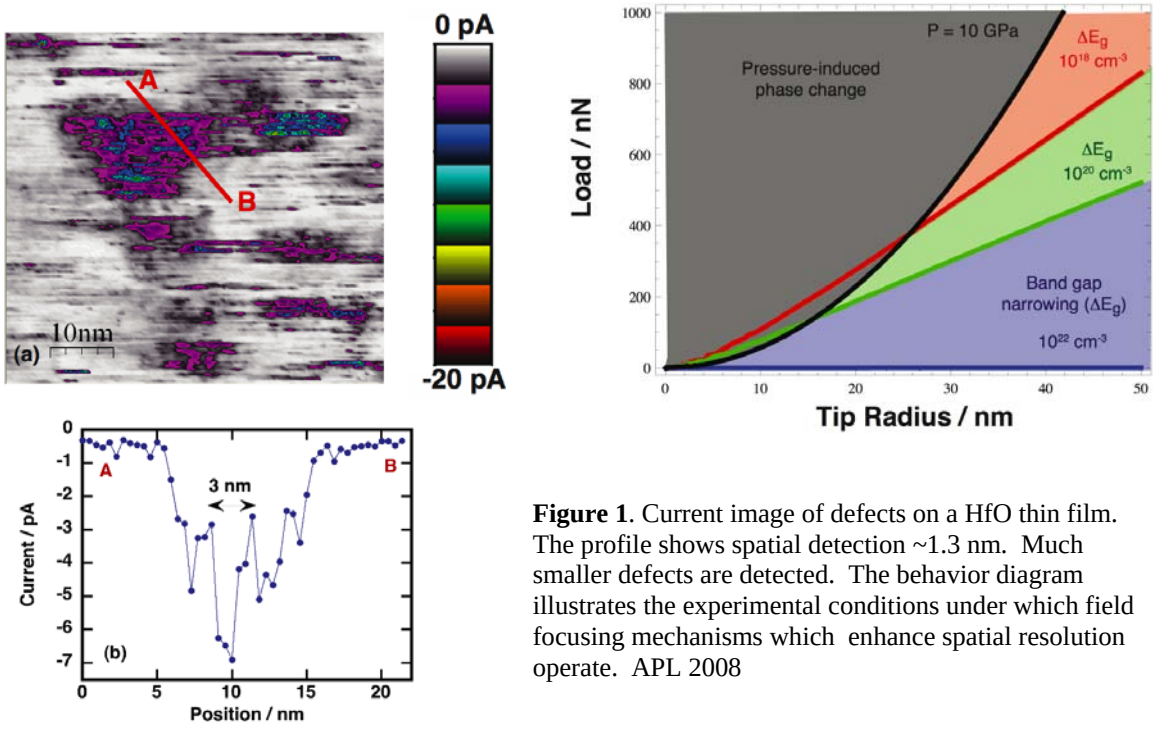

Figure 1. Current image of defects on a HfO thin film. The profile shows spatial detection ~1.3 nm. Much smaller defects are detected. The behavior diagram illustrates the experimental conditions under which field focusing mechanisms which enhance spatial resolution operate. APL 2008

The second metrology challenge is to introduce frequency dependent measurements such as impedance to nm sized metal contacts. This requires: locating nano contacts with an imaging mode, making contact without deforming the interface, detecting pico amp currents over long times with lateral drift less than A/min, preferably with the capability for temperature variation. In order to accomplish this we have developed a modification for commercial instruments that exploits high a gain amplifier, can interrupt an imaging process to control tip contact to a nanoparticle and deliver and extract transport properties. Preliminary data demonstrate that the modifications are successful.

To make nano-sized metal-oxide interfaces Au particle colloids were spin cast onto SrTiO3 (100) substrates and annealed at a temperature sufficiently high to eliminate organic surfactants and allow the particles to achieve equilibrium shape. Initial conditions for annealing were determined on oxidized Si, graphite and SrTiO3 (100) substrates with temperatures ranging from 500 C to 900 C. The most prevalent shape was the truncated octahedron, the lowest energy state for au nanoparticles 100nm in size or greater, bound by {111}hexagonal and {100} square planes,. Nanoparticles on the HOPG showed no

preference for lying on the hexagonal or square plane. The ratio of square planes to hexagons is approximately 2.6, meaning 72% of the particles to rest on the hexagonal plane and 28% to rest on the square facets if the surface does not prefer one facet over the other. Approximately this ratio was observed on HOPG substrates. This analysis is being used to sort geometries on the other substrates in order to control the interface structure.

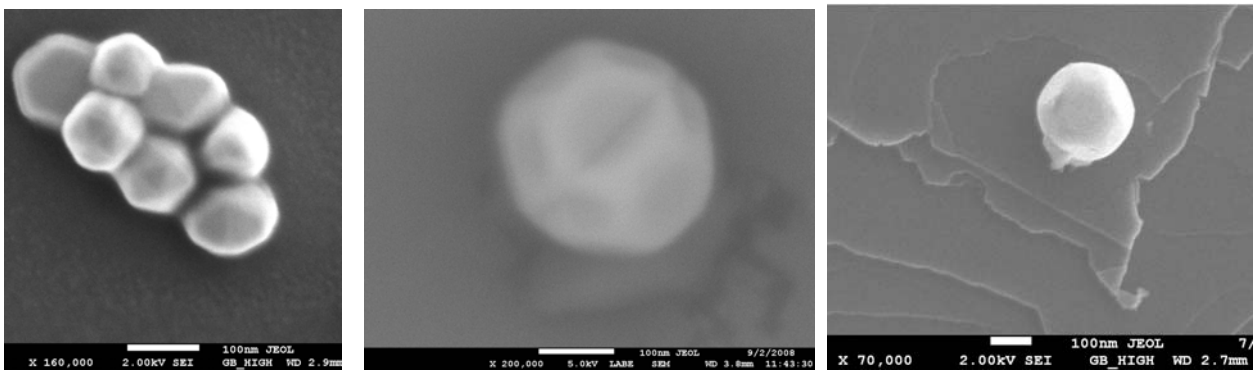

Figure 2. 100 nm Au particles on oxidized Si annealed at 850C for 1 hr (left), on SrTiO3 (100) annealed at 900 C for 1.5hr,on HOPG annealed at 900 C for 1 hr (right).

Future Plans

The next stage of the project involves characterizing the interfaces transport properties of Au/SrTiO3 nano-sized interfaces as a function of interface state density, particle size, and relate it to the atomic structure of the nanoparticle/oxide interface determined by high resolution TEM in collaboration with G. Duscher at NCSU.

Recent References

Scanning Probe Microscopy in Materials Science
M. Nikiforov, D. A. Bonnell Science of Microscopy ed P. Hawkes, J. Spence Springer (2007)

Atomic Structures of Oxide Surfaces
J. Garra, D. A Bonnell *Progress in Modern Physics* (2008)

High Resolution Characterization of Defects on Thin Oxide Films
M. Nikifrov, M. Brukman, D. Bonnell APL (2008)

Probing Physical Properties at the Nanoscale
M. Brukman, D. Bonnell Phyics Today (June 2008)

Properties at Atomic Resolution
D. Bonnell ACS Nano (Sept 2008)

Observing Materials Dynamics on the Fundamental Atomic Scale by Ultrafast In-Situ TEM

N. D. Browning (PI), M. L. Taheri, N. Goldman, B. W. Reed, J. E. Evans, and G. H. Campbell
browning20@llnl.gov, mtaheri@coe.drexel.edu, goldman14@llnl.gov, reed12@llnl.gov, evans80@llnl.gov, ghcampbell@llnl.gov.

Materials Science and Technology Division, Chemistry, Materials, Earth and Life Sciences Directorate, Lawrence Livermore National Laboratory, PO Box 808, Livermore, Ca 94550

Program Scope

The aim of this project is to develop a fundamental understanding of materials dynamics (from microseconds to nanoseconds) in systems where the required combination of spatial and temporal resolution can only be reached by the dynamic transmission electron microscope (DTEM). Although the DTEM can cover a broad time range, the emphasis of the work in this proposal will be around the microsecond timescale. In this regime, the DTEM is expected to have atomic scale resolution, providing an in-situ TEM capable of studying nanoscale dynamic phenomena with several orders of magnitude time resolution advantage over any existing in-situ TEM, i.e. it is an ultra-fast atomic scale in-situ TEM. This capability will be used to develop new insights into long-standing scientific problems related to the identification and control of the active sites on the nanoscale catalysts that are responsible for the selectivity of chemical reactions and the nucleation of nanostructures. The results will be used to study the nucleation and growth of nanowires for solid state lighting applications and the interaction of nanoscale metal clusters used for catalysis. Work in this proposal will also coordinate with other experiments on structural materials, biological materials and electronic materials to fully develop the range of fundamental ultrafast measurements possible in the DTEM.

Recent Progress

The first year of this project has emphasized the use of the DTEM to establish the basic capabilities for studying nucleation and growth phenomena (aspects of this research have led to the DTEM receiving both R&D 100 and Nano 50 awards in 2008). The first example of this has been the utilization of the DTEM to grow Si nanowires (NWs) by *in situ* pulsed laser ablation (Figure 1). One of the unique aspects of this work is that the Si NWs were fabricated without resistive heating or the flow of reactant gases. Although the result was obtained without time resolution (this experiment was a test of the specimen drive laser) this result establishes the ability to fabricate nanoscale systems in the DTEM under non-equilibrium conditions while simultaneously having the ability to image the growing nanostructures after each laser pulse. In future studies, dynamic observations will be incorporated into the experiment that may allow for a more complete understanding of the origin of texture, morphology and extended defects in NWs during nucleation and growth. Such observations should allow for a more comprehensive model of the mechanisms involved in 1D nanostructure production, and hence have a great impact on the future of the use of NWs in electronic device fabrication. Thus, in future we will be able to determine the local microstructure and morphology before, during and after laser-assisted NW formation, giving us insight into the processing parameters that influence growth.

In addition to the study of nanowires, the first year of this project has also examined the capabilities required to observe catalytic reactions in the DTEM. In this case, many of the

catalysts for which surface interactions are critical, consist of nanoclusters of metal dispersed on porous high-surface-area supports. These nanomaterials are not well understood, in part because they are highly non-uniform and their properties depend strongly on their interactions with the substrates (which are also highly non-uniform). A model example of such a catalyst is Au on TiO_2, which is a highly active catalyst for CO oxidation and selective for various partial oxidations. This processes that take place in this catalyst are the subject of intense debate, as it is unclear what the catalytically active species are within the system, with candidates being the Au nanoparticles themselves, isolated Au cations on the substrate, and Au cations at the metal–substrate interface. As a first step in understanding these processes an *in-situ* stage was used to investigate the clustering of Au on TiO_2. The initial results show that the *in-situ* stage (see future plans) designed to control the environment around the sample during analysis can function in the TEM and will be used in future years to investigate the details of the reactions.

One of the key metrics for understanding catalytic phenomena is to be able to determine nanoscale cluster sizes accurately under all environmental conditions. This becomes particularly challenging when the signal levels become very small and when the cluster sizes approach the resolution of the microscope. To be able to make measurements of cluster sizes under the DTEM low signal and high time resolution conditions, we have therefore developed a methodology to quantify cluster sizes that at least for the high vacuum case appears to have ~10pm precision for the smallest cluster sizes (3 to 10 atoms). The mathematical models for defining the size of the clusters and for dealing with noise and background variability should allow cluster sizes, shapes/orientations and compositions to be determined with a high degree of accuracy, allowing direct correlation with theoretical models and analyses by other experimental methods (such as EXAFS).

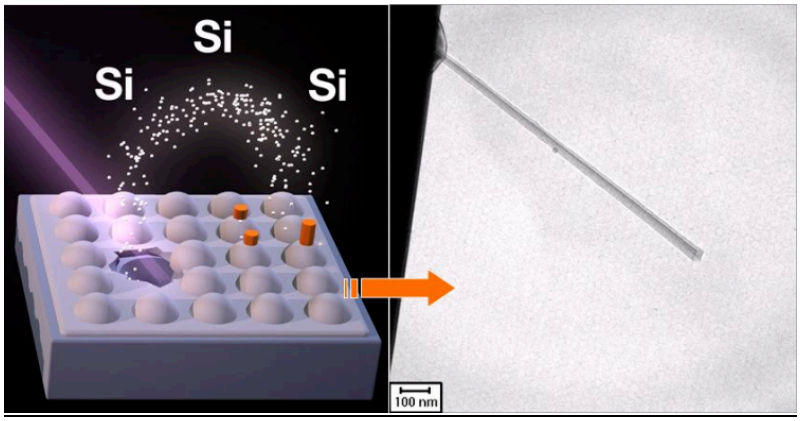

Figure 1: *In situ* pulsed laser ablation synthesis of Si nanowires within the DTEM.

To fully investigate the nature of the metal/oxide bond and the fundamental processes behind the catalytic activity of oxide-supported metal catalysts [1] we have also started computer simulations of the phenomena observed in the DTEM. This includes the role of TiO_2 surface defect, mechanisms for catalysis on the nanoparticles, and the degree of hydroxylation of the TiO_2 surface [1-3]. From a theoretical standpoint, a number of studies exist wherein zero-temperature Au nanostructures have been determined through energy minimization calculations of structures thought to be relevant to catalysis [1,3,4]. However, such calculations explicitly exclude any temperature effects, which can have a large effect on the associated free energy

barriers, particle migration, and aggregation. In addition, energy minimization calculations cannot explicitly determine particle diffusion pathways, the kinetic rate laws governing nanocluster formation, and other dynamic properties which are vital in order to fully characterize the catalytic system. To this end, we are elucidating the dynamic processes that govern Au nanoparticle catalysis through a combination of the fast chemical imaging on the DTEM and Molecular Dynamics (MD) simulations using *ab initio* codes. In order to accurately model particle aggregation or the catalysis of CO oxidation, we are required to perform computationally demanding Density Functional Theory (DFT) calculations. Previously calculated zero-temperature energetic barriers [3] suggest Au particle diffusion occurs on the microsecond time-scale and beyond, which are exceedingly difficult to achieve with standard simulation techniques. This is due to the fact that the free energy surfaces governing these reactions often contain multiple minima with large energy barriers. The high free energy barriers can be surpassed via the *metadynamics* simulation technique [5]. *Metadynamics* is a self-adaptive free energy calculation based on a "collective variable" that describes the reaction coordinate of interest. Our simulations (Figure 2) show that even fairly low temperatures (300 K) can reduce the energetic barrier for the diffusion of Au particles to 4 kcal/mol. Future work will elucidate the energetic barriers for different diffusion pathways and studies of larger Au clusters on both stoichiomechtric and nonstoichiometric surfaces. The simultaneous knowledge of the free-energy landscape and the electronic and atomic structure will allow for a more detailed understanding of ultrafast experimental results, through comparison to imaging and spectroscopic signatures in order to infer mechanisms and reaction rates.

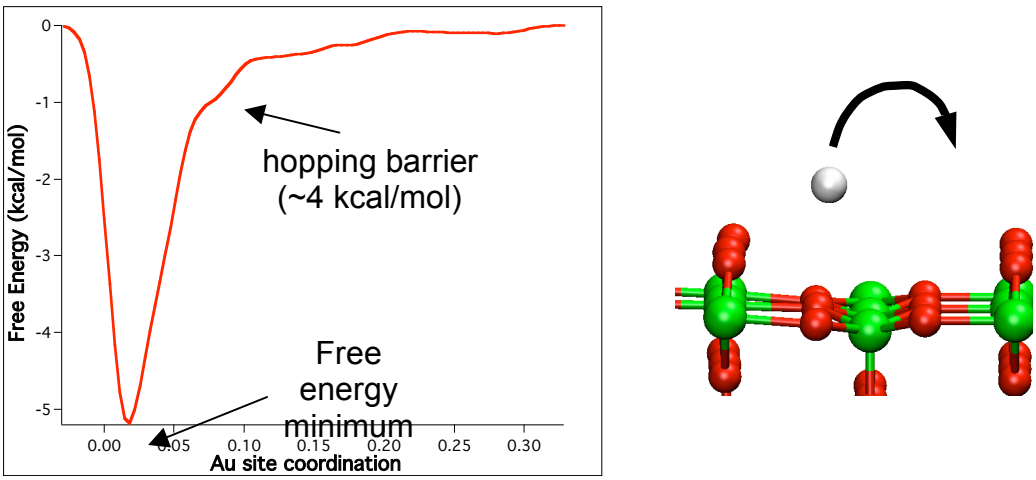

Figure 2: Free energy barrier calculated by metadynamics at a temperature of 150 K for the hopping of a single Au particle along a stoichiometric rutile TiO_2 (110) surface.

Future Plans

The research performed during the first year of this project has established the experimental and theoretical framework for analyzing the dynamic properties of nanoscale systems. The aim for the second year of this project is to complete the following tasks

1. Complete the installation and calibration of the in-situ stage for both high spatial resolution STEM experiments (not in the DTEM) and high temporal resolution measurements. This calibration includes the effect of the windows and the gas pressure on the resolution

achievable in the microscope. This work will also calibrate particle size measurements from annular dark field TEM with the Z-contrast STEM.

2. Install the capabilities for annular dark field TEM imaging with variable temporal resolution in the DTEM. The variable temporal resolution will be achieved by installing an arbitrary waveform generator that will allow the source laser (and hence the electron beam) to be varied between 10μs and 10ns in duration. The dark field TEM imaging will allow the DTEM characterization to be approximated to Z-contrast STEM and permit the quantified size, shape/orientation and composition analysis to be performed in the DTEM.
3. Correlate DTEM observations of Au nanocluster mobility/sintering under variable gas pressures and temperatures directly with MD simulations to elucidate the effects of metal-support interactions on catalytic properties.

This work performed under the auspices of the U.S. Department of Energy, Office of Science, Office of Basic Energy Sciences, Division of Materials Sciences and Engineering by Lawrence Livermore National Laboratory under Contract DE-AC52-07NA27344

References

1. E. Wahlström, N. Lopez, R. Schaub, P. Thostrup, A. Rønnau, C. Africh, E. Lægsgaaard, J. K. Nørskov and F. Besenbacher, *Phys. Rev. Lett.*, **90**, 026101, 2003.
2. D. Matthey, J. G. Wang, S. Wendt, J. Matthiesen, R. Schaub, E. Lægsgaard, B. Hammer, F. Besenbacher, *Science*, **315**, 1692, 2007.
3. H. Iddir, S. Ögut, N. D. Browning and M. M. Disko, *Phys. Rev. B*, **72**, 081407, 2005.
4. S. Chrétien and H. Metiu, *J. Chem. Phys.*, **127**, 084704, 2007.
5. A. Laio, M. Parrinello, *PNAS* **99**, 12562, 2002.

DOE Sponsored Publications 2008

"In-Situ Synthesis of Nanowires in the Dynamic TEM", M. L. Taheri, B. W. Reed, T. B. Lagrange, B. S. Simpkins, and N. D. Browning, in press *Small*

"Imaging of Transient Structures using Nanosecond in situ TEM", J. S. Kim, T. B. LaGrange, B. W. Reed, M. L. Taheri, M. R. Armstrong, W. E. King, N. D. Browning and G. H. Campbell, in press *Science*

"Nanosecond time resolved investigations using the *in situ* of Dynamic Transmission Electron Microscope (DTEM)", Thomas B. LaGrange, Geoffrey H. Campbell, Bryan W. Reed, Mitra L. Taheri, J. Bradley Pesavento, Judy S. Kim and Nigel D. Browning, in press *Ultramicroscopy*

"Laser Based *In Situ* Techniques: Novel Methods for Generating Extreme Conditions in TEM Samples", M. L. Taheri, T. B. Lagrange, B. W. Reed, M. R. Armstrong, G. H. Campbell, W. J. DeHope, J. S. Kim, W. E. King, D. J. Masiel, and N. D. Browning, in press *Microscopy Research and Techniques*

"In Situ Laser Crystallization of Amorphous Silicon for TFT Applications: Controlled Ultrafast Studies in the Dynamic TEM", M. L. Taheri, N. Teslich, J. P. Lu, D. G. Morgan, and N. D. Browning, submitted *Applied Physics Letters*

*"*Validation and Generalization of a Method for Precise Size Measurements of Metal Nanoclusters*",* B. W. Reed, D. G. Morgan, N. L. Okamoto, A. Kulkarni, B. C. Gates, and N. D. Browning, *in preparation*

Materials Properties at Interfaces in Nanostructured Materials: Fundamental Atomic Scale Issues

N. D. Browning, nbrowning@ucdavis.edu.

Department of Chemical Engineering and Materials Science, University of California-Davis, One Shields Avenue, Davis, CA 95616

Program Scope

The aim of the research program is to develop a robust method to investigate the fundamental changes in electronic structure/properties occurring at surfaces and interfaces in nanostructured materials. This research utilizes the development of two new atomic resolution scanning transmission electron microscopes (STEM), one with the ability to perform electron energy loss spectroscopy (EELS) with ~0.1nm spatial resolution and ~0.1eV energy resolution and another with ~0.2nm spatial resolution and ~0.8 eV energy resolution under a variety of atmospheric conditions. The spatial and energy resolution of these two microscopes allows experiments to be performed to investigate the effect of size, shape and composition, interface structure and surface termination on the local band structure of quantum dots. Here the aim is to use dielectric models to understand all the effects controlling the reactivity and optoelectronic response of isolated metal, oxide, and semiconductor quantum dots and the same systems embedded in either an organic or inorganic matrix. This will be achieved through controlled ex-situ synthesis of the quantum dots and systematic in-situ oxidation/reduction and reaction of the quantum dots in the microscope. Systems of interest to be studied include Si nanoparticles for hydrogen storage, doped Si and functionalized II-VI core shell nanoparticles for magnetic applications, and metal/oxide nanoparticles for solar power applications. The detailed atomic scale characterization of the individual quantum dots in the microscope will be compared with the standard optical characterization methods to develop a complete model for the effect of particular defect/surface/interface structures on the ensemble average properties of the quantum dot system. Through such measurements it is anticipated that fundamental models to guide the atomic scale processing of quantum dot systems for specific functionalities can be determined.

Recent Progress

The main aim of this work is to be able to quantify the effects of size, shape, composition and bulk/surface/interface structure on the electronic properties of nanostructures. The first year of work in this area has focused on the development of the TEM and STEM methods that will allow these features to be characterized at high spatial resolution with atomic scale sensitivity. While the techniques necessary for the characterization are well established, applying them to nanostructures present unique challenges. Typically nanostructures are sensitive to beam damage effects and can move under the beam, making characterization difficult. Additionally, for nanostructures embedded in organic media, beam damage can significantly modify the structure. Emphasis has therefore been placed on developing high resolution methods under low-dose conditions.

To achieve the very high spatial resolution (~0.1nm) that can potentially be provided by aberration correctors, the study of organic materials requires the microscope to be operated under hybrid conditions: low electron dose on the specimen in a liquid nitrogen cryo-stage (optimum for organics) at low defocus values (optimum for inorganics). Initial TEM images from standard organic test specimens (Figure 1) have indicated that under these conditions C_s-correction

provides a significant improvement in resolution for direct imaging of organic/biological samples (~0.16 nm). This shows that the electron dose can be reduced significantly and still provide atomic resolution for beam sensitive materials. Similar results have also been achieved using low-dose STEM operating conditions. In this case, a reduction of electron dose from a typical ~5x10^6 electrons/Å^2 used for inorganic materials to ~400 electrons/Å^2 still resulted in ~0.2nm resolution in an image of $SrTiO_3$.

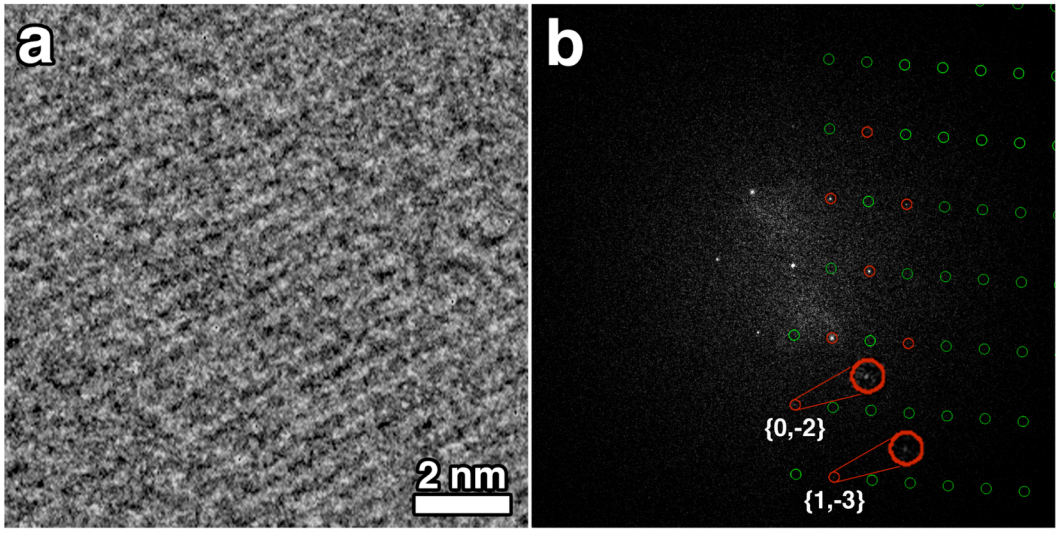

Figure 1: (a) Cs corrected TEM image of paraffin imaged with <10 electrons/Å^2. (b) The Fourier Transform indicates information transfer out to ~1.6 Å.

Another aspect of imaging nanostructures with high spatial resolution is to make the most of the information present in each image. In this case, typical zone axis Z-contrast STEM images contain many sub-images of the crystal unit cell and/or interface structure. The repetitive nature of these images allows standard image processing techniques that have been developed for the electron crystallography of biological macromolecules to be applied to increase the precision of the structural determination. These methods can be used to enhance the signal-to-noise present in the original images, to remove distortions in the images that arise from either the instrumentation or the specimen itself and to quantify properties of the material in ways that are difficult without such data processing. As a demonstration of the use of these methods, they have been applied to high resolution STEM images of Si_{46} clathrates, currently being developed for hydrogen storage (Figure 2), to determine the partial occupancy of the guest sites.

In the case of the nanostructures systems of interest for this research, many of the potential dopants in the matrix are lighter elements, making them extremely difficult to observe in both STEM and TEM. Using the same methods for image processing mentioned above, however, it is possible to quantify the presence of dilute levels of light elements inside a heavier matrix. This type of analysis has been demonstrated for the incorporation of Nitrogen into GaAs. Here films were prepared with variable N content from 0.5% to 2%. What is initially surprising about the Z-contrast images of these films is that the incorporation of N into the structure (presumably substitutional) increases the contrast. This can be understood in terms of the static displacements in the atomic columns caused by the size difference between N and As and this also highlights a means to interpret the level of contrast with doping. By evaluating the average contrast change in and between the columns from the experimental images as a function of doping (Figure 3a), the effect of each type of structure, either substitutional, interstitial etc, can be determined. A

series of first principles calculations was performed for the various structures that were then used for inputs to the Z-contrast image simulations (Figure 3b). By comparing the trends in the simulations with the experimental data and by also considering the effect of each on the average dumbbell spacing, the onset of N clustering could be observed in the structures. Clustering appears to take place below the solubility limit of N in GaAs and appears to be the precursor to the formation of GaN precipitates.

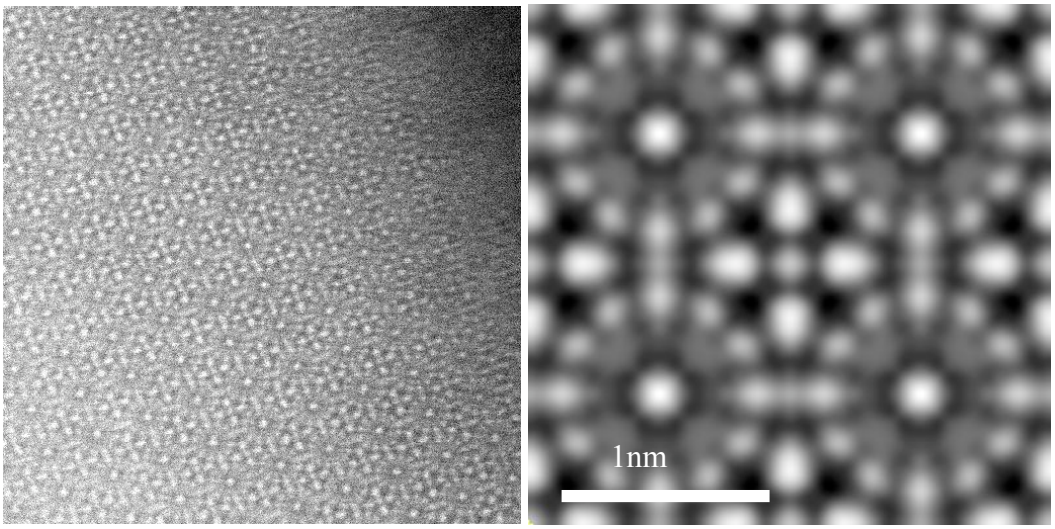

Figure 2: (a) Raw Z-contrast Image of the Si_{46} clathrate structure and (b) processed image.

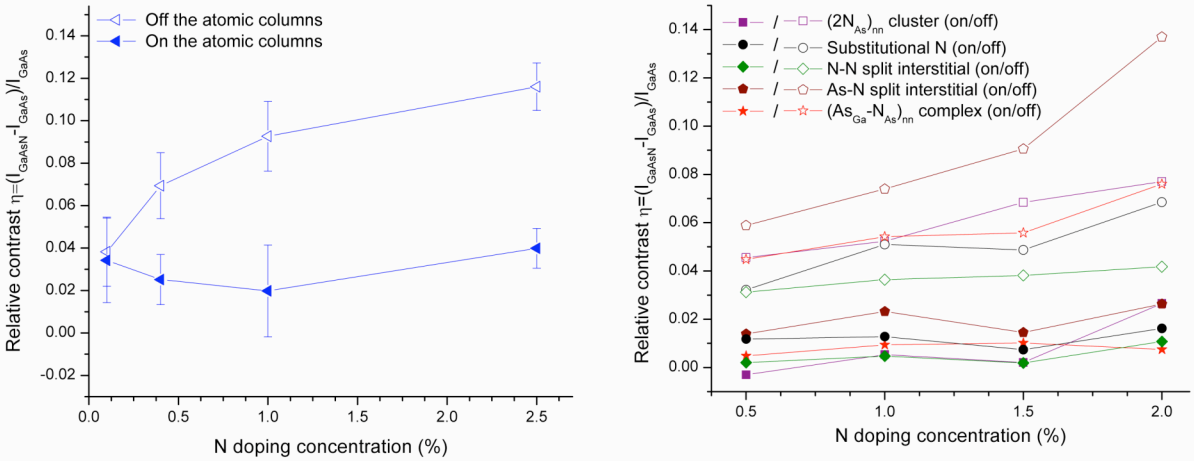

Figure 3: (a) Experimental image intensity off and on the GaAsN columns (b) simulations of the potential defect complexes.

Future Plans

The results from this years work and previous tomography experiments show that the size, shape, structure and composition of nanostructures can be characterized with atomic scale precision. The aim for the future is to correlate this analysis with the optoelectronic properties. To achieve this, the following tasks will be addressed.

1. Develop a simulation package for low-loss spectroscopy that includes bulk/surface losses, retardation effects and can be solved for the penetrating beam case.

2. Incorporate a high-resolution in-situ stage for the analysis of nanostructures under different gaseous environments
3. Analyze doped Si nanostructures, core-shell semiconductor heterostructures and metal nanocluster/perovskite sheet catalysts in the in-situ stage to quantify the effect of preparation/embedding medium on the overall optoelectronic properties.

DOE Sponsored Publications 2007-2008

"Application of Two-dimensional Crystallography and Image Processing to Atomic Resolution Z-contrast Images", David Gene Morgan, Quentin M. Ramasse and Nigel D. Browning, submitted *Journal of Electron Microscopy*

"Observation of Atomic Scale Clusters in Dilute Nitrides of GaAs", M. Herrera, Q. M. Ramasse, D. G. Morgan, D. Gonzalez, J. Pizarro, A. Yáñez, P. Galindo, R. Garcia, M.-H. Du, S.B. Zhang, M. Hopkinson and N. D. Browning, submitted *Physical Review Letters*

"Towards Low-dose Imaging in STEM", J. P. Buban, H. Stahlberg, N. D. Browning, submitted *Journal of Electron Microscopy*

"$K_4Nb_6O_{17}$-Derived Photocatalysts for Hydrogen Evolution from Water: Nanoscrolls versus Nanosheets", Frank Osterloh, Michael S Sarahan, Elizabeth C Carroll, Mark Allen, Delmar S Larsen, Nigel D Browning, in press *J. Solid State Chemistry*

"Low-dose aberration corrected cryo-electron microscopy for organic specimens", James E. Evans, Crispin Hetherington, Angus Kirkland, Henning Stahlberg, and Nigel D. Browning, in press *Ultramicroscopy*

"Atomic Scale Analysis Of The Effect Of The SiO_2 Passivation Treatment On InAs/GaSb Superlattice Mesa Sidewall" **,** M. Herrera, M. Chi, M. Bonds, N. D. Browning**,** J. N. Woolman, R. E. Kvaas, S. F. Harris, D. R. Rhiger**,** C. J. Hill, *Applied Physics Letters* **93**, 093106 (2008)

"First demonstration of CdSe as a photocatalyst for hydrogen evolution from water under UV and visible light", A. F. Frame, E. C. Carroll, D. S. Larson, M. Sarahan, N. D. Browning, F. E. Osterloh, *Chemical Communications* **19**, 2206-2208 (2008)

"Prospects for Analyzing the Electronic Properties of Nanostructures by VEELS", R. Erni, S. Lazar, N. D. Browning, *Ultramicroscopy* **108**, 270-276 (2008)

"The Impact of Surface and Retardation Losses on Valence Electron Energy-Loss Spectroscopy", R. Erni and N. D. Browning, *Ultramicroscopy***108**, 84-99 (2008)

"Hydrogen Encapsulation in a Silicon Clathrate Type I Structure: $Na_{55}(H_2)_{2.15}Si_{46}$: Synthesis and Characterization", Doinita Neiner, Norihiko L. Okamoto, Cathie L. Condron, Quentin M. Ramasse, Ping Yu, Nigel D. Browning and Susan M. Kauzlarich, *Journal of the American Chemical Society* **129**, 13857-13862 (2007)

"A Structural and Spectroscopic Study on Copper and Oxygen Incorporation into Wurtzite-Type Gallium Nitride", B. Seipel, R. Erni, C. Li, L. Noice, A. Gupta, K.V. Rao, N. D. Browning, P. Moeck, *J. Materials Science***22**, 1396-1405 (2007)

"Growth and structure of $PbVO_3$ Thin Films", L. W. Martin, Q. Zhian, Y. Suzuki, R. Ramesh, M. Chi, N. D. Browning, T. Mizoguchi, J. Kreisel, *Applied Physics Letters* **90**, 062903 (2007)

"Quantification of the Size-Dependent Band Gap of Individual Quantum Dots", Rolf Erni, Nigel D. Browning, *Ultramicroscopy***107**, 267-273 (2007)

Complex Transient Events in Materials Studied Using Ultrafast Electron Probes and Terascale Simulation

Geoffrey H. Campbell, PI
Thomas LaGrange, Nigel D. Browning, Judy S. Kim, Co-I
Lawrence Livermore National Laboratory, Materials Science and Technology Division
PO Box 808, Mailstop L-356, Livermore, CA 94550
E-mail: ghcampbell@llnl.gov

Project Scope

The thrust of the project is to study martensitic transformations [1] and rapid chemical reactions [2] with the novel capabilities offered by the newly developed DTEM instrumentation [3] (which has led to R&D100 and NANO50 awards). We strive to map the kinetics of martensitic phase transformations by developing time-temperature-transformation diagrams with nanosecond time resolution. By investigating materials with differing scales of initial microstructure, we observe the differing influences of nucleation behavior on the final microstructure. Our observations are used to constrain analytical models of the transformation kinetics.

We also study nucleation and growth kinetics in diffusive systems that are strongly driven. These recent DTEM results have shown that the nucleation rates can vary by up six orders of magnitude from those predicted by scaling the known kinetics data to the temperatures used in the DTEM experiments. These differences point to changes in nucleation behavior, from homogenous to heterogeneous, where surface nucleation sites may be predominant and enhance the nucleation rate.

We also made observations of morphological details of the reaction front in energetic nanolaminates. The DTEM reveals transient structures at the reaction front in these rapid solid-state chemical reactions. In this abstract we focus on the phase transformation results.

Recent Results

Titanium is a dimorphic element, which undergoes a crystal structure change from HCP (α-phase) to the BCC (β-phase) atomic coordination upon heating above 1155K, which is accomplished by a simple shear strain of the HCP unit cell. The rapid α to β transition in nanocrystalline Ti was studied using the

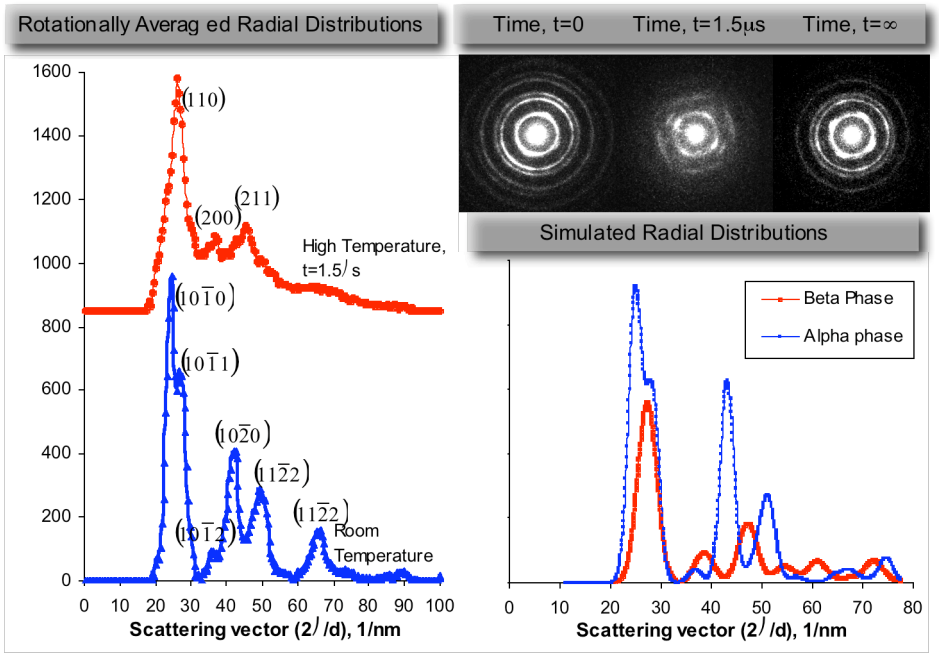

Figure 1 – 15 ns exposure, single-shot electron diffraction data of the α to β transformation in nanocrystalline Ti occurring by pulsed laser induced temperatures of 1300 K. Upper-right diffraction patterns show the transformation occurring from α-phase to β-phase at 1300 K and time delay of 1.5 μs, which after cooling back through the transition temperature transforms back to α-phase (t=∞). Comparison of the rotationally averaged radial intensity distributions (plot on left-hand side) with simulated diffraction data (plot on lower right-hand side) indicate that transform to the β-phase was complete at 1.5 μs.

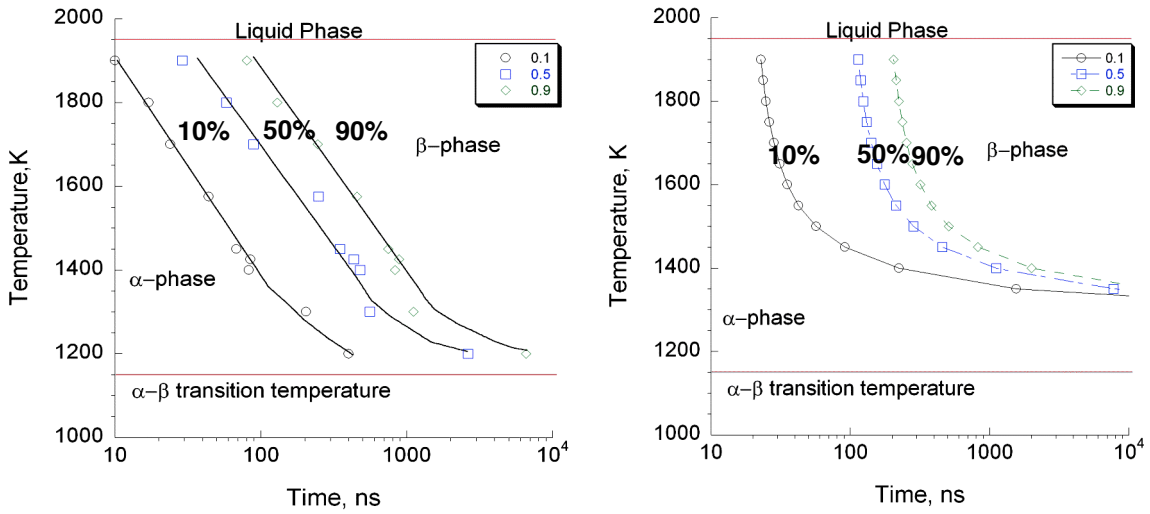

Figure 2 – a) Experimental isothermal phase diagram for nanocrystalline Ti film constructed from quantitative analysis of the pulsed electron selected area diffraction data. Lines through are a smoothing curve fit through the data set. b) TTT curves calculated using the Kaufman-Cohen description for isothermal martensite transformation kinetics and available thermodynamic data.

DTEM (Fig.1), which at high heating rates (>10^3 K/s) occurs by an isothermal martensitic-type mechanism. The transformation kinetics were studied through a series of nanosecond, time-resolved diffraction patterns acquired from the transition temperature to the melting point taken at different stages of the transformation. From quantitative analysis of the patterns using Rietveld fitting routines, the phase fractions and corresponding α to β transformation rates were determined as a function of temperature, and the first reported time temperature transformation diagram (TTT curves) for Ti was constructed [1] (Fig. 2). Theoretical TTT curves were calculated using analytical models for isothermal martensite from available thermodynamic data and experimental data gathered from pulsed electron brightfield TEM images. Above 1400 K, there is excellent agreement between experiment and the analytical model proposed by Kaufman and Cohen [4], suggesting that the α to β transformation rate in Ti is governed by nucleation kinetics. However below 1400K, theory predicts much slower transformation rates than experiment. Experimental data fits using the Pati-Cohen model for isothermal martensite transformation kinetics [5, 6]suggests that an increase in autocatalytic nucleation may account for the fast transformation rates at lower temperatures.

Complementary DTEM experiments on coarse-grained materials were also conducted. It was found that, although the transformation rates are similar, a drastic change in transformed microstructure morphology was observed in the coarse-grained material, suggesting that grain size alters the nucleation behavior, see Fig. 3. Pulsed laser heating of the TEM foil above α to β transition temperature rapidly transforms the initial equiaxed α-phase grains (100 ns) into large laths of β-phase having a distinct, jagged interface with preexisting, untransformed α-grains (Figure 3b). It is also noted that the orientation of the laths is different across the α-grain boundaries due to distinct habit planes for nucleation and growth and the crystallographic orientation relationships associated with the martensitic phase transformation. Since the electropolished TEM foil is wedge-shaped, the material transforms first in the thin regions near the perforation and then radiates outward into the thicker regions of the foil. The interface designates the boundary where the temperature and thermodynamic driving force become too low to kinetically drive the transformation. Substantial refinement of the β-phase lath structure is observed when cooled to room temperature and the reverse transformation back into α-phase has taken place. Overall lath domains persist, but are sectioned by fine acicular α-phase, having up to 12 different crystallographic orientations (which can be noted by the high amount of contrast observed in Figure 3c) and suggesting that the forward and reverse transformation behaviors are different.

These morphological differences created by forward and reverse transformation were not observed in the nanocrystalline Ti foils, where the morphologies and grain size of the α-phase and β-phase were similar

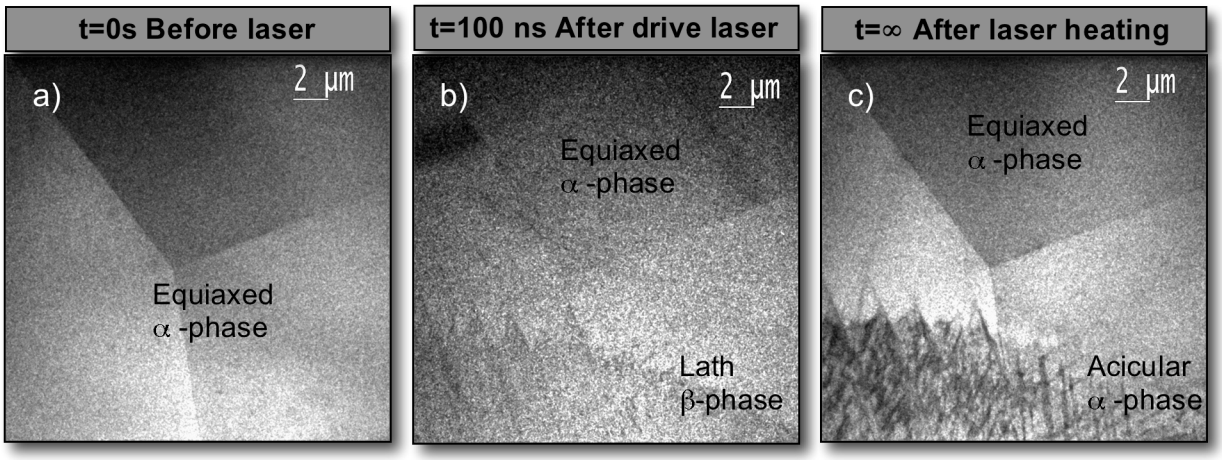

Figure 3 – A series of single-shot bright-field, 15 ns time-resolved TEM images showing the change in grain morphology induced by the α→β phase transformation in coarse-grained Ti material. a) The left image is taken at room temperature before the laser strikes the film. b) The center image is taken 100 ns after the laser hits the film, showing that preexisting α-grains transform into β-phase laths at high temperatures (estimated temperature rise ~1800K). Also, notice the jagged interface that is indicative the martensitic phase transformation. c) Image of the α-phase after cooling back down to room temperature, note the degree of refinement in the microstructure that has occurred due to the forward and reverse transformation.

before and after transformation. It appears that the number of nucleation sites was not altered in the nanocrystalline material due to transformation of the foil, whereas, in the coarse-grained material, excursions through the forward and reverse transformation led to substantial refinement of the microstructure, suggesting a change in the number and type of active nucleation sites. Future experiments will continue to characterize the nucleation behavior in materials by observing the interplay between the phase front interface dynamics and the role of local microstructural features on heterogeneous nucleation events.

In the area of strongly driven crystallization of an amorphous material, pulsed laser heating was used to anneal an amorphous NiTi film in the DTEM and revealed striking differences in the devitrification processes as compared to slower, "furnace-based" anneals. The extraordinarily fast crystallization rates and the observed fine microstructures after crystallization were not expected and do not correlate with literature reported kinetic data, leading us to find that these observations have not been previously described.

Devitrification of NiTi films has been studied extensively using differential scanning calorimetry (DSC) [7] and *in situ* TEM [8]. The crystallization temperature (exotherm) has been found to vary in DSC measurements from 700K to 775K depending on the composition, prior thermal treatment, thickness, and residual stress in the film. From kinetics analysis of DSC data using the Kissinger method or Johnson-Mehl-Avarami-Kolomogrov (JMAK) rate theory, activation energies for polymorphic crystallization have been calculated that range from 250 to 500 kJ/mol (2.6 to 5.2 eV), indicating the sluggish nature and long-range diffusion required for devitrification at low temperatures and slow heating rates. From *in situ* TEM observations, Lee et al. determined a growth and nucleation rate for crystallization, 0.01 μm s^{-1} and 0.017 nuclei per μm^{-2} s^{-1} at 763 K, respectively [8]. The current DTEM results on the nucleation kinetics differ strongly with these previous observations showing nucleation rates that are six orders of magnitude faster than predicted from these reported kinetic data. Extrapolation of the kinetic parameter derived from these data to temperatures of 1200K for the DTEM experiment yields a predicted nucleation rate at these temperatures of 4 μm^{-2} s^{-1}, orders of magnitude lower than observed in the DTEM experiments described next.

In contrast to the expected crystallization rates under pulsed laser irradiation, the amorphous NiTi films rapidly laser heated to temperatures of 1200K crystallizes within <5 μs, see Figure 4. These crystallization rates do not correspond with measured kinetic data, e.g., activation energies and rate constants, and known nucleation behavior observed in differential scanning calorimetry (DSC) or by *in situ* TEM. In fact, the

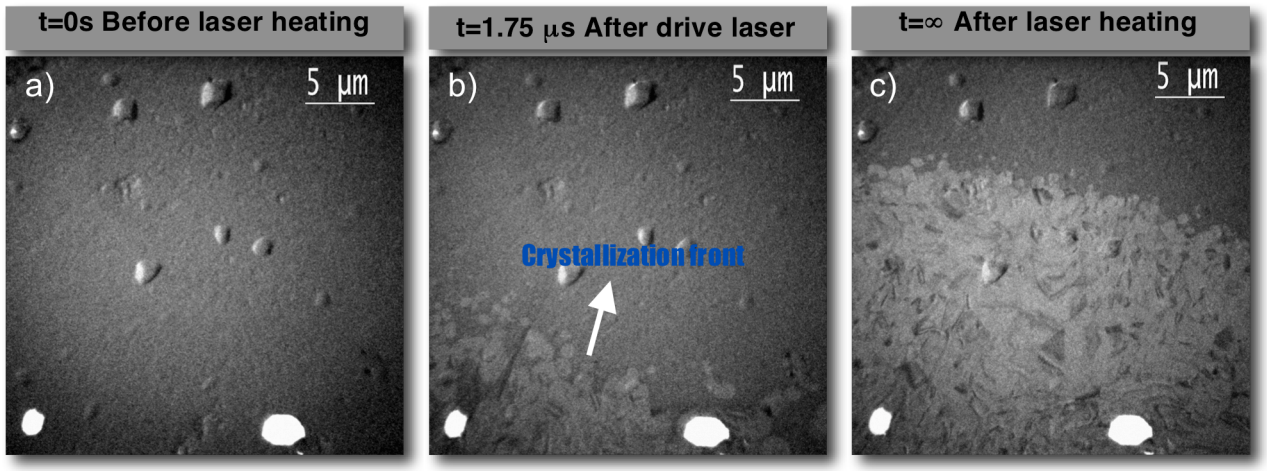

Figure 4 – Time-resolved TEM brightfield images taken with 15ns exposure, a) image of the amorphous NiTi film taken at room temperature before laser heating and crystallization, b) a "snap-shot" image of the propagating crystallization front taken at a temperatures of 1200K and 1.75μs after laser heating pulse, c) image taken of room temperature crystallized microstructure. The nucleation rate is estimated from multiple experiments by counting and comparing the number of crystallites in a given area at a particular time step.

measured nucleation rates in the DTEM experiments are six orders of magnitude larger than those predicted by rate theory at temperatures of 1200K. This difference infers that the potency of nucleation sites changes at high temperature (>800K), e.g., free surfaces and local density variations in the amorphous film may become active heterogeneous sites, which are not commonly observed at lower crystallization temperatures. The recent DTEM images shown in Fig. 4 are a first step in understanding the extraordinary crystallization rates in strongly driven conditions. However, elucidation of complex nucleation behavior requires movie capabilities.

Future Work

The interesting interaction of microstructure with the martensite transformation will be pursued. However, we are evaluating a change in system to ease experimental complications brought about by the study of Ti. The phase transformation in Ti occurs at high temperature and observations of the specimen at high temperature have increased background levels in both the diffraction patterns and the images cause by thermal diffuse scattering. We will, therefore, investigate NiTi based martensite transformations, which can be thermally driven at temperatures just above room temperature, significantly improving the quality of our data.

We will also continue our studies of crystallization from the amorphous phase under strongly driven conditions. We will use double exposures enabled by the soon to be operational arbitrary waveform cathode laser on the DTEM to allow precise measurement of crystallization front velocity for a more accurate separation of nucleation and growth activation energies.

This work performed under the auspices of the Office of Basic Energy Sciences, U.S. Department of Energy by Lawrence Livermore National Laboratory under Contract DE-AC52-07NA27344.

Literature Cited

[1] LaGrange T, *et al*. Acta Mater 2007; 55:5211.
[2] Kim JS, *et al*. Science in press;
[3] LaGrange T, *et al*. App Phys Lett 2006; 89:
[4] Kaufman L and Cohen M. Progress In Metal Physics 1958; 7:165.
[5] Pati SR and Cohen M. Acta Metall 1969; 17:189.
[6] Pati SR and Cohen M. Acta Metall 1971; 19:1327.
[7] Kim JJ, *et al*. Scripta Metall 1986; 20:243.
[8] Lee HJ, *et al*. App Phys Lett 2005; 87:

Electronic structure and properties of complex ceramics and their microstructures

Wai-Yim Ching, Chingw@umkc.edu
Department of Physics, University of Missouri-Kansas City, Kansas City, Missouri 64110

Program Scope

This program consists of large-scale *ab initio* and broad-ranged computational efforts to study the structure and properties of complex ceramics and their microstructures. The project takes advantage of the rapidly growing computing power and state-of-the-art computational methods that can be applied to much larger and more complex systems. It enables us to explore, investigate, and verify the structure/properties relationship for complex microstructures in ceramics including grain boundaries (GBs), intergranular glassy films (IGF), defects, surfaces and interfaces. The electronic structure and spectroscopic properties of novel materials and configurations are emphasized. These investigations are carried out in close collaboration with experimental groups. In the next few years, focuses will be on two main projects: (1) The development of a new spectral imaging (SI) technique using *ab initio* data; and (2) fundamental study of mullite ceramics. The goal of the SI project is to provide a new method to interpret electron microscopy measurements. The goal of the mullite project is to model and understand mullite ceramics down to the atomistic and electronic level.

Recent Progress

(A). *Deformation pattern and failure mechanism of IGF models in Si_3N_4.*

One of the major accomplishments is the exploration of the atomic-scale structure and properties of IGFs in β-Si_3N_4. Large-scale *ab initio* calculations in the form of "theoretical experiments" were carried out on a basal-IGF model by applying various forms of strained deformations including tensile, compression, and shear. These results were analyzed in the form of strain field images to apprehend the atomic scale mechanisms that lead to failure within the IGF or at the interface. It shows the deformation behavior to be extremely complex and exhibits regions of compressive strains in significant violation to the Cauchy-Born rule. This work connects atomic-scale simulations to engineering mechanics. The electronic structure of this complex IGF model is also calculated, showing the role of defective atoms at the interphase boundary. This work offers a new level of understanding on the microscopic deformation behavior in complex ceramics and could stimulate innovative experimental designs for their direct observation. This work is now extended to a different and larger IGF model with prismatic surfaces. Preliminary data indicate a very different mechanical response from the basal-IGF model.

(B). *Electronic structure and properties of grain boundary models in Al_2O_3.*

Significant progress has been made on the large-scale modeling of GBs in Al_2O_3. In collaboration with an experimental group at the University of Tokyo, research showed the direct observation of segregated Y atoms at the Σ31 GB core using STEM [1]. Theoretical calculation provided evidence that the strengthening is due to the replacement of Al by Y at strategic locations in the GB core with a favorable energy gain which simultaneously results in an increased number of interatomic bonds and overall bond strength. More recently, research on GBs has been extended from structural aspects to EELS spectroscopy. The atom specific calculations of these models not only revealed the spectral differences for differently bonded atoms but also form the basis for developing a SI technique. Such calculations complement experimental measurements in pursuit of more accurate GB characterization. Another important accomplishment in the study of GB models is the *ab initio* calculation of the phonon spectra of these models which are necessary for *ab intio* thermodynamic calculations.

(C). *Electronic, structural, and spectroscopic properties of complex ceramics.*

The structures and properties of many complex ceramic crystals have been investigated. Recent accomplishments include Al_2SiO_5 crystals (andalusite, sillimanite, kyanite). In particular, a comprehensive paper on the XANES/ELNES spectral calculations in the Y-Si-O-N system has been published [2]. Because many different types of bonding between cations (Si, Y) and anions (O, N) exist in these crystals consisting of six binary (α-SiO_2, stishovite SiO_2, β-Si_3N_4, α-Si_3N_4, γ-Si_3N_4, Y_2O_3), three ternary (Si_2N_2O, $Y_2Si_2O_7$, Y_2SiO_5) and three quaternary ($Y_2Si_3N_4O_3$, $Y_4Si_2O_7N_2$, $Y_3Si_5N_9O$) crystals, this system provides a rich data base when seeking meaningful correlations of the ELNES edges of the ions with their local structural environments. 45 spectra of ions in different local coordination were calculated and analyzed. Another system studied is $AlPO_4$ which has three phases: hexagonal (α-), orthorhombic (o-) and monoclinic (m-) formed at different pressures [3]. The rich variations in local bonding in crystals with the same formula unit and same types of atoms in equal proportions offer a rare opportunity for the precise characterization of their XANES/ELNES spectra. On the basis of these calculations, we have questioned the long standing practice of using the so-called "fingerprinting" technique for ELNES interpretation. This will change the way the experimental data are analyzed in future. Another very important publication for ceramic crystals is the calculation of elastic constants and bulk structural parameters of 44 crystals (oxides, nitrides, carbides, and others) with different crystal structures [4]. This work will lead to a systematic study of the mechanical properties of complex ceramics crystals.

(D). *Structure and bonding of the (001) surfaces of fluorapatite and hydoxyapaite.*

Bioceramics is an important part of ceramic materials research. We have completed the study of the (001) surface structure of fluorapatite (FAP or $Ca_5(PO_4)_3F$) and hydoxyapaite (HAP or $Ca_5(PO_4)_3OH$) crystals [5]. This has been a very challenging project due to the complexity of the crystal structure and the stability issues related to surface termination. Our calculation showed that the stable (001) surfaces are O-terminated in both crystals with surface energies of 0.865 and 0.871 J/m^2 respectively for FAP and HAP. There are significant atomic displacements of Ca and other ions near the surface. [see Fig.1]. The most important conclusion is that the (001) surfaces in both crystals are positively charged. This result has important implications on the adsorption and interaction of organic molecules and proteins on apatite surfaces in an aqueous solution that is important for bioactivity. Similar work on another bioceramic, tri-calciumphosphate (TCP) is currently in progress.

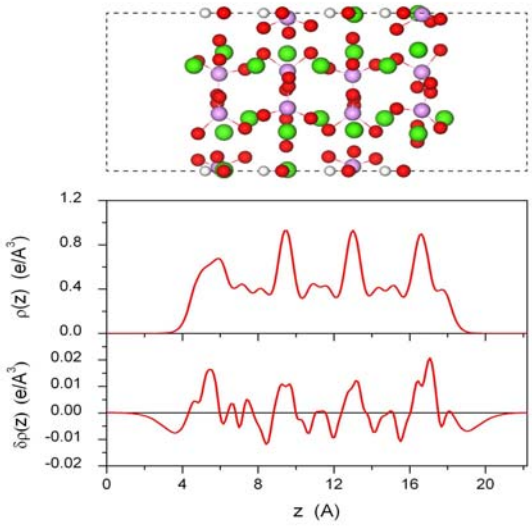

Fig. 1. Upper panels shows the relaxed supercell slab model of the HAP (001) surface atoms, Ca (green), P (violet), O (red), and H (white). The vacuum region of the surface model is shown on the either side of the two surfaces. The lower panel shows the valence charge density ρ(r) and its deviation Δρ(r) from neutral atom charge across the bulk and surfaces in HAP (001) model.

(E). *A comprehensive study of the properties of γ-Al_2O_3.*

γ-Al_2O_3 is one of the most important transition alumina with many important applications especially in cΣ31 GB Σ31 GB atalysis. There has been much controversy regarding its structure and various properties. We have investigated theoretically [6] the lattice dynamics and phonon spectrum [see Fig.2**],** elastic constants and bulk structural parameters, electronic structure and interatomic bonding, optical properties and ELNES spectra. These results are in good agreements with most experimental data but the effect of the porosity of the γ-Al_2O_3 samples should be properly assessed. The most important conclusion of this work is that the traditional view that γ-Al_2O_3 as a defective spinel with cation vacancies (or its variations) should be modified. γ-Al_2O_3 is better described as an amorphous network-like structure with specific ratio of Al_{tet} to

Al_{oct} (0.6); and that the O ions are either in 3-fold or 4-fold coordination in equal proportion. This work is the most comprehensive calculation to date on the physical properties of γ-Al_2O_3 and will have a large impact on research in this transition alumina.

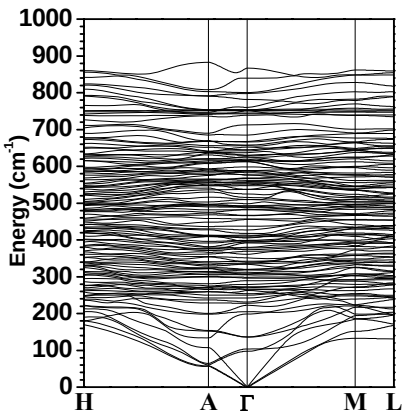

Fig. 2. Calculated phonon dispersion spectrum of γ-Al_2O_3.

Futures Plans

(A) *Initiation of the development of spectral imaging technique*.

We have just started a new and ambitious initiative to develop an effective imaging technique based on the ELNES data calculated using the *ab initio* approach. The supercell method for ELNES/XANES spectral calculation was developed in the PI's laboratory. It has been recognized as one of the most competitive methods for spectroscopic calculations of materials. Numerous papers have been published using this method in recent years. The goal now is to capitalize on this method and to develop a practical spectral imaging (SI) technique that contains the information about interatomic bonding and electronic structure in the imaging of the materials. This method is complementary to experimental probes using aberration corrected STEM and EELS, but is also more versatile. Eventually, we hope it will be a standard imaging technique like many other image simulations codes used in all major laboratories. Experimentally, spectral imaging using the most advanced microscopes is a major area of research at many DOE laboratories. Preliminary application of this method to a passive defect model in crystalline Si and the Σ5 GB in crystalline $SrTiO_3$ is underway.

(B) *Structural modeling for the Mullite ($Al_{4+2x}Si_{2-2x}O_{10-x}$) system*.

Mullites, or alumino silicates, are one of the most important classes of ceramic materials which Robert B. Sosman coined as the ceramic phase par excellence. In recent years, in addition to its traditional application in conventional ceramics, such as clay, mullite has found strong applications in advanced structural and functional ceramics due to many of its outstanding properties such as low thermal expansion, low thermo conductivity, and superior creep resistance. Surprisingly, no calculations on the electronic structure or other fundamental properties of mullite are available. This is mainly due to uncertainty in the underlying structure of mullites which are always described as crystalline phases with partial site occupations for both cations and O sites. Electronic structure theory in condensed matter physics is incompatible with the notion of partial atomic occupation. We plan to fill this void by large-scale supercell modeling of mullites followed by comprehensive investigations of their various physical and thermodynamic properties. We have already studied one end member of the mullite series *($Al_{4+x}Si_{2-2x}O_{10-x}$)* with x = 0 (silliminite) and have determined the structure of the other elusive end member with x = 1, the iota phase of alumina (ι-Al_2O_3).

References

[1] J. Buban, K. Matsunaga, J. Chen, N. Shibata, W.Y. Ching, T. Yamamoto, Y. Ikuhara, Science, 311, 212 (2006).

[2] W.Y. Ching, and P. Rulis, Phys. Rev. B17, 35125-1-17 (2008).

[3] W.Y. Ching, and P. Rulis, Phys. Rev. B77, 125116-1-7 (2008).

[4] Hongzhi Yao, L. Ouyang and W.Y. Ching, J. Am. Ceram. Soc. 90 [10] 3194-3204 (2007).

[5] P. Rulis, Hongzhi Yao, L. Ouyang, and W.Y. Ching , Phys. Rev. B76, 245410-1-15, (2007).

[6] W.Y. Ching, L. Ouyang, Paul Rulis, and Hongzhi Yao, Phys. Rev. B 78, 014106-1-13 (2008).

DOE Sponsored Publications (2006-2008)

1).J. Buban, K. Matsunaga, J. Chen, N. Shibata, W.Y. Ching, T. Yamamoto, Y. Ikuhara, "Grain Boundary Strengthening in Alumina by Rare Earth Impurities", Science, 311, 212-215 (2006).

2). W.Y Ching and Paul Rulis, "Ab-initio calculation of the electronic and spectroscopic properties of spinel Sn_3N_4", Phys. Rev. B73, 045202-1-9 (2006).

3). W.Y. Ching, Paul Rulis, Yong-Nian Xu and L. Ouyang, "The electronic structure and spectroscopic properties of 3C, 2H, 4H, 6H, 15R, 21R polymorphs of SiC", Materials Science and Engineering A, 422 C1-2, 147-156 (2006).

4). A. Zerr, R. Riedel, T. Sikine, T. Lowther, W.Y. Ching, and I. Tanaka, "Recent Advances in New Nitrides", Advanced Materials, 18, 2933-2948 (2006).

5). W. Y. Ching, Jun Chen, Paul Rulis, Lizhi Ouyang, and Anil Misra, "*Ab initio* Modeling of Clean and Y-doped Grain Boundaries in Alumina and Intergranular Glassy Films (IGF) in β-Si_3N_4", J. Materials Scence, 41 (16) 5061-5067, (2006).

6). A. Hunt, W.Y. Ching, Y.-M. Chiang, and A. Moewes "Electronic structure of $LiFePO_4$ and $FePO_4$ studied using resonant inelastic x-ray scattering", Phys. Rev. B73, 205120-1-10 (2006).

7). J.B. MacNaughton, A. Mowes, J.S. Lee, S.D. Wetting, H.-B. Kraatz, L. Ouyang, W.Y. Ching and E.Z. Kurmaev, "Dependence of the DNA Electronic structure on environmental and structural variations", J. Phys. Chem. 110(32), 15742-748 (2006).

8). Jun Chen, Paul Rulis, Lizhi Ouyang, S. Satpathy, and W.Y. Ching,"Vacancy enhanced ferromagnetism in Fe-doped rutile TiO_2", Phys. Rev. B74, 235207-1-5 (2006).

9). R. F. Rajter, W.Y. Ching, R. H. French, W. C. Carter, and Y.M. Chiang, "van der Waals-London dispersion interactions of optically uniaxial metallic and semiconducting carbon nanotubes determined from ab initio optical properties", J. Appl. Phys., 101, 54303-1-5 (2007).

10). A. Misra, L. Ouyang, J. Chen and W.Y. Ching, "Ab initio calculations of strain field and failure pattern in silicon nitride intergranular glassy films", Philosophical Magazine A. 87(25), 3839-3852 (2007).

11). Hongzhi Yao, L. Ouyang and W.Y. Ching, "Ab initio Calculation of the elastic constants of ceramic crystals", J. Am. Ceram. Soc. 90 [10] 3194-3204 (2007).

12). R. F. Rajter, R. Podgornik, A. Parsegian, R.H. French, and W.Y. Ching, "van der Waals-London dispersion interactions for optically anisotropic cylinders: Metallic and semiconducting single wall carbon nanotubes",Phys. Rev. B76, 045417-1-16 (2007).

13). T. Mizoguchi, A. Seko, M. Yoshiya, H. Yoshida, W.Y. Ching and I. Tanaka, "X-ray absorption near-edge structure of disordered $Mg_{1-x}Zn_xO$ solid solutions First-principles", Phys. Rev. B76, 195125-1-7 (2007).

14). P. Rulis, H. Yao, L. Ouyang, and W.Y. Ching "Electronic structure, bonding, charge distribution and X-ray absorption spectra of the (001) surfaces of fluorapatite and hydroxyapatite", Phys. Rev. B76, 245410-1-15, (2007).

15). Sitaram Aryal, Paul Rulis and W. Y. Ching, "Density functional calculation of the electronic structure and optical properties of Aluminosilicate polymorphs (Al_2SiO_5)", American Mineralogist, 93, 114-123 (2008).

16). W.Y. Ching, and P. Rulis, "*Ab initio* calculation of the O-K, N-K, Si-K, Si-L_3, Y-K, Y-L_3 edges in the Y-Si-O-N system: A new strategy for ELNES/XANES spectral modeling in complex materials", Phys. Rev. B. 77, 35125-1-17 (2008).

17). W.Y. Ching, and P. Rulis, "Large differences in the electronic and spectroscopic properties of the three phases of $AlPO_4$", Phys. Rev. B77, 125116-1-7 (2008).

18). S.K. Arora, H. C. Wu, R.J. Choudhary, I.V. Shvets, O.N. Mryasov, H. Yao, and W.Y. Ching, "Giant magnetic moment in epitaxial magnetite thin films grown by molecular beam epitaxy", Phys. Rev. B77, 134443,(2008).

19). W.Y. Ching, L. Ouyang, Paul Rulis, and Hongzhi Yao "*Ab initio* study of the physical properties of γ-Al_2O_3: lattice dynamics, bulk properties, electronic structures and bonding, optical properties and ELNES/XANES spectra", Phys. Rev. B 78, 014106-1-13 (2008).

20). R. F. Rajter, R.H. French, R. Podgornik, W.Y. Ching and A. Parsegian, "Mixing of optical properties for the determination of accurate far-limit effective vdW-Ld spectra and total vdW-Ld interaction energies", J. Appl. Phys. (accepted, 2008).

21). S.K. Arora, H. C. Wu, H. Yao, and W.Y. Ching, I.V. Shvets, O.N. Mryasov, "Magnetic Properties of Ultra-thin Magnetite Films Grown by Molecular Beam Epitaxy", IEEE Transactions on Magnetics. (accepted, 2008).

Atomic and Electronic Structure of Polar Oxide Interfaces

Marija Gajdardziska-Josifovska (*mgj@uwm.edu*)
Michael Weinert (*weinert@uwm.edu*)
Department of Physics, University of Wisconsin-Milwaukee
Milwaukee, WI 53201-0413

Scott Chambers (*sa.chambers@pnl.gov*)
Chemical and Materials Science Division
Pacific Northwest National Laboratory
P. O. Box 999, Richland, WA 99352

Program Scope:

In this project we strive to develop a fundamental understanding of the atomic and electronic mechanisms related to the stabilization of polar oxide interfaces. We use an integrated experimental and theoretical approach – combining sample growth, advanced characterization via electron microscopy, and first-principles calculations – to elucidate the properties of this important new class of low-dimensional ionic materials at the atomic scale. Understanding and harnessing the effects of polarity to tailor the properties of nanomaterials has implications for multiple branches of the basic and applied energy sciences.

Recent Progress:

Building on our initial results on the growth and experimental characterizations of a comprehensive set of iron oxide films on polar magnesia and alumina substrates, we focused on several important aspects:

- Experimental determination of the atomic structure and transport properties of hematite films grown on unreconstructed hydrogen-stabilized and on reconstruction-stabilized polar oxide surfaces;
- Theoretical modeling of ultrathin hematite films on unreconstructed magnesia surfaces;
- First-principles modeling of the stability and charge transfer in polar nano-slabs;
- Preliminary investigation of aging effects at the magnesia and iron oxides interfaces.

A. Effects of Unreconstructed and Reconstructed Polar Surface Terminations on Growth, Structure and Magnetic Properties of Hematite Films

Controlled growth of hematite and magnetite films has been a subject of intense studies, inspired by the many possible technological applications in catalysis, gas sensing, sequestration of toxic metals, and magnetic devices. Bulk hematite is a high Néel temperature (953K) canted antiferromagnetic oxide, with 2.2 eV band gap, and with potential for use in exchange-biased devices and sensors to pin the magnetization of an adjacent ferromagnetic layer. Magnetite is a high Curie temperature (854K) ferrimagnet that is of interest as a source of spin-polarized electrons. In combination with a tunneling barrier from an insulating oxide such as MgO or Al_2O_3, magnetite is of interest for spintronic devices such as magnetic tunnel junctions. The combination is also of great interest due to the close lattice match offering opportunities for electronic and magnetic

device engineering through a combination of polarity, strain, spin, and band-gap engineering.

We explore two basic questions: 1) Can polar hematite films be grown on hydrogen-stabilized unreconstructed polar oxide substrates without phase separation? 2) Does the surface stabilization mechanism for a polar oxide substrate has any noticeable effect(s) on the growth, structure and properties of the polar hematite films?

Iron oxide films were grown at PNNL by oxygen plasma-assisted molecular beam epitaxy (OPA-MBE) under the same iron flux (~0.1 Å/s) and oxygen partial pressure (~2×10^{-5} torr) on unreconstructed and reconstructed MgO (111) and α-Al_2O_3 (0001) single crystal surfaces. *In situ* characterization of the substrate and film surfaces was performed using reflection high-energy electron diffraction (RHEED) and x-ray photoelectron spectroscopy (XPS). Upon removal from ultrahigh vacuum, the film crystal structure was characterized with high-resolution x-ray diffraction (XRD), and with selected area and convergent beam electron diffraction (SAD and CBED) and high-resolution transmission electron microscopy (HRTEM). The film composition was characterized by electron energy loss spectroscopy (EELS) and energy filtered microscopy, and the magnetic properties were also characterized using room-temperature magnetometry and x-ray magnetic circular dischroism (XMCD) and x-ray absorption spectroscopy (XAS).

Electron microscopy and diffraction data show that hematite films on the unreconstructed MgO(111) surface grow in a continuous fashion. Previously in magnetite films films grown on unreconstructed MgO(111) surfaces, Fe nanocrystals were detected; such metallic nanocrystals are absent from all hematite films studied to date. The film thickness is quite uniform, but the actual average thickness (112 ± 3 nm) measured by TEM is drastically smaller than the nominal thickness (200 nm) obtained based on calibrations for Fe_2O_3 growth on sapphire (0001) and on neutral magnesia (100) surfaces.

On the unreconstructed MgO(111) surface, the hematite structure initiates abruptly at the interface (Fig. 1a) and propagates throughout the film; the interface is sharp, albeit with a narrow transition region. In contrast, on a reconstructed MgO(111) surface (Fig.1b), the growth initiates with a ~7 nm interface phase of a different crystal structure and then transforms into hematite. The SAD patterns shows additional reflections that appear half way between the MgO Bragg beams, as would be expected for a [11-2] zone of the magnetite lattice. Detailed lattice spacing measurements from SAD and from numerical diffractograms confirm that the structure of the interfacial band is consistent with Fe_3O_4 growing with its (111) planes parallel to the interface.

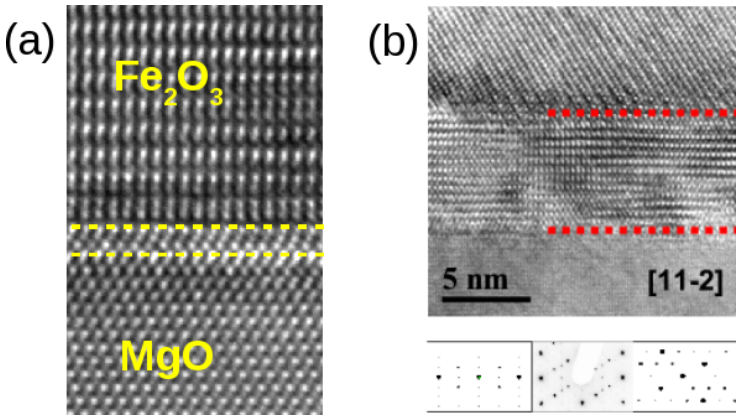

Fig. 1. HRTEM images of the hematite on (a) unreconstructed and (b) reconstructed MgO(111) surfaces. SAD patterns fo hematite on the reconstructed substrate (center) compared to calculated patterns for magnetite (left) and hematite(right).

This study shows that different modes of polar surface stabilization have profound

effect on the growth mode, phase composition and magnetic properties of polar hematite films.

B. DFT modeling of hematite/magnesia polar interface structure and properties

The first-principles calculations have focused on the initial stages of growth of Fe_2O_3 on the unreconstructed polar MgO(111) surface. There is good epitaxial matching of Fe_2O_3(0001)-(1×1) to MgO(111)-(1×1) surface in a ($\sqrt{3}\times\sqrt{3}$) R30° orientation. Both because the structure of the reconstructed surface is unknown (and we are also continuing to revisit this issue) and because the best experimental data we have (Fig. 1a) is for hematite grown on the unreconstructed surface, our calculations are limited to this case. The first question that arises is whether the interface is oxygen-metal (...O-Mg-O-Fe-O...) or metal-metal (...O-Mg-Fe-O...). The calculations clearly indicate that the interface is oxygen-metal, by an energy of ~0.3 eV/Å^2. In light of the long standing arguments that polar systems could avoid the electrostatic catastrophe by intermixing at an interface, we have considered various types of intermixing. Fe-O (as well as Mg-O) interchanges are unstable, i.e., the calculations find that the forces on the Fe and O atoms will try to exchange places directly. Likewise, mixing of Fe and Mg across the interface is energetically costly, ~2 eV. Thus, the calculated results strongly support abrupt interfaces, which are very effective in screening the internal electric fields.

The magnetic structure of bulk hematite consists of antiferromagnetic ordering of ferromagnetic planes of Fe along the (0001) axis. At the initial stages of growth, the first Fe layer is ferromagnetic, as expected from the bulk ordering. For two Fe (bi)layers, the magnetic ordering is still antiferromagnetic, but now the magnetic ordering in the first layer is antiferromagnetic – or more properly, ferrimagnetic – and as well as AFM between the layers. The energy difference favoring this new ordering is significant, ~0.4 eV/Fe_2O_3 unit. (Coupling the AFM layers ferromagnetically costs 0.3 eV.) This change in magnetic ordering is unexpected, but can be traced to the fact that the interface is semi-metallic. In addition, there is a strong coupling of the magnetic ordering and the structure, with significantly different interlayer spacings of the Fe.

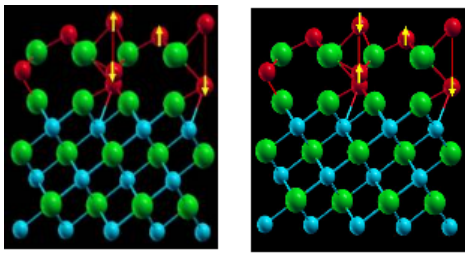

Fig. 2. Magnetic structure of the interface for "bulk" and the calculated ground state.

The magnetic ordering for free-standing hematite films also show thickness-dependent behavior, with 5 Fe bilayers having AFM bilayers, but by 9 bilayers, the structure throughout the whole film has reverted to the bulk-like ordering.

Recent results for different thicknesses of Fe_2O_3 on MgO(111) show significant changes in the atomic structure. In particular, for 3 bilayers of Fe, the surface Fe and O layers exchange places, without a barrier. At smaller (1 or 2 bilayers), no such exchange is observed; nor is this behavior observed for films of free-standing hematite, i..e., this is an effect associated with the polar interface, *not* with the pure materials, and may be related to the Mott mechanism of oxidation. Moreover, this calculated behavior provides a basis for understanding several puzzling experimental observations such as the formation of small Fe nanoparticles and the need for much higher oxygen pressures in order to grow uniform films on the polar surfaces compared to the non-polar ones.

Future Plans:

Our data from both Fe-O on MgO(111) and the Ti:Fe_2O_3 samples exhibit more

complicated – and interesting – behavior than expected. For example, the dependence on the Fe and oxygen rates, not just the Fe/O ratio, suggests there may be a kinetic contribution to the growth. The discovered dependence of hematite film structure and magnetic properties on surface reconstructions is of particular interest and will be explored in the magnetite and iron regimes. Our previous Fe-O data lead us to hypothesize that the oxide surface polarity presents a barrier for iron oxidation. Further characterization of the existing samples, in particular additional TEM studies of samples grown under less oxidizing environments, will provide information about the atomic structure at the polar interfaces and in the films. These results will be used to guide calculations directed towards understanding the fundamental mechanisms behind polar oxide interface stabilization. Calculations will continue to focus on the Fe_2O_3-MgO(111) and Fe-MgO(111) interfaces, and on possible structures of the Ti-Fe-O films. The different layer-dependent structures, both atomic and magnetic, observed in the calculations for the hematite films on MgO(111) are particularly intriguing in that they appear to provide mechanisms capable of addressing some of the puzzling aspects seen in the experiments. Modeling of the growth through series of calculations will be essential in untangling this issues. Although we do not yet know the detailed structure of hematite on the (1×1) MgO(111) surface, the recent HRTEM results (Fig. 1a) coupled with image simulations and first-principles calculations should enable us to solve this interface in the near future. Understanding the difference in growth of different iron oxides on the unreconstructed and reconstructed MgO(111) surfaces will be a topic of great interest to be investigated both experimentally and theoretically, especially in light of the fact that there is still not a consensus regarding the atomic structure of the reconstructed (√3×√3)R30° MgO(111) substrate. As we develop new insights regarding the growth, new samples will be grown under different conditions to test these hypotheses.

Publications of DOE-sponsored research (2006-2008):

1. "Effects of Unreconstructed and Reconstructed Polar Surface Terminations on Growth, Structure and Magnetic Properties of Hematite Films," S. H. Cheung, A. Celik-Aktas, P. Day, M. Weinert, B. Kabius, D. Keavney, V. K. Lazarov, S. A. Chambers and M. Gajdardziska-Josifovska,, *Phys. Rev. B* (to appear).
2. "Role of Mn and H in formation of cubic and hexagonal GaMnN," V. K. Lazarov, S. H. Cheung, Y. Cui, L. Li and M. Gajdardziska-Josifovska, *Appl. Phys. Lett.* **92,** 101914(1-3) (2008).
3. "FLAPW: Applications and implementations," M. Weinert, G. Schneider, R. Podloucky, and J. Redinger, *J. Phys. Condens. Matter* **21**, xxxx (2009).
4. "The Role of Polar Oxide Surface Reconstruction on the Atomic Structure of Polar Oxide Films: HRTEM and SAD Study of Hematite Growth on Magnesia," S. H. Cheung, A. Celik-Aktas, M. Weinert, S. A. Chambers and M. Gajdardziska-Josifovska, *Microscopy and Microanalysis* **13**, 814 (2007).
5. "Dopant Ordering in Antiferromagnetic Semiconducting Ti Doped Alpha-Fe_2O_3 Revealed by Electron Diffraction," A. Celik-Aktas, T. Droubay, S.A. Chambers and M. Gajdardziska-Josifovska, *Microscopy and Microanalysis* **13**, 820 (2007).
6. "The structure and magnetic properties of Fe thin films grown on (1×1) and (√3×√3)R30° reconstructed MgO(111)," V.K. Lazarov, S.H. Cheung, S.A. Chamb ers, M. Gajdardziska-Josifovska, and A. Kohn, *Microscopy and Microanalysis* **13**, 1044 (2007).
7. "Initial phases in sputter-deposited HfO_2-Al_2O_3 nanolaminate films", E. E. Hoppe, C. R. Aita, M. Gajdardziska-Josifovska, *Appl. Phys. Lett.* **91** 203105(1-3) (2007).

Discovering the Role of Grain Boundary Complexions in Materials

Martin P. Harmer, Christopher J. Kiely and Shen J. Dillon
Mph2@lehigh.edu chk5@lehigh.edu sjd6@lehigh.edu
Department of Materials Science and Engineering,
Lehigh University, Bethlehem PA 18015

Program Scope

Interfaces, their properties and atomic motion within them play a crucial role in determining the processing and properties of virtually all materials. It has long been a theme in materials science to link material performance with the structure of internal interfaces. Unfortunately, the nature of these interfaces is highly complex and it has been an ongoing challenge to link properties to the internal interface structure.

Grain boundary complexions offer a new missing link between grain boundaries, microstructure, and properties. Complexions represent grain boundaries as true three-dimensional phases, which are essentially distinct equilibrium interfacial phases that can transform to different phases (complexions) as a function of temperature, interfacial chemistry, stress and grain misorientation. This is in sharp contrast to the traditional view that interfaces are planar, non-transformable two-dimensional defects that depend only on the macroscopic degrees of freedom of the interface. Furthermore, these interface complexions exhibit drastically different transport kinetics (parallel and perpendicular) and possibly very different physical properties. Grain boundaries may display a number of thermodynamically stable features such as facets, atomic roughness, solute adsorption, intergranular films, etc. The multiplicity of possible behaviors requires a rational identification scheme for such features. We are applying an extension of the Gibbs definition of phase (which applies to identifiable *volumes* that differ in their state, composition, or symmetry and not their geometrical features) to interfacial features. These grain boundary phenomena contain a common element; an equilibrium interfacial feature with associated thermodynamic properties that cannot be separated from their abutting bulk phases. We have designated these equilibrium features as *complexions*.

One example of a grain boundary complexion is the intergranular film which has been observed in several of systems, most notably; zinc oxide[1], silicon nitride[2], titanates[3], and, a tungsten alloy[4]. Our recent work on alumina suggests that these intergranular films are evidence of a more widespread phenomenon that needs to be more thoroughly explored in a range of different systems.

An extensive kinetic study of grain boundary transport kinetics in alumina has been performed recently.[5] The data for grain boundary mobilities are summarized in figure 1. The samples exhibited various degrees of normal and abnormal grain growth with various morphologies. The rather remarkable result is that all of the data points fell onto one of six different lines. Six distinct types of kinetic behavior are exhibited by alumina varying by ~4 orders of magnitude. These are labeled type I through VI in the

plot. The agreement amongst the data is in spite of the fact that the grains in the samples exhibit distinctly different morphologies and microstructural evolution behavior.

Individual grain boundaries of known mobility were removed from the bulk material and fashioned into samples for transmission electron microscopy (TEM) using a focused ion beam. This allowed for a direct correlation between the grain growth kinetics and the observed grain boundary complexions. The six different kinetic types (type I-VI) are intimately related to six different grain boundary complexions (complexion I-VI).

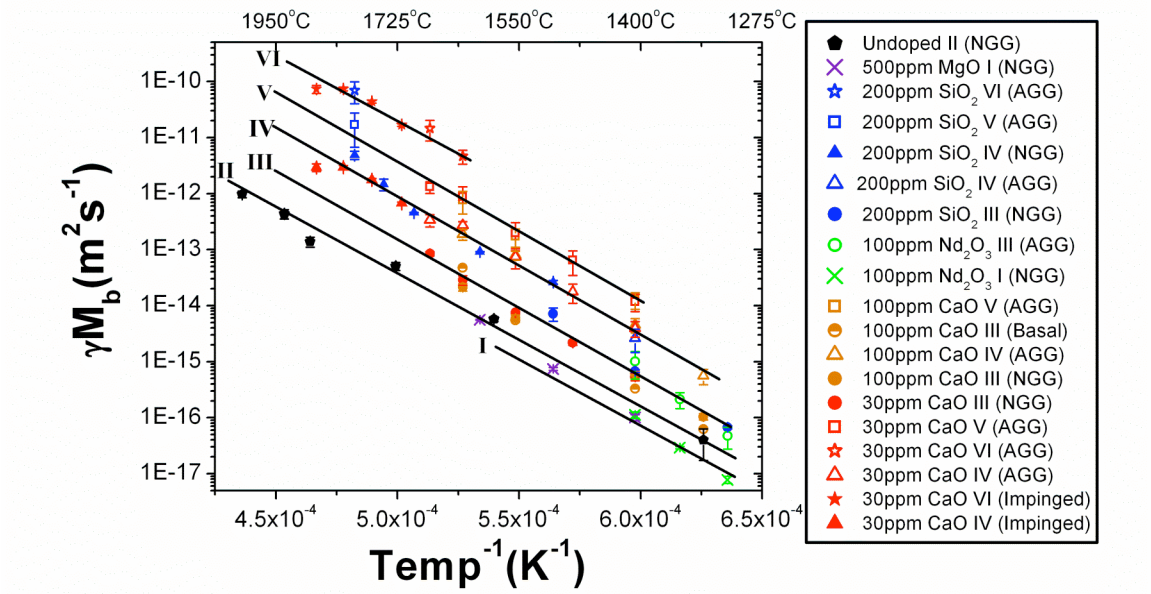

Figure 1: Summary of data for grain boundary mobility (times grain boundary energy) for normal and abnormal grain growth in a number of doped aluminas.

Three of the complexions are not differentiable by HRTEM. Atomic resolution Z-contrast scanning TEM (STEM) images of boundaries corresponding to type I through type III grain growth kinetics which does enable distinctions between the complexions to be made are shown in figure 2.

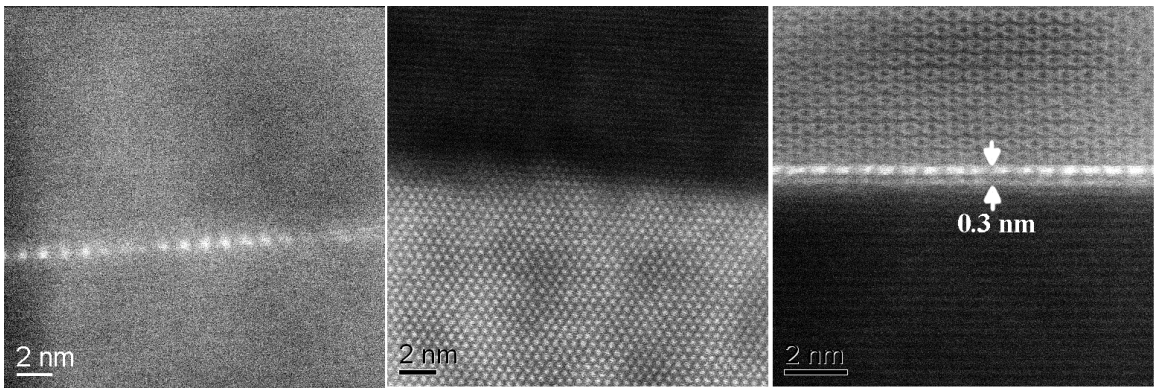

Figure 2: HAADF-STEM images of complexions I, II, and III, respectively.

Future studies

There are three major goals associated with the current project. Understanding the effect of the macroscopic degrees of freedom on the stability of different grain boundary complexions, in addition to temperature and chemistry, is critical to understanding how to engineer them. The atomic structures of grain boundaries affect their mechanical properties and a second goal is to evaluate the role of complexions in mechanical properties. Finally, while much insight has been gained into grain boundaries in alumina, it is important to explore complexions in other systems of interest.

Information on grain boundary structure will be obtained using a combination of conventional TEM, high-resolution electron microscopy (HREM) and high angle annular dark field (HAADF) STEM imaging. In order to perform detailed atomistic analysis of grain boundaries it is important to have that boundary aligned parallel to the electron beam with both adjacent grains oriented to a zone axis. Bicrystals are typically produced to fulfill this condition by joining two flat single crystals with specific misorientations, typically twist or tilt boundaries. This provides the opportunity to explore the effects of the macroscopic degrees of freedom on complexion stability. Unfortunately, these types of idealized boundaries do not necessarily represent the structure of general high angle boundaries. A novel approach to producing bicrystals it to join two curved single crystals (a cylinder and a mating surface) such that they have two zone axes oriented parallel to the plane of the curved grain boundary and the beam. This is shown schematically in Figure 3, where hot-pressing two ceramic single crystals together (diffusion bonding) may produce such geometry. The curved boundaries will produce more realistic atomistic structures that better represent higher energy boundaries.

In order to more generally understand chemistry effects on grain boundary complexions, it is important to thoroughly explore their existence and properties in different systems and different classes of materials. There are a number of characteristic traits that suggest that multiple grain boundary complexions may be present in a system. These include; abnormal grain growth in the absence of bulk liquid, crystallographic preference in abnormal grain growth, 'activated sintering', an exponential temperature dependence of the number density of abnormal grains and chemically induced grain boundary embrittlement. These indicators will be especially important when a system displays all of them simultaneously. Some systems of particular interest include, Fe-Si, Y_2O_3, $Y_3Al_5O_{12}$-SiO_2, Al-Ga, Cu-Bi, and $MgAl_2O_4$-LiF.

It is known that higher order complexions (more disordered) reduce the strength of silicon carbide grain boundaries[6]. There have been no direct experimental investigations of the lower order complexions since these have only recently been identified by the authors. However, a number of researchers have observed an anomalous decrease in the strength of alumina polycrystals with increasing grain size (outside of the Hall-Petch effect) [7]. The effect of complexions on mechanical properties will be evaluated in bulk polycrystals and idealized bicrystals.

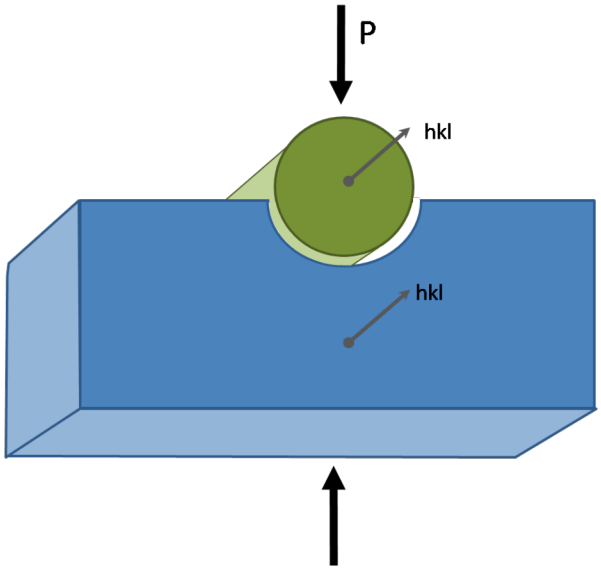

Figure 3: Schematic of a novel bicrystal geometry designed to observe curved high-energy grain boundaries in 'edge-on' conditions with parallel zone axes.

References

[1] J. Luo, M. Tang, R. M. Cannon, W. C. Carter, and Y.-M. Chiang, "Pressure-balance and diffuse-interface models for surficial amorphous films," *Materials Science & Engineering, A: Structural Materials: Properties, Microstructure and Processing,* **A422**[**1-2**] 19-28(2006).

[2] S. Bhattacharyya, C. T. Koch, and M. Ruehle, "Projected potential profiles across intergranular glassy films," *Journal of the Ceramic Society of Japan,* **114**[**Nov.**] 1005-1012(2006).

[3] S.-Y. Choi, D.-Y. Yoon, and S.-J. L. Kang, "Kinetic formation and thickening of intergranular amorphous films at grain boundaries in barium titanate," *Acta Materialia,* **52**[**12**] 3721-3726(2004).

[4] J. Luo, V. K. Gupta, D. H. Yoon, andH. M. Meyer, III, "Segregation-induced grain boundary premelting in nickel-doped tungsten," *Applied Physics Letters,* **87**[**23**] 231902/231901-231902/231903(2005).

[5] S. J. Dillon, M. Tang, W. C. Carter, and M. P. Harmer, "Complexion: A New Concept for Kinetic Engineering in Materials Science," *Acta Materialia,* **55**[**18**] 6208-6218(2007).

[6] R. O. Ritchie, X. F. Zhang, and L. C. de Jonghe, "On the role of grain-boundary films in optimizing the mechanical properties of silicon carbide ceramics," *Materials Research Society Symposium Proceedings,* **819**[**Interfacial Engineering for Optimized Properties III**] 3-14(2004).

[7] F. Guiberteau, N. P. Padture, and B. R. Lawn, "Effect of grain size of Hertzian contact damage in alumina," *Journal of the American Ceramic Society,* **77**[**7**] 1825-1831(1994).

Grain Boundary Complexions and Transitions in Doped Silicon

Jian Luo
School of Materials Science and Engineering, Clemson University
Olin 206, Clemson, SC 29634
jianluo@clemson.edu

Program Scope

Background: A *grain boundary (GB) complexion* is a GB "phase" with characteristic structure, chemistry and morphology [1, 2]. One particular liquid-like GB complexion that has generated much recent research interest is represented by impurity-based equilibrium-thickness intergranular films (IGFs) in ceramics [3, 4]. This research project was motivated by several recent research advancements:

- Carter and co-workers predicted coupled GB prewetting and premelting transitions in binary alloys [1].
- Sutton and co-workers revealed a temperature-induced GB structural transition in Si using atomistic simulations [5].
- Harmer and co-workers revealed the existence of six distinct GB complexions in doped Al_2O_3 with increasing level of structural disorder [2].
- We have made two intriguing observations regarding to metallic counterparts [6, 7] and free-surface counterparts [8] to IGFs in ceramics, namely **i)** stabilization of subsolidus (subeutectic) quasi-liquid IGFs in binary metals [6] and **ii)** a first-order monolayer-to-multilayer adsorption transition on oxide surfaces [9, 10]. Consequently, a unifying thermodynamic framework is envisaged [4].
- The concepts of liquid-like GB complexions and GB transitions were used to solve outstanding scientific problems, such as the origins of abnormal grain growth [2] and subsolidus activated sintering [7, 11, 12], both of which had puzzled the materials community for > 50 years.

However, no quantitative and systematic data yet exists that allow development and a critical test of a fundamental thermodynamic model of liquid-like GB complexions and related GB transitions.

Objectives: This project aims to discover the atomic-level and thermodynamic factors that control GB complexion stability and GB transitions through systematic investigation of doped Si as a proof-of-principle system. An emphasis is placed on nanoscale quasi-liquid IGFs and other derivative GB complexions. A combined experimental and theoretical study will **a)** establish a basic thermodynamic model for predicting GB transitions and GB diagrams, **b)** explore the effects of variations in several key parameters in stabilizing liquid-like GB complexions, and **c)** establish a basis to develop more sophisticated models for understanding complex ceramics and alloys. Additionally, this study will develop an effective method to measure GB complexion diagrams.

Selection of the Model System: We selected doped silicon for the following reasons. First, doped Si is the best proof-of-principle system for validating a basic model; extensive data exist for thermodynamic and atomistic modeling. Second, we are able to control the trace impurities in Si to the level that cannot be achieved for ceramic materials such as Si_3N_4. It is known that the presence of trace impurities can profoundly influence the occurrence of IGFs in ceramics. Third, the confirmed existence of IGF-like GB complexions in nitrides, oxides, carbides and metals [4] makes the search for analogous GB complexions in a simpler prototypical covalent material a logical extension with distinct scientific merit. Finally, this model system is also technologically important because of the increasing usage of less-pure polycrystalline Si for solar cells.

Recent Progress

On-Going Experiments: We have started a series of isothermal GB penetration experiments to probe GB transitions by annealing bi-crystals or polycrystals with "clean" GBs in contact with a liquid or solid reservoir (Fig. 1). Specimens will be characterized through the use of i) a focused ion beam to cut high-resolution transmission electron microscopy (HRTEM) specimens along the GBs to examine the atomic structures and ii) a scanning Auger nanoprobe to examine the composition along the GBs.

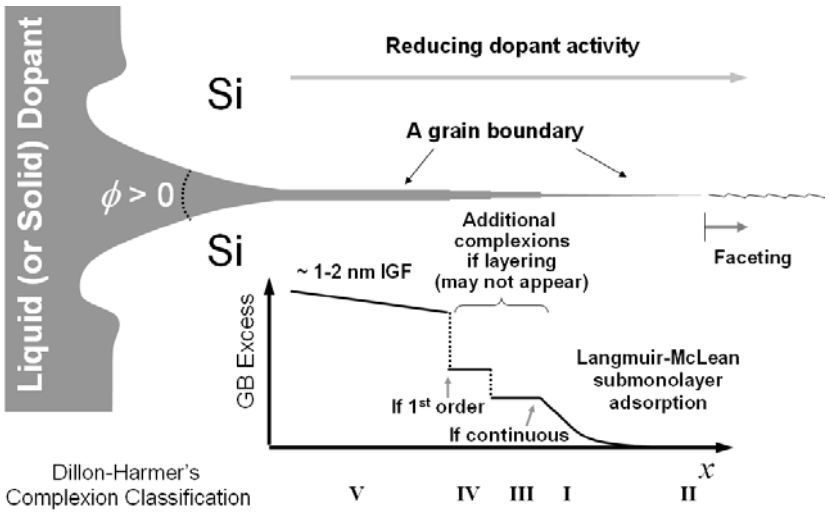

Figure 1: GB penetration experiments to probe GB transitions and construct GB diagrams. A series of GB complexions is expected to form along the penetration direction with reducing dopant activity dictated by the measurable local bulk chemical potential. The specific sequence of GB complexions may vary. If a GB transition is first-order, a discrete jump in GB excess is expected.

Initial Progress: Since the launch of this DOE-ESPM research project in July 2008, we have made the following progresses: **a)** a special quick quench furnace has been designed for conducting the planned experiments (Fig. 2) and a purchase order has been placed; **b)** we are working with Prof. Minghao Qi at Purdue University to make Si bi-crystals with controlled twisted GBs via a wafer bonding method and our initial experiments achieved good results (Fig. 3); and **c)** we are working to extend a recently developed thermodynamic model [12] to quantitatively predict the stability of nanoscale liquid-like IGFs to Si based binary systems.

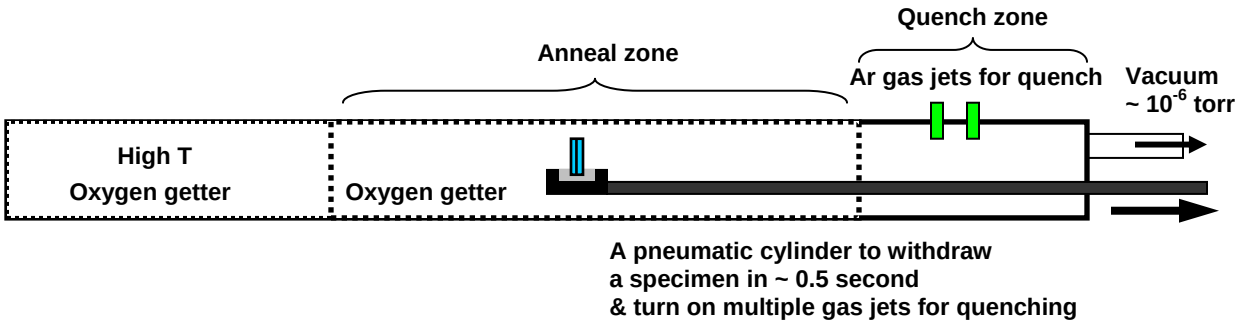

Figure 2: A furnace system has been designed for annealing and quenching a Si bi-crystal in contact with a liquid.

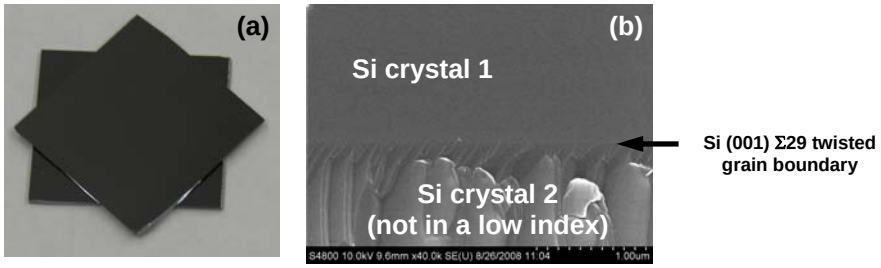

Figure 3: (a) Optical and (b) SEM images of a Si bi-crystal with a (001) Σ29 twisted grain boundary that was made via wafer bonding by our Purdue collaborator (subcontractor), Prof. Qi and his student.

Future Plans

Probing GB Transitions and Constructing GB Diagrams: We will continue to conduct the isothermal GB penetration experiments as illustrated in Fig. 1. At a given temperature and isothermal annealing time, a series of GB complexions is expected to form along the penetration direction with reducing dopant activity. After conducting a series of isothermal penetration experiments as a function of temperature and time, GB complexion diagrams will be constructed. Additionally, the character of GB transitions (e.g., first-order vs. continuous) will be probed. The coupled bulk and GB diffusion kinetics will be analyzed within the well-established Harrison framework. We will first examine polycrystalline specimens, where electron backscatter diffraction will be used to determine the GB crystallography; here GBs of different misorientation will be examined, to represent a general statistics. Then, focused experiments will be conducted using bi-crystals, where a low-symmetry twisted GB, e.g. the (100) Σ29 twisted GB, and a non-coincident twisted GB will be chosen as representative general GBs.

Modeling: The theoretical thrust is to utilize phenomenological force-balance and diffuse-interface models [4]. We will: **1)** quantify the models to construct GB diagrams; **2)** analyze the temperature- and dopant activity-dependent IGF stability; and **3)** establish and elaborate the conditions for GB transitions. These models will address areas in which we can robustly quantify interfacial thermodynamic models and critically compare model predictions with results of our experiments. Complementary atomistic and first-principle simulations will be pursued via external collaborations.

Selection Criteria: One particular goal of this 4-year research project is to develop a set of criteria to predict material systems and conditions for which nanoscale quasi-liquid IGFs and other derivative GB complexions are likely stable. This will be done via critical comparison of modeling and experimental results, and in particular, by intentionally selecting an array of dopants to represent different values of these key variables. Key parameters that determine the stability of nanoscale quasi-liquid IGFs include relative interfacial energies, fusion entropies, mixing enthalpy and strengths of several interfacial forces.

Extending Bulk CALPHAD Methods to GBs and Critical Experimental Validation: Recently, we have extended bulk CALPHAD methods to predict the stability of nanoscale quasi-liquid IGFs in binary alloys [12]. Using onset subsolidus activated sintering as an indicator of GB disordering (i.e., the initial formation of a liquid-like GB complexion), we validated this model for five binary tungsten alloys (Fig. 4 & Table 1) [12]. In this project, we will extend this model to Si based systems, where we can do much more critical experiment-model comparisons. We will seek direct experimental evidence (via HRTEM, AC-STEM and Auger) to critically validate the key model predictions. Furthermore, we will explore the conditions where additional derivative liquid-like GB complexions may form. We recently showed that introduction of an oscillation structural interaction related to the finite atomic size (which is well-known in colloidal theories) will result in layering transitions that produce two additional derivative GB complexions (Fig. 5) [12], similar to those revealed by Dillon *et al.* for doped Al_2O_3 [2]. We will further test this prediction with systematic experiments using Si based model systems.

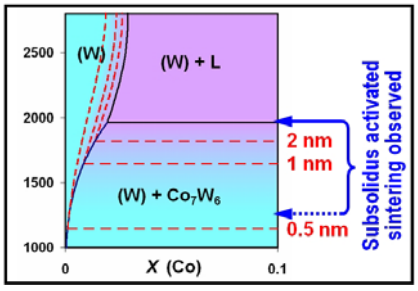

Figure 4: Red dashed lines: predicted conditions where 2, 1 and 0.5 nm thick quasi-liquid IGFs are stable [12].

Table 1: Observed GB disordering temperatures (as indicated by onset subsolidus activated sintering) vs. predicted GB disordering temperatures [12].

	Observed (K)	Predicted (K)
W-Pd	1090±23	<1141
W-Ni	1150±18	1121-1470
W-Co	1301±49	1140-1644
W-Fe	1308±50	1273-1664
W-Cu	No effect	No IGF

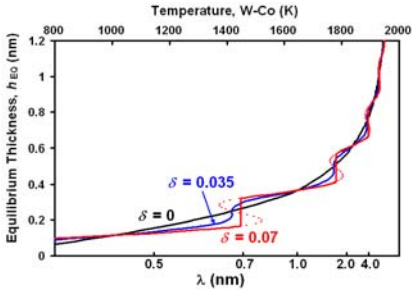

Figure 5: A finite atomic size effect produces layering transitions, leading to two new GB complexions [12].

A Long-Range Scientific Goal:

GB Diagrams – A New Tool for Materials-by-Design: Our long-range scientific goal is to develop quantitative GB (complexion) diagrams as a crucial component for the predictable fabrication of materials by design. Importance and novelty stem from the large changes in properties that accompany GB transitions, and to the fact that high-temperature GB structures can often be retained on cooling. Specifically, quantitative GB diagrams can be used in three ways:

- Guided by GB diagrams, fabrication protocols can be designed to utilize the most appropriate GB structures to achieve optimal microstructures, e.g., utilizing liquid-like GBs for low-*T* sintering.
- Heat treatment protocols can be devised to optimize GB structures for the desired performance properties, e.g., "drying" liquid-like GBs to improve creep resistance.
- GB diagrams provide necessary information for predicting high-*T* materials properties.

An Example: The necessity of developing such GB diagrams is demonstrated by recent studies of subsolidus activated sintering for both ceramic [11] and metallic [7] systems. These studies demonstrated that bulk phase diagrams are not adequate for designing optimal activated sintering protocols. This is because nanoscale quasi-liquid IGFs can form at as low as 60-85% of bulk solidus (eutectic or peritectic) temperatures, thereby resulting in enhanced sintering behaviors similar to liquid-phase sintering [12]. In general, nanometer-thick interfacial films are not expected to follow the same thermodynamic relations as bulk phases! On the other hand, our most recent results showed that the onset of subsolidus activated sintering can indeed be predicted from computed GB diagrams (Fig. 4 and Table 1).

Impact of This Study: This proposed study is a critical step towards our long-range scientific goal of developing GB diagrams as fundamental information leading to controlled materials design. Successful completion of this study will achieve highly systematic data of GB complexions and GB transitions in a prototypical covalent material – knowledge that is crucial for development of fundamental interfacial thermodynamic models. We will also develop effective experimental and modeling techniques to investigate GB transitions and construct quantitative GB diagrams.

DOE Sponsored Publications: N/A (*This is a new award starting in July 2008.*)

References

1. M. Tang, W. C. Carter, and R. M. Cannon, "Grain Boundary Transitions in Binary Alloys," *Physical Review Letters*, **97**, 075502 (2006).
2. S. J. Dillon, M. Tang, W. C. Carter, and M. P. Harmer, "Complexion: A New Concept for Kinetic Engineering in Materials Science," *Acta Materialia*, **55**, 6208 (2007).
3. D. R. Clarke, "On the Equilibrium Thickness of Intergranular Glass Phases in Ceramic Materials," *Journal of the American Ceramic Society*, **70**, 15 (1987).
4. J. Luo, "Stabilization of Nanoscale Quasi-Liquid Interfacial Films in Inorganic Materials: A Review and Critical Assessment," *Critical Reviews in Solid State and Material Sciences*, **32**, 67 (2007).
5. S. von Alfthan, K. Kaski, and A. P. Sutton, "Temperature-Induced Structural Transition at Twist Boundaries in Silicon," *Physical Review B* (2007, submitted).
6. J. Luo, V. K. Gupta, D. H. Yoon, and H. M. Meyer, "Segregation-Induced Grain Boundary Premelting in Nickel-Doped Tungsten," *Applied Physics Letters*, **87**, 231902 (2005).
7. V. K. Gupta, D. H. Yoon, H. M. Meyer III, and J. Luo, "Thin Intergranular Films and Solid-State Activated Sintering in Nickel-Doped Tungsten," *Acta Materialia*, **55**, 3131 (2007).
8. J. Luo and Y.-M. Chiang, "Wetting and Prewetting on Ceramic Surfaces," *Annual Review of Materials Research*, **38**, 227 (2008).
9. H. Qian and J. Luo, "Vanadia-Based Equilibrium-Thickness Amorphous Films on Anatase (101) Surfaces," *Applied Physics Letters*, **91**, 061909 (2007).
10. H. Qian and J. Luo, "Nanoscale Surficial Films and a Surface Transition in V_2O_5-TiO_2-Based Ternary Oxide Systems," *Acta Materialia*, in press (2008).
11. J. Luo, H. Wang, and Y.-M. Chiang, "Origin of Solid State Activated Sintering in Bi2O3-Doped ZnO," *Journal of the American Ceramic Society*, **82**, 916 (1999).
12. J. Luo and X. Shi, "Grain Boundary Disordering in Binary Alloys," *Applied Physics Letters*, **92**, 101901 (2008).

Atomic Structure and Function of Internal Interfaces

D.L. Medlin, J.C. Hamilton, F. Léonard, C. Spataru
dlmedli@sandia.gov, jchamil@sandia.gov, fleonar@sandia.gov, and cdspata@sandia.gov
MS 9161, Sandia National Laboratories, Livermore, CA 94551

Program Scope

Our program seeks to establish the fundamental principles that underpin the structure and function of internal interfaces in materials. A central goal of our work is to explain how the incompatibilities and discontinuities that arise at an interface—whether these are structural, compositional, or electronic—are accommodated and what the implications of these relaxations are on interfacial behavior and properties. We make progress against such problems by closely integrating experimental microscopic observations of interfaces with detailed theory and modeling. We pay particular attention to interfacial defects, such as dislocations, steps, and junctions, since these entities provide a route to extending our understanding of ideal, high-symmetry interfaces to more complex configurations. Our experimental work employs conventional and high-resolution electron microscopy and atom probe tomography to investigate interfacial structure and composition. In these measurements we seek to obtain quantitative information that can be linked to theory. Our theoretical work combines continuum elasticity, interfacial crystallography, atomistic simulations, and first-principles, *ab initio* computation. In recent years, we have focused primarily on metallic interfaces, investigating both grain boundaries and heterophase interfaces. In our future work, we will increasingly focus on materials where interfaces more directly control the functional electronic and thermal properties of the material. To this end, we have begun investigating interfaces in thermoelectric materials because of the important role of interfaces in controlling the thermal and electronic transport processes that govern energy conversion efficiency in these materials.

Recent Progress

A long-standing focus in this program has been to establish the detailed structure and function of line defects at grain boundaries and other internal interfaces. We seek to arrive at analytical descriptions of interfaces that capture details of the atomic-scale interfacial structure in terms of longer-length-scale entities. One area where the study of interfacial defects provides great insight is in explaining interfacial reconstructions. For instance, we have recently

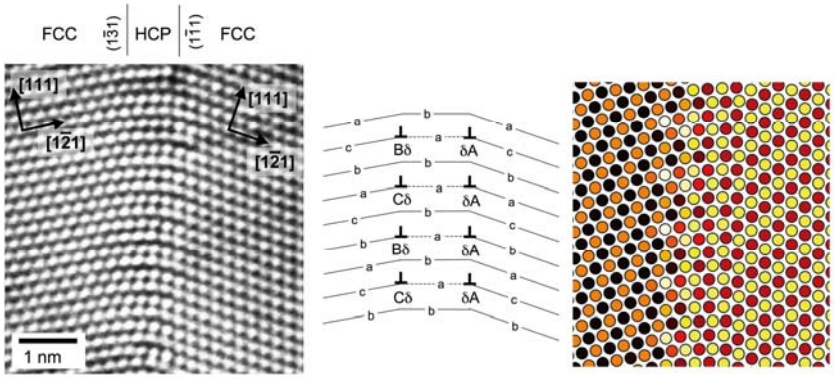

Fig. 1 HRTEM image, dislocation model, and atomistic simulation for a 29°<110> boundary in Au. This boundary reconstructs to form an intermediate layer of HCP stacking by the dissociation of a dense array of lattice dislocations into Shockley partials and intervening stacking faults. The screw-character of the dislocations in the left array produce an interfacial planar offset (in the viewing direction) of half the {220} spacing. This shift is seen in the atomistic calculation by the shading of atoms by depth.

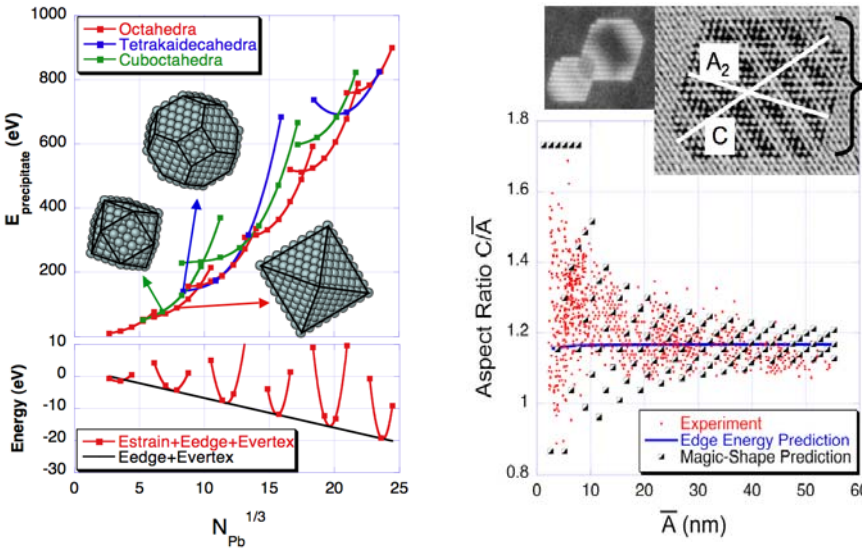

Fig. 2. (Left): Extraction of edge energy from atomistic calculation of precipitate energy, top graph. The sum of strain, edge and vertex energies (bottom graph) is obtained by subtracting the total interface energy. The slope of the black tangent line gives the edge energy. (Right): Top micrograph defines precipitate dimensions used to calculate the aspect ratio. The red points show the experimental distribution of aspect ratios vs. size. The blue line shows that the edge-energy theory cannot explain the shapes. The squares show the distribution of aspect ratios predicted by magic shape theory.

investigated the formation of a narrow slab of hexagonal-close-packed (HCP) material at a grain boundary in face-centered-cubic (FCC) gold (Fig. 1)[1]. This interfacial HCP layer results from the dissociation of a dense array of crystal-lattice dislocations, which accommodate the boundary's 29° misorientation, into pairs of Shockley partial dislocations, producing stacking faults on alternating {111} planes. By establishing the quantitative details of this dislocation arrangement, we have shown how this structure is related to dissociated grain boundary structures found at higher misorientation angles.

We are also investigating the mechanisms that control interface morphology between compositionally distinct phases. One issue is the role of elastic strain at the nanometer scale. We have recently collaborated with U. Dahmen (LBL-NCEM) to explain how the *shape* of embedded nanoprecipitates varies as a function of size [2,3]. We considered Pb precipitates in Al (Fig. 2). In contrast to initial hypotheses [4], our work has shown that facet edge energies play a negligible role in controlling the strong variation in the distribution of precipitate aspect ratios with size. The answer, instead, is that for the nanoprecipitates in this system to be strain-free, they can only be assembled by combining two fundamental building blocks, namely tetrahedral and square pyramids, which must be of a specific size (edge length of 16Å). By filtering this set of "magic" shapes by an energy criterion, we successfully explained the experimental measurements of aspect ratio as a function of size (Fig. 2).

We have also begun to investigate interfaces in thermoelectric materials because of the critical role that interfaces can play in controlling the thermal and electronic transport processes that govern thermoelectric energy conversion efficiency. The central materials challenge to improving this efficiency is to balance the competing requirements of high electrical conductivity, high Seebeck coefficient, and low thermal conductivity. While these properties are highly inter-related in traditional, single-phase, solid-solution alloys, it is possible to decouple these transport properties using nanometer-scale distributions of interfaces. For instance, we have recently developed a theory and performed numerical calculations to explain how embedded metallic nanoparticles can enhance the thermoelectric properties of bulk semiconductors [5]. The basic idea of our model is illustrated in Fig. 3. Band bending at the interfaces between the semiconductor host and randomly distributed metallic islands causes energy-dependent scattering of electrons, preferentially scattering the low-energy electrons. Because the Seebeck coefficient depends on the energy derivative of the relaxation time at the Fermi energy, $d\ln t(E)/dE$, this type of energy filtering increases the Seebeck coefficient. This

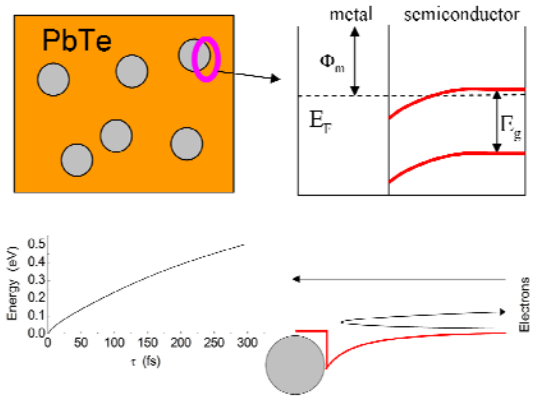

Fig. 3. (a) Schematic of the semiconductor host with metallic nanoinclusions. Panel (b) shows an example of the calculated potential and the energy diagram for PbTe with Pb nanoinclusions of radius 1.5 nm. Panel (c) illustrates the concept of energy filtering: low energy electrons scatter strongly with the potential, but high energy electrons are unaffected. The calculated electronic relaxation time for the potential of panel (b) is also shown.

model provides an explicit, physical explanation for the recently proposed energy filtering effect [6]. By also accounting for changes in thermal conductivity, using a previous model for the scattering of phonons on nanoinclusions [7], we have shown how such nanoinclusions can significantly enhance the thermoelectric energy conversion efficiency.

We are also investigating the mechanisms of solid-state phase separation in thermoelectric alloys, since this is one route to producing nanostructured bulk thermoelectric materials. In our initial work [8], we have investigated the rock-salt structured compound $AgSbTe_2$, which is of great interest both because of its specific thermoelectric properties and because it is a constituent of two classes of high performance thermoelectric alloys: $(PbTe)_x(AgSbTe_2)_{1-x}$ [9] and $(GeTe)_x(AgSbTe_2)_{1-x}$ [10] We have investigated the decomposition of this compound to form embedded, nanoscale precipitates of monoclinic Ag_2Te. By establishing the details of this orientation relationship, we have shown that the Te-sublattice remains aligned in both the matrix and precipitate phase. Because the monoclinic and high-temperature cubic phases of Ag_2Te differ by only small, local distortions of the crystal lattice, this result suggests a facile transformation path for the Ag_2Te precipitation, requiring only the clustering of excess silver. We have also observed this same orientation relationship for Ag_2Te precipitates in Ag-rich PbTe and $(PbTe)_x(AgSbTe_2)_{1-x}$, suggesting that this mechanism is generic for silver-telluride precipitates in rock-salt structured tellurides.

Future Plans

In the future, we plan to increase our emphasis on interfaces that directly control the macroscopic, functional properties of materials, focusing initially on interfaces in thermoelectric materials. Combining electron microscopic and first-principles atomistic calculations, we will investigate the atomic structure and composition of both grain boundaries and heterophase interfaces in these materials. We have started work on grain boundary structures in tetradymite-structured materials, initially concentrating on bismuth telluride (Bi_2Te_3). We are starting with relatively simple interfaces, such as twin boundaries, and moving to more complex configurations by analyzing the line defects that arise at such interfaces. We are also continuing our work investigating the boundaries that form through solid-state phase separation in the $AgSbTe_2$ system and are determining how these transformations are controlled by the interfacial defect configurations. We will also continue work on the theory of electronic and thermal transport at nanoscale interfaces. Our theoretical work thus far has considered the interfaces between metallic nanoparticles and the host semiconductor from a general perspective by considering a range of electronic band alignments at these interfaces, and has modeled their impact on phonon transport from the difference in the sound velocities of the two materials. We will study in more detail the properties of these interfaces by combining higher-level continuum theories with *ab initio* calculations. In particular, we will study how the band bending at an

embedded metallic inclusion depends on radius of the particle and more directly establish the phonon scattering mechanisms by directly calculating the phonon-band structure at planar metal/semiconductor interfaces.

References

[1] D. L. Medlin and J. C. Hamilton, *Formation of Hexagonal Close Packing at a Grain Boundary in Gold by the Dissociation of a Dense Array of Crystal Lattice Dislocations*, submitted to J. Mat. Sci. (2008).
[2] J. C. Hamilton, *Edge energies: Atomistic calculations of a continuum quantity*, Phys. Rev. B 73, 125447 (2006).
[3] J. C. Hamilton, F. Léonard, E. Johnson and U. Dahmen, *Pb nanoprecipitates in Al: Magic-shape effects due to elastic strain*, Phys. Rev. Lett. 98, 236102 (2007).
[4] E. Johnson, A. Johansen, U. Dahmen, S. Chen and T. Fujii, *Shapes and sizes of nanoscale Pb inclusions in Al*, Mat. Sci. Eng. A 304, 187 (2001).
[5]S. V. Faleev and F. Léonard, *Theory of enhancement of thermoelectric properties of materials with nanoinclusions*, Phys. Rev. B 77, 214304 (2008).
[6]J. P. Heremans, C. M. Thrush and D. T. Morelli, *Thermopower enhancement in PbTe with Pb precipitates*, J. Appl. Phys. 98, 063703 (2005).
[7]W. Kim, J. Zide, A. Gossard, D. Klenov, S. Stemmer, A. Shakouri and A. Majumdar, *Thermal conductivity reduction and thermoelectric figure of merit increase by embedding nanoparticles in crystalline semiconductors*, Phys. Rev. Lett. 96, 045901 (2006).
[8] J. D. Sugar and D. L. Medlin, *Precipitation of Ag_2Te in the Thermoelectric Alloy $AgSbTe_2$*, submitted to the J. Alloy. Compd. (2008).
[9] K. F. Hsu, S. Loo, F. Guo, W. Chen, J. S. Dyck, C. Uher, T. Hogan, E. K. Polychroniadis and M. G. Kanatzidis, *Cubic $AgPb_mSbTe_{2+m}$: Bulk thermoelectric materials with high figure of merit*, Science 303, 818 (2004).
[10] E. A. Skrabek and D. S. Trimmer, P*roperties of the General TAGS System*, in CRC Handbook of Thermoelectrics, edited by D.M. Rowe (CRC Press, Boca Raton 1995), pp. 267.

DOE Sponsored Publications (2006-2008)

•J. C. Hamilton, *Edge energies: Atomistic calculations of a continuum quantity*, Phys. Rev. B **73**, 125447 (2006).
•P. L. Williams, Y. Mishin and J. C. Hamilton, *An embedded-atom potential for the Cu-Ag system*, Model. Simul. Mater. Sci. Eng. **14**, 817 (2006).
•R. C. Pond, D. L. Medlin and A. Serra, *A study of the accommodation of coherency strain by interfacial defects at a grain boundary in gold*, Philos. Mag. **86**, 4667 (2006).
•S. V. Faleev, M. van Schilfgaarde, T. Kotani, F. Léonard and M. P. Desjarlais, *Finite-temperature quasiparticle self-consistent GW approximation*, Phys. Rev. B **74**, 033101 (2006).
•M. van Schilfgaarde, T. Kotani and S. Faleev, *Quasiparticle self-consistent GW theory*, Phys. Rev. Lett. **96**, 226402 (2006).
•M. van Schilfgaarde, T. Kotani and S. V. Faleev, *Adequacy of approximations in GW theory*, Phys. Rev. B **74**, 245125 (2006).
•J. C. Hamilton, F. Léonard, E. Johnson and U. Dahmen, *Pb nanoprecipitates in Al: Magic-shape effects due to elastic strain*, Phys. Rev. Lett. **98**, 236102 (2007).
•T. Kotani, M. van Schilfgaarde and S. V. Faleev, *Quasiparticle self-consistent GW method: A basis for the independent-particle approximation*, Phys. Rev. B **76**, 165106 (2007).
•T. Kotani, M. van Schilfgaarde, S. V. Faleev and A. Chantis, *Quasiparticle self-consistent GW method: a short summary*, J. Phys.-Condens. Matter **19**, 365236 (2007).
•E. A. Marquis, *A reassessment of the metastable miscibility gap in Al-Ag alloys by atom probe tomography*, Microsc. Microanal. **13**, 484 (2007).
•E. A. Marquis, D. L. Medlin and F. Léonard, *Stabilization of extended stacking faults by {111}/{112} twin junction interactions*, Acta Mater. **55**, 5917 (2007).
•S. V. Faleev and F. Léonard, *Theory of enhancement of thermoelectric properties of materials with nanoinclusions*, Phys. Rev. B **77**, 214304 (2008).
•I. A. Arslan, E. A. Marquis, M. Homer, M. Hekmaty and N. C. Bartelt, *Towards better 3D reconstructions by combining electron tomography and atom probe tomography*, Ultramicroscopy, in press (2008).
•J. C. Hamilton and D. L. Medlin, *Theory for planar offsets at heterophase interfaces in metals*, submitted to Phys. Rev. (2008).
•D. L. Medlin and J. C. Hamilton, *Formation of hexagonal close packing at a grain boundary in gold by the dissociation of a dense array of crystal lattice dislocations*, submitted to J. Mat. Sci. (2008).
•J. D. Sugar and D. L. Medlin, *Precipitation of Ag_2Te in the thermoelectric alloy $AgSbTe_2$*, submitted to J. Alloy. Compd. (2008).

Scanning Transmission Electron Microscopy: Atomic Structure and Properties of Materials

Stephen J. Pennycook, Maria Varela, Andrew R. Lupini, Albina Y. Borisevich, Matthew F. Chisholm
Research Professors: Mark P. Oxley, Weidong Luo
pennycooksj@ornl.gov, mvarela@ornl.gov, 9az@ornl.gov, albinab@ornl.gov, chisholmmf@ornl.gov
Materials Science and Technology Division, Oak Ridge National Laboratory, Oak Ridge, TN 37831

Program Scope

Over the last seven years this program has been involved in the development and application of the aberration-corrected scanning transmission electron microscope (STEM). Beyond the factor of two or more improvement in lateral resolution, useful resolution is gained also in the third dimension, sensitivity to light elements is enormously improved and simultaneous, aberration-corrected phase-contrast imaging is available. Single atom sensitivity at atomic resolution is achieved in electron energy loss spectroscopy (EELS). These new capabilities have been investigated and applied to a variety of important materials issues.

Recent Progress

Resolution and localization in STEM imaging: A quantitative definition of image resolution was proposed and a method developed for determining thickness, defocus and incoherent broadening through comparison to image simulations (Peng et al., 2008). The longstanding view that spectroscopic images using low-lying edges such as Si $L_{2,3}$ at ~ 100 eV would be too delocalized to show atomic resolution was disproved (Oxley et al., 2007, 2008). Simulations are essential to distinguish contrast artifacts from compositional changes.

Defect-mediated ferromagnetism in insulating Co-doped anatase TiO_2 thin films: The nature of the defect responsible for room-temperature ferromagnetism in Co-doped anatase TiO_2 was identified using atomic-resolution Z-contrast images, EELS and density-functional calculations as $Co\text{-}Ti^{+3}\text{-}V_O$ complexes (Roberts et al., 2008). The role of O defects has also been examined in double perovskites such as Bi_2NiMnO_6 and La_2CoMnO_6.

Point defect configurations of supersaturated Au atoms inside Si nanowires: 3D imaging showed a high density of Au atoms not only on the surface of the nanowires, but inside the bulk of the nanowire. Substitutional and three interstitial configurations are found. Density functional theory (DFT) confirmed these to be associated with stable (substitutional) or metastable (interstitial) sites (Oh et al., 2008).

Colossal ionic conductivity at interfaces of epitaxial ZrO_2 : Y_2O_3/$SrTiO_3$ heterostructures: Eight orders of magnitude enhancement in lateral ionic conductivity near room temperature has been observed in yttria stabilized zirconia / $SrTiO_3$ epitaxial heterostructures. Microscopy showed that this phenomenon is a genuine interface process (Garcia-Barriocanal et al., 2008).

Nonstoichiometric dislocation cores in alpha-alumina: Nonstoichiometric core structures were observed in Al_2O_3 implying that for basal slip to occur, synchronized motion of the partial dislocations on adjacent planes is required (Shibata et al., 2007).

Complex Oxides: Manganites. In mixed-valence transition-metal oxides such as $La_xCa_{1-x}MnO_3$ a spatial ordering of two inequivalent Mn atoms known as "charge ordering" occurs. Atomic-resolution EELS in doped $CaMnO_3$ also reveals two distinct Mn L_{23} spectra in an ABBABB… pattern. DFT, including spin polarization, gives excellent predictions for all structural, electronic and magnetic ground-state properties. Results demonstrated that there is practically no charge ordering, instead, there is ordering of orbital occupancy (Luo et al., 2007).

Atomic resolution spectroscopy: The near edge structure of the O K edge of $LaCoO_3$ has been shown to be sensitive to spin state (Klie et al., 2007). Changes in the Cu L and O K fine structure between the CuO chains and the CuO_2 planes of $YBa_2Cu_3O_{7-x}$ show directly that holes are located in the chains (Mizoguchi et al., 2008). Z-contrast images and EELS have identified a novel ferromagnetic phase in nanophase FeGe (Zeng et al., 2006), and correlations between structure and properties in semiconducting systems (Molina et al., 2006, 2007, 2008).

Catalysis: We have expanded the understanding and characterization of catalysts synthesized by conventional (Rashkeev et al., 2007) and novel techniques (Veith et al., 2007).

Future Plans

A full 5th order aberration-corrected Nion UltraSTEM will be delivered to ORNL in October 2008, providing spectroscopic imaging with high spatial and energy resolution and high efficiency. We propose to focus on atomic-resolution mapping of spectral fine structure and theoretical interpretation in terms of materials electronic structure. Some specific areas of study will include:

Image simulation: Simulations of high-resolution STEM images will explore possible origins of the reduced contrast seen in experimental images compared to theory. New simulation methods are also needed for EELS fine structure that combine DFT with dynamical electron scattering.

Complex Oxides: EELS imaging will be carried out on a wide portfolio of systems with sub-unit-cell resolution including the new Fe-based superconductors, $YBa_2Cu_3O_{7-x}$ and cobaltites. A broad spectrum of oxide superlattice and heterostructures will be investigated, aimed at probing charge leakage and the interfacial origins of novel properties. Results will be correlated with density-functional calculations

Ferroelectrics: The direct interpretability of the Z-contrast image will be combined with the much greater contrast variations possible by phase contrast imaging to investigate unresolved questions in the physics of ferroelectrics, the mechanisms by which screening occurs at electrode/ferroelectric interfaces and the extent to which polarization varies at various interfaces.

DOE-sponsored journal publications 2006-2008

Agassi, D., D. K. Christen and S. J. Pennycook, "Thickness-dependent pinning in a superconductor thin film," *J. Appl. Phys.*, **101,** 023916 (2007).

Borisevich, A. Y., S. W. Wang, S. N. Rashkeev, M. Glazoff, S. J. Pennycook and S. T. Pantelides, "Dual nanoparticle/substrate control of catalytic dehydrogenation," *Adv. Mater.*, **19**, 2129-2133 (2007).

Chisholm, M. F. and S. J. Pennycook, "Direct imaging of dislocation core structures by Z-contrast STEM," *Philos. Mag.*, **86**, 4699-4725 (2006).

Christen, H. M., M. Varela, D. H. Kim. "The Effect of Strain and Strain Symmetry on the Charge-Order Transition in $Bi_{0.4}Ca_{0.6}MnO_3$ Films" *Phase Transitions*, 81, 717-727 (2008).

D'Alfonso, A. J., S. D. Findlay, M. P. Oxley, S. J. Pennycook, K. van Benthem and L. J. Allen, "Depth sectioning in scanning transmission electron microscopy based on core-loss spectroscopy," *Ultramic.*, **108**, 17-28 (2007).

D'Alfonso, A. J., S. D. Findlay, M. P. Oxley and L. J. Allen, "Volcano structure in atomic resolution core-loss images," *Ultramicrosc.*, 108, 677-687 (2008).

Du, S. X., H. J. Gao, C. Seidel, L. Tsetseris, W. Ji, H. Kopf, L. F. Chi, H. Fuchs, S. J. Pennycook and S. T. Pantelides, "Selective nontemplated adsorption of organic molecules on nanofacets and the role of bonding patterns," *Phys. Rev. Lett.*, **97**, 156105 (2006).

Dwyer, C., A. Ziegler, N. Shibata, G. B. Winkelman, R. L. Satet, M. J. Hoffmann, M. K. Cinibulk, P. F. Becher, G. S. Painter, N. D. Browning, D. J. H. Cockayne, R. O. Ritchie and S. J. Pennycook, "Interfacial structure in silicon nitride sintered with lanthanide oxide," *J. Mat. Sci.*, **41**, 4405-4412 (2006).

Findlay, S. D., M. P. Oxley and L. J. Allen, "Modeling Atomic-Resolution Scanning Transmission Electron Microscopy Images," *Microsc. Microanal.,* 14, 48-59 (2007).

Garcia-Barriocanal, J., A. Rivera-Calzada, M. Varela, Z. Sefrioui, E. Iborra, C. Leon, S. J. Pennycook and J. Santamaria, "Colossal ionic conductivity at interfaces of epitaxial ZrO_2 : Y_2O_3/$SrTiO_3$ heterostructures," *Science*, **321**, 676-680 (2008).

Garrett, M. D., A. D. Dukes, J. R. McBride, N. J. Smith, S. J. Pennycook and S. J. Rosenthal, "Band edge recombination in CdSe, CdS and CdS_xSe_{1-x} alloy nanocrystals observed by ultrafast fluorescence upconversion: The effect of surface trap states," *Journal of Physical Chemistry C*, **112**, 12736-12746 (2008).

Guo, H. Z., J. Burgess, E. Ada, S. Street, A. Gupta, M. N. Iliev, A. J. Kellock, C. Magen, M. Varela and S. J. Pennycook, "Influence of defects on structural and magnetic properties of multifunctional La_2NiMnO_6 thin films," *Phys. Rev. B*, **77**, 174423 (2008).

Guo, H. Z., A. Gupta, J. Zhang, M. Varela and S. J. Pennycook, "Effect of oxygen concentration on the magnetic properties of La_2CoMnO_6 thin films," *Appl. Phys. Lett.*, **91**, 202509 (2007).

Halabica, A., J. C. Idrobo, S. T. Pantelides, R. H. Magruder, S. J. Pennycook and R. F. Haglund, "Pulsed infrared laser annealing of gold nanoparticles embedded in a silica matrix," *J. Appl. Phys.*, **103**, 083545 (2008).

Henini, M., J. Ibanez, M. Schmidbauer, M. Shafi, S. V. Novikov, L. Turyanska, S. I. Molina, D. L. Sales, M. F. Chisholm and J. Misiewicz, "Molecular beam epitaxy of GaBiAs on (311)B GaAs substrates," *Appl. Phys. Lett.*, **91** (2007).

Herndon, N. B., S. H. Oh, J. T. Abiade, D. Pai, J. Sankar, S. J. Pennycook and D. Kumar, "Effect of spacer layer thickness on magnetic interactions in self-assembled single domain iron nanoparticles," *J. Appl. Phys.*, **103**, 07D515 (2008).

Kim, K., Y. Zhang, R. Feenstra, D. K. Christen, H. M. Christen, S. Cook, F. A. List, J. Tao, S. J. Pennycook and Y. Zuev, "$YBa_2Cu_3O_{7-\delta}$ formation by processing of laser-ablated, fluorine-free precursor films," *IEEE Trans. Appl. Supercond.*, **17**, 3624-3627 (2007).

Klie, R. F., J. C. Zheng, Y. Zhu, M. Varela, J. Wu and C. Leighton, "Direct measurement of the low-temperature spin-state transition in $LaCoO_3$," *Phys. Rev. Lett.,* **99**, 047203 (2007).

Lee, H. N., S. M. Nakhmanson, M. F. Chisholm, H. M. Christen, K. M. Rabe and D. Vanderbilt, "Suppressed dependence of polarization on epitaxial strain in highly polar ferroelectrics," *Phys. Rev. Lett.*, **98,** 217602 (2007).

Lee, H. N., S. M. Nakhmanson, M. F. Chisholm, H. M. Christen, K. M. Rabe and D. Vanderbilt, "Suppressed dependence of polarization on epitaxial strain in highly polar ferroelectrics (vol 98, art no 217602, 2007)," *Phys. Rev. Lett.*, **98**, 217602 (2007).

Li, A. P., C. Zeng, K. van Benthem, M. F. Chisholm, J. Shen, S. Rao, S. K. Dixit, L. C. Feldman, A. G. Petukhov, M. Foygel and H. H. Weitering, "Dopant segregation and giant magnetoresistance in manganese-doped germanium," *Phys. Rev. B*, **75,** 201201 (2007).

Liu, C. T., C. L. Fu, M. F. Chisholm, J. R. Thompson, M. Krcmar and X. L. Wang, "Magnetism and solid solution effects in NiAl (40% Al) alloys," *Prog. Mater Sci.*, **52**, 352-370 (2007).

Liu, F., R. Collazo, S. Mita, Z. Sitar, G. Duscher and S. J. Pennycook, "The mechanism for polarity inversion of GaN via a thin AlN layer: Direct experimental evidence," *Appl. Phys. Lett.*, **91**, Art. No. 203115 (2007).

Liu, F., R. Collazo, S. Mita, Z. Sitar, S. J. Pennycook and G. Duscher, "Direct observation of inversion domain boundaries of GaN on c-sapphire at sub-Angstrom resolution," *Adv. Mater.*, **20**, 2162-2165 (2008).

Luo, W., A. Franceschetti, M. Varela, J. Tao, S. J. Pennycook and S. T. Pantelides, "Orbital-occupancy versus charge ordering and the strength of electron correlations in electron-doped $CaMnO_3$," *Phys. Rev. Lett.*, **99**, 036402 (2007).

Luo, W., S. J. Pennycook and S. T. Pantelides, "s-electron ferromagnetism on gold and silver nanoclusters," *Nano Lett.*, **7**, 3134-3137 (2007).

Marinopoulos, A. G., K. van Benthem, S. N. Rashkeev, S. J. Pennycook and S. T. Pantelides, "Impurity segregation and ordering in $Si/SiO_2/HfO_2$ structures," *Phys. Rev. B*, **77**, 195317 (2008).

Mizoguchi, T., M. Varela, J. P. Buban, T. Yamamoto and Y. Ikuhara. "Site dependence and peak assignment of $YBa_2Cu_3O_{7-x}$ O K edge electron energy loss near edge fine structure," *Phys. Rev. B.* **77,** 024504 (2008).

Molina, S. I., T. Ben, D. L. Sales, J. Pizarro, P. L. Galindo, M. Varela, S. J. Pennycook, D. Fuster, Y. Gonzalez and L. Gonzalez, "Determination of the strain generated in InAs/InP quantum wires: prediction of nucleation sites," *Nanotech.*, **17**, 5652-5658 (2006).

Molina, S. I., A. M. Sanchez, A. M. Beltran, D. L. Sales, T. Ben, M. F. Chisholm, M. Varela, S. J. Pennycook, P. L. Galindo, A. J. Papworth, P. J. Goodhew and J. M. Ripalda, "Incorporation of Sb in InAs/GaAs quantum dots," *Appl. Phys. Lett.*, **91**, 263105 (2007).

Molina, S. I., M. Varela, D. L. Sales, T. Ben, J. Pizarro, P. L. Galindo, D. Fuster, Y. Gonzalez, L. Gonzalez and S. J. Pennycook, "Direct imaging of quantum wires nucleated at diatomic steps," *Appl. Phys. Lett.*, **91**, 143112 (2007).

Molina, S. I., M. Varela, T. Ben, D. L. Sales, J. Pizarro, P. L. Galindo, D. Fuster, Gonz, Y. lez, Gonz, L. lez and S. J. Pennycook, "A Method to Determine the Strain and Nucleation Sites of Stacked Nano-Objects," *J. Nanosci. Nanotech.*, **8**, 3422-3426 (2008).

Nicolosi, V., P. D. Nellist, S. Sanvito, E. C. Cosgriff, S. Krishnamurthy, W. J. Blau, M. L. H. Green, D. Vengust, D. Dvorsek, D. Mihailovic, G. Compagnini, J. Sloan, V. Stolojan, J. D. Carey, S. J. Pennycook and J. N. Coleman, "Observation of van der Waals driven self-assembly of MoSI nanowires into a low-symmetry structure using aberration-corrected electron microscopy," *Adv. Mater.*, **19**, 543-547 (2007).

Oh, S. H., K. van Benthem, S. I. Molina, A. Y. Borisevich, W. D. Luo, P. Werner, N. D. Zakharov, D. Kumar, S. T. Pantelides and S. J. Pennycook, "Point defect configurations of supersaturated Au atoms inside Si nanowires," *Nano Lett.*, **8**, 1016-1019 (2008).

Oxley, M. P. and S. J. Pennycook, "Image simulation for electron energy loss spectroscopy," *Micron*, **39**, 676-684 (2008).

Oxley, M. P., M. Varela, T. J. Pennycook, K. van Benthem, S. D. Findlay, A. J. D'Alfonso, L. J. Allen and S. J. Pennycook, "Interpreting atomic-resolution spectroscopic images," *Phys. Rev. B*, **76**, 064303 (2007).

Allen, L. J., S. D. Findlay, M. P. Oxley, C. Witte and N. J. Zaluzec, "Modelling high-resolution electron microscopy based on core-loss spectroscopy," *Ultramicrosc.*, 106, 1001-1011 (2006).

Peng, Y., M. P. Oxley, A. R. Lupini, M. F. Chisholm and S. J. Pennycook, "Spatial Resolution and Information Transfer in Scanning Transmission Electron Microscopy," *Microsc. Microanal.*, **14**, 36-47 (2008).

Pennycook, S. J., "Investigating the Optical Properties of Dislocations by Scanning Transmission Electron Microscopy," *Scanning*, **30**, 287-298 (2008).

Rashkeev, S. N., A. R. Lupini, S. H. Overbury, S. J. Pennycook and S. T. Pantelides, "Role of the nanoscale in catalytic CO oxidation by supported Au and Pt nanostructures," *Phys. Rev. B*, **76**, 035438 (2007).

Roberts, K. G., M. Varela, S. Rashkeev, S. T. Pantelides, S. J. Pennycook and K. M. Krishnan, "Defect-mediated ferromagnetism in insulating Co-doped anatase TiO2 thin films," *Phys. Rev. B*, **78**, 014409 (2008).

Rosenberg, R. A., G. K. Shenoy, M. F. Chisholm, L. C. Tien, D. Norton and S. Pearton, "Getting to the core of the problem: Origin of the luminescence from (Mg,Zn)O heterostructured nanowires," *Nano Lett.*, **7**, 1521-1525 (2007).

Rosenthal, S. J., J. McBride, S. J. Pennycook and L. C. Feldman, "Synthesis, surface studies, composition and structural characterization of CdSe, core/shell and biologically active nanocrystals," *Surf. Sci. Rep.*, **62**, 111-157 (2007).

Seo, S. S. A., J. H. Lee, H. N. Lee, M. F. Chisholm, W. S. Choi, D. J. Kim, J. Y. Jo, H. Kim, J. Yu and T. W. Noh, "Ferroelectricity in artificial bicolor oxide superlattices," *Adv. Mater.*, **19**, 2460-2464 (2007).

Shin, J., S. V. Kalinin, A. Y. Borisevich, E. W. Plummer and A. P. Baddorf, "Layer-by-layer and pseudo-two-dimensional growth modes for heteroepitaxial $BaTiO_3$ films by exploiting kinetic limitations," *Appl. Phys. Lett.,* **91**, 202901 (2007).

Shin, J., S. V. Kalinin, A. Y. Borisevich, E. W. Plummer and A. P. Baddorf, "Layer-by-layer and pseudo-two dimensional growth modes for heteroepitaxial $BaTiO_3$ films by exploiting kinetic limitations (vol 91, art no 202901, 2007)," *Appl. Phys. Lett.,* **91**, 249901 (2007).

Shibata, N., M. F. Chisholm, A. Nakamura, S. J. Pennycook, T. Yamamoto and Y. Ikuhara, "Nonstoichiometric dislocation cores in alpha-alumina," *Science*, **316**, 82-85 (2007).

Shibata, N., G. S. Painter, P. F. Becher and S. J. Pennycook, "Atomic ordering at an amorphous/crystal interface," *Appl. Phys. Lett.*, **89**, 051908 (2006).

Torija, M. A., M. Sharma, M. R. Fitzsimmons, M. Varela and C. Leighton, "Epitaxial $La_{0.5}Sr_{0.5}CoO_3$ thin fims: Structure, magnetism and transport," *J. Appl. Phys.,* **104,** 023901 (2008).

van Benthem, K., G. S. Painter, F. W. Averill, S. J. Pennycook and P. F. Becher, "Experimental probe of adsorbate binding energies at internal crystalline/amorphous interfaces in Gd-doped Si_3N_4," *Appl. Phys. Lett.*, **92**, 163110 (2008).

Veith, G. M., A. R. Lupini, S. J. Pennycook, A. Villa, L. Prati and N. J. Dudney, "Magnetron sputtering of gold nanoparticles onto WO_3 and activated carbon," *Catal. Today*, **122**, 248-253 (2007).

Viswanathan, S. K., A. A. Gapud, M. Varela, J. T. Abiade, D. K. Christen, S. J. Pennycook and D. Kumar, "Enhancement of critical current density of $YBa_2Cu_3O_{7-\delta}$ thin films by self-assembly of Y_2O_3 nanoparticulates," *Thin Solid Films*, **515**, 6452-6455 (2007).

Walkosz, W., R. F. Klie, S. Ogut, A. Borisevich, P. F. Becher, S. J. Pennycook and J. C. Idrobo, "Atomic resolution study of the interfacial bonding at $Si_3N_4/CeO_{2-\delta}$ grain boundaries," *Appl. Phys. Lett.*, **93**, 053104 (2008).

Xiao, K., J. Tao, Z. W. Pan, A. A. Puretzky, I. N. Ivanov, S. J. Pennycook and D. B. Geohegan, "Single-crystal organic nanowires of copper-tetracyanoquinodimethane: Synthesis, patterning, characterization, and device applications," *Angewandte Chemie-International Edition*, **46**, 2650-2654 (2007).

Zeng, C., P.R.C. Kent, M. Varela, M. Eisenbach, G. M. Stocks, M. Torija, J. Shen, H. Weitering. "Epitaxial stabilization of ferromagnetism in the nanophase of FeGe," *Phys. Rev. Lett.*, **96**, 127201 (2006)

Zeng, C. G., Z. Y. Zhang, K. van Benthem, M. F. Chisholm and H. H. Weitering, "Optimal doping control of magnetic semiconductors via subsurfactant epitaxy," *Phys. Rev. Lett.*, **100**, 066101 (2008).

Visualization and quantification of deformation processes controlling the mechanical response of alloys in aggressive environments.

Ian M. Robertson.
Department of Materials Science and Engineering,
University of Illinois, 1304 West Green Street
Urbana IL 61801. ianr@illinois.edu

The objective of this effort is to determine the atomistic processes occurring at elevated temperatures that govern the macroscopic mechanical response of metals and alloys relevant for deployment in the aggressive environments envisioned for Generation IV reactors. Realization of this objective will be achieved through a combination of bulk mechanical property tests and post-mortem characterization studies as well as *time-resolved* straining experiments conducted as a function of temperature in the transmission electron microscope. The latter approach allows visualization and quantification of interactions of dislocations with obstacles which provides unique insight to the pathways governing microstructure evolution. The program focuses on understanding the interaction of dislocations with interfaces, with precipitates of varying degrees of coherency, and with radiation defects as a function of temperature. Using this combination of approaches it is possible to determine the dominant processes and to use this information to develop, test and refine predictive models for effects such as irradiation-assisted intergranular failure, high-temperature creep behavior, and radiation embrittlement.

The visualization and quantification of reactions by transmission electron microscopy are obscured by the fact that what is observed is a projection of the microstructure. The three-dimensional aspect of the microstructure is lost. This information can be recovered by using stereomicroscopy techniques but this approach is limited. Part of this effort will focus on development and application of image reconstruction, with appropriate image processing to reveal high fidelity and high spatial resolution images of dislocation structures, to produce three-dimensional images featuring the interaction. This capability will greatly enhance our ability to understand dislocation-defect interactions as the interactions can be viewed from different directions. This is a relatively new technique in the area of dislocation-defect interactions and requires significant development.

Interfaces serve as both sources and sinks for dislocations, fast diffusion pathways for impurities and as sites at which defects and impurities segregate to and aggregate. These processes can change the internal structure and chemistry of the interface with the consequence that the response mechanism can be changed to the extent of favoring crack nucleation and propagation along the interface rather than slip transmission through it. Temperature also plays a role in how a grain boundary responds to a local stress concentration through changing the spreading kinetics of the accumulated strain energy along the interface; this effectively diffuses the local stress concentration. Changing the matrix strength can impact how an interface responds by influencing not the dislocation nucleation stress but rather the propagation stress. Our efforts in the first year of this program have emphasized dislocation interactions with grain boundaries and radiation produced defects as a function of temperature.

At room temperature the interaction of dislocations with interfaces is governed by competition between the local stress state, applied stress plus the stress due to a dislocation pile-up, and the strain energy density in the interface which is altered by the accommodation and release of dislocations from it. These transfer conditions are well established and appear applicable for both grain boundaries and interfaces.[1-3] At elevated temperatures, the possibility of distributing the strain energy density along the length of the grain boundary is increased and this capability changes the strain energy density distribution and the need for the grain boundary to activate a source and eject dislocations. A key observation in the preliminary study is the tendency for increased grain boundary mobility of dislocations which spreads the accumulated strain energy density along the boundary. An example of this process is shown in Figure 1. The bright-field time-resolved images presented in Figure 1a show glissile grain boundary dislocations being ejected from a triple junction as perfect dislocations. Confirmation this is a triple junction along with a static bright-field image showing emission of the first eight dislocations is shown in Figure 1b. The significance of this result is the high frequency of occurrence at elevated temperatures compared to low temperatures. We are currently in the process of completing the characterization of the grain boundary and the dislocations. An interesting, but yet unanswered question is the nature of the step created at the triple junction by this ejection process but clearly there is no obvious sign of the formation of a void or crack. After we have understood the criteria governing such reactions, we will introduce obstacles into the matrix by irradiation to determine if the emission processes are altered by the presence of strong obstacles. That is, we will determine if the criterion governing dislocation emission from a grain boundary is changed from nucleation- to propagation-controlled. Such a transition in governing mechanism could result in the development of a high local stress that could be the driving force for nucleating and propagating a crack along the grain boundary; this effect would have important consequences for our understanding and mitigation of processes such as irradiation assisted stress corrosion cracking.[4]

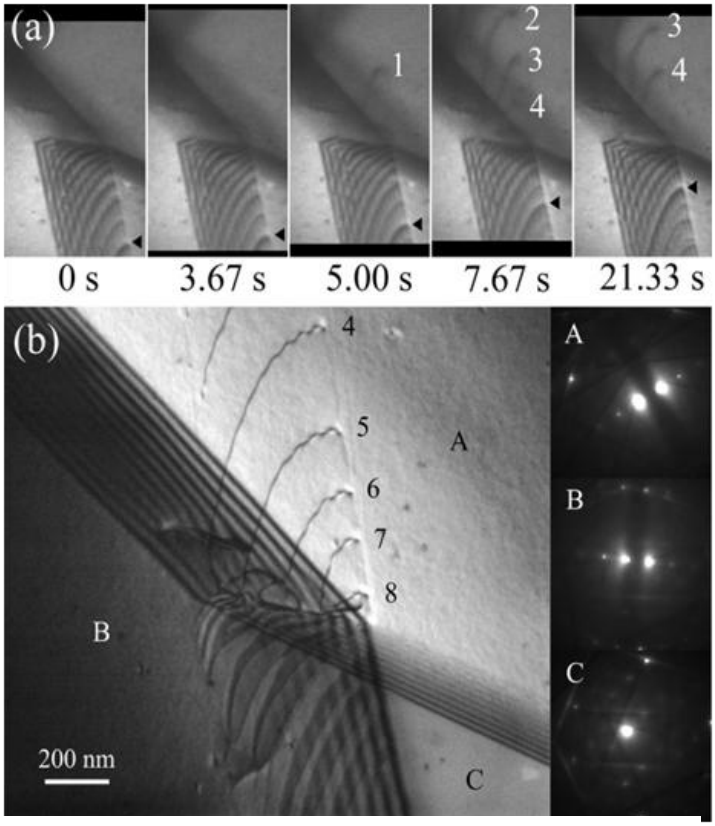

Figure 1. a) series of time-resolved images showing the propagation of dislocations along a grain boundary and the emission of perfect dislocations from a triple junction. b) static image with corresponding selected area diffraction patterns showing the emission of eight dislocations and confirming this is a triple junction.

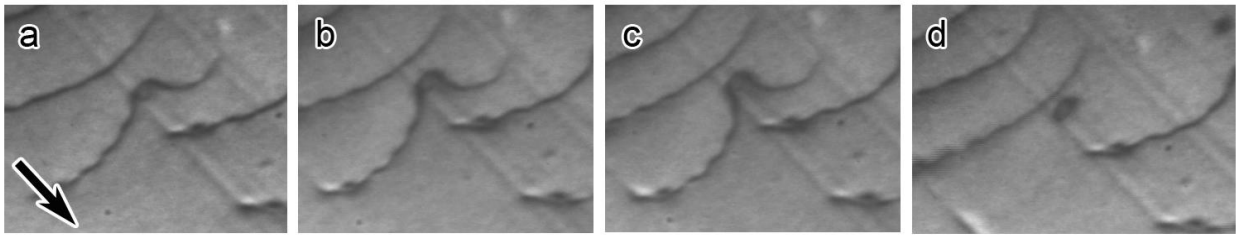

Figure 2. Time resolved series of images showing the interaction of a dislocation with a carbide in a stainless steel at room temperature. This appears to be an example of the classical "Orowan" bypass process but no loop is created around the particle.

Dislocation interactions with precipitates have also been observed to change as a function of the number of interactions. The time-resolved series of images presented in Figures 2 and 3 show the initial and final dislocations bypass processes as a function of the number of interactions at room temperature. The initial bypass process involves the two unpinned dislocation segments bowing around the obstacle as a function of the applied stress. As the segments sweep towards each other they are attracted together because they have opposite sign, recombine and break free of the obstacle. This process appears to be the classical Orowan bypass mechanism but, surprisingly, there is no visible "Orowan" loop.[5] This could be an example of the loop collapsing back onto the particle as has been suggested by some simulations.[6] As the number of interactions increases, the bypass process changes as seen in the series of images presented in Figure 3. Now one arm of the dislocation moves around the obstacle independent of the other until it impacts the free surface where it is breaks apart and releases a dislocation, Figure 3d. As other dislocations move to interact with the particle, the dislocation segment still attached to the particle reverses direction and annihilates part of the next incoming dislocation. This is seen in Figures 3f and 3g, with the outcome shown in Figure 3h. The bypass process has changed from

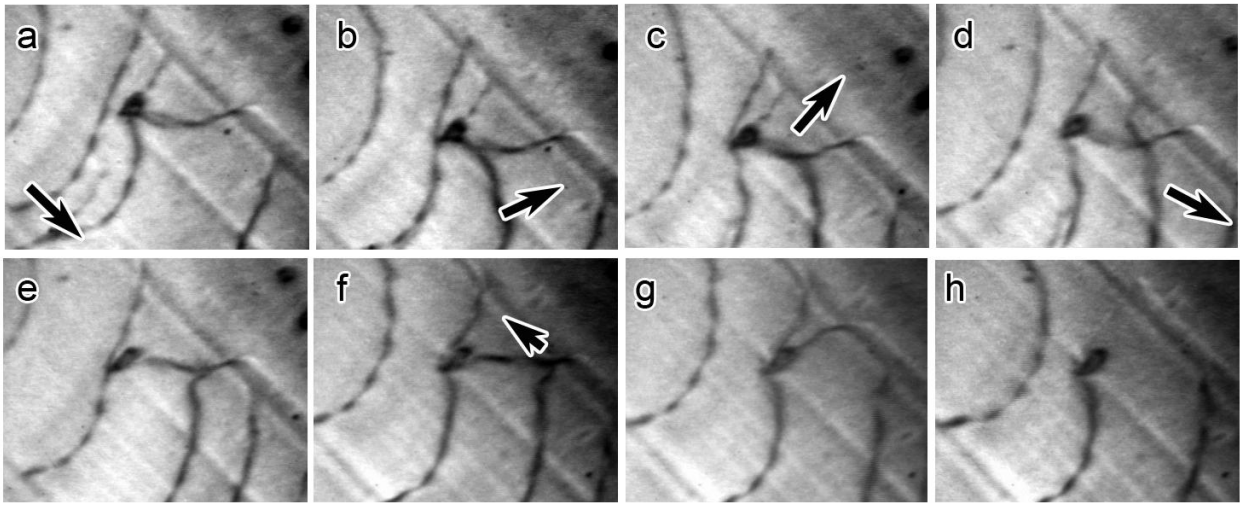

Figure 3. Change in the bypass mode following interaction with multiple dislocations. The process now involves cross slip to create two well separated dislocation segments that can move independently of each other.

a simply mechanism to one involving cross-slip such that the unpinned dislocation segments move independent of each other. This change appears to have occurred for dislocations on acoplanar slip plane and without noticeable debris being accumulated at the carbide. The reasons for this change are currently under investigation.

Our future work will emphasize quantifying dislocation interactions with grain boundaries as a function of grain boundary type and deformation temperature as well as dislocation interactions with other obstacles as a function of temperature. To reveal the interactions in more detail we have begun to explore the use of tomographic reconstruction of these complex interactions from multiple images taken over large angles of tilt. [7] Preliminary efforts have been successful to the extent that for the tilt angles achievable images can be reconstructed but these still suffer from aberrations due to inadequate tilt. However, the feasibility study has proved promising and in the next fiscal period we will explore further the use of this technique to reveal complex dislocation reactions.

PUBLICATIONS:

Combining *in situ* Transmission Electron Microscopy and Molecular Dynamics Computer Simulations to Reveal the Interaction Mechanisms of Dislocations with Stacking-fault Tetrahedron in Nuclear Materials
Yoshitaka Matsukawa, Martha Briceno and Ian M. Robertson. Accepted for publication in Journal of Electron Microscopy Technique.

REFERENCES.

[1] Clark WAT, Wagoner RH, Shen ZY, Lee TC, Robertson IM, Birnbaum HK. On the criteria for slip transmission across interfaces in polycrystals. Scripta Metallurgica et Materialia 1992;26:203.

[2] Lee TC, Robertson IM, Birnbaum HK. In situ transmission electron microscope deformation study of the slip transfer mechanisms in metals. Metallurgical Transactions 1990:2437.

[3] Lee TC, Robertson IM, Birnbaum HK. TEM in situ deformation study of the interaction of lattice dislocations with grain boundaries in metals. Philosophical Magazine A Physics of Condensed Matter Defects & Mechanical Properties 1990;A 62:131.

[4] Was GS, Busby JT. Role of irradiated microstructure and microchemistry in irradiation-assisted stress corrosion cracking. Philosophical Magazine 2005;85:443.

[5] Meyers MA, Chawla KK. Mechanical Behavior of Materials: Prentice-Hall, 1999.

[6] Xiang Y, Srolovitz DJ, Cheng LT, E W. Level set simulations of dislocation-particle bypass mechanisms. Acta Materialia 2004;52:1745.

[7] Barnard JS, Sharp J, Tong JR, Midgley PA. High-resolution three-dimensional imaging of dislocations. Science 2006;313:319.

Research Summaries IV:

Surfaces

Dynamic Surface Microscopy of Functional Materials

Norman C. Bartelt, John C. Hamilton, Kevin F. McCarty, and Konrad Thürmer
bartelt@sandia.gov, jchamil@sandia.gov, mccarty@sandia.gov, kthurme@sandia.gov
MS 9161, Sandia National Laboratories, Livermore, CA 94551

Program Scope

This project's goal is to quantify the fundamental atomic processes governing the dynamics of surface structure and morphology of functional materials. We use state-of-the-art microscopy (LEEM and STM) to measure, often in real time, the time evolution of surface structure on nanometer length scales. We use these measurements to write down precise equations of motion to describe the observed time dependence and then relate these equations of motion to atomic processes. This approach has obtained new insight into how real, multicomponent surfaces behave in different environments. We have used this general approach on a variety of different problems in surface science, including quantitatively determining the forces that stabilize self-assembling patterns, identifying the kinetic pathways that cause films to be unstable, and showing that unexpected diffusion processes, such as cluster diffusion and bulk/surface mass exchange, can dominate surface properties. We emphasize materials systems that can simultaneously reveal fundamental mechanisms and have importance to energy-related technologies. We also develop new microscopic experimental techniques and new theory/models, balancing technique development with application. Examples of technique development include a method for imaging insulating ice films by STM and our ongoing development of a method to measure local adsorbate concentrations using electron reflectivity (see below). Our recent and future work is focused in three areas: 1) The factors that control the stability of thin films; 2) The complex diffusion pathways that occur in multicomponent systems; and 3) The nanoscale pattern formation that can occur on surfaces. We next briefly highlight one result from each area.

Recent Progress

Thin-film stability – Ice films on Pt(111)

While water and ice next to surfaces plays critical roles in many phenomena, the fundamental nature of water/ice films has been remarkably poorly characterized. Microscopic techniques that are powerful for metals (e.g., TEM, SEM or LEEM) fail for ice films because they use electrons that immediately destroy ice. STM also had not been successful in studying multilayer ice because it requires an electric current to flow between the STM tip and sample. But ice is an insulator and cannot, under normal conditions, supply the electrons needed for imaging. Due to this lack of suitable high-resolution microscopies, how ice multilayers grow and what atomic mechanisms determine the stability of these films remained largely unknown. We discovered that nondestructive imaging is possible using extremely low tunneling currents and a large negative sample bias [1]. Water first forms a thin wetting layer upon which 3D crystallites grow (Fig. 1a). Upon dosing more

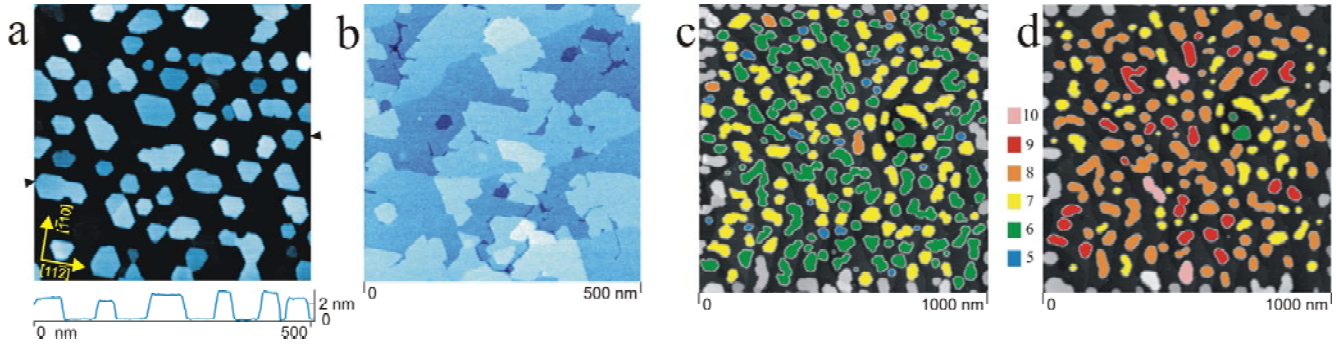

Fig. 1. STM images demonstrating the capability to investigate ice multilayers nondestructively. a) 0.8-nm-thick ice film with individual ~3-nm-high crystallites embedded in a one-molecule-thick wetting layer (black). b) 4-nm-thick continuous ice film, showing the first-ever images of molecular-height surface steps. c,d) Nucleation-limited dewetting. c) Ice film with each crystallite's height color-coded. d) Image of the same region after annealing.

water, these crystallites coalesce into a continuous film (Fig. 1b). By deciphering this coalescence, we determined the origin of the metastable phase cubic ice. We found that the substrate steps modify how the molecular layers of merging crystallites connect. As a result, screw dislocations are created around which growth spirals form where cubic ice is being produced [2]. To probe the stability of ice/Pt(111), we monitored with STM how the morphology changes when a film is annealed. Figures 1c,d reveal that the ice crystals grow thicker to expose more of the wetting-layer-covered Pt surface. This means that the dewetting driving force is strong enough to *nucleate* new layers, in contrast to metal/metal systems where no nucleation occurs.[a] The results show that the rate of new-layer nucleation, and not surface diffusion, determines how fast individual crystallite shapes equilibrate.

Complex diffusion mechanisms -- Graphene grows by adding clusters of C atoms

To better understand surface phenomena such as diffusion, we have developed a new technique for accurate, sensitive measurements of surface adsorbate concentrations [3]. The method uses changes in electron reflectivity from a surface. When performed in a LEEM instrument, our method gives a spatial map of adsorbate concentration, as the reflectivity change is determined locally from the intensity of LEEM images. We have applied our technique to understand how graphene (single layer sheets of graphitic carbon) grow on Ru, a model transition metal [4]. Figure 2 shows how carbon adatom concentrations can be measured while simultaneously imaging graphene growing from deposited C. We determined the relationship between the rate at which a graphene step edge advances and the adatom concentration. Such detailed knowledge has occasionally been obtained in crystal growth from solutions but has never been achieved in vapor-phase growth.[b] We find that graphene's growth rate is not the linear function of the adatom concentration expected for growth by addition of individual C atoms. Instead, a statistical-mechanical analysis shows that graphene grows by adding C *clusters*, most likely of five C atoms. This mechanism is in striking contrast to all known cases of metal and semiconductor growth.

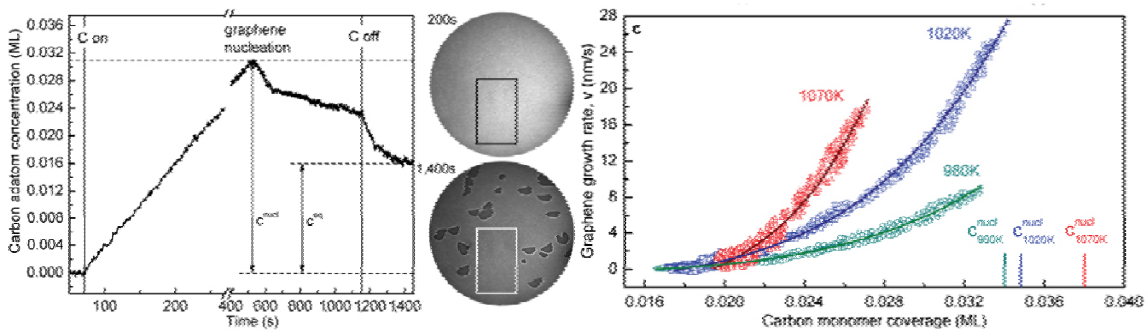

Fig. 2. Left: C adatom concentration during graphene nucleation and growth measured from electron reflectivity. Middle: LEEM images (46 μm field-of-view)where the boxes mark the graphene-free region where the C monomer concentration was determined. c^{nucl} *and* c^{eq} *are the monomer concentrations needed to nucleate graphene and be in equilibrium with graphene, respectively. Right: Non-linear dependence of growth rate on C monomer concentration.*

Nanoscale-pattern formation -- Nanoscale periodicity in the high-temperature limit

Key questions in surface pattern formation are quantifying the forces responsible for self-assembly and determining the generality of different possible mechanisms. We have used our approach of quantitative, real-time microscopy measurements combined with theory to gain new insight into why stripe patterns with long-range order form in the Au on W(110) system [5]. We find that the pattern amplitude decreases steadily with temperature and vanishes at the critical point, a signature of a 2nd-order phase transition. However, the pattern wavelength maintains a finite value of 100 nm. These observations are inconsistent with standard theories of pattern formation at solid surfaces, which focus on the low-temperature limit, where sharp boundaries exist between the surface phases. In contrast, we find that a mean-field description of patterns with diffuse interfaces successfully

describes the measured dependence of wavelength and amplitude. This work demonstrates the first experimental observation of nanoscale surface self-assembly close to the order-disorder transition. Importantly, the wavelength of the pattern at the critical point depends only on basic quantities like the stress difference and the boundary energy, which tend to be only weakly material-dependent. Thus, we expect that stress-domain patterns near the order-disorder transition will have this 100-nm-length scale.

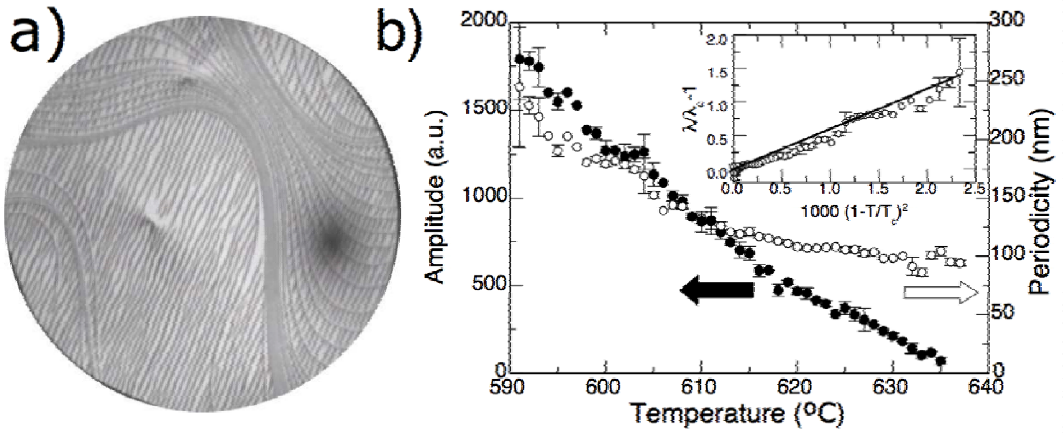

Fig. 3. a) LEEM image of Au stripes, which appear dark, on W(110) at 619°C. The field-of-view is 7 μm. b). Amplitude and period of the stripe pattern near the critical point, where the pattern vanishes.

Future Plans

Thin-film stability Future work will address the energetic driving forces that make flat films unstable. Our work reveals that even flat films that are not strained by the substrate can be unstable relative to being undulated. That is, we directly observe mass transfer that simultaneously thins and thickens, respectively, adjacent film areas. We will explore whether *surface stress* causes the instability. Additionally, we will examine the conversion of amorphous ice to crystalline ice.[c] Whereas amorphous ice grows layer-by-layer, crystalline films grow three dimensionally on top of the wetting layer. Thus, the structural transition from amorphous to crystalline ice is expected to occur simultaneously with a morphological transformation due to the dewetting instability.

Complex diffusion mechanisms We will determine whether the morphological evolution of crystalline ice is governed by the competing pathways of diffusion through the bulk, on the surface, or through the gas phase. Additionally, using a combined experimental and theoretical approach, we will deduce the origin and generality of the cluster-addition kinetics we have observed for graphene growth (Fig. 2) by characterizing growth on other metal substrates. Finally, we will use LEEM and STM to study diffusion under electrical bias, as occurs in electrochemical devices for energy storage and conversion.[d]

Nanoscale pattern formation We will explore how and why patterns form in the wetting layer of water (ice) on metal substrates. Finally, we will thoroughly study 3D pattern formation in the system of Cr on W(110). By observing the motion of individual atomic steps on the film surface, we should be able to elucidate which processes allow the remarkable transformation of a flat film into a fairly well-ordered array of 3D stripes.

References

[a]W. L. Ling, T. Giessel, K. Thürmer, R. Q. Hwang, N. C. Bartelt and K. F. McCarty, *Crucial role of substrate steps in de-wetting of crystalline thin films*, Surf. Sci. **570**, L297 (2004).

[b]L. N. Rashkovich, J. J. De Yoreo, C. A. Orme and A. A. Chernov, *In situ atomic force microscopy of layer-by-layer crystal growth and key growth concepts*, Crystallogr. Rep. **51**, 1063 (2006).

[c]A. Verdaguer, G. M. Sacha, H. Bluhm and M. Salmeron, *Molecular structure of water at interfaces: Wetting at the nanometer scale*, Chem. Rev. **106**, 1478 (2006).

[d]*Basic Research Needs for Electrical Energy Storage*. (Office of Basic Energy Sciences, U.S. Department of Energy, Washington, DC, 2007).

DOE Sponsored Publications 2006-2008

[1] K. Thürmer and N. C. Bartelt, *Nucleation-limited dewetting of ice films on Pt(111)*, Phys. Rev. Lett. **100**, 4 (2008).

[2] K. Thürmer and N. C. Bartelt, *Growth of multilayer ice films and the formation of cubic ice imaged with STM*, Phys. Rev. B **77**, 195425 (2008).

[3] J. de la Figuera, N. C. Bartelt and K. F. McCarty, *Electron reflectivity measurements of Ag adatom concentrations on W(110)*, Surf. Sci. **600**, 4062-6 (2006).

[4] E. Loginova; N. C. Bartelt; P. J. Feibelman; K. F. McCarty, *Evidence for graphene growth by C cluster attachment*, New Journal of Physics, accepted (2008).

[5] J. de la Figuera, F. Leonard, N. C. Bartelt, R. Stumpf and K. F. McCarty, *Nanoscale periodicity in stripe-forming systems at high temperature: Au/W(110)*, Phys. Rev. Lett. **100**, 4 (2008).

- M. L. Anderson, N. C. Bartelt, P. J. Feibelman, B. S. Swartzentruber and G. L. Kellogg, *The effect of embedded Pb on Cu diffusion on Pb/Cu(111) surface alloys*, Surf. Sci. **600**, 1901-8 (2006).
- J. de la Figuera, J. M. Puerta, J. I. Cerda, F. El Gabaly and K. F. McCarty, *Determining the structure of Ru(0001) from low-energy electron diffraction of a single terrace*, Surf. Sci. **600**, L105-9 (2006).
- F. El Gabaly, S. Gallego, C. Munoz, L. Szunyogh, P. Weinberger, C. Klein, A. K. Schmid, K. F. McCarty and J. de la Figuera, *Imaging spin-reorientation transitions in consecutive atomic Co layers on Ru(0001)*, Phys. Rev. Lett. **96**, 147202-4 (2006).
- P. Y. Hou and K. F. McCarty, *Surface and interface segregation in beta-NiAl with and without Pt addition*, Scripta Mater. **54**, 937-41 (2006).
- W. L. Ling, J. C. Hamilton, K. Thürmer, G. E. Thayer, J. de la Figuera, R. Q. Hwang, C. B. Carter, N. C. Bartelt and K. F. McCarty, *Herringbone and triangular patterns of dislocations in Ag, Au, and AgAu alloy films on Ru(0001)*, Surf. Sci. **600**, 1735-57 (2006).
- K. F. McCarty, *Deterministic positioning of three-dimensional structures on a substrate by film growth*, Nano Letters **6**, 858-61 (2006).
- K. F. McCarty, J. P. Pierce and C. B. Carter, *Translation-related domain boundaries form to relieve strain in a thin alumina film on NiAl (110)*, Appl. Phys. Lett. **88**, 141902-1 (2006).
- K. Thürmer, R. Q. Hwang and N. C. Bartelt, *Surface self-organization caused by dislocation networks*, Science **311**, 1272-4 (2006).
- R. van Gastel, N. C. Bartelt and G. L. Kellogg, *Reversible shape transition of Pb islands on Cu(111)*, Phys. Rev. Lett. **96**, 036106-4 (2006).
- M. L. Anderson, N. C. Bartelt, P. J. Feibelman, B. S. Swartzentruber and G. L. Kellogg, *How Pb-overlayer islands move fast enough to self-assemble on Pb-Cu surface alloys*, Phys. Rev. Lett. **98**, 096106 (2007).
- F. El Gabaly, J. M. Puerta, C. Klein, A. Saa, A. K. Schmid, K. F. McCarty, J. I. Cerda and J. de la Figuera, *Structure and morphology of ultrathin Co/Ru(0001) films*, New J. Phys. **9**, 80 (2007).
- S. Helveg, W. X. Li, N. C. Bartelt, S. Horch, E. Laegsgaard, B. Hammer and F. Besenbacher, *Role of surface elastic relaxations in an O-induced nanopattern on Pt(110)-(1 x 2)*, Phys. Rev. Lett. **98**, 115501 (2007).
- J. P. Pierce, N. C. Bartelt and K. F. McCarty, *Evolution of a reactive surface via subsurface defect dynamics*, Phys. Rev. Lett. **99**, 026101 (2007).
- N. Rougemaille, F. El Gabaly, R. Stumpf, A. K. Schmid, K. Thürmer, N. C. Bartelt and J. de la Figuera, *Labyrinthine island growth during Pd/Ru(0001) heteroepitaxy*, Phys. Rev. Lett. **99**, 4 (2007).
- Y. Sato, S. Chiang and N. C. Bartelt, *Spontaneous domain switching during phase separation of Pb on Ge(111)*, Phys. Rev. Lett. **99**, 4 (2007).
- R. Stumpf, *Nano-faceting of fcc(110) surfaces controlled by adsorbates and atom deposition or removal*, Surf. Sci. **601**, L115-L9 (2007).
- F. El Gabaly, K. F. McCarty, A. K. Schmid, J. de la Figuera, S. Gallego, L. Szunyogh, P. Weinberger and M. C. Muñoz, *Coinage-metal capping effects on the spin-reorientation transitions of Co/Ru(0001)*, New J. Phys. **10**, 73024 (2008).
- J. P. Pierce, N. C. Bartelt, R. Stumpf and K. F. McCarty, *Stability of ultrathin alumina layers on NiAl(110)*, Phys. Rev. B **77**, 195438 (2008).
- B. Santos, J. M. Puerta, J. I. Cerda, R. Stumpf, K. von Bergmann, R. Wiesendanger, M. Bode, K. F. McCarty and J. de la Figuera, *Structure and magnetism of ultra-thin chromium layers on W(110)*, New J. Phys. **10**, 16 (2008).
- R. Stumpf, R. Bastasz, J. A. Whaley and W. P. Ellis, *Effect of adsorbed hydrogen on the stability of titanium atoms on aluminum surfaces*, Phys. Rev. B **77**, 235413 (2008).

Fundamentals of kinetics on clean surfaces using LEEM.

C P Flynn and W Swiech,
University of Illinois at Urbana Champaign,
Physics Department and Materials Research Laboratory,
Urbana, IL 61801.
cpf@mrl.uiuc.edu

1. Program Scope.

The program, at this point of its initiation, is founded on equipment and ideas developed under DOE support over the past five years. Surface steps of atomic height are clearly visible in images taken by low energy electron microscopy (LEEM), which thus offers surface topography at atomic resolution. The lateral resolution is typically 10 nm, although recent instruments are improved in this regard by almost an order of magnitude. In our LEEM, the evolution of such surface features in time can be recorded at video rates with a 10^{-10} torr ambient vacuum and at temperatures up to 1700K. On this project the surface kinetics revealed by the observed evolution are employed to explore the fundamental defect kinetic processes that take place on clean surfaces near equilibrium at high temperatures that approach the melting point T_m.

The power of these methods has been greatly enhanced by the recent incorporation of an ion beam of tunable energy into the LEEM, including use of self-ions, e.g., Pt- ions on Pt(111). Self-ions eliminate possible effects of chemical contamination on kinetics driven by ion beam processes. Upon irradiating surfaces with ion beams of energy 50 - 3000 eV the processes observed at lower energies comprise epitaxial growth with hyperthermal ions, while at higher energies there is a net loss of atoms from the surface by beam-induced sputtering. In both limits the ion beam intensity at the surface permits driving rates ~ 0.1 ML/s. The former (low energy) regime may be regarded as a surface driven by the creation of excess adatoms while the latter is driven by excess advacancies. The driven steady states of the surface in these regimes has offered rich new information about surface defect processes. This augments and complements measurements of equilibrium kinetics on the surface in the absence of irradiation. The combination of intense ion beams and high experimental temperatures permits, in addition, atomic resolution studies under simultaneous extreme combinations of driving irradiation and operating temperature.

Experimental research on this project has established that driven steady states achieved at high temperatures fall within the regime in which the response remains linearly dependent on the ion beam intensity. The experimental program has been complemented by a theoretical effort in which the linear response of the driven surface is analyzed in terms of defect processes. These include both the creation and annihilation of adatoms and advacancies at fixed sinks such as step edges, their diffusion from one site to the next on the surface, and their spontaneous creation and annihilation as pairs on otherwise perfect terrace sites. The theory permits a quantitative interpretation of kinetic observations that could not be achieves in the absence of a detailed theoretical understanding. The full generality of the theory proves essential as the experiments show that, under typical operating conditions on the surfaces studied, the defect lifetimes are

dominated by reactions through pair events rather than by independent processes of adatoms and advacancies separately at fixed sinks.

2. Recent Results.

While microscopies have, on occasion, been derogated as the source only of 'pretty pictures' our own efforts have in substantial part focused on measurements that yield quantitative information that is otherwise inaccessible. Examples of recent progress in four such areas are summarized here.

A. Surface mass diffusion using step fluctuation spectroscopy. Adatoms and advacancies in equilibrium attach to and detach from step edges at rates that precisely determine the surface mass diffusion coefficient D_s. The statistical fluctuations of the step location appear as Fourier modes on straight steps. Their decay times can be determined from video sequences and the dependence of rms amplitude on wave vector employed to identify surface and bulk contributions to the step process. By these means quantitative values of D_s have been determined as a function of temperature for close packed surfaces of a number of important materials including Ni(111), Pd(111) and Pt(111). Prefactors D_0 and activation energies Q for different metals appear fairly systematic with $D_0 \sim 10^{-3}$ cm^2/s and $Q \sim 6k_BT_m$.

B. Driven island nucleation. The way a beam of self ions changes the chemical potential μ^* on a surface depends on the local fixed sinks and on the rates K_1 and K_2 per site at which the beam creates adatoms and advacancies. We have devised an valuable method using such ion beams by which large arenas formed as pans or mesas of perfect terrace ~ 6 μm wide can be created to buffer local processes from external perturbations. The beam-driven $\mu^*(\mathbf{r})$ on the terrace at steady state is independent of Ds and determined in terms of K_1 and K_2 by the theory mentioned above. The theory affords a description of the conditions under which new islands nucleate near the center of the driven terrace. A novel prediction is that equal but opposite values of μ^* are required for adatom islands and advacancy islands regardless of differences between the properties of the two antidefect species. In an investigation of Pt^- irradiation of Pt(111), the critical beam flux for island nucleation has been determined over a range of temperatures and the symmetry prediction confirmed. The observed critical rates agree within a small factor with rates predicted from fundamental theories of nucleation.

C. Driven island growth. Once nucleated by irradiation, an adatom island growns larger in a low-energy (adatom) beam and shrinks in a high energy (advacancy) beam whose overall effect is to sputter. The reverse is the case for advacancy islands in which the peripheral step edge is reversed to step up radially outwards. We have examined these processes for islands nucleated on pans and mesas to find that the process is universal and independent of diffusion coefficient, determined only by the defect creation rate from the ion beam. The simplified geometry of the synthesized pans and mesas permits a description of the process using the theory mentioned above, and this provides a precise prediction of the time evolution of the universal behavior. So much is this the case that the growth measurements yield experimental values of $K_1 - K_2$, the excess adatom creation rate for the beam energy emploted. With R. Averback et al. of Illinois we have

compared these observations as a function of beam energy with the detailed predictions from advanced molecular dynamics simulations of the surface processes and find that the two agree within an experimental uncertainty ~ 10 %. In this way the irradiation research is providing an absolute calibration for the molecular dynamics programs.
Other processes. From a variety of kinetic observations by LEEM just two are selected for mention here. First, screw dislocations threading to the surface form spirals when driven by an ion beam and the rotation provides a clock whose period is exactly one monolayer of surface modification. This applies likewise when two neighboring screws of opposite sign form a Frank-Reed source that operates by climb of a surface step (rather than slip, as in the original concept). The exactitude of these processes offers an alternative to island growth as a calibration for calculated rates of beam damage.

Second, the ability to operate a LEEM with the sample at very high temperatures brings the prospect of observations under extreme conditions in which the surface is eroding by sublimation. The ion beam introduces the possibility of scientific observation under simultaneous extreme conditions of irradiation and temperature which are surely pertinent to future interests in energy production. Thus far we have explored sublimation in the absence of irradiation for Pt(111), Cr (011) and V(011) and have successfully observed the step flow resulting from sublimation in each case. The observed activation energy is approximately the cohesive energy in each case.

3. Future Plans.

Two areas of projected activity are identified here. One is quickly explained. We will explore sublimation near the melting temperature of selected crystals both with and without intense ion beam self-irradiation. It is our expectation that new effects may emerge as the ion beam and evaporation interact in a non-linear manner. Mechanisms by which this can happen are readily conceived. Sublimation from flat surfaces is, for example, limited by available step-edge sources. Then the creation of new steps by irradiation can cause sublimation to increase.

A main thrust of future work will be a focus on the time domain. It is possible to switch a driving ion beam on or off very rapidly. The subsequent relaxation of the surface to a new steady state offers the opportunity to examine the time sequence of change, and this in turn involves the hopping diffusion coefficient rather than the mass diffusion measured as described above. Given both diffusion coefficients, the surface concentration of surface thermal defects becomes quantitatively accessible-- a major long-term goal for much effort directed to metal surfaces, not yet successfully accomplished. From among alternative possibilities we expect to use the island nucleation process (see 2A above) to determine the response rate of the surface, and hence the hopping diffusion coefficient. Probe rates down to μsecs are visualized. The LEEM is capable of measurements at still faster rates, should they be needed.

4. DOE-Sponsored Publications.

S.-J. Tang, S. Kodambaka, W. Swiech, I. Petrov, C. P. Flynn, and T.-C. Chiang, Phys. Rev. Lett. 96, 126106 (2006). Sublimation of atomic layers from a chromium surface.
M. Ondrejcek, M. Rajappan, W. Swiech and C.P. Flynn, Phys.Rev B 73, 035418 (2006) Step fluctuation studies of surface diffusion and step stiffness for the Ni(111) surface.

C P Flynn, J. Phys.:Condens. Matter, 18, 5239 (2006). Why is diffusion in metals and on metal surfaces universal?
M. Ondrejcek, W. Swiech and C.P. Flynn, Phil. Mag. 86,1387 (2006). From step fluctuations to nanostructure energetics on Nb(011).
M Ondrejcek, W Swiech and C P Flynn, Surf. Sci., 600, 4673 (2006). Surface mass diffusion and step stiffness on an anisotropic surface: Mo(011).
M Ondrejcek, M Rajappan, W Swiech and C P Flynn, J Appl Phys, 100, 083523 (2006). Surface mass diffusion and step stiffness on V(011).
C P Flynn, Phys. Rev B71, 1 (2006). Coupling among bulk, surface and edge diffusion.
C P Flynn, Phys. Rev. B 75, 134106 1-11 (2007). Exact linear response of reacting thermal defects driven by creation processes.
C P Flynn, Surf. Sci. 601, 1648-1658 (2007). Flow of Defects from Bulk to Surfaces.
M. Rajappan, W. Swiech, M. Ondrejcek, and C.P. Flynn, J. Phys.: Condens. Matter, 19, 226006 (2007). Surface mass diffusion over an extended temperature range on Pt(111)
M Rajappan, W Swiech, M Ondrejcek and C P Flynn, Phil. Mag. 87, 4501-4518 (2007). Surface sink action during irradiation for Pt^- on Pt(111) by LEEM
W. Swiech, M. Rajappan, M. Ondrejcek, E. Sammann, S. Burdin, I. Petrov and C.P. Flynn, Ultramicroscopy 108 646–655 (2008). Real-time imaging of surface evolution driven by variable energy ion irradiation.
C. P. Flynn, W. Swiech, M. Ondrejcek and M. Rajappan, Phys. Rev. B 77, 045406 1-7 (2008). Surface islands nucleated by a beam of energetic self-ions.
M Ondrejcek, W Swiech, I Petrov, M Rajappan and C P Flynn, Microscopy Research and Techniques: special issue on 'In situ electron microscopy methods' (in press). LEEM investigations of surfaces using a beam of energetic self-ions.
C P Flynn, W Swiech and M Ondrejcek, Phys. Rev. B 78, 075420 (2008). Universal growth of islands driven by ion beams.
C P Flynn, M Ondrejcek and C P Flynn, J. Phys.: Condens. Matter 20, 395001 (2008). Synthesis of pans and mesas using a beam of self ions.

Abstract for Electron and Scanning Probe Microscopies Contractors Meeting 2008

1. **DOE Award Number**: DE-FG02-84ER45076

   Recipient Organization: Board of Regents of the University of Wisconsin System, University of Wisconsin-Milwaukee, P.O. Box 340, Milwaukee, WI 53201

2. **Project Title**: "Electron Scattering from Surfaces"

   PI: Dilano K. Saldin

3. **Recent Progress**

Low energy electron diffraction (LEED) [1] is an almost ideal tool for experimentally revealing the atomic-scale structure of the outermost layers of a crystal surface. This is because the strong interaction of such electrons with matter results in a short inelastic scattering length of the depth of only a few surface atomic layers. Thus the backscattered signal is sensitive only to the structure of these few outermost layers.

However, the very strength of this interaction also results in LEED being a strong multiple-scattering problem for which there is as yet no inverse method – that is one in which the structure of the surface may be determined directly from the diffraction data. The traditional method of solving surface structures by LEED is that of comparing a large number of simulated LEED spectra for guessed models with experiment. While such a method is admirable for the final stages of refinement, due to the exponential scaling of the required computer time with the number of parameters varied, it is often inadequate for finding a completely unknown structure.

In most developed branches of crystallography, where structures of even biological macromolecules are determined routinely, structure solution proceeds in two steps: (1) the application of some kind of direct method which rapidly reveals the approximate structure, and (2) a step in which structural parameters are refined against the experimental data. It is to provide the missing step (1) for LEED that this work is directed.

The key idea [2] is to write the dynamical (multiple-scattering) structure factor as:

$$F_\varepsilon^{(c)} = R_\varepsilon + S_\varepsilon \qquad (1)$$

where the partial structure factor (reference wave) R_ε represents the sum of all multiple-scattering paths that include only scattering by atoms of the known (bulk) structure, while

$$S_\varepsilon = \sum_j p_j O_{\varepsilon j} \qquad (2)$$

is an object wave consisting of a sum of *calculable elementary object waves,* $O_{\varepsilon j}$, [3] which may be regarded as a *renormalized structure factor* of a test 2D Bravais lattice containing an average atom at a position j in a surface unit cell (in Eqs. (1) and (2), the subscript ε represents a measured data point, specified

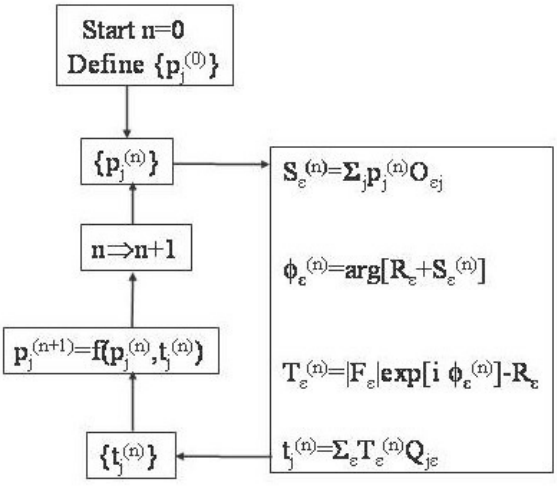

Figure 1 Flow chart for an iterative algorithm for LEED structure completion.

by a combination of the Miller indices (*h, k*) of a Bragg reflection and the electron beam energy, *E*). The inverse problem in this case may be defined as that of recovering the real-space distribution $\{p_j\}$ of surface *atoms* from a set of measured LEED intensities $|F_\varepsilon^{(e)}|^2$. The flow chart of the algorithm for accomplishing this is illustrated in Fig. 1, above.

From some initial guessed distribution, $\{p_j^{(0)}\}$, of atoms of unknown position, Eq.(2) is used to construct a set of "theoretical" structure factors $\{S_\varepsilon^{(n)}\}$ of the unknown part of the structure at the current iteration, *n*. Adding these to the structure factors R_ε of the known part of the structure and taking the arguments of the sums yields current estimates, $\varphi_\varepsilon^{(n)}$ of the phases of the total structure factors. Associating these with their experimentally-measured amplitudes $|F_\varepsilon|$, followed by subtraction of the structure factors R_ε of the known part gives improved estimates, $T_\varepsilon^{(n)}$ of the structure factors of the unknown part. Extraction from these quantities of the estimate of the spatial distribution $\{t_j^{(n)}\}$ of the atoms of unknown positions that are consistent with the measured structure factors $|F_\varepsilon|$ may now be performed by the equations in the bottom right hand corner of the flow chart with the aid of the quantities $Q_{j\varepsilon}$ defined by

$$\sum_\varepsilon Q_{j\varepsilon} O_{\varepsilon i} = \delta_{ji} \tag{4}$$

i.e. the matrix $\{Q_{j\varepsilon}\}$ is the inverse of $\{O_{\varepsilon i}\}$, and may be found by the robust method of singular value decomposition (SVD). We have termed this algorithm the Phase and Amplitude Recovery And Diffraction Image Generation Method (or PARADIGM, for short).

The solution is reached by iteratively satisfying constraints in real and reciprocal space. We followed an initial successful test of the algorithm on simulated LEED data for c(2x2)-CO/Ni(001) [2] with its use to recover directly the structures of the surface unit cells of c(2x2)-Br/Pt(110) [2], (3x1)-Br/Pt(110) [4], and (5x1)-H/Ir(100) [4] from experimental data.

We have recently demonstrated further applications of this method [5] to the (5x1)-Ir(001) surface. The clean surface of (5x1)-Ir(001) has been the subject of investigations for several decades. It is a fascinating structure in which the top surface layer accommodates an extra row of atoms parallel to a (100) direction every five subsurface rows. More recent LEED work has uncovered exquisite details of this structure, including minute bucklings and relaxations down to the fourth layer from the surface.

A remarkable change in the structure is induced upon exposure to H at temperatures above 180 K (Hammer et al. [6]). The strain of the outermost Ir layer is relieved by one atom per (5x1) unit cell "popping out" of this layer to form an adatom, while the previously compressed layer deconstructs to form a normal bulk-like face-centered cubic (001) layer. The ejected atom takes up an adatom structure on a hollow site on the deconstructed surface. The string of single adatoms per (5x1) surface unit cell aligns in a direction parallel to the short axis of the resulting surface unit cell to form a one-atom-wide surface nanowire. This structure was correctly recovered by our PARADIGM algorithm from experimental LEED data measured by Heinz and co-workers.

The self-assembly of single-atom-wide nanowires is of great interest due to potential applications in nanotechnology. Such nanowires may form templates for other interesting nanoscale structures (Klein et al. [7], Heinz et al. [8]). It has been found that dosing with enough Fe to form 0.4 of a monolayer results in Fe atoms decorating the Ir nanowire from both sides to form a *ribbon* structure. Further adsorption of

Fe results in the complete filling of the nanotrenches between the decorated nanowires when the coverage reaches 0.8 monolayers. The PARADIGM algorithm was able to correctly find these structures from experimental LEED data [5].

During this year also, together with the visiting Japanese student Shohgo Higashi, we have applied this method successfully to recover the structure of the surface alloy p(2x2)Sb/Cu(001) [9] from LEED data from the group of Prof. Hiroshi Tochihara of Kyushu University.

In summary, the PARADIGM algorithm shows much promise of developing into a general direct method for the strong multiple-scattering problem of LEED

References

[1] J. B. Pendry, *Low Energy Electron Diffraction*. (London, Academic Press).
[2] D. K. Saldin, A. Seubert, and K. Heinz, Phys. Rev. Lett. **88**, 115507 (2002).
[3] A. Szöke, Phys. Rev. B **47**, 14044 (1993).
[4] A. Seubert, K. Heinz, and D. K. Saldin, Phys. Rev. B **67**, 25417 (2003).
[5] D. K. Saldin and V. L. Shneerson, J. Phys.: Condens. Matter **20**, 304208 (2008).
[6] L. Hammer, W. Meier, A. Klein, P. Landfried, A. Schmidt, and K. Heinz, Phys. Rev. Lett. **91**, 156102 (2003).
[7] A. Klein, A. Schmidt, L. Hammer, and K. Heinz, Europhys. Lett. **65**, 830 (2004).
[8] K. Heinz, L. Hammer, A. Klein, and A. Schmidt, Appl. Surf. Sci. **237**, 519 (2004).
[9] S. Higashi, H. Tochihara, V. L. Shneerson, and D. K. Saldin, Surf. Sci. **602**, 2473 (2008).

4. Planned Activities for Next Year

LEED Studies with a Low Beam Currents

There are two circumstances in which use of an ultra-low beam current is essential for LEED: (1) the study of fragile organic adsorbates on surfaces, and (2) the study of insulating surfaces, such as those of metal oxides where, due to lack of a conduction channel, such samples charge up due to an accumulation of electrons from the incident beam. The apparatus developed in the laboratory of one of the PI's colleagues, Prof. Carol Hirschmugl, which uses a low-current, and a high-count-rate delay-line detector, enables precisely such experiments. We have analyzed such data to determine the structure and reactivity of 2-butanol on Pd(111), and work is in progress on the unsolved structure of MgO(111)-($\sqrt{3}$x$\sqrt{3}$) and on surface structures of ZnO and TiO.

LEED Studies of Chiral Surfaces

It is well known chirally-related molecules cannot be distinguished x-ray crystallography since an x-ray diffraction pattern from a molecule and its enantiomorph are identical. The theoretical argument for this proposition is based on the kinematical (or single-scattering) theory. It is not expected to be valid in a circumstance of strong multiple scattering as in LEED. We have indeed found that LEED is an excellent tool for distinguishing enantiomerically-related structures.

The PI has recently been awarded computer time for this project on the NSF-funded TeraGrid. which uses high-performance network connections, to integrate high-performance computers, data resources and tools, and high-end experimental facilities around the country. Currently, TeraGrid resources include more than 750 teraflops of computing capability and more than 30 petabytes of online and archival data storage, with rapid access and retrieval over high-performance networks. Work will also continue on exploring the capabilities of LEED to investigate chiral surfaces, and on further developing our direct method for LEED, making use of opportunities offered by the TeraGrid.

5. Publications Acknowledging DOE Support on this Project in 2006-2008

[1] "Structure of hydrogen-stabilized MgO(111)-(1x1) surface from low-energy electron diffraction"
H. C. Poon, X. F. Hu, S. E. Chamberlin, D. K. Saldin, and C. J. Hirschmugl
Surf. Sci. **600**, 2505-2509 (2006).

[2] "Spontaneous symmetry breaking of the Ir(100)-(5x1) surface from low energy electron diffraction"
H. C. Poon, D. K. Saldin, D. Lerch, W. Meier, A. Schmidt, A. Klein, S. Müller, L. Hammer, and K. Heinz
Phys. Rev. B **74**, art. no. 125413 (8 pages) (2006).

[3] "Surface Segregation of Gold on Au/Pd(111) Alloys Measured by Low Energy Electron Diffraction"
J. Li, O. Furlong, F. Calaza, L. Burkholder, H. C. Poon, D. K. Saldin, and W. T. Tysoe
Surf. Sci. **602**, 1084-1091 (2008).

[4] "The Structure and Reactivity of 2-Butanol on Pd(111)"
F. Gao, Y. Wang, L. Burkholder, C. Hirschmugl, D. K. Saldin, H. C. Poon, D. Sholl, J. James, and W. T. Tysoe
Surf. Sci. **602**, 2264-2270 (2008).

[5] "Direct Methods for Surface Crystallography"
D. K. Saldin and V. L. Shneerson
Invited Paper in Festschrift to honor the 65th birthday of Prof. Sir John Pendry, F. R. S.
J. Phys.: Condens. Matter **20**, 304208 (2008).

[6] "Surface Alloy Model of p(2x2)Sb/Cu(001) from LEED I/V data"
S. Higashi, H. Tochihara, V. L. Shneerson, and D. K. Saldin
Surf. Sci. **602**, 2473-2477 (2008).

Grant Number: DE-FG02-07ER46442

Title: "In Situ Characterization of the Nanoscale Catalysts during Anodic Redox Process"

PI: Renu Sharma, LeRoy Eyring Center for Solid State Science, 501 Tyler Mall, ECG 307, Arizona State University, Tempe, AZ 85287-9506.
CoPI: Peter Crozier and James Adams, School of Materials, Arizona State University.

SCOPE OF THE PROJECT:

In order to obtain basic understanding of the dynamic behavior of anode catalyst for solid oxide fuel cell (SOFC) at the nanoscale, our objective is to follow the changes in the anode's structure of and its redox properties, in situ, at atomic scale using a powerful Environmental (Scanning)Transmission Electron Microscope (E(S)TEM).[1,2,3] We employ this unique in situ technique for atomic-scale imaging, nano-diffraction and also for nanospectroscopic analysis (electron energy-loss spectroscopy) to investigate structural and compositional changes under redox conditions, and to observe changes in redox performance. Our primary objectives are:

- T***o obtain an atomic level understanding of the structure and composition of doped ceria oxides (without metal) and Co, Cu or Ni based cermet (after impregnation with metal)***

  Samples of high surface area Gd and Pr doped ceria with and without transition metal catalyst (Co, Cu or Ni particles), subjected to different redox cycles, will be analyzed using high resolution electron microscopy (HREM), nano-electron diffraction (NED) and nanospectroscopy (electron-energy-loss spectroscopy). This powerful combination of in situ methods will provide a nanoscale understanding of the structure and composition of the anode.[4]

- ***To determine the reactivity of individual nanoparticles and measure the kinetics of oxidation reactions on anode cermets.***

  We will follow the structural and chemical changes of individual particles in the anode cermet during oxidation of hydrogen and methane using in situ electron diffraction, high resolution electron microscopy (HREM) images and electron energy loss spectroscopy (EELS). Our ability to follow the evolution of individual particles will allow us to directly investigate the factors that affect the anodic reactions.[5]

- ***To establish the effect of operation conditions on structure and morphology of anode cermets.***

  In situ characterization at reaction temperatures in reducing atmospheres (H_2 and CH_4) will be used to track the evolution of individual particles, rate of coke formation and observe how structural and compositional inhomogeneities affect redox properties of the anode material.

- ***To develop theoretical models to assist us in understanding and improving nanoscale catalysis on anode cermets.***

We will compare our measurements with theoretical calculations of the cermet, including calculations of the electronic structure, surface energy, oxygen vacancy formation in ceria (including the effect of Gd and Pr dopants), and EELS spectra.

Altogether, this work will provide a detailed understanding of the fundamental science of nanoscale catalysis occurring at the anode. Such knowledge can be used to improve the composition and structure of anode cermet for better performance.

RECENT PROGRESS:

Spray Drying System for nano-particle synthesis

We have designed and built a system for synthesizing mixed oxides and cermets by spray-drying method (Figure1). This technique is expected to provide a better control on the size of nano particles.The spray drying system consists of a glass vessel, with several alternative inlet positions for salt solution sprayer, inlet for hot air at controlled temperature and pressure, and removable sample collector. We will monitor the effect air flow-rate, temperature, concentration of solution, position of air brush on the particle size. A combination of these factors should result in optimizing conditions for nanoparticles size control.

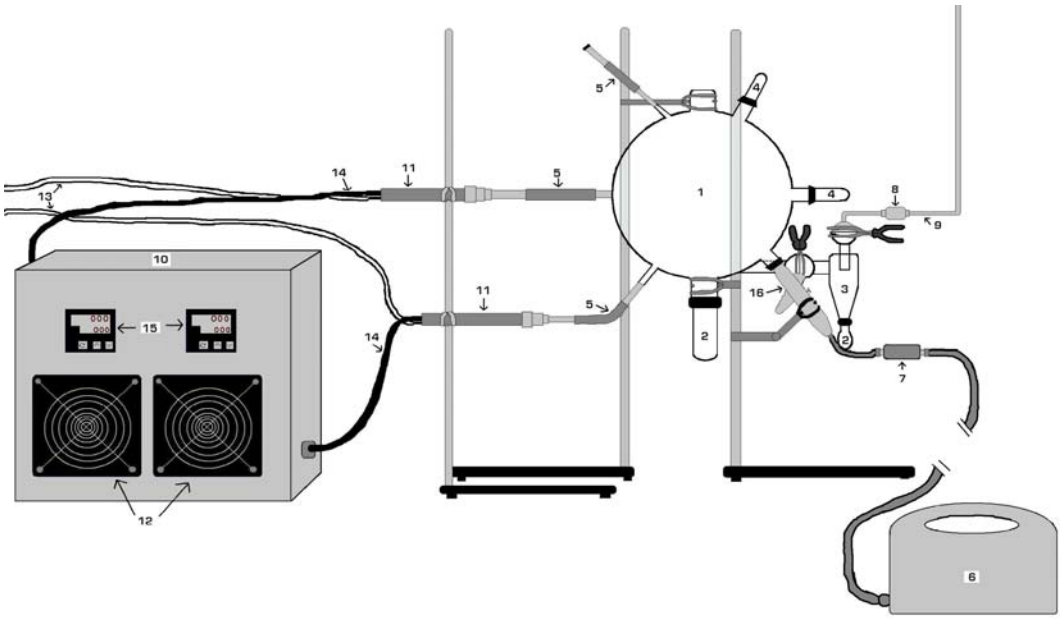

Spray Drying System Key

1. Spray drying chamber	*2. Sample collection container*
3. Vortex	*4. End caps for alternate air brush ports*
5. Heat gun ports	*6. Air compressor*
7. Moisture trap	*8. Exhaust filter*
9. Exhaust line	*10. Electrical component box*
11. Heat gun	*12. Cooling fan for heat gun power controller*
13. Compressed air line	*14. Connections to heat gun*
15. Digital temperature controller	*16. Air brush – (spraying system)*

Figure1

Ex-situ Characterization:

During the first year, we have characterized two samples; $Ce(Gd)O_2$ support (A) and with 1% Co catalyst particles (B) synthesized by precipitation method provided by Dr. Kang (collaborator from China) and compared with ceria powder. X-ray diffraction data confirm the samples to have fluorite structure, with average particle size 6 and 10 nm, an average lattice strain of 0.27% and 0.07% for sample A and B respectively. This is quite low compared to ceria-zirconia sample (0.78%) with compositional heterogeneity. Nano-characterization of individual particles, using and EELS, has also established that the samples are compositionally homogeneous as measured from the background subtracted Ce/Gd ionization intensity ratios as expected from samples with low strain.[4] The particle size, as measured from HREM images (Figure 2) also is in agreement with the X-ray data.

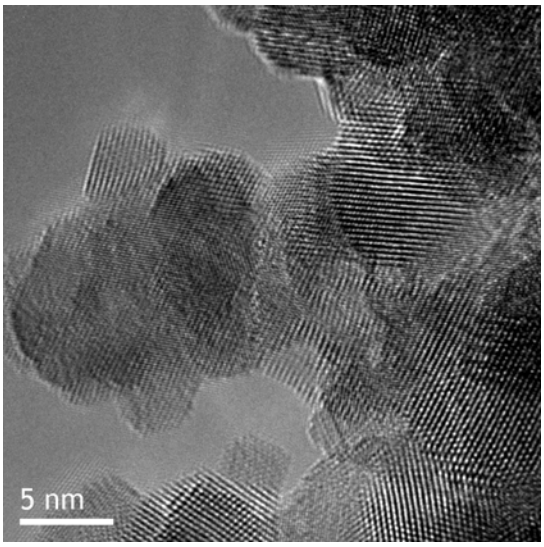

Figure2*. High resolution image from $(CeGd)O_2$ sample showing 3-7 nm particles with fluorite structure.*

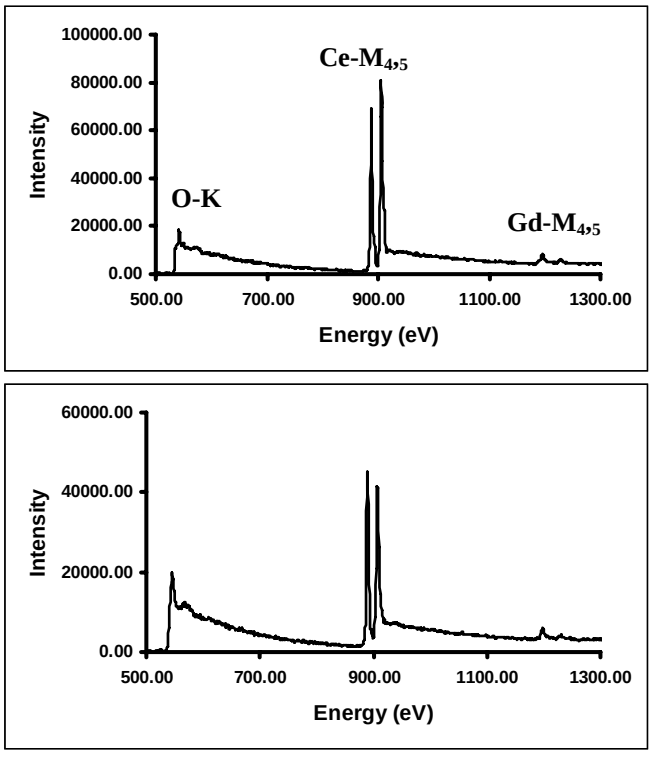

Figure 3*. Electron energy loss spectra recorded from a particle in the $Ce(Gd)O_2$ sample with 1% Co loading at (a) room temperature and (b) 700°C in 1 Torr of dry hydrogen. Note the reversal in the relative intensities of Ce M_4 and Ce M_5 peaks.*

Thermogravimetric analysis (TGA) showed that both samples have similar reducibility with reduction temperature around 650°C.

In-situ Redox behavior of individual particles:

We have also used environmental transmission electron microscopy (ESTEM) to follow the reducibility of individual particles from room temperature up to 700°C under 1.5 Torr of dry H_2. HREM images show that particle size of as prepared sample A varied between 5-20 nm, in agreements with XRD data. Electron energy-loss spectra (EELS) were collected at different temperatures in 1 Torr of dry hydrogen. Cerium in both the support oxide and one with 1% Co loading was observed to reduce between 640-700°C as indicated by the reversal of $M_{4,5}$ peak Figure 2a shows a typical spectra collected at room temperature from a particle from the $Ce(Gd)O_2$ sample with 1% loading of Co. While O-K and $M_{4,5}$

peaks (white-lines) from both Ce and Gd are clearly present, Co-$L_{2,3}$ peaks are missing. It appears that the low loading amount for Co is below the detection limit for EELS therefore we checked the samples with EDX and found that we do have Co in the samples. Our preliminary data is not conclusive enough to pin point the exact location of Co. Intensity ratios of Ce white lines, obtained after background subtraction, were used to obtain the change in Ce oxidation state with temperature. Although Gd doped oxide reduced at lower temperature (650º C) compared to pure ceria (750º C), our preliminary results do not show any appreciable change in the reducibility of Ce with or without metal loading. It is possible that the loading is too low or Co is not a good catalyst for Ce reduction.

Prof. Herbert Schroeder (Julich, Germany) visited us to finalize the design of an in situ biasing holder capable of simultaneously heating the sample up to 800ºC. We plan to use this holder (time permitting) for in situ measurement of SOFC functioning in the 3rd year of the project.

Future Plans:

1. Synthesize and characterize other compositions of Gd and Pr doped samples using spray dry technique and find the most suitable sample for low temperature reduction.
2. Continue to characterize samples prepared by precipitation technique (Dr. Kang) and compare with our samples especially using STEM imaging to locate Co particles.
3. Vaneet Sharma will continue in-situ characterization of anode catalysts under reaction conditions
4. Katie Eberhard will start working on the synthesis and bulk characterization of Pr doped Ce as her Master's project.
5. We will employ another Ph.D student starting from the Spring Semester.
6. A post doc., Dr. Dholabhai has started working with us from September 1, 2008. He will use density functional methods to investigate the structure and properties of doped ceria. Initially the focus will be on oxygen vacancy formation energies as a function of structure and composition.

REFERENCES

1. Gai, P. L., Environmental high resolution electron microscopy of gas-catalyst reactions. *Topics in Catalysis* **1999** 8, 97-113.
2. Sharma, R., Crozier, Peter A., Environmental Transmission Electron Microscopy in Nanotechnology. In *Transmission Electron microscopy for nanotechnology*, Wang, N. Y. Z. L., Ed. Springer-Verlag and Tsinghua University Press: 2005; pp 531-565.
3. Sharma, R., An environmental transmission electron microscope for in situ synthesis and characterization of nanomaterials. *Journal of Materials Research* **2005,** 20, (7), 1695-1707.
4. Wang, R., Crozier, Peter A., Sharma, Renu, and Adams, James B., Nanoscale heterogeneity in ceria zirconia with low temperature redox properties. *Journal of Physical Chemistry* **2006,** B110, (37), 18278-18285.
5. Wang, R., Crozier, Peter A., Sharma, Renu, and Adams, James B., Measuring the Redox Activity of Individual Catalytic Nanoparticles in Cerium-Based Oxides. *Nano Letters* **2008,** 8, (3), 962-967.

Atomistic Transport Mechanisms in Reversible Complex Metal Hydrides

PIs: Peter Sutter[1] (psutter@bnl.gov), James Muckerman[2], Jason Graetz[3]
Collaborators: Yves Chabal[4], C. Ciobanu[5], Eli Sutter[1]
[1]Center for Functional Nanomaterials, [2]Chemistry Department, [3]Energy Science & Technology Department, Brookhaven National Laboratory, Upton, NY 11978,
[4]Materials Science & Engineering Department, University of Texas at Dallas, Richardson, TX 75083
[5]Engineering Division, Colorado School of Mines, Golden, CO 80401

Program Scope

The development of materials for efficient hydrogen storage has been recognized as a major obstacle on the way to a hydrogen economy. Most solid-state H-storage materials, for instance, cannot be cycled reversibly between H-rich and depleted phases and exhibit slow reaction kinetics. Dopants and catalysts, nanostructuring, and finely tuned reaction environments could provide improved properties.

This research program aims to establish a scientific basis for such improvements in two interlinked thrusts: **(i)** development of a comprehensive understanding of the fundamental, atomic-scale mechanisms underlying the facile reversible H storage in titanium-doped sodium aluminum hydride ($NaAlH_4$), one of very few known complex hydrides allowing *reversible hydrogen storage with fast reaction rates.* And **ii)** Utilization of this basic knowledge for the development of new reversible H-storage materials with high storage capacity and fast reaction kinetics.

We consider the *hydrogenation reaction*, proceeding from a H-depleted phase (NaH and metallic Al) via Na_3AlH_6 to the H-rich $NaAlH_4$, as the basis for understanding reversible H storage, and in particular dopant and catalyst effects. Surface processes are expected to be of central importance. In contrast to previous research on bulk compounds with complex reaction pathways, microstructures, and unknown impurity concentrations, the present program emphasizes the use of *well-defined model systems* and of state-of-the-art surface experiments to achieve a quantitative understanding of the important reaction mechanisms. This approach is generating data accessible directly to density-functional theory (DFT) and atomistic modeling, and thus allows an unprecedented level of interaction between experiment and theory. Key questions addressed via combined experimental and theoretical efforts include:

- The mechanisms by which a Ti catalyst facilitates H_2 dissociation, a key initial step in the reaction transforming metallic Al to Al-H species and, ultimately, to a complex hydride.
- The fundamental factors determining the formation and diffusion kinetics of alanes, which we have identified as primary carriers of mass transport during hydrogenation.
- The possibility that kinetic bottlenecks in the hydrogenation reaction can be circumvented by tailoring the reaction environment, thus allowing the facile hydrogenation of previously irreversible materials.

The long-term goal of this project is to develop an atomistic understanding of the interaction of hydrogen with metal, metal alloy, and alkali metal surfaces as well as nanostructures, hence providing a scientific basis for solid-state hydrogen storage in support of the DOE BES hydrogen fuel initiative (HFI).

Recent Progress

1. Role of Ti in enabling reversible hydrogen storage in $NaAlH_4$

Following our theoretical prediction that specific atomic titanium (Ti) complexes on aluminum (Al) surfaces efficiently dissociate H_2 adsorbing from the gas phase (a crucial first step in the hydrogenation reaction),[1] and having studied the formation of such complexes by combined atom-resolved STM and density-functional theory,[2] atomic-resolution microscopy was used to establish how hydrogen interacts with Ti-doped Al surfaces.[3] These recent studies resulted in the following main findings:

- Kinetic barriers slow the dissociation of adsorbing H_2 sufficiently to make it impractical to observe H_2 dissociation near Ti at low H_2 pressures typically accessible to scanning tunneling microscopy (STM). We have thus developed an *elevated pressure STM* capability extending the operating range to at least 10 torr while maintaining impurity levels near 10^{-10} torr. This new experimental capability is now being used for atomic-resolution studies of hydrogen-metal interactions near practically relevant conditions.

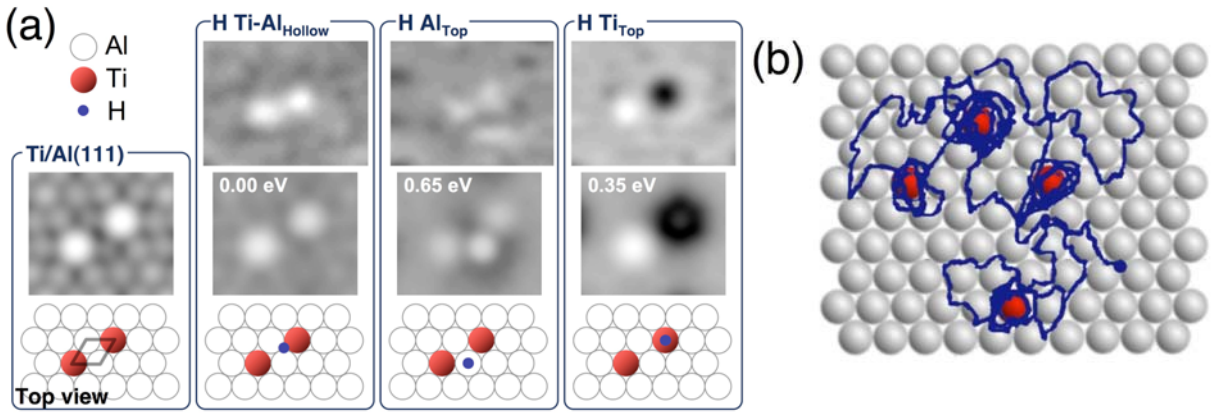

Figure 1: (a) Identification of H-binding sites by STM imaging **(top)** and DFT-based image simulation for second-nearest neighbor Ti-Ti pairs on Al(111), with and without a H-atom in different sites **(bottom)**. **(b)** Kinetic Monte Carlo simulation of H-atom diffusion near Ti/Al(111) at room temperature, showing the transient trapping of H near Ti atoms.

- Combined STM imaging and DFT were used to establish the interaction of atomic H with dispersed Ti on Al(111). Individual H atoms near surface Ti dopants were identified by STM, and followed by time-lapse STM over extended periods (fig. 1a).[3] Combined with ab-initio calculations and kinetic Monte-Carlo (KMC) simulations, these experiments have identified *specific binding sites for H atoms*, and have demonstrated that H can easily *diffuse onto all-Al surface sites*, thereby regenerating the catalytic Ti complex and allowing further H_2 dissociation.

- In an effort to develop a comprehensive theoretical understanding of H storage processes, we combined DFT with KMC simulations to use atomic-level information in determining the behavior of the system over much larger length and time scales. As a first application, we have elucidated the diffusivity of different species (H, Al, Al_xH_y) on Ti-doped Al(111). Shallow potential wells around embedded Ti atoms transiently trap H and reduce its diffusivity (fig. 1b), but not that of the other species. This effect has important consequences on hydrogenation reactions in the presence of Ti dopants: unexpectedly, Al and alane (Al-H) species diffuse much faster than H; and the rate of mobile alane formation is slowed considerably, since it involves the rather slow "harvesting" of H by diffusing Al.

2. Identification of the carriers of long-range mass transport

- STM and IR spectroscopy on Al(111) in UHV, combined with DFT, have established how H atoms interact with the Al surface to form mobile Al_xH_y (alane) species, and how these alanes interact, grow, diffuse, and desorb. STM shows a pronounced etching of Al surface steps during exposure to atomic H. Although difficult to interpret, IR spectra analyzed by comparison with DFT-prediced vibrational frequencies have unambiguously demonstrated the *formation of progressively larger alane species* with increasing H-coverage and temperature, demonstrating the high surface mobility of these species.[4]

- The assignment of alanes as a primary carrier of mass transport in the hydrogenation of alanates was confirmed by a series of targeted solid-state-chemistry experiments. Specifically, we were able to show that the hydrogenation proceeds readily *without the need for a catalyst* once alane is available.[5] This finding shows that alane formation is a critical step in the hydrogenation, and that this step is indeed enabled and accelerated by Ti doping.

3. Development of new reversible hydrogen storage materials

Experiments on bulk materials, accompanying our work on model systems in UHV, have focused on AlH_3, a very promising H storage material with 10.1 wt. % H-capacity. Little has been known about the crystallographic and thermodynamic properties of AlH_3, and these have now been established:

- The thermodynamic and vibrational properties relevant for hydrogen storage of three different polymorphs, α, β, and γ-AlH_3 have been determined.[6,7]
- High-pressure induced structural, chemical, and thermodynamic changes have been determined for α-AlH_3, using combined high-pressure synchrotron x-ray diffraction and ab-initio calculations.[8]
- The previously unknown crystal structures of β and γ-AlH_3 have been determined. For this purpose, a synthesis route for β-AlH_3 had to be established.[9,10]
- The stability and decomposition pathways of the three AlH_3 polymorphs have been determined, showing an actual release of 10 wt. % hydrogen at temperatures below 100°C.[11,12]

Our findings for both single crystal model systems and bulk materials suggest rational regeneration routes for AlH_3 and high-capacity alanates, by dissociating H_2 over Al doped with transition metals (Ti), generating molecular alane, which can then be collected and aggregated to a H-rich AlH_3 or alanate phase. Based on free energy arguments *regeneration in solution* holds the most promise. Fundamental research on the interaction of H with doped light metals (e.g., Al:Ti) in complex environments (e.g, liquids), necessary to establish the complex processes involved, have begun in FY 2008:

- We demonstrated a low energy route to regenerate $LiAlH_4$ (10.6 wt. % H) from LiH and Ti-catalyzed Al.[13] The initial hydrogenation in tetrahydrofuran (THF) forms the adduct $LiAlH_4 \cdot 4THF$. The free energy change in this reversible reaction is small and slightly negative, suggesting an equilibrium H_2 pressure of ~1 bar at 300 K. The adduct $LiAlH_4 \cdot 4THF$ was successfully desolvated at low T to yield crystalline $LiAlH_4$. Regeneration of $LiAlH_4$ from LiH and Al hence is achieved in the two-step process:

$$LiH + Al^{*} + 3/2\ H_2 \xrightarrow{THF} LiAlH_4 \cdot 4THF \xrightarrow{Vacuum} LiAlH_4 + 4THF\uparrow$$

  The possibility of using this regeneration process for other metastable hydrides (e.g., $Mg(AlH_4)_2$) is currently being investigated.

Future Plans

In future work we aim to provide a comprehensive understanding of the role of dopants and of complex reaction environments (e.g., fluids) in facilitating the hydrogenation and dehydrogenation of solid and nanostructured H storage materials. A brief summary of new research directions is given below:

1. H_2 dissociation at surface Ti complexes on Al single crystals

- Elevated-pressure STM is being used to establish how the hydrogen fuel to be stored (i.e., H_2) interacts with dopant sites on the surface of light metals, such as Al. Working closely with theory and IR spectroscopy important questions regarding the mechanism of H_2 dissociation and the formation of mobile molecular adsorbates (alanes) will be addressed.
- Impurities such as O_2 and H_2O, invariably present in practical storage materials, may fundamentally alter the interaction of hydrogen with light metals. UHV-STM and IR will be used to study their effects, in particular a possible enhancement or decrease in the activity of dopants.

2. Interaction of hydrogen with light metal nanoparticles

- Nanostructures could significantly enhance the kinetics of hydrogen storage reactions, but experiments at the atomic scale are needed to evaluate this possibility and identify the underlying mechanisms. We are preparing a study on the interaction of H with small metal and alloy nanoparticles in UHV, to understand the effects of nanoparticle size, of dopants at various concentrations, and of impurities.

3. Surface mass transport and initial hydrogenation stages

- Our previous work has shown complex H-metal interactions even for seemingly simple systems. A comprehensive model of the hydrogenation process will be invaluable to understand these interactions. By coupling DFT with KMC, we have begun to build a computational framework for different Al(hkl) surfaces. The energetics of atomic level processes, established by DFT, feed into KMC calculations on the evolution over large length and time scales. Once fully developed, this approach will serve to capture the complex processes involved in hydrogenation reactions and their modification by dopants.
- Experiments on surface mass transport during hydrogenation reactions will be carried out by STM and in-situ low-energy electron microscopy. We will probe surface diffusion on Al and Ti doped Al surfaces, with and without H or H_2 exposure, as well as the initial nucleation and growth of hydrogen-rich phases on Al in the presence of NaH and H.

4. Fundamental mechanisms of solution-phase hydrogenation of Al – Role of dopants

- AlH_3 has recently been identified as a promising H-storage material with high storage capacity (>10 wt. %) and fast dehydrogenation kinetics near ambient temperature. The key bottleneck to the widespread use of AlH_3, as well as of high-capacity complex hydrides that cannot be cycled reversibly in H_2 gas, is the lack of a viable regeneration route following its decomposition to H_2 and Al metal. Regeneration in solution appears promising. Yet it remains unknown how Al and doped Al interact with H_2 dissolved in a solvent such as tetrahydrofuran (THF). We are preparing to use powerful in-situ spectroscopy experiments (Raman and infrared) in a microfluidic setup to study the reaction of H_2 on immersed Al (and Al-Ti) surfaces and the resulting formation of H-rich species (e.g., alanes) in solution. This work connects strongly with our studies on Ti catalyzed model systems in UHV, and will establish hydrogen-metal interactions and their modification by dopants in complex environments, such as the liquid-solid interface.

References (2006 – 2008)

1. S. Chaudhuri and J.T. Muckerman, J. Phys. Chem. B **109**, 6952 (2005).
2. E. Muller, E. Sutter, P. Zahl, C.V. Ciobanu, and P. Sutter, Appl. Phys. Lett. **90**, 151917 (2007).
3. E. Muller, T. Davies, A. Karim, P. Zahl, J.T. Muckerman, C.V. Ciobanu, and P. Sutter, submitted.
4. S. Chaudhuri, S. Rangan, J.-F. Veyan, J.T. Muckerman, and Y.J. Chabal, J. Am. Chem. Soc. **130**, 10576 (2008).
5. S. Chaudhuri, J. Graetz, A. Ignatov, J.J. Reilly, and J.T. Muckerman, J. Am. Chem. Soc. **128**, 11404 (2006).
6. J. Graetz and J.J. Reilly, J. Alloys Comp. **424**, 262 (2006).
7. M. Tkacz, T. Palasyuk, J. Graetz, and S. Saxena, J. Raman Spectr. **39**, 922 (2008).
8. J. Graetz, S. Chaudhuri, Y. Lee, T. Vogt, J.T. Muckerman, and J.J. Reilly, Phys. Rev. B **74**, 214114 (2006).
9. H.W. Brinks, C. Brown, C.M. Jensen, J. Graetz, J.J. Reilly, and B.C. Hauback, J. Alloys Comp. **441**, 364 (2007).
10. H.W. Brinks, W. Langley, C.M. Jensen, J. Graetz, J.J. Reilly, and B.C. Hauback, J. Alloys Comp. **433**, 180 (2007).
11. J. Graetz, J.J. Reilly, J.G. Kulleck, and R.C. Bowman, J. Alloys Comp. **446-447**, 271 (2007).
12. S.-H. Hwang, R.C. Bowman, J. Graetz, J.J. Reilly, W. Langley, and C.M. Jensen, J. Alloys Comp. **446-447**, 290 (2007).
13. J. Graetz, Chem. Soc. Rev. (invited article), in press (2008).
14. S. Chaudhuri and J.T. Muckerman, "Catalytic activity of Ti-doped NaH nanoclusters towards hydrogenation of terminal alkenes," Molecular Simulation **33**, 919 (2007).

Atomic--Scale Chemical, Physical and Electronic Properties of the Subsurface Hydride of Palladium

Paul S. Weiss, Principal Investigator

Departments of Chemistry and Physics, 104 Davey Laboratory, The Pennsylvania State University, University Park, PA 16802-6300
Email: stm@psu.edu; Web: www.nano.psu.edu

Overall research goals: We will elucidate the chemical, physical and electronic properties of the subsurface hydride of Pd, the key material and reactant, hypothesized to be critical both to hydrogenation reactions and metal embrittlement, and a model for hydrogen storage. We are able to create this species for direct measurement and for use as a chemical reagent. We will utilize our unique ultrastable scanning tunneling microscopes (STMs) for these studies. With insight gained from these STM measurements, we will develop more general methods for the preparation and study of this reagent. We will also determine how far such atomic manipulation techniques can be extended.

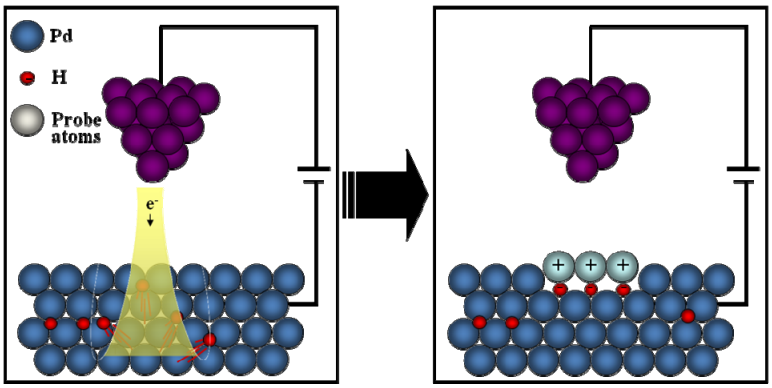

Inelastic scattering of ballistic electrons injected into Pd mobilizes "illuminated" H atoms in the bulk. When any of these atoms reach the stable subsurface site, they remain trapped there and perturb the surface physical and electronic structure. They are hypothesized to be the reactive species in hydrogenation reactions.

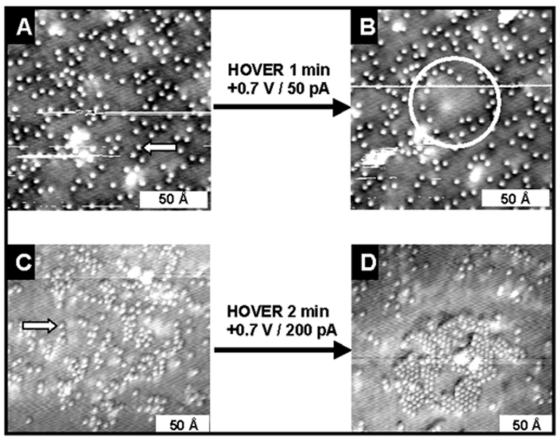

(A and B) STM images demonstrating hydrogen (protrusions under these conditions) segregation from the area over which the tip hovered (circle) (150 Å × 150 Å, V_{sample} = +0.070 V, I_t = 50 pA). (C and D) STM images depicting hydrogen overlayer vacancy (protrusions under these conditions) aggregation in the area over which the tip was hovered (200 Å × 200 Å, V_{sample} = +0.050 V, I_t = 100 pA).

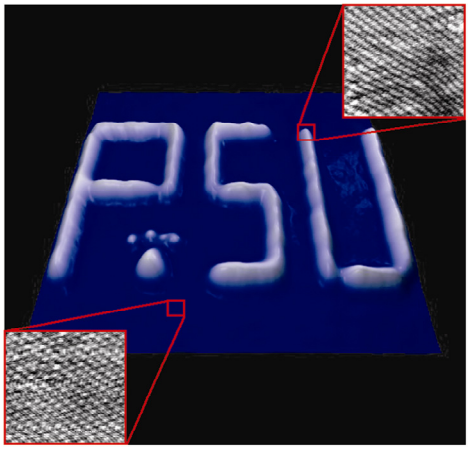

STM image of the Pd{111} surface with an arbitrary pattern written in subsurface hydride. The upper right inset shows the lattice distortion due to the subsurface hydride. The lower left inset shows the unperturbed lattice.

Significant achievements to date: This project began August 2008.

Science objectives for 2008-2009:

- Measure the electronic structural perturbation of subsurface hydride on the Pd{111} surface.
- Measure the effects of the subsurface hydride on the Pd lattice.
- Measure the effects of the subsurface hydride on surface adsorbates.

DE-FG02-07ER46446: MULTISCALE ATOMISTIC SIMULATION OF METAL-OXYGEN SURFACE INTERACTIONS: METHODOLOGICAL DEVELOPMENT, THEORETICAL INVESTIGATION, AND CORRELATION WITH EXPERIMENT

PI: Judith Yang, Department of Mechanical Engineering and Materials Science, University of Pittsburgh (UPitt), Pittsburgh PA, jyang@engr.pitt.edu

Co-PIs: Alan McGaughey, Department of Mechanical Engineering, Carnegie Mellon University (CMU), Pittsburgh PA, mcgaughey@cmu.edu

Simon Phillpot, Department of Materials Science and Engineering, University of Florida, Gainesville FL, sphil@mse.ufl.edu.

Susan Sinnott, Department of Materials Science and Engineering, University of Florida (UF), Gainesville FL, ssinn@mse.ufl.edu

PROGRAM SCOPE

Our long-term vision is the comprehensive and fundamental understanding of a critical gas-surface reaction, nano-oxidation— from the adsorption of oxygen atoms on the metal surface to the coalescence of the bulk oxide—via coordinated multi-scale theoretical and *in situ* experimental efforts. Reaching this goal necessitates close collaborations between theorists and experimentalists. The purpose of this specific DOE program is the development of new theoretical and computational tools that can be used to model nano-oxidation, and the correlation of these predictions with our abundant experimental observations acquired by a unique *in situ* ultra-high vacuum transmission electron microscope (UHV-TEM).

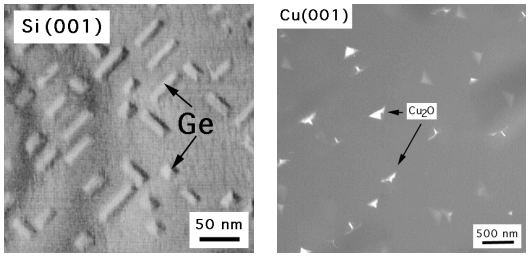

Figure 1: Comparison of Ge on Si heteroepitaxy and Cu_2O nucleation on Cu(001).

The PI has previously shown that heteroepitaxial concepts describe the nucleation and growth to coalescence of Cu_2O islands on Cu(001) surprisingly well (Fig. 1). Models of heteroepitaxial growth, where nucleation rate theory is a standard model used to describe the atomistic processes, have been developed and used successfully to describe metal-on-metal heteroepitaxy. However, these models have not yet been developed to include gas-surface reactions. ***The objective of this program is to further develop heteroepitaxial theories for application to oxidation using a multiscale theoretical approach, and thus allow the direct quantification of the associated experimental observations and lead to a fundamental understanding of nanoscale oxygen gas – metal surface reactions.***

To achieve this goal, we are (i) developing a kinetic Monte Carlo (KMC) approach, called Thin Film oxidation (TFOx), to simulate the atomistics of transport, nucleation and growth of metal oxides during the oxidation process, and (ii) determining realistic input parameters for TFOx through coordinated electronic structure and molecular dynamics. The TFOx development is the primary responsibility of the PI. The electronic-structure calculations and atomic-level simulations are the prime responsibilities of the CMU and UF co-PIs. This is a multi-scale approach, where molecular dynamics (MD) and electronic structure (ES) calculations will be used to determine the parameters used in TFOx, and then TFOx will be compared to experiments in order to validate and challenge each method. Our specific goals include gaining fundamental and quantitative insights into the nucleation behavior, morphological evolution of oxide islands during nano-oxidation and coalescence, and provide the surface and interface energies required to

augment the available theoretical treatment of island stability. Each of these aspects has not been demonstrated before for gas-surface reactions and, hence, each represents a potential ground-breaking fundamental science in surfaces and interfaces.

RECENT PROGRESS

Development and Optimization of KMC Code: We have developed a Kinetic Monte Carlo (KMC) code to simulate the complexities of oxygen interactions with a metal surface in 2-D called Thin Film Oxidation (TFOx), and presently converted it to TFOx-3D (www.tfox.org). TFOx-2D presently simulates the general behavior of irreversible 2-dimensional nucleation and growth of epitaxial islands on a square or rectangular lattice. The TFOx model explicitly considers a very large range of elementary steps, including deposition, adsorption, dissociation of gas molecules (such as O_2), surface diffusion, aggregation, desorption and substrate-mediated indirect interactions between static adatoms. Through a detailed systematic exploration of affect of various physical parameters, we have already shown that TFOx-2D is capable of displaying a wide variety of thin film oxidation processes, leading to a large number of morphologies, many of which have been observed experimentally. Recently, TFOx-2D has undergone a massive overhaul. Now consisting of separate console (C++) and GUI (Python) applications, TFOx has seen two orders of magnitude in speed increase. In addition to this, parameterized testing, parallel execution, and initial 3D simulation capabilities have been added to its repertoire.

Prediction of Adsorption Energies and Energy Barriers from ES Calculations: Our initial electronic structure calculations have focused on the interaction of a single oxygen molecule/atom with a bare and reconstructed Cu (100) surfaces. The bare system has previously been studied [1], allowing us to validate our computational procedures. The VASP software package is used.

Single point energy calculations for the adsorption energy of an oxygen atom or molecule at the FCC and bridge sites on the copper surface are provided in Table 1 as an example of the calculations we have performed. These results are in reasonable agreement with those of Alatalo et al [1], with small differences attributable to the size of the calculation domain and the relaxation procedures. To predict diffusion energy barriers, we apply the nudged elastic band method, where the minimum energy pathway between an initial condition and a final condition is determined. Results are provided in Table 1 for the movement of a single copper or oxygen atom on the bare copper surface.

Table 1: Predicted adsorption energies and energy barriers from electronic structure calculations.

Molecule/Site	Adsorption Energy, eV	Atomic Move	Energy Barrier, eV
O2@FCC	**-1.858**	**O(FCC) → O(FCC)**	**1.044**
O@FCC	**-6.634**	**Cu(FCC) →Cu(FCC)**	**0.522**
O@Bridge	**-5.884**		

Current work is focused on exploring the energy barrier for an oxygen atom penetrating a copper surface as a function of the surface oxygen coverage and reconstruction configuration.

Examination of aluminum-oxygen charge transfer potentials: Successful simulation of a metal-oxide system requires a method that is 'smart' enough that it can autonomously distinguish between a metal ion in the metallic state and one in an ionic oxide phase. This requires, at a minimum, that the charges on the metal and oxygen ions be determined in a self-consistent and physically reasonable manner. Furthermore, the goal of accurately modeling a range of oxides requires a highly transferable potential that can accurately model the oxygen anion in various bond and coordination environments. To prepare for generating a copper-oxygen charge transfer potential, which does not currently exist in the literature, we have explored the previous work on

aluminum-oxygen systems. We found that while these potentials do a reasonable job for bulk phases, they perform poorly for systems containing metal/oxide interfaces.

Earlier variable charge potentials have proven to be an efficient form to simulate bulk alumina [4]. However, we have found that in simulations of interfaces, where the constraints of charge conservation and stoichiometry are removed, the oxide invariably evolves to the high symmetry closed packed rocksalt structure. Zhou et al. [5] modified the potential of Streitz and Mintmire to better control the charges. We find that their potential, however, also fails in the modeling of interfaces, as shown in Fig. 2. While the alumina phase remains stable, we find that the metal phase becomes disordered at temperatures above 150 K.

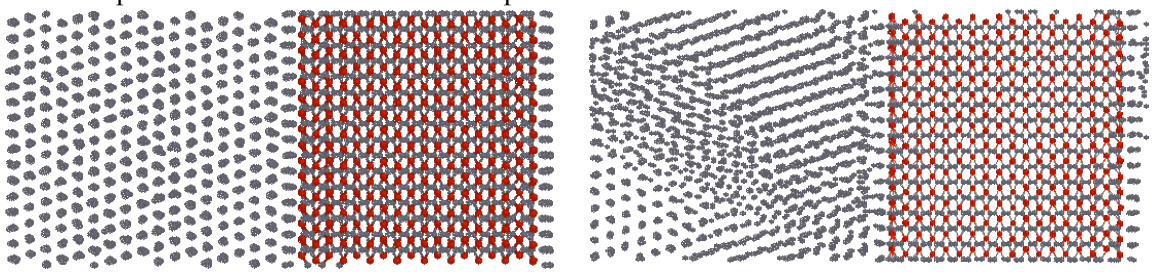

Figure 2: Aluminum/alumina interface at temperatures of (a) 150 K and (b) 175 K based on molecular dynamics simulations using the charge transfer potential of Zhou et al. [5]. Note that the metal phase becomes disordered at the higher temperature, indicating that this potential is not suitable for modeling interfaces.

Based on these results, we believe that the Charge Optimized Many-Body (COMB) potential that we have developed to model silicon/silica interfaces, will be a more suitable choice for copper and copper oxide. Substantial progress has been made in the development of this potential, and is described in the next section.

Development of copper-oxygen charge transfer potential: The fitting of a COMB potential for the copper-oxygen system proceeds in two steps. First, the parameters for bulk copper are specified. Then, the more complicated oxide phase is considered. Our COMB potential for Cu predicts the lattice parameter, the cohesive energy, and the bulk modulus, with high accuracy. The elastic constants, C_{11} and C_{12}, not included in the fitting data, are very well reproduced. The C_{44} elastic constant, however, is substantially lower than the experimental value; this should be considered as a weakness of the current potential. The (100), (110), and (111) surface energies are also well predicted. Additionally, at room temperature, the tCOMB potential predicts the thermal expansion being $14 \times 10^{-6}\,K^{-1}$, which compares well to the experimental value of $16.5 \times 10^{-6}\,K^{-1}$. We have expanded this COMB potential for copper to include copper oxide. We have a first generation potential that demonstrates that the structure and basic properties of this material, which have not been previously well described at the atomic level, can be well described within the COMB framework. This potential is currently undergoing refinement to bring the predicted properties in better agreement with the experimental and DFT results.

Reference

1. Alatalo, M.; Jaatinen, S.; Salo, P.; Laasonen, K. *Phys. Rev. B*. **70**, 245417 (2004).
2. Zhang, Q.; Cagin, T.; van Duin, A.; Goodard, W.A.; Qi, Y.; Hector, L.G.; *Phys. Rev. B* 69, 045423 (2004).
3. Jahn, S.; Madden, P.A.; Wilson, M.; *Phys. Rev. B* 74, 024112 (2006)
4. Streitz, F; Mintmire, J.M.; *Phys. Rev. B* 50, 11996 (1994)
5. Zhou, X. W.; Wadley, H. N. G. *J. Phys.: Cond. Matt*. 17, 3619 (2005).
6. Yu, J.-G.; Sinnott, S.B.; Phillpot, S. R.; *Phys. Rev. Lett*. **In review**.
7. Beg, M. M.; Shapiro, S. M.; *Phys. Rev. B* 13, 1728 (1976)
8. Ruiz, E.; Alvarez, S.; Alemany, P.; Evarestov, R.; *Phys. Rev. B* 56, 12 7188 (1997)

9. Soon, A.; Todorova, M.; Delley, B.; Stampfl, C.; *Phys. Rev. B* 75, 125420 (2007)
10. Soon, A.; Sohnel, T.; Idriss, H.; *Sur. Sci.* 579, 131 (2005)

FUTURE PLANS

Bridging the gap between simulations and experiment is one primary target. The optimization of TFOx-2D led to 100x faster simulations on a PC, and TFOx-2D can now run on computer clusters. The purchase and attachment of a fast CCD camera to the *in situ* UHV-TEM provides a temporal resolution of <1 second. TFOx-2D has made a qualitative leap to TFOx-3D in order to simulate nucleation and growth in 3-dimensions, i.e. into the substrate, and not just laterally on the surface, since cross-sectional TEM images of the Cu_2O/Cu interface revealed that Cu_2O primarily grows into the Cu film. A second key component of this DOE program is the determination of real input parameters in TFOx-3D for copper-oxygen systems. This task will be accomplished by performing electronic structure calculations and molecular dynamics simulations of Cu-O systems. The TFOx-3D predictions, utilizing the input parameters obtained via first principles and molecular dynamics will then be directly correlated with *in situ* transmission electron microscopy (TEM) experiments.

Specifically, our future goals include:

- Complete work on polarizable aluminum-oxygen charge transfer potential, prepare and submit publications.
- Electronic structure calculations of the interaction of oxygen molecules/atoms with reconstructed copper (100) surfaces. Dissociation energies and energy barriers will be calculated and fed into the development of the COMB copper-oxygen potential.
- Complete the refinement the Cu_2O COMB potential to better reproduce properties such as elastic constants, surface energies, stacking fault energies, defect formation energies and thermal expansion coefficients. A portion of the fitting/testing input will be provided from electronic structure calculations.
- Carry out MD simulations of the oxidation of copper and aluminum surfaces to validate the interatomic potentials and input (and a comparison point) for the KMC simulations.
- Compare the simulation results for the oxidation of copper and aluminum to better understand the mechanisms responsible for their differing oxidative behaviors.
- Parallelize the TFOx program and modify it to allow for the handling of three-dimensional systems and reaction.
- Begin TFOx simulations to compare with experiments.

PUBLICATIONS

- X. Han, R. McAfee, Judith C. Yang, "Development of a Versatile Kinetic Monte Carlo Code to Simulate Physical Processes in Thin Film Nucleation and Growth", *Multidiscipline Modeling in Materials and Structures* 3 (2007) 43-54.
- X. Han, R. McAfee, J. C. Yang, "Kinetic Monte Carlo Simulations of the Dramatic Effects of Attachment Probability and Potential Gradients on Island Morphology Variations under Heteroepitaxial Growth Conditions", *J. Computational and Theoretical Nanoscience* 4 (2007) 1-12.
- J. Yu, S.B. Sinnott, and S.R. Phillpot, "Optimized Many Body Potential for fcc Metals," *Physical Review Letters* (in review)
- B. Devine, A. J. H. McGaughey, M. Lee, S.B. Sinnott, S.R. Phillpot, "Adaptation of Dynamic Charge Potentials in Massively Parallel Molecular Dynamics Simulations", *Journal of Physics. Condensed Matter* (in preparation).

Research Summaries V:

Structure Determination

Program title: Development of Microcharacterization Tools for Soft Matter based on Advanced Electron Microscopy

Principal Investigators: Nitash Balsara (nbalsara@lbl.gov), Kenneth Downing (khdowning@lbl.gov), Jay Groves (jtgroves@lbl.gov), Christian Kisielowski (cfkisielowski@lbl.gov), Andrew Minor (aminor@lbl.gov),

Program Scope

Our objective is to refine and use new electron scattering and microscopy techniques to investigate structure, composition and transport properties of soft matter. We focus on three-dimensional characterization of systems ranging from molecularly thin membranes formed by phospholipids to 50 μm thick synthetic polymer membranes used in fuel cells. The microscopy techniques focus on maximizing spatial and energetic resolution while minimizing radiation exposure and damage.

Recent Progress

Nanostructured fuel cell membranes which get wetter as the temperature of the surrounding air gets hotter at constant relative humidity were synthesized using block copolymer self-assembly. Transmission electron microscopy (TEM) of hydrated block copolymer membranes without heavy ion doping was used to establish nanoscale morphology. This enabled determination of the relationship between water retention and morphology. The orientation of the hydrated channels in contact with humid air was determined by TEM of samples prepared by the shadow focused ion beam technique. Energy-filtered TEM was used to image lithium ions in nanostructured block copolymer electrolytes.

Using two levels electron beam lithography, vapor phase deposition techniques and FIB etching, we have fabricated an electrostatic phase plate for phase contrast imaging of weak phase objects. The dimensions of this phase plate are suitable for the imaging of large biologic samples without affect the high resolution imaging of hard materials. This micro-device has been inserted into the Zeiss Libra EFTEM and its position in the back focal plan of the objective lens is controlled with a piezo-driven manipulator. A quantitative study of the phase shift induced by the phase plate has been realized by analyzing the influence of the electrode potential on the power spectra of the images.

Procedures for visualizing, in three dimensions, how lipid vesicle shape can be altered by proteins have been developed. Cryo-electron tomography was used to investigate model systems that incorporate peptides into vesicles of specific composition.

We have successfully designed and built a custom in situ electrical biasing holder for the Zeiss Libra TEM. This holder will enable in situ electrical biasing of polymers under energy filtered imaging conditions. Our goal is to directly image charge transport in polymer membranes in order to better understand the influence of polymer microstructure on ion conductivity.

Future Plans:
We will continue to study the systems that were initiated during the first year of the program. This includes studying polymer electrolytes for fuel cells and batteries, development of a robust electrostatic phase plate for electron microscopy, measuring the distortion of vesicles by proteins, and the development of *in situ* probes for studying ion motion by electron microscopy.

Publications
1. "Control of Domain Orientation in Block Copolymer Electrolyte Membranes at the Interface with Humid Air", M.J. Park, S. Kim, A.M. Minor, A. Hexemer, N.P. Balsara, *Advanced Materials*, accepted, **2008**.

2. "Phase Behavior of Symmetric Sulfonated Block Copolymers", M.J. Park, N.P. Balsara, *Macromolecules*, vol. 41, pg. 3678-3687, **2008**.

3. "Humidity-Induced Phase Transitions in Ion-Containing Block Copolymer Membranes", M.J. Park, A.J. Nedoma, P.L. Geissler, A. Jackson, D. Cookson, *Macromolecules*, vol. 41, pg. 2271-2277, **2008**.

4. "Interfacial Concentration Profiles of Rubbery Polyolefin Lamellae Determined by Quantitative Electron Microscopy", E.D. Gomez, M.L. Ruegg, A.M. Minor, C. Kisielowski, K.H. Downing, R.M. Glaeser, N.P. Balsara, *Macromolecules*, vol. 41, p. 156-162, **2008**.

5. "Increased Water Retention in Polymer Electrolyte Membranes at Elevated Temperatures Assisted by Capillary Condensation", M.J. Park, K.H. Downing, A. Jackson, E.D. Gomez, A.M. Minor, D. Cookson, A.Z. Weber, N.P. Balsara, *Nano Letters*, vol. 7, pg. 3547-3552, **2007**. Web coverage: science@ berkeley lab, December 12, 2007; fuelcellworks.com, Jan 13, 2008; greentechnologyforum.net, February 17, 2008; fuelcelltoday.com, February 14, 2008.

Program Title: Electron and Scanned Probe Microscopy of sp^2-bonded Nanostructures

PI's:
Alex Zettl, Materials Sciences Division, Lawrence Berkeley National Laboratory, Berkeley, California 94720, azettl@berkeley.edu, and

Michael F. Crommie, Materials Sciences Division, Lawrence Berkeley National Laboratory, Berkeley, California 94720, crommie@berkeley.edu

Program Scope: To understand and control the electronic, magnetic, and mechanical properties of novel sp^2-bonded nanostructures, including fullerenes, nanotubes, and graphitic layers.

Recent Progress: Here we describe our recent progress at performing microscopy on graphene. Graphene is a covalently bonded network of carbon only one atom thick which has very exciting technological potential due to its unique magneto-electronic and mechanical properties, as well as its great tunability. While the intrinsic nanoscale nature of graphene holds great promise, it also poses great challenges. One of the greatest challenges comes from the fact that in order to efficiently exploit the properties of graphene we must understand and control its behavior at the nanometer and even subnanometer scale.

Electron and scanned probe microscopies are ideally suited for exploring the properties of graphene. Here we describe our progress at using two powerful microscopies for this purpose: transmission electron microscopy (TEM) and scanning tunneling microscopy (STM). These microscopy techniques are complementary in that they can provide different information regarding nanoscale processes that occur in a material such as graphene. TEM, for example, can provide fast, dynamical information on structural processes that occur in real-time at the atomic scale in suspended graphene films. STM, on the other hand, is useful for its highly resolved spectroscopic capabilities that can be performed at the atomic scale on graphene films attached to substrates and in a back-gate geometry. We have exploited all of these capabilities to explore the nanoscale physics of graphene films and devices.

Using TEM we have demonstrated a means to observe even the smallest atoms and molecules on a clean single-layer graphene membrane, including adsorbates such as atomic hydrogen and carbon.[1] We have directly imaged individual adatoms, along with carbon chains and vacancies, and investigated their dynamics in real time.[1] Our new sensitivity-enhancing techniques open a way to reveal dynamics of more complex chemical reactions or identification of atomic-scale structure of unknown adsorbates. We have made significant progress by using a state-of-the-art transmission electron aberration-corrected microscope (TEAM) at the National Center for Electron Microscopy at Lawrence Berkeley National Laboratory. This has allowed us to achieve one-Ångstrom resolution at an acceleration voltage of only 80 kV.[2] As a result, every individual carbon atom in our graphene samples is detected and resolved (see figure 1). We have clearly observed the graphene crystalline lattice, point defects, and the formation and annealing of Stone-Wales defects.[2] We also observe that multiple five- and seven-membered rings exclusively appear in combinations that avoid dislocations and disclinations, in contrast to

previous observations on highly curved (tube- or fullerene-like) graphene surfaces.

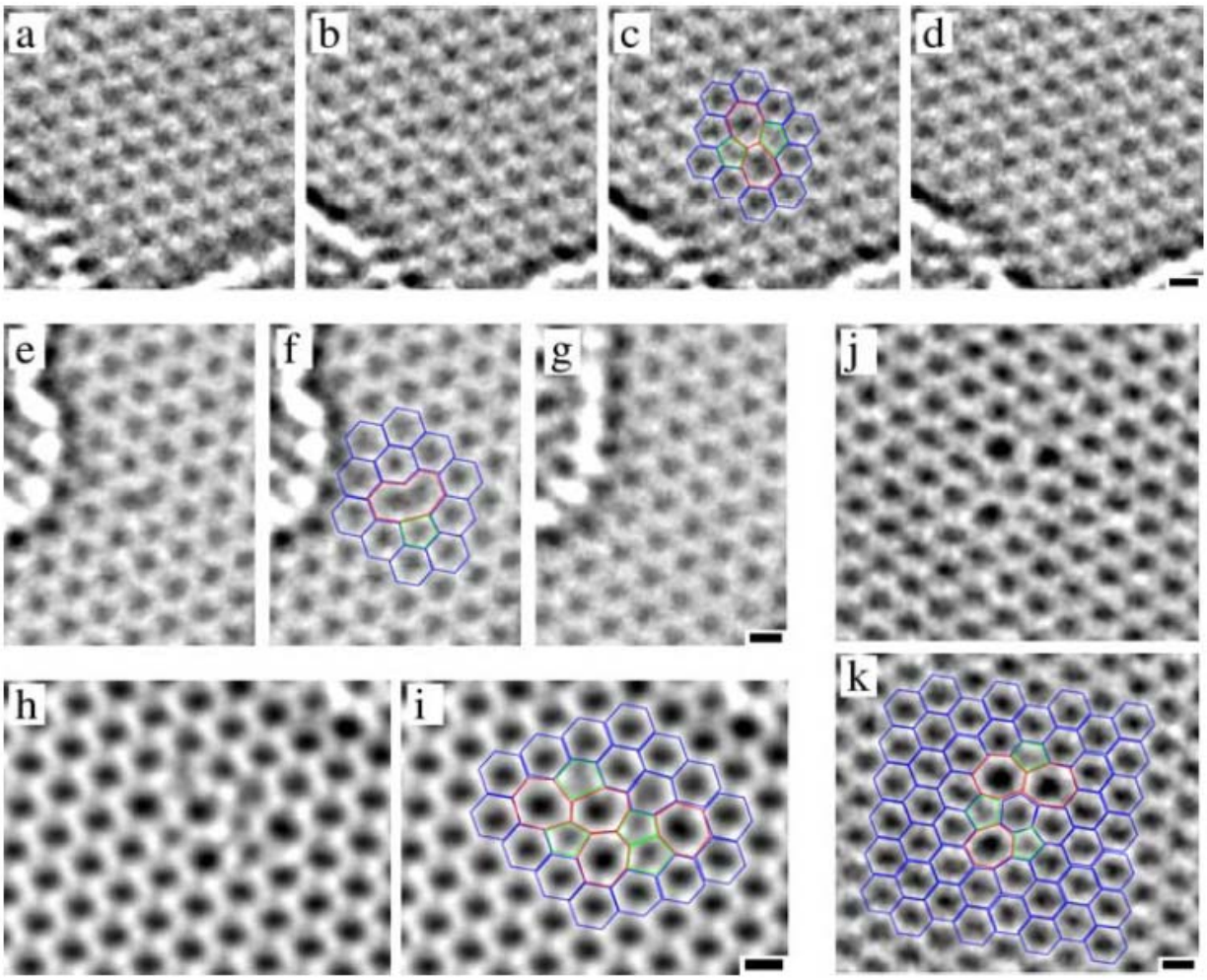

Fig. 1: Metastable defects found in HRTEM image sequences. (a-d) Stone-Wales (SW) defect: (a) unperturbed lattice before appearance of the defect, (b) SW defect (c) same image with atomic configuration superimposed, (d) relaxation to unperturbed lattice (after ca. 4s). (e-g) Reconstructed vacancy: (e) original image and (f) with atomic configuration; a pentagon is indicated in green. (g) Unperturbed lattice, 4s later. (h,i) Defect image and configuration consisting of four pentagons (green) and heptagons (red). Note the two adjacent pentagons. (j,k) Defect image and configuration consisting of three pentagons (green) and three heptagons (red). This defect returned to the unperturbed lattice after 8s. In spite of the odd number of 5-7 pairs, this is not a dislocation core (it is compensated by the rotated hexagon near the center of the structure). All scale bars are 2 Å. (From ref. [2]).

Using STM techniques we have performed atomically-resolved scanning tunneling spectroscopy measurements of graphene flake devices having tunable back-gates (figure 2). We find that the tunneling spectra of graphene displays an unexpected gap-like feature that is pinned to the Fermi level for different gate voltages.[3] This feature coexists with an additional depression in the graphene density-of-states (DOS) that shifts energetically with gate voltage. Our analysis reveals that the pinned gap-feature is due to phonon-assisted inelastic tunneling, while the DOS depression directly marks the location of the graphene Dirac point.[3] Our ability

to locally probe the energetic location of the Dirac point via STM spectroscopy has allowed us to spatially map out electron density inhomogeneities in graphene with a resolution that is two orders of magnitude higher than previous experiments. In this way we have measured graphene charge inhomogeneities that coexist with energy-dependent electronic interference patterns, and which can be directly correlated with nanometer-scale topographic features, thus revealing new impurity scattering behavior for Dirac fermions in graphene. These results are significant for understanding the sources of electron density inhomogeneity and scattering in graphene, as well as the microscopic mechanisms that determine graphene electron mobility.

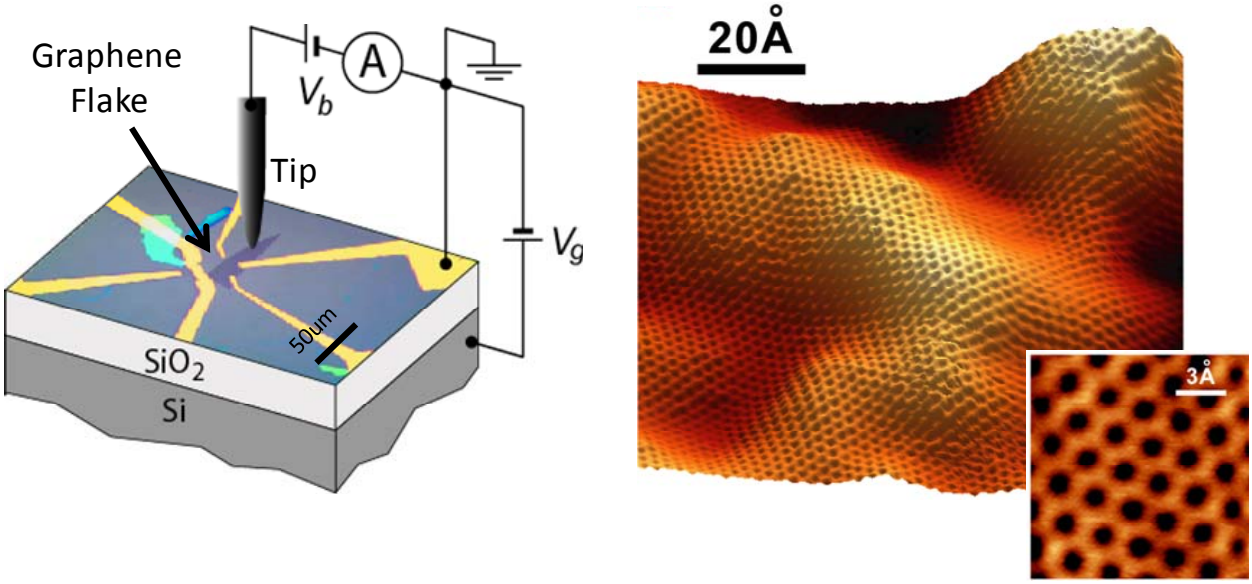

Fig. 2: Left panel shows gated graphene flake nanodevice used for scanning tunneling spectroscopy studies of graphene nanodevices. Right panel shows STM image of graphene surface for gated graphene nanodevice on left. (From ref. [3]).

Future Plans: For the future we intend to explore and control the fundamental properties of different nanoscale structures in graphene, including graphene edges, graphene nanoribbons, suspended films, and adsorbate coated surfaces. An important component of this program will be the simultaneous integration of functional nanodevices with atomic-scale microscopy, and the use of microscopy techniques not only to image, but to modify graphene structures at the atomic scale.

References:

[1] J. C. Meyer, C. O. Girit, M. F. Crommie, and A. Zettl, "Imaging and dynamics of light atoms and molecules on graphene", *Nature* **454**, 319 (2008).
[2] J. C. Meyer, C. Kisielowski, R. Erni, M. D. Rossell, M. F. Crommie, and A. Zettl, "Direct Imaging of Lattice Atoms and Topological Defects in Graphene Membranes", *Nano Lett.* (2008).
[3] Y. Zhang, V. Brar, F. Wang, C. Girit, Y. Yayon, M. Panlasigui, A. Zettl, and M. F. Crommie, "Giant phonon-induced conductance in scanning tunneling spectroscopy of gate-tunable graphene", *Nature Physics* **4**, 627 (2008).

New Methods for Atomic Structure Definition of Materials

Laurence D. Marks
Department of Materials Science and Engineering
Northestern University
Evanston, IL 60208
Email: L-marks@northwestern.edu

Program Scope

This program has two objectives. One is to understand the details of precession electron diffraction and push this technique to its technical limits. This technique shows considerable promise as a new method to quantitatively characterize material structures and their evolution over atomic to micron length scales. The second objective is to compare the thermodynamics and energetics of oxide surfaces as revealed using advanced electron microscopy with first-principles theoretical calculations, to determine the degree to which they agree.

Recent Progress

Since renewal of this proposal in 2008 we have made substantial progress in understanding oxide surfaces. Two things had become apparent in our work as well as that of others on oxide surfaces: obtaining agreement between experimental and theoretical results for equilibrium surface structures, is an unsolved problem. As an example, the structure of the $SrTiO_3$ (001) 2x1 surface is relatively conclusively solved, as is the more complicated c4x2 structure. Several theoretical analyses have been performed of these two surfaces (e.g. [1-7]), and they all come to the conclusion that the experimental surfaces are higher in energy than alternatives. Are the surface structures metastable kinetically-limited structures rather than the true thermodynamic minimum energy structures, or are the theoretical calculations not accurate enough due to fundamental problems with the density functionals?

One hard case is the NiO (111) surface. It has been argued, based upon surface x-ray diffraction data, that the surface either forms an octapolar structure or a spinel, the later under reducing conditions, and does not react with water to form hydroxide in reasonable vacuums [8-11]; this is a unexpected because NiO is normally considered to be very similar to MgO (ignoring the antiferromagnetic d-electrons), and MgO (111) is known to readily form a hydroxide [12]. In addition to possible problems with the interpretation of the diffraction data, which is not always unique, there are for certain problems with appropriately calculating the energetics of NiO; for instance conventional GGA will grossly underestimate the ionicity so can be expected to do a poor job of representing the energy of forming a hydroxide.

We have been recently able to resolve these issues by combining careful TEM surface structure analysis with XPS and more advanced DFT methods, in particularly the use of an on-site PBE0 method [13, 14] to include a dynamically adjusting Hubbard U terms for the d-electrons which will take account of changes in the shielding at the surface, which can be calculated with full account of the forces [15]. The combined analysis clearly indicates that the surfaces are hydroxylated and that rather than obtaining the thermodynamically stable structures what is

taking place is dehydration of an initial hydroxide terminated 1x1 surface which follows a kinetic pathway as sketched in Figure 1. Note that while the PBE calculations are qualitatively similar to those of the more accurate PBE0 functional, the former severely underestimates the energy of hydration as would be expected.

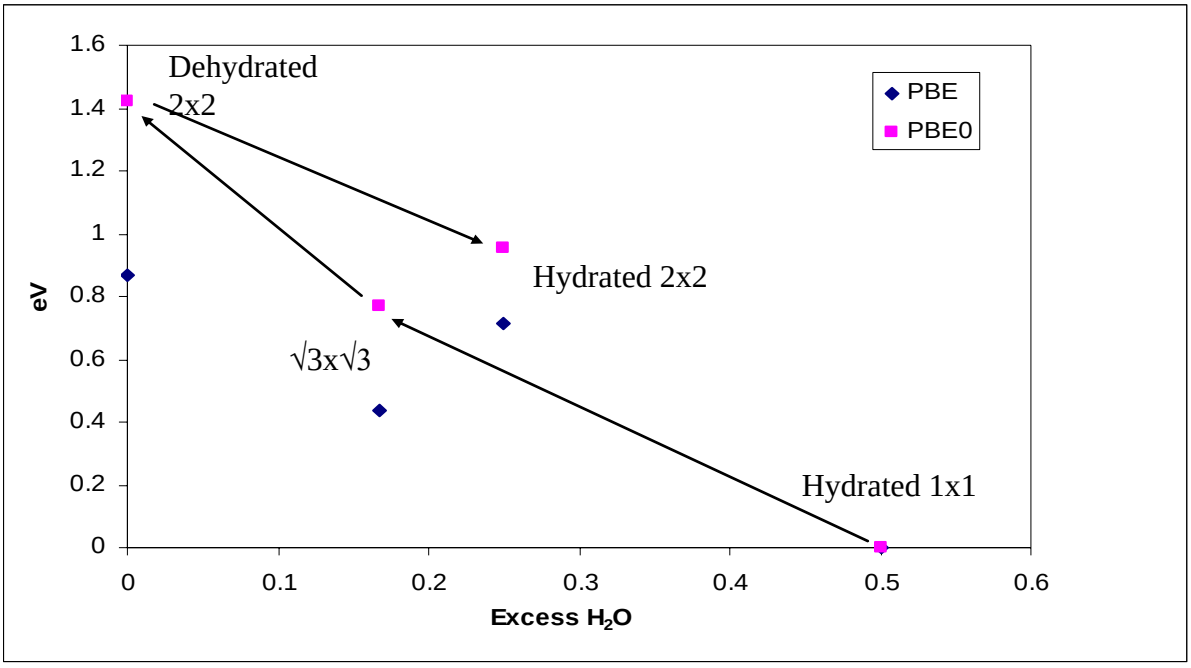

Figure 1: Surface energy per 1x1 cell normalized to the hydrated 1x1 surface in blue for the PBE functional and in purple for PBE0. The kinetic pathway of dehydration and rehydration found experimentally is shown and is not the thermodynamically lowest energy path but is determined by the kinetics of proton diffusion on the surface.

For the $SrTiO_3$ (001) surface we have made one important step forward; we have been able to measure and solve the structure of the √13x√13 R33.7 structure (see Figure 1). Whereas all the previously solved surface structures on $SrTiO_3$ (001) have the same composition, an excess coverage of 1.5 monolayers of TiO_2, this surface has a lower surface TiO_2 content of 1.115. For the first time we now have an *experimental* structure with a different composition so we can start to compare, rigorously, DFT calculated energies for the surface phase diagram as a function of composition and experimental data. These are currently being performed using both the standard PBE functional as well as more accurate PBE0; even for titanium conventional GGA underestimates the ionicity although this is less severe than for nickel.

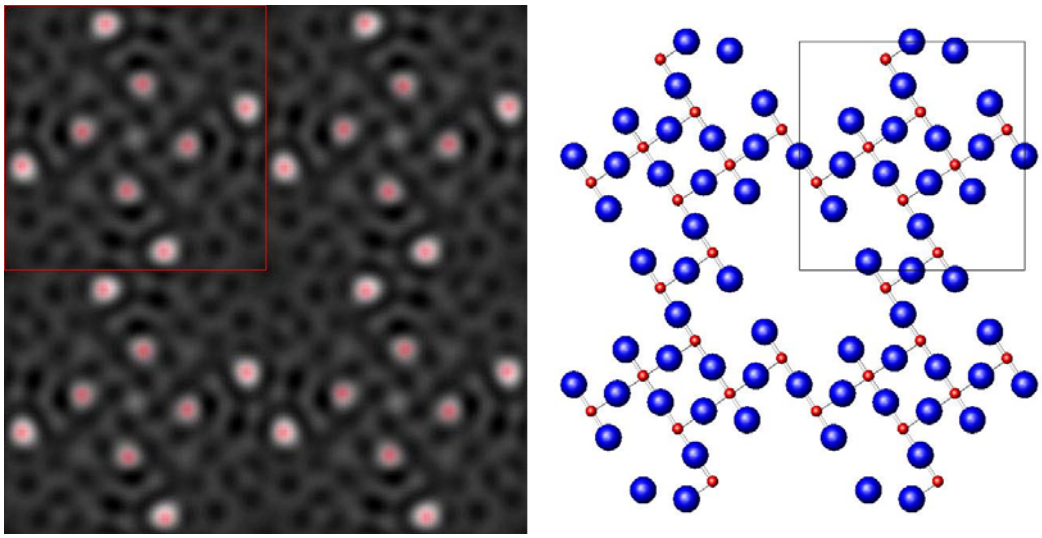

Figure 2: Map (left) and structure (right) with the Ti atoms red and the oxygen atoms blue.

Publications partially or fully supported by this funding 2006-2008

i. Own, C.S., L.D. Marks, and W. Sinkler, *Precession electron diffraction 1: multislice simulation.* Acta Crystallographica Section A, 2006. **62**: p. 434-443.

ii. Own, C.S., W. Sinkler, and L.D. Marks, *Rapid structure determination of a metal oxide from pseudo-kinematical electron diffraction data.* Ultramicroscopy, 2006. **106**(2): p. 114-122.

iii. Ciston, J., B. Deng, L.D. Marks, C.S. Own, and W. Sinkler, *Precession electron diffraction: delivering a knockout blow to kinematically forbidden reflections.* Ultramicroscopy, submitted, 2007.

iv. Own, C.S., W. Sinkler, and L.D. Marks, *Prospects for aberration corrected electron precession.* Ultramicroscopy, 2007. **107**(6-7): p. 534-542.

v. Sinkler, W., C.S. Own, and L.D. Marks, *Application of a 2-beam model for improving the structure factors from precession electron diffraction intensities.* Ultramicroscopy, 2007. **107**(6-7): p. 543-550.

vi. Deng, B. and L.D. Marks, *Theoretical structure factors for selected oxides and their effects in high-resolution electron-microscope (HREM) images.* Acta Crystallographica Section A, 2006. **62**: p. 208-216.

vii. Deng, B., L.D. Marks, and J.M. Rondinelli, *Charge defects glowing in the dark.* Ultramicroscopy, 2007. **107**(4-5): p. 374-381.

viii. Rondinelli, J., D. Bin, and L.D. Marks, *Enhancing structure relaxations for first-principles codes: an approximate Hessian approach.* Computational Materials Science, 2007. **40**: p. 345-353.

ix. Lanier, C.H., J.M. Rondinelli, B. Deng, R. Kilaas, K.R. Poeppelmeier, and L.D. Marks, *Surface reconstruction with a fractional hole: (root 5x root 5)R26.6 degrees LaAlO3(001).* Physical Review Letters, 2007. **98**(8).

x. Merkle, A.P. and L.D. Marks, *Friction in full view.* Applied Physics Letters, 2007. **90**(6): p. 064101.

xi. Merkle, A. and L.D. Marks, *Liquid-Like Sliding Deformation.* Wear, submitted, 2007.

xii. Merkle, A., L.D. Marks, O. Eryilmaz, and A. Erdimer, *In-Situ Observation of Graphitization of Nearly Frictionless Carbon.* In Preparation, 2007.
xiii. Merkle, A.P. and L.D. Marks, *A predictive analytical friction model from basic theories of interfaces, contacts and dislocations.* Tribology Letters, 2007. **26**(1): p. 73-84.
ivx. Merkle, A.P. and L.D. Marks, *Comment on "friction between incommensurate crystals".* Philosophical Magazine Letters, 2007. **87**(8): p. 527-532.
vx. Warchkow, O., et al., *Structure and Thermodynamics of the c(2x2) reconstruction of TiO2 (100).* Physical Review Letters, 2008. **100**: p. 86102.
vxi. Ciston, J., et al., *A quantitative analysis of the cone-angle dependence in precession electron diffraction.* Ultramicroscopy, 2008. **108**(6): p. 514-522.

References

1. Johnston, K., et al., *SrTiO3(001)(2x1) reconstructions: First-principles calculations of surface energy and atomic structure compared with scanning tunneling microscopy images.* Physical Review B, 2004. **70**(8).
2. Warschkow, O., et al., *TiO2-rich reconstructions of SrTiO3(001): a theoretical study of structural patterns.* Surface Science, 2004. **573**(3): p. 446-456.
3. Liborio, L.M., et al., *Stability of Sr adatom model structures for SrTiO3(001) surface reconstructions.* Journal of Physics-Condensed Matter, 2005. **17**(23): p. L223-L230.
4. Piskunov, S., et al., *Hybrid DFT calculations of the atomic and electronic structure for ABO(3) perovskite (001) surfaces.* Surface Science, 2005. **575**(1-2): p. 75-88.
5. Evarestov, R.A., A.V. Bandura, and V.E. Alexandrov, *Hybrid HF-DFT comparative study of SrZrO3 and SrTiO3(001) surface properties.* Physica Status Solidi B-Basic Solid State Physics, 2006. **243**(12): p. 2756-2763.
6. Evarestov, R.A., A.V. Bandura, and V.E. Alexandrov, *Adsorption of water on (001) surface of SrTiO3 and SrZrO3 cubic perovskites: Hybrid HF-DFT LCAO calculations.* Surface Science, 2007. **601**(8): p. 1844-1856.
7. Heifets, E., et al., *Electronic structure and thermodynamic stability of double-layered SrTiO3(001) surfaces: Ab initio simulations.* Physical Review B, 2007. **75**(11).
8. Barbier, A., et al., *Atomic structure of the polar NiO(111)-p(2 x 2) surface.* Physical Review Letters, 2000. **84**(13): p. 2897-2900.
9. Barbier, A., C. Mocuta, and G. Renaud, *Structure, transformation, and reduction of the polar NiO(111) surface.* Physical Review B, 2000. **62**(23): p. 16056-16062.
10. Finocchi, F., et al., *Stability of rocksalt (111) polar surfaces: Beyond the octopole.* Physical Review Letters, 2004. **92**(13).
11. Goniakowski, J., F. Finocchi, and C. Noguera, *Polarity of oxide surfaces and nanostructures.* Reports on Progress in Physics, 2008. **71**(1).
12. Lazarov, V.K., et al., *Structure of the hydrogen-stabilized MgO(111)-(1x1) polar surface: Integrated experimental and theoretical studies.* Physical Review B, 2005. **71**(11).
13. Tran, F., et al., *Hybrid exchange-correlation energy functionals for strongly correlated electrons: Applications to transition-metal monoxides.* Physical Review B, 2006. **74**(15).
14. Novak, P., et al., *Exact exchange for correlated electrons.* Physica Status Solidi B-Basic Solid State Physics, 2006. **243**(3): p. 563-572.
15. Tran, F., et al., *Force calculation for orbital-dependent potentials with FP-(L)APW+lo basis sets.* 2008: p. Submitted.

Electron Diffraction Determination of Nanoscale Structures

Joel H. Parks and Xi Li
parks@rowland.harvard.edu
The Rowland Institute at Harvard, 100 Edwin H. Land Boulevard, Cambridge, MA 02142

Program Scope

Structure determination is one of the outstanding challenges of cluster science. Structural determination via analysis of diffraction measurements is most desirable, since the scattering data is related to the spatial arrangement of the scattering atoms in a direct manner. Development of a unique diffraction instrument under DOE support has allowed direct measurements of the size-dependent evolutions of cluster structures and the physical and chemical properties of finite nanoscale materials aggregates. Trapped ion electron diffraction (TIED)[1,2] has enabled the first direct measurements of metal cluster structures[3,4]. The TIED technique is based on storing cluster ions in an ion trap to enable the accumulation of *size selected* clusters, collisional relaxation of the vibrational energy and exposure to a high energy electron beam for sufficient time to collect electron diffraction data. Collaborations with theorists have provided an essential contribution to this program because comparisons between the measured diffraction patterns and those calculated for theoretically optimized structures is required in order to fully determine the atomic arrangement. Current research continues TIED measurements of metal cluster structures with an emphasis to determine how structure plays a role in the dynamical processes of metal cluster nanocatalysis and cluster melting. Diffraction measurements and associated adsorption measurements are being pursued for metal cluster materials of both pure and alloyed compositions. This research program relates to the DOE Materials Science and Engineering Division mission by providing a method for confirming the design of nanosize materials at the atomic level; by providing an experimental tool for characterization of nanoscale phenomena; and by allowing a more complete understanding of nanoscale properties.

Recent Progress

Water adsorption on gold clusters continues to be an important area of study as a result of enhanced catalytic reactivity on hydrated clusters[5]. Initial measurements of the chemisorption of H_2O on both gold cluster anions and cations have been performed over the cluster size range $3 \leq n \leq 22$. The measurement of adsorption rates and their saturation have observed a dependence on specific cluster structures in this size range.

Cation H_2O adsorption. Adsorption of H_2O on gold cluster cations only occurs for planar structures with $n \leq 7$ with adsorption strength and saturation number depending strongly on size. Adsorption also exhibits isomer structural variations. The mass spectrum of reaction products $Au_n(H_2O)_x^+$ with $3 \leq n \leq 11$ is shown in Fig. 1. Saturated adsorption occurs for 3 molecules on n=3-5 and 2 molecules for n=6,7 and sizes greater than Au_7^+ exhibit only weak physisorption of multiple water molecules under these experimental conditions. The structures shown in Fig. 1 are the lowest energy isomers of pure gold cluster cations resulting from density functional calculations[6] and have been identified through comparison with mobility and photoelectron spectroscopy experiments since diffraction data was not available for such small species.

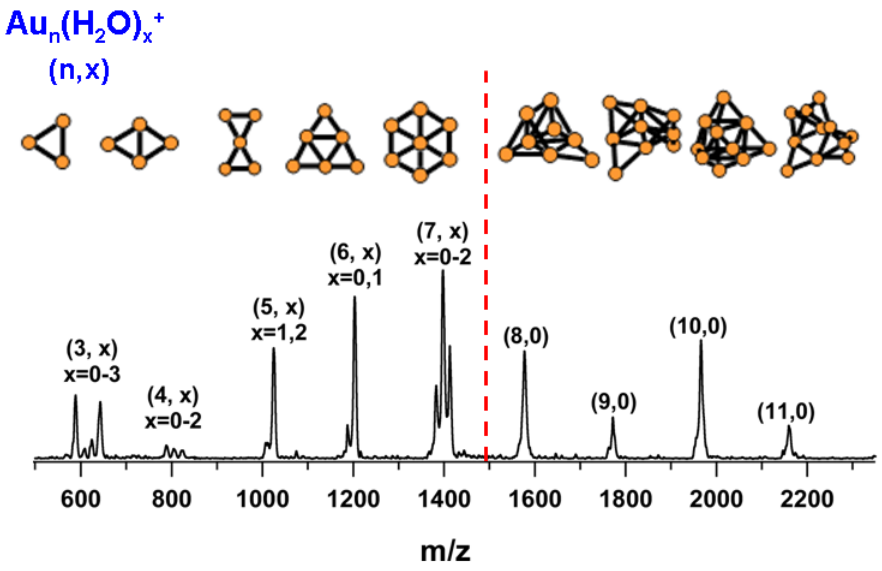

Figure 1. Mass spectrum of $Au_n(H_2O)_x^+$ indicates adsorption is occurring primarily on planar structures. The saturation number of adsorbed molecules is given in parentheses above the cluster structures. The spectrum is obtained at 298 K, $p_{H2O}=2x10^{-8}$ Torr, $p_{He}=5x10^{-3}$ Torr, exposure time 20 s.

Anion H_2O adsorption. The mass spectrum of reaction products $Au_n(H_2O)_x^-$ with $3\leq n\leq 11$ and $0\leq x\leq 2$ is shown in Fig. 2. The bare Au_n^- structures shown in Fig. 2 were taken from Refs. 4,7,8. Water molecules adsorb on only three gold anion clusters (Au_4^-, Au_5^-, and Au_6^-) with a maximum saturation number of 2 molecules. Similar to the adsorption for Au_3^+, acceleration of the second water is observed for all three anions for which the $Au_n(H_2O)_2^-$ adsorption mass intensity is much greater than $Au_nH_2O^-$. For all the clusters studied here, we observed weak physisorption of multiple water molecules. It is worthwhile to note that unlike Au_3^+ and Au_7^+, adsorption of H_2O molecules is not observed on Au_3^- and Au_7^-.

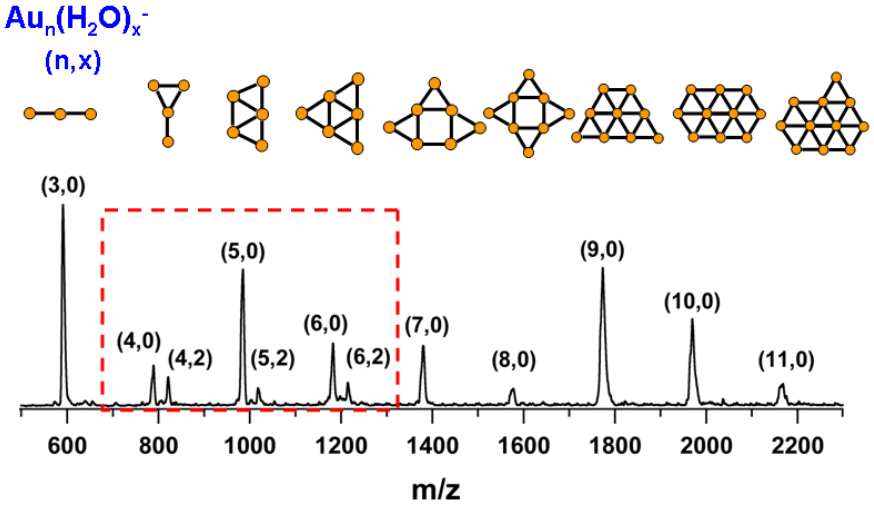

Figure 2. Mass spectrum of $Au_n(H_2O)_x^-$ indicates adsorption is occurring primarily on planar structures. The spectrum is obtained at 298 K, $p_{H2O}=2.4x10^{-7}$ Torr, $p_{He}=5x10^{-3}$ Torr, exposure time 20 s.

Future Plans

Catalytic Reactivity on Metal Clusters. Gas phase measurements of clusters having identified structures can serve to guide the search for efficient heterogeneous systems based on supported metal clusters. In addition, metal cluster nanocatalysis offers interesting possibilities to increase catalytic reactivity and perhaps reaction specificity. It is particularly important to be able to identify the relationship, or correlation between structure and reactivity for gas phase clusters. In

this case, the utility of diffraction data and calculations to identify the isomer structure of a gas phase reactant may allow such a correlation to be discerned and related to catalytic processes. The quadrupole ion trap is particularly well suited to measure both the kinetic and steady state adsorption properties of metal clusters over a wide range of temperature and pressure. It is clear from our initial measurements that a broad spectrum of structure related effects are dominating the adsorption of small molecules on gold clusters. Many questions related to the structural dependence are currently unanswered. How is this sensitivity to structure related to the cluster electronic states? At what size does this structure dependence cease to be a dominating characteristic? Does such a structure-sensitivity extend to reactions, eg. CO_2 generation from the co-adsorption of O_2 and CO?

Studies will continue to investigate the structure dependence of cluster reactivity on gold, silver and aluminum clusters. The adsorption of H_2O, O_2, CO and their co-adsorption will be measured on TIED/DFT determined structures. In particular, adsorption on cations and anions of Au_6 will be compared theoretically to determine how the charge state determines the adsorption process on this initially planar cluster. For example, is a transition 2D to 3D involved in the sharp reduction in gold anion water adsorption.

Diffraction of Reactive Metal Clusters. Diffraction measurements of metal cluster structures will be performed as a function of size and temperature. Preliminary data for gold anion and cation clusters will be compared with theoretical calculations to search for transitions between structural motifs and symmetries for larger size gold clusters with up to 75 atoms. Clusters of palladium and gold clusters with palladium surface impurities will be studied to relate their structures to recent gas phase nanocatalysis measurements[9-11] observed for these clusters supported on TiO_2 substrates.

Cluster structures identified by these diffraction measurements can be further characterized by measuring their adsorption of small molecules known to be involved in efficient nanocatalysis reactivity. Equilibrium adsorption measurements will be performed as a function of temperature, pressure and cluster size to determine the dependence of saturated adsorption and reactivity on cluster structure. These experiments will be performed on structures identified by the diffraction measurements and will be conducted in the same cluster source/trap apparatus used for diffraction. The adsorption on trapped, mass selected clusters is the only technique which can assure that cluster adsorption measurements represent thermal equilibrium and are not the result of transient kinetics. Questions related to the rearrangement of cluster atoms after adsorption will be investigated by diffraction measurements. Calculations will analyze the interactions between adsorbed molecules and the electronic states associated with specific structures.

The size dependence of the melting transition of metal clusters has long been recognized as a measurement critical for the study of many body interactions in cluster structures. As a result of our recent measurements silver and gold cluster structures, specific cluster sizes of both metals including Ag_{38}^+, Ag_{55}^+, Au_{20}^- and Au_{24}^-, have been identified[3,4] which will allow unambiguous diffraction measurements to follow the melting transitions for these cluster structures.

References

(1) M. Maier-Borst, D. B. Cameron, M. Rokni and J. H. Parks Phys. Rev. A **59**, R3162 (1999).
(2) S. Krückeberg, D. Schooss, M. Maier-Borst and J.H. Parks, Phys. Rev. Lett.**85**, 4494 (2000).
(3) X. Xing, R. M. Danell, I. L. Garzón, K. Michaelian, M. N. Blom, M. M. Burns, and J. H. Parks, Phys. Rev. B **72**, 081405 R (2005).
(4) X. Xing, B. Yoon, U. Landman, J. H. Parks, Phys. Rev. B **74** (2006) 165423.
(5) M. Daté and M. Haruta, J. Catal. **201**, 221 (2001).
(6) S. Gilb, P. Weis, F. Furche, R. Ahlrichs, and M. M. Kappes, J. Chem. Phys.**116**, 4094(2002).
(7) F. Furche, R. Ahlrichs, P. Weis, C. Jacob, S. Gilb, T. Bierweiler, and M. M. Kappes, J. Chem. Phys. **117**, 6982 (2002).
(8) Anion structures: Refs. 6 and 3; B. Yoon, H. Ha1kkinen, and U. Landman, J. Chem. Phys. **107**, 4066 (2003).
(9) M. D. Hughes, Y-J. Xu, P. Jenkins, P. McMorn, P. Landon, D. I. Enache, A. F. Carley, G. A. Attard, G. J. Hutchings, F. King, E. H. Stitt, P. Johnston, K. Griffin and C. J. Kiely, Nature **437**, 20 (2005).
(10) D. I. Enache, J. K. Edwards, P. Landon, B. Solsona-Espriu, A. F. Carley, A. A. Herzing, M. Watanabe, C. J. Kiely, D. W. Knight, G. J. Hutchings, Science **311** (2006).
(11) M. Chen, D. Kumar, C.-W. Yi, D. W. Goodman, Science **310**, 14 (2005).

Publications

Structural evolution of Au nanoclusters: From planar to cage to tubular motifs, X. Xing, B. Yoon, U. Landman, J. H. Parks, Phys. Rev. B 74 (2006) 165423.

Trapped Ion Electron Diffraction: Structural Transitions in Silver and Gold Clusters, J. H. Parks and X. Xing in: The Chemical Physics of Solid Surfaces Volume 12, "Atomic Clusters: from Gas Phase to Deposited", Ed. D. Woodruff, Elsevier.

Structure and Dynamics of Trapped Ions, J. H. Parks in: PRACTICAL ASPECTS OF TRAPPED ION MASS SPECTROMETRY, Volume 5: Applications, Eds. R. March and J. Todd, CRC Press. (in press)

Automated Nanocrystallography

Prof J.C.H Spence
Physics. Arizona State University
Tempe, Az. 85282. Spence@asu.edu
DE-FG02-02ER45996

The aim of this research program is to develop nanocrystallography for nanomaterials. In addition, we are developing strain-mapping by CBED for devices.

Our nanocrystallography is based on electron microdiffraction in a TEM, and is based on the realisation that a) The host of new nanostructures being created urgently requires a method for rapid determination of nanocrystal atomic structure, and 2) Because these nanocrystals are so small, multiple-scattering artifacts, which have hitherto prevented much success in electron crystallography, are minimized. 3) The new charge-flipping algorithm (see G. Oszlányi and A. Süto. *Acta Cryst.,* A60, 134 (2004)), which performs well with poor quality diffraction data, is ideally suited to the phase problem in this application. The electron probe size is about 20nm diameter. Our aim is to develop a method which will collect three-dimensional diffraction data sets automatically from 50nm regions, analyse them (and solve the phase problem), and present a three-dimensional charge-density map of the crystal structure to the user while at the electron microscope.

Over the last year we have made significant progress toward this goal. We are developing two approaches - first based on kinematic convergent-beam patterns (KCBED), and the second on the electron precession method. The KCBED method has the following advantages: 1. CBED patterns with uniformly illuminated disks are collected from very thin regions at the edge of samples where single scattering conditions apply, and the nm-sized probe of the CBED mode can be used, rather than the much larger probe in precession mode. 2. The central disk may be recorded, allowing absolute scaling of intensities. 3. Angular integration may be performed across the disks. Over the last year we have

i) Developed software code to implement the 3D flipping algorithm, to solve the phase problem (370, 375), and analysed three-dimensional experimental diffraction data with it from thin crystals of spinel.

ii) Purchased and installed a precession electron diffraction system for our CM200 electron microscope, and obtained first results with it, also from spinel (393). Work continues on the challenging problem of automated collection of 3D diffraction data. Our plan is to automate single-axis data collection, then deduce the exact orientation and indexing of the spots later by computer, rather than by attempting to set up pre-determined orientations at Bragg conditions.

In addition to this work , we have continued our work on the accurate measurement of charge-densities and chemical bonding in crystals, by applying it to the case of GaN, as used for solid state lighting.

The most industrially significant work of the last two years has been our use of the Libra Omega TEM at NCEM in energy-filtered CBED mode to map out the strain around a single transistor, in collaboration with Intel. This method is based on the quantitative analysis of HOLZ lines. This work resulted from a statement on the

semiconductor industry Roadmap web site, that "no techniques currently exist for the crucial problem of mapping strain at the nanoscale". In current computers, speed is increased by using intentionally induced strain-fields to increase carrier mobility.

The most visible work undertaken is our three-dimensional X-ray imaging inside porous media (362). These diffractive (lensless) images of a ceramic nanofoam provide insights for the modelling of the percolation of water and oil flow in minerals, and insight into the strength and failure mechanisms of foam materials. In other projects we have developed a new method of diffractive imaging, based on Fourier Transform holography using a Uniformly Redundant Array as a reference. This avoids the uncertainties associated with convergence of iterative phasing methods.

Book chapters on electron crystallography and related topics have been written for the International Tables for Crystallography, and for the new edition of the Carter-Williams text on Electron Microscopy in Materials Science.

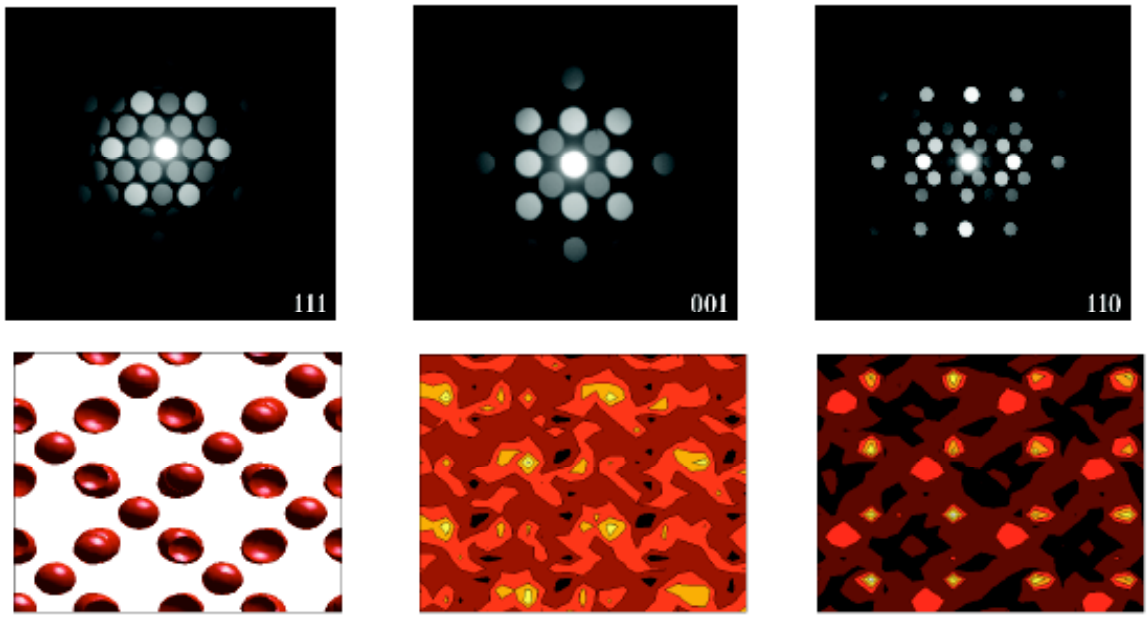

Figure 1. Experimental Kinematic (single-scattering) CBED patterns from cubic spinel nanocrystals in three orientations. Below are shown reconstructed real-space potentials, left (001), middle (at start of iterations with random phases), right (converged).

References (Publications of last two years).

295 "Valence charge density distribution and chemical bonding in MgB2". B. Jiang, N. Jiang and J.C.H.Spence. AXkive on-line **(2006).**

316. Ab initio calculation of the phase stability, mechanical properties and electronic structure of ZrCr2 Laves phase compounds. J.Sun, B.Jiang Phil Mag 84, 3133 (2004)

322 Electron crystallography. The way forward. J.Spence. In "Electron crystallography". T.E.Weirich et al. Ed. Nato Science Series Vol 211 (2006) Erice 04. (Summer school) DOE . ISBN 1-4020-3919-0

327 An assessment of the resolution limitation due to radiation-damage in X-ray diffraction microscopy. M.Howells, T. Beetz, H. Chapman, C. Cui, J. Holton, C. Jacobsen, J. Kirz, E. Lima, S. Marchesini, H. Miao, D. Sayre, D. Shapiro, J. Spence. J. Elec. Spectr. Rel Phenom. (2008). In press. http://arxiv.org/abs/physics/0502059.

333 Imaging dislocation cores - the way forward. J.C.H.Spence , H. Kolar, G. Hembree, C. Humphreys, J. Barnard, R. Datta, C. Koch, F. Ross, J. Justo. Phil. Mag. 86, 4781 (2006). Special issue for 50 years since first observation of dislocations by TEM.

342 A Simple constraint for phase retrieval with high efficiency. H. He. J.Opt. Soc. Am, 23, p. 550. (2006)

354 "Analysis of nanoscale stress in strained silicon materials and microelectronic devices by energy-filtered CBED. P. Zhang, A. Istratov, H. He, C. Nelson, J. Ager, E. Stach, J. Spence, C. Kiselowski, E. Weber. J. Electrochemical Soc. (2006). In press. .

357 "Direct strain measurement in a 65nm node locally strained silicon device by energy-filtered convergent beam diffraction". P. Zhang, C. Kisielowski, A. A. Istratov, H. He, C. Nelson, J. Mardinly, E. Weber, J. Spence. Applied Phys Letts. 89, 161907, (2006).

360 "Direct measurement of strain in 65nm uniaxially strained PMOS and STI by CBED". P. Zhang, C. Kisielowski, J. Mardinly, O. Karpenko, A. Istratov, J. Spence, E. Weber. Int. Elec Device Meeting., 2006. San Francisco.

362 Three-dimensional ceramic nanofoam lattice structure determination using coherent X-ray diffractive imaging: insights into deformation mechansisms. A. Barty, S. Marchesini, H. Chapman, M. Howells, C. Cui, A. Minor, J.Spence, U. Weierstall, A. Noy, A. Artyukhin, T. Baumann, T. Willey, T. van Buuren, J. Stolken, J. Kinney. **Phys Rev Letts**. 101, 055501 (2008).

365 A method of combining STEM image with parallel beam diffraction and electron-optical conditions for diffractive imaging. H. He, C. Nelson. Ultramic. 107, 340 (2007).

368 "Electron Crystallography, Charge-density mapping and Nanodiffraction". Ch 7 in "Electron Microscopy in Materials Science". Eds D. Williams and B. Carter. (2007) 2nd Edition.

370 Automated electron nanocrystallography. J. Spence, J. McKeown, H. He and J.Wu. Proc. MRS. Symp. Quantitative Electron Microscopy 2008.

372 Observation of long-range compositional fluctuations in glasses: implications for atomic and electronic structure. N. Jiang, J. Qiu, J.C.H.Spence and C.J.Humphreys. Micron. submitted (2007). Special issue for R. Egerton.

373 "Absorption spectroscopy with sub-Angstrom beams: EELS in STEM" J.C.H. Spence. Rep. Prog. Phys. 69, 725 - 758 (2006).

377 Ultrafast, ultrabright, X-ray holography using a uniformly redundant array. Stefano Marchesini[1,2], Sébastien Boutet[3,4], Anne E. Sakdinawat[5], Michael J. Bogan[1], Saša Bajt[1], Anton Barty[1], Henry N. Chapman[1], Matthias Frank[1], Stefan P. Hau-Riege[1], Abraham Szöke[1], Congwu Cui[2], David A. Shapiro[2], Malcolm R. Howells[2], John C. H. Spence[6], Joshua W. Shaevitz[7] , Johanna Y. Lee[8], Janos Hajdu[4,3], Marvin M. Seibert[4]. (2008) **Nature Photonics** 2, 560 - 563 (2008).

383 "Iterative phase retrieval for electron diffraction patterns by charge flipping". J. Wu, C. Koch and J.C.H.Spence. J. Chinese Elec. Micros. Soc. (2007) 27, 520.
384 "Electron diffraction and electron microscopy". J.Cowley and J. Spence. Chapter 2.5. International Tables for Crystallography. (2008).
390 Bonding in GaN. D. Holec, B. Jiang, V. Duggi, C. Humphreys, J.C.H.Spence. (2008). In preparation.
391 J.T. McKeown, V.R. Radmilovic, R.Gronsky, and A.M. Glaeser. "Niobium silicide formation at alumina-niobium interfaces," *Philos. Mag.*, in prep.
392 J.T. McKeown, J.D. Sugar, V.R. Radmilovic, A.M. Glaeser, and R. Gronsky. "Nanoscale phase-patterned alloys by constrained spinodal decomposition," *Nature Mater.*, in preparation.
393 Electron Nanocrystallography. J. McKeown and J. Spence. Proc Int Union of Crystallography, Conference, Osaka, 2008.

Quantitative Electron Nanocrystallography

Jian-Min Zuo
jianzuo@illinois.edu
Dept. of Materials Science and Engineering and Materials Research Laboratory,
University of Illinois, Urbana-Champaign, IL 61801

Program Scope

The properties of materials ultimately depend on their local atomic structure. While there are well-established diffraction techniques for structure determination of crystals with 2-D or 3-D periodicities, there are no such techniques for nonperiodic structures including many nanostructured materials. Understanding structure-property relationships in these materials thus depends critically on further progress in our ability of characterizing non-periodic structures. This proposal aims to develop quantitative and robust atomic structure determination techniques for nanoparticles, small crystals and one-dimensional materials whose structure cannot be addressed by conventional crystal diffraction techniques. The tool we use to address this problem is based on the nanoarea electron diffraction (NED) technique developed under prior DOE support. Significant improvement to this technique is expected from the new field emission gun transmission electron microscope with an electron probe aberration corrector and an in-column energy filter at University of Illinois. The improvement in resolution (with a smaller probe) and diffraction pattern quality (with energy filtering) will be coupled with new developments in electron diffraction modeling and inversion algorithms. Modeling will be performed for those nanoparticles where good structural models can be generated using atomic potentials. Small metal nanoparticles and quantum dots will be used as model systems to develop the electron diffraction technique. Broad impact is expected from the structural knowledge obtained with the new high-resolution electron diffraction technique, especially in areas of surface and interfacial structures characterization of nanomaterials.

Recent Progress:

Various forms of carbon nanotubes (CNT) as building blocks for nanoscience and nanotechnology have attracted considerable interest since their initial discovery by transmission electron microscopes[1]. However, their structure can be highly complex and their growth mechanism is poorly understood. In case of a carbon double wall nanotube (DWNT), the tube consists of two concentric tubes, the structure is incommensurate if the outer and inner tubes have different chiral angles. The combination multiplies further for multi-wall nanotubes (MWNT). The interaction between inner and outer tubes determines a variety of properties in both DWNTs and MWNTs[2]. For CNT nanotube bundles, interactions are expected between different tubes. While there are several techniques for characterizing single wall carbon nanotubes (SWCNT)[3], MWNT and CNT bundle structure determination require a penetrating probe, which has been done only in few cases of DWNT using electron diffraction[4]. As the result, our knowledge of MWNT and nanotube bundle structures is very limited[5].

We have developed a general solution to nanotube structure determination based on nanoarea electron diffraction (NED) technique that we developed under the previous DOE support[6]. The method is based on the analysis of single tube diffraction pattern recorded with a very small electron beam (tens of nanometers in diameter). First, the intensity peaks in the diffraction pattern are measured and their positions are used to calculate the chiral angles of different walls. Secondly, the tube diameter is measured by fitting the diffraction intensity profile using the Bessel function. The combination of tube diameter and chiral angle gives the average structure of the tube. The method developed here is general and can be applied to other cylindrical nanotubes or nanotube bundles. Most significantly, the structural knowledge obtained with the new electron diffraction method provides the basis for fundamental understanding of nanotube properties and it also provides a diagnosis tool for scientists to use in order to optimize nanotube growth.

In a separate study, we demonstrated that deformations of single wall CNT induced by van der Waals (vdW) forces can be measured from changes in electron diffraction intensities[7]. A bundle of two SWCNTs (d=2.05 nm and 1.56 nm) was studied. We used deformation model predicted by atomistic simulations to fit the experiment. We show that the best fit gives a flattening of 0.7 Å and 0.35 Å at the middle of the binding surface for the two SWCNTs. The work was motivated by the large amount of works on mechanic deformation of CNTs using TEM and atomic force microscopy (AFM) [8,9]. However, small deformation expected from the attractive vdW forces between different CNTs has not been possible so far. AFM tip itself asserts a force on CNTs and can only be used to study extreme deformations[10]. Since CNT deformations have a large effect on tube electron structures[11] and mechanical properties[8], the knowledge of vdW force deformation acquired here is extremely useful for understanding the electronic transport and mechanical properties of CNT bundles.

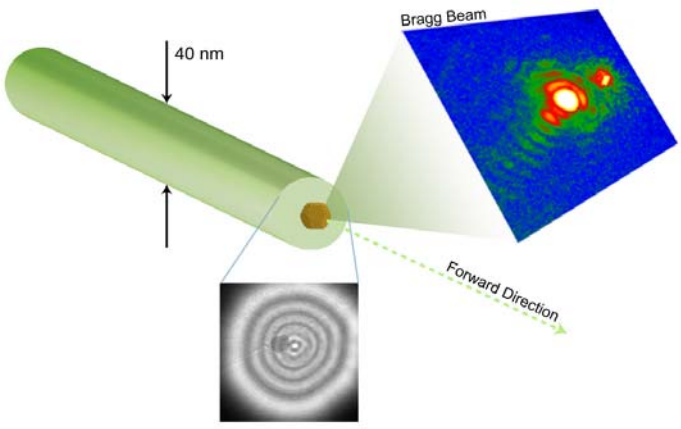

Figure 1. A schematic illustration of the coherence electron diffraction technique used to probe the surface structure of Au nanocrystals. A parallel electron beam of 40 nm is illuminated on a single Au nanocrystal to record a diffraction pattern. Electrons scattered off the surface gives speckles around the Bragg beam, which is used to study the nanocrystal surface.

In another exciting development, we show that coherent electron diffraction patterns recorded from individual nanocrystals as illustrated in Figure 1 are very sensitive to, and can be used to study, the structures of nanocrystal surfaces[12]. In a paper recently published[12], we show that both the experimental electron diffraction data and molecular

dynamics (MD) simulations strongly suggest an inhomogeneous model of the relaxation, involving large out-of-plane bond length contractions for the edge atoms; a significant contraction for {100} surface atoms; and a much smaller contraction for atoms in the middle of the {111} facets. The coordination/facet dependent contraction is markedly different from bulk crystalline surfaces and demonstrates a new pattern of structural dynamics for nanocrystalline materials. The unprecedented, atomistic, structural details we reported about nanocrystal surfaces were achieved by taking advantage of coherent interference between scattered waves from small nanocrystals containing few thousands of atoms. Experimentally we knew very little about their surface structure. Surface structures are studied by medium energy ion scattering, low energy electron diffraction, and X-ray reflectivity. However those probes generally require large flat surfaces, which exclude nanocrystals. Without the necessary structural information, our understanding of nanocrystals has been limited to the prevailing, phenomenological, models that often treat nanocrystal surface as an extension of bulk crystalline surfaces.

Future Plans:

We plan to address the following issues in next one to two years: 1) To improve the iterative transformation algorithm for inversion of electron diffraction patterns and to push the resolution of diffractive imaging and use this technique to overcome the information limit of the microscope. The intended applications are to image nanoparticles. We are especially interested in the atomic structure of quantum dots. 2) To test the limit of electron diffraction for the study of nanoparticles. We intend to carry out a systematic study of electron diffraction of ultrafine nanoparticles to examine the information limit placed by atomic scattering and detector noise. This will be coupled with a simulation study. 3) To image nanoparticles in multiple projections to examine their 3-D structure. We are especially interested in imaging at high index zone axes from diffraction patterns, which can be used to supplement or complement information obtained by electron direct imaging.

Reference:

[1] S. Iijima, Nature **354** (6348), 56-58 (1991); D. S. Bethune et al., Nature **363**, 605-607 (1993); S. Iijima and T. Ichihashi, Nature **363**, 603-605 (1993).

[2] J. Cumings and A. Zettl, Science **289**, 602-604 (2000).

[3] M. S. Dresselhaus, G. Dresselhaus, R. Saito, and A. Jorio, Physics Reports-Review Section of Physics Letters **409**, 47-99 (2005); M. Gao, et al., Applied Physics Letters **82**, 2703-2705 (2003); Hua Jiang et al., Physical Review B **74**, 035427-035428 (2006); L. C. Qin, Reports on Progress in Physics **69**, 2761-2821 (2006).

[4] M. Gao et al., Journal of Materials Science **41**, 4382-4388 (2006); K. Hirahara, et al., Physical Review B **73**, 195420 (2006).

[5] Z. J. Liu, Q. Zhang, and L. C. Qin, Applied Physics Letters **86**, 191903 (2005).

[6] J. M. Zuo et al., Zeitschrift Fur Kristallographie **222**, 625-633 (2007).

[7] Y. Y. Jiang et al., Physical Review B **77** (15), 153405 (2008).

[8] A. Pantano, D. M. Parks, and M. C. Boyce, Journal of the Mechanics and Physics of Solids **52**, 789-821 (2004).

[9] M. F. Yu, T. Kowalewski, and R. S. Ruoff, Physical Review Letters **85**, 1456-1459 (2000).
[10] T. Hertel, R. Martel, and P. Avouris, Journal of Physical Chemistry B **102**, 910-915 (1998).
[11] L. Yang and J. Han, Physical Review Letters **85**, 154-157 (2000); E. D. Minot et al., Physical Review Letters **90** (15), 156401 (2003).
[12] W. J. Huang et al., Nature Materials **7** (4), 308-313 (2008).

DOE Sponsored Publications in 2007-2008

1) M. Gao, J. M. Zuo, R. Zhang, L. A. Nagahara, " Structure determinations of double-wall carbon nanotubes grown by catalytic chemical vapor deposition", Journal of Materials Science, 42, 4382-4388, (2006)
2) Hao Chen and J.M. Zuo, “Structure and phase separation of Ag–Cu alloy thin films”, Acta Mater. In press (2006)
3) W.J. Huang, B. Jiang, R.S. Sun and J.M. Zuo, “Towards Sub-Å Atomic Resolution Electron Diffraction Imaging of Metallic Nanoclusters: A Simulation Study of Experimental Parameters and Reconstruction Algorithms”, Ultramicroscopy, 107, 1159-1170, (2007)
4) (Invited) J.M. Zuo, T. Kim, A. Celik-Aktas, J. Tao, “Quantitative Structural Analysis of Individual Nanotubes by Electron Diffraction”, Zeitschrift fur Kristallographie 222, 625-633 (2007)
5) A. Celik-Aktas, J. F. Stubbins, and J. M. Zuo, "Electron beam machining of nanometer-sized tips from multiwalled boron nitride nanotubes," Journal of Applied Physics 102, 024310 (2007).
6) W. J. Huang, R. Sun, J. Tao, L. D. Menard, R. G. Nuzzo and J. M. Zuo, “Coordination-dependent surface atomic contraction in nanocrystals revealed by coherent diffraction” Nature Materials, 7, 308-313 (2008)
7) S.W. Kim, J.M. Zuo, N.T. Nguyen, D.C. Johnson, and D.G. Cahill, “Structure of layered WSe_2 thin films with ultralow thermal conductivity”, J. Materials Research, 23, 1064-1067, (2008)
8) T Kim, S Kim, E Olson, and J. M. Zuo, "In situ measurements and transmission electron microscopy of carbon nanotube field-effect transistors," Ultramicroscopy, In print (2008).
9) Y. Y. Jiang, W. Zhou, T. Kim, Y. Huang, and J. M. Zuo, "Measurement of radial deformation of single-wall carbon nanotubes induced by intertube van der Waals forces," Physical Review B 77 (15), 153405 (2008).
10) D. Niebieskikwiat, J. Tao, J. M. Zuo, and M. B. Salamon, "Time-dependent phenomena in phase-separated electron-doped manganites," Physical Review B **78** (1), 014434 (2008).
11) A. Bhattacharya, S. J. May, Sget Velthuis, M. Warusawithana, X. Zhai, B. Jiang, J. M. Zuo, M. R. Fitzsimmons, S. D. Bader, and J. N. Eckstein, "Metal-insulator transition and its relation to magnetic structure in (LaMnO3)(2n)/(SrMnO3)(n) superlattices," Physical Review Letters **100** (25), 257203 (2008).

Research Summaries VI:

Nanoscale Materials

Toward the Development of Cluster-Based Materials

Kit H. Bowen
kbowen@jhu.edu
Depts. of Chemistry and Materials Science, Johns Hopkins University, Baltimore, MD 21218

Program Scope

Clusters are aggregates of atoms and/or molecules held together by the same cohesive forces responsible for binding atoms and/or molecules to one another in solids and liquids. Free clusters tend to have unique geometric structures. In fact, some of them exhibit low dimensionalities, eg., strings and planes of atoms, but when three-dimensional, as most are, they tend to have large surface area-to-volume ratios. They also display other intriguing geometric structures, such as empty shells, cuboids ('baby crystals'), and shells encapsulating atoms or other clusters ('core shells'). In addition, clusters often display extraordinarily novel electronic, magnetic, and reactivity properties. For example, the optical (electronic) properties (band gaps) of clusters can be tailored by controlling their size and composition. Moreover, some clusters enjoy enhanced stability ('magic clusters') due to having achieved closed shell electronic configurations under the 'shell model'. Clusters of non-magnetic elements can also be magnetic, while those of antiferromagnetic elements can become ferromagnetic. Together, their unique size-dependent electronic and magnetic properties provide a unique opportunity for manipulating and controlling electrons in finite size regimes. Furthermore, clusters of noble metals can be reactive, while those consisting of reactive elements can be made chemically inert by suitably changing their size, charge state, and/or composition. Moreover, the valency of some elements can change depending on the number of atoms per cluster. With these novel properties, clusters provide a means of manipulating physical and chemical properties. Indeed, if clusters, instead of atoms or molecules, could be incorporated into materials as building blocks, viz., 'cluster-based materials', whole new worlds of materials properties would become available.

Our program provides experimental results which make fundamental contributions to the elucidation of cluster properties and to the development of cluster-based materials. Toward these goals, we have utilized negative ion photoelectron (photodetachment) spectroscopy as our principal tool. By photodetaching excess electrons from size- and composition-selected cluster anions, we obtain a detailed picture of the electronic structure of the anions' corresponding neutral counterpart. Moreover, due to mass selection, we can follow the evolution of these properties as function of size and composition. Our program is currently in the process of extending its grasp beyond the study of the electronic properties of free (gas phase) clusters to include the study of the same electronic properties for the same (size and composition) clusters deposited on surfaces. In this way, we will determine how the electronic properties of free clusters are modified by their interactions with specific substrates.

Recent Progress

Silicon-Encapsulated, Rare Earth Atom Clusters Our work with silicon-encapsulated, rare earth (RE) atoms was motivated by two observations: (1) the fact that silicon clusters have a propensity to encapsulate metal atoms, forming relatively stable cages and (2) the potential, inherent in their f-electron electronic configurations, for rare earth atoms to exhibit large magnetic moments. If both high magnetic moments and stability (perhaps due to caging) could be achieved in particular silicon-encapsulated, rare earth cluster sizes, $RE(Si)_n$, these clusters might provide a pathway for obtaining magnetic, silicon-based cluster-assembled materials. Such materials could serve as transitional materials between today's silicon-based semiconductor technology and the emerging field of spintronics. We studied six different $RE(Si)_n^-$ systems by photoelectron spectroscopy: $Eu(Si)_n^-$, $3 \le n \le 17$; $Ho(Si)_n^-$, $3 \le n \le 13$; $Gd(Si)_n^-$, $2 \le n \le 13$; $Yb(Si)_n^-$,

$4 \leq n \leq 13$; $Sm(Si)_n^-$, $3 \leq n \leq 13$; and $Pr(Si)_n^-$, $4 \leq n \leq 9$. Even though each rare earth element possesses a different number of f-electrons, we found striking spectral similarities among groups of $RE(Si)_n^-$ clusters having the same rare earth oxidation numbers. This implied that their f-electrons were not strongly interacting with their silicon environments, suggesting the possibility of high magnetic moments. Measured electron affinity trends implied encapsulation at n=12 for the +2 oxidation state rare earths and at n=10 for the +3 cases.

Transition Metal-Molecular Organic Complexes Transition metal-organic complexes in which one or more transition metal atoms interact with one or more organic molecules exhibit a wide variety of structural, electronic, and magnetic properties, these being largely the result of their proximate d-electron – π-electron interactions. These complexes may be considered as models for the interaction of transition metal atoms and clusters with surfaces. Small transition metal clusters often have larger per-atom magnetic moments than the same metal in its bulk state. If these metal clusters were deposited onto suitable substrates, with organic films being important candidates, there is potential for information storage applications. To acquire information about these properties, we have measured the photoelectron spectra of size- and composition-selected, transition metal-organic molecular cluster anions. Not only do these spectra relate the electronic properties of the cluster anions to their corresponding neutral forms, but they also provide the energy differences between the neutrals' ground and various electronically excited states. Simultaneously, our theoretical collaborators, Dr. P. Jena and Dr. A. Kandalam calculated the geometries and corresponding energies of the same cluster anions and their neutral counterparts using density functional theoretical methods. This allowed them to predict the photoelectron spectra that we measured along with electron affinities and vertical detachment energies. A match between their calculated values and our spectra validated their calculations. In addition to providing geometries and electronic energy differences, their calculations also provided spin multiplicities. These imply the values of spin magnetic moments, since the spin multiplicity (2S + 1) minus one (1) equals 2S, the value of the spin magnetic moment in units of Bohr magnetons, μ_B. We and our theoretical collaborators have applied this synergetic protocol to the following transition metal-organic molecular anion complexes: $Co_n(benzene)_m^-$, $Ti_n(benzene)_m^-$, $Ni_n(benzene)_m^-$, $Co_n(pyridine)_m^-$, $Co_n(coronene)^-$, $Fe_n(coronene)_m^-$, $Co_n(pyrene)_m^-$, $Fe_n(pyrene)_m^-$, $Co(COT)^-$, and $Fe_n(COT)^-$. Our results with transition metal-organic complexes confirmed the existence of sandwich structures and found that organic molecules can exert strong influences on the magnetic properties of transition metal atoms or clusters. Also quite importantly, our experimental/theoretical studies of both anionic and neutral $Fe_2(organic)_{1,2}$ and $Co_2(organic)_{1,2}$ clusters showed that their metal atoms tend to aggregate instead of being separated by organic molecules. The tendency for aggregation of metal atoms in transition metal - organic complexes has important implications for transition metal *atom*-decorated nanostructures as hydrogen storage materials.

Heavy Group IV Element-Encapsulated, Transition Metal Atom Clusters The synthesis of laboratory quantities of transition metal encapsulated tin and lead cluster solids has sparked considerable interest, these being bona vide cluster based materials with potentially exciting optical and magnetic properties. In cooperation with Eichhorm who synthesized them and with Pederson who did calculations on them, we have measured the photoelectron spectra of $Pt@Pb_{12}^-$ and related clusters, finding close correlations with bulk structural determinations and with theoretical calculations.

Non-Metal to Metallic Transitions Following up on our earlier work on this topic, we have measured the evolving anion photoelectron spectra of manganese and calcium cluster anions and collaborated with several theorists in the process. Results include the discovery of half-metallicity in manganese clusters with Jellinek, the determination of the geometric structure of Mn_{13}^- with Gutsev and Bauschlicher, and the mapping of the electronic structure of Ca_n with Blaisten-Barojas.

Zintl Phase Clusters The term, Zintl anion, refers to the family of multiply-charged polyatomic anions formed by the heavier (and mildly electronegative) post-transition elements. Zintl anions can combine with cations of highly electropositive elements, such as alkali metals, to form solids and "melts" which are usually referred to as Zintl phases. These are important because they are bulk scale precedents

for cluster-based materials. We have continued our work with sodium-tin clusters, mesurung anion photoelectron spectra of $(Na_nSn_4)^-/(Na_nSn_4)$, n=0-4 and $(NaSn_m)^-/(NaSn_m)$, m=4-7. Collaborative work with Khanna has been very productive in determining the structures of these species though comparisons with his calculations.

Baby Crystals of Lead Sulfide Only a few clusters are known to form tiny cuboids due to the packing of their atoms into well-defined nano-lattices. Our work with $(PbS)_n^-$ together with the calculations of Kiran suggest that these systems fall into that category.

Transition Metal Oxides We have also studied the electronic properties of several transition metal oxides, measuring electron affinities and assigning electronic spectra of systems such as TaO^-, TaO_2^-, and TaO_3^-.

Cluster Deposition and TEM Studies of Possible Inorganic Fullerenes Together with Gantefoer and Pennycook, we have been involved in depositing mass-selected beams of molybdenum sulfide clusters and examining them with HR TEM. The expected geometric structures of the deposited clusters appear to correlate with the shapes of Pennycook's TEM images, raising the possibility that we have made and observed some exciting structures.

Future Plans

Clusters possess many novel properties, but to harness them, most clusters will have to be deposited on surfaces, where interactions between them and their substrates may alter the clusters' original properties. Thus, it is important to determine how the intrinsic properties of clusters are changed by surface interactions. To address this issue, experiments are needed that measure both the properties of free (gas phase) clusters and those same properties of the same cluster sizes and compositions deposited on various substrates. The key property to measure is electronic structure, since it is linked to optical characteristics, geometric structure, magnetism, and reactivity. Electronic structure can be measured directly in both the free and the supported cluster environments. We plan a research effort with two, highly complementary parts to do just that. In one part, we will conduct photoelectron spectroscopic studies of size- and composition-selected cluster anions of materials science interest to map the intrinsic electronic properties of their *neutral* counterparts under conditions which are free from environmental effects. Photoelectron spectroscopy (PES) of anions provides HOMO-LUMO gaps and electronic state splittings (electronic spectra) for their corresponding neutrals. In the other part, we will deposit the *same* size and composition, mass-selected cluster anions onto suitable substrates, where we will use *in situ* scanning tunneling microscopy (STM) and ultraviolet photoelectron spectroscopy (UPS) to measure the electronic properties of their *neutral* counterparts. [Mass-selected cluster anions will be soft-landed, where they will lose their negative charges to the surface and become neutral clusters.] STM measurements will be performed to measure the HOMO-LUMO gaps of individual clusters, while at higher coverages, UPS will supply information on their densities of states (electronic spectra). In this way, the same electronic properties (HOMO-LUMO gaps and electronic spectra) will be mirrored both in the gas phase and on surfaces for the same size and composition (neutral) clusters, thereby determining how the electronic properties of free clusters are modified by their interactions with substrates.

This work will involve two sophisticated apparatus, an anion photoelectron spectrometer and a cluster deposition/surface characterization apparatus. The latter apparatus was recently brought to Johns Hopkins from Konstanz University in Germany by Prof. Gerd Gantefoer on long-term loan as part of the collaboration between himself, us, and Prof. Howard Fairbrother, a surface chemist and colleague of mine. Both apparatus are located either in or near my lab. In addition to his home position, Dr. Gantefoer holds an appointment as Research Professor at Johns Hopkins University.

We are proposing to conduct beam/deposition studies on five categories of cluster systems. (1) Clusters in which Group IV atoms encapsulate transition metal or rare earth metal atoms, such as $Pt@Pb_n$. The macroscopic counterparts of some such clusters have been synthesized. (2) Gold-silica and gold-iron clusters. These are of interest due to their optical absorption and/or their magnetic properties. (3) Small

clusters of divalent metals, eg., Mg_n, which are known to have large HOMO-LUMO gaps. (4) Zinc oxide clusters doped with transition metal atoms, eg., $Co(ZnO)_n$. These are models of dilute magnetic semiconductor candidates. (5) Transition metal and rare earth metal/organic molecular complexes, such as $Fe_n(coronene)_m$. Depending on their sizes and compositions, such complexes are thought to exhibit extended sandwich ('nanowire') and 'rice-ball' geometric structures. We will have considerable theoretical support from Dr. Jena, a solid state theorist at Virginia Commonwealth University who is well known for his work with clusters. Also, Dr. Eichhorn, an inorganic chemist at the University of Maryland will provide us with samples of his endohedral Group IV cluster compounds, and Dr. Pederson, a solid state theorist formerly at the Naval Research Laboratory will supply theoretical support for that topic.

References to Publications of DOE-Sponsored Research (2006-2008)

1. "Structure and Stability of $Co_n(pyridine)_m^-$ Clusters: Absence of Metal Inserted Structures", B. D. Edmonds, A. K. Kandalam, S. N. Khanna, X. Li, A. Grubisic, I. Khanna, and K. H. Bowen, J. Chem. Phys. 124, 074316/1-6 (2006).
2. "Mn_n^- Clusters: Size-Induced Transition to Half-Metallicity", J. Jellinek, P. H. Acioli, J. Garcia-Rojeda, W. Zheng, O. C. Thomas, and K. H. Bowen, Phys. Rev. B, 74, 153401/1-4 (2006).
2a. "Mn_n^- Clusters: Size-Induced Transition to Half-Metallicity", J. Jellinek, P. H. Acioli, J. Garcia-Rojeda, W. Zheng, O. C. Thomas, and K. H. Bowen, selected for republication in the Virtual Journal of Nanoscale Science & Technology, 14, issue 16 (2006).
3. "Photoelectron Spectroscopy of Metal, Metal/Organic, and Biological Cluster Anions", W.-J. Zheng, J. M. Nilles, D. Radisic, S. T. Stokes, B. A. Trotter, S. Eustis, A. Grubisic, X. Li, and K.H. Bowen, in Proc. of Indo-US Conference on Materials and Biological Applications, ed. S. N. Saku, R. K. Choudhury, and P. Jena, (Nova Publishers, New York, 2006).
4. "The Ionic KAl_{13} Molecule: A Stepping Stone to Cluster-Assembled Materials", W. Zheng, O. C. Thomas, T. P. Lippa, S.-J. Xu, and K. H. Bowen, J. Chem. Phys. 124, 144304/1-5 (2006).
5. "Ground State Structures and Photoelectorn Spectroscopy of $[Co_m(coronene)]^-$ Complexes", A. K. Kandalam, B. Kiran, P. Jena, X. Li, A. Grubisic, and K. H. Bowen, J. Chem. Phys. 126, 084306/1-9 (2007).
6. "Anion Photoelectron Spectroscopy of TaO_n^- (n=1-3)", W.-J. Zheng, X. Li, S. Eustis, and K. H. Bowen, Chem. Phys. Lett. 460, 68-71 (2008).
7. "Electronic and Geometrical Structure of Mn_{13} Anions, Cations, and Neutrals', G. L. Gutsev, M. D. Mochena, C. W. Bauschlicher, Jr., W.-J. Zheng, O. C. Thomas, and K. H. Bowen, J. Chem. Phys. 129, 044310/1-5 (2008).
8. "Photoelectron Spectroscopic Study of Iron-Benzene Cluster Anions", W.-J. Zheng, S. N. Eustis, X. Li, J. M. Nilles, O. C. Thomas, K. H. Bowen, and A. K. Kandalam, Chem. Phys. Lett., **462**, 35-39 (2008).
9. "Photoelectron Spectroscopy of Europium-Silicon Mixed Cluster Anions, $EuSi_n^-$ ($3 \leq, n \leq 17$)", A. Grubisic, H-P Wang, Y.J. Ko, and K.H. Bowen, J. Chem. Phys. **129**, 054302/1-5 (2008).
10. "Photoelectron Spectroscopic and Theoretical Studies of $Fe_m^-(Coronene)_n$ (m=1,2, n=1,2) Complexes", X. Li, S. N. Eustis, K. H. Bowen, A. K. Kandalam, and P. Jena, J. Chem. Phys. **129**, 074313/1-11 (2008).
11. "Photoelectron Spectroscopic Study of the Anion Transition Metal-Organic Complexes, $[Fe_{1,2}(COT)]^-$ and $[Co(COT)]^-$', X. Li, S. N. Eustis, K. H. Bowen, A. K. Kandalam, and P. Jena, J. Chem. Phys. (in press).
12. "Photoelectron Spectroscopy and Theoretical Studies of $[Co_m(Pyrene)_n]^-$ (m = 1,2 and n = 1,2) Complexes", A. K. Kandalam, P. Jena, X. Li, S.N. Eustis, and K. H. Bowen, J. Chem. Phys. (in press).
13. "Heteroborane Analogs of Silicon Clusters: Experimental and Theoretical Studies of Bi_2Si_5", X. Li, H.-P. Wang, A. Grubisic, D. Wang, K. H. Bowen, M. Jackson, and B. Kiran, J. Chem. Phys. (in press).

Structure and Phase Transformations of Nanophases Embedded in Solids

U. Dahmen and V. Radmilovic
National Center for Electron Microscopy
Lawrence Berkeley National Laboratory
Berkeley, Ca 94720
Emails: UDahmen@lbl.gov; VRRadmilovic@lbl.gov

Program Scope

This program is aimed at understanding the fundamental features that underlie the behavior of nanoscale phases embedded in a solid matrix and their role in the evolution of microstructure in materials. Because of the scale and nature of such microstructures, electron microscopy is an integral part of these investigations - as an analytical tool as well as a subject of technique development. The goal is to understand and ultimately gain control of the structure, distribution and shape of nanophase inclusions by establishing the basic relationship between crystallographic variables and microstructural features. Such relationships are put to use both analytically, to examine the structure of particles and defects, and synthetically, to produce new and unique microstructures with defect configurations reflecting composite symmetries. The ability to observe the kinetics and mechanisms of phase transformations directly by electron microscopy and to correlate the effects of size and shape with measurable local properties is a key element of this research. The fundamental principles established using model alloy systems are employed in the design and testing of new materials such as Al-based alloys of interest for energy-related technologies.

The long-term objective is to develop an understanding of individual embedded nanostructures as a function of their size, shape and embedding parameters such as elastic strain and crystallographic alignment. This understanding will be critical for the application of nanomaterials because it addresses the fundamental question of their interaction with a solid environment.

Recent Progress

In collaboration with the Hamilton group at Sandia, we have developed an explanation of our observation that nanoprecipitates of Pb in Al have shapes that depend on size. This theory predicts a series of "magic shapes" in good agreement with the experimental observations.

A unique microstructure of sputter deposited thin films has been utilized to create new NEMS devices and to study the resonance properties of 20 nm thick cantilevers fabricated from a metallic Al–32 at. %Mo nanocomposite. The strength and near-atomic surface smoothness of this alloy enable fabrication of single-anchored metallic cantilevers with length-to-thickness ratios as high as 400:1. This yields uniquely compliant structures with exquisite force sensitivity.

After our earlier discovery of a core-shell precipitate structure in ternary Al-Sc-Zr alloys we have performed detailed TEM characterization of these unique structures and found the Zr to be distributed primarily in a shell surrounding a Sc-rich core. It was subsequently shown by Clouet et al. that the Zr-rich shell acts as a diffusion barrier and modifies the growth rate of the Sc-rich core, slowing down precipitation kinetics. Recent elastic modeling by the group of Voorhees indicates an equilibrium shell thickness close to the observed range.

Based on previous work under this program, we have now been able to produce more pronounced core-shell precipitates by adding lithium to ternary Al-Sc-Zr alloys. By exploiting kinetic and thermodynamic parameters, we were able to obtain an extremely uniform distribution

of monodisperse particles with a Sc-rich core surrounded by a Li-rich shell a few nanometers thick. The structure and kinetics of these core/shell precipitates has been studied by means of aberration-corrected electron microscopy, supplemented by atom probe tomography.

Figure 1 illustrates the microstructure of the alloy. The superlattice dark field image in (a) shows a monodisperse array of precipitates with a bright shell surrounding a dark core. The high resolution image in (b) demonstrates the fully ordered $L1_2$ structure of the shell. Energy filtered jump ratio maps of Li and Sc (b,c) indicate that Sc is confined to the core while Li is primarily located in the shell. The aberration-corrected ADF STEM image of the core/shell interface confirms that the core region also maintains $L1_2$ order, with the bright Sc atom columns defining a square pattern (d).

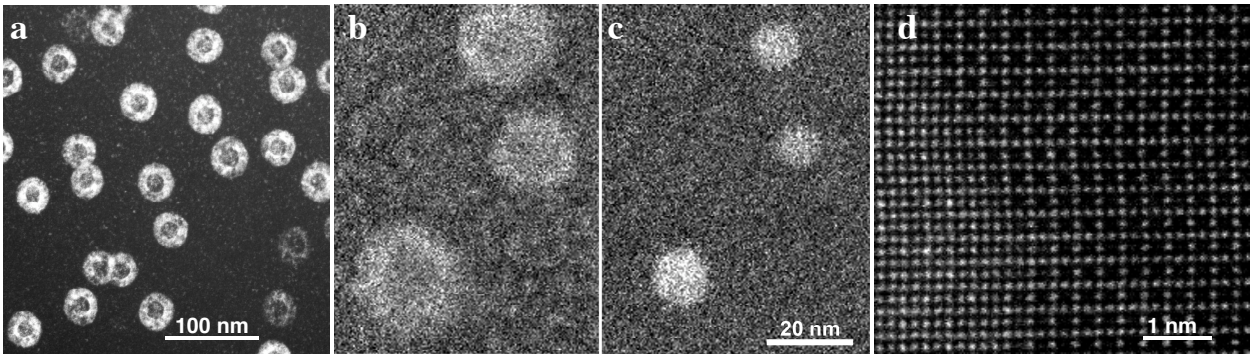

Figure 1: Dark field image of an Al-(LiScZr) alloy (a); energy filtered jump ratio maps of three core/shell precipitates showing distribution of Li (b) and Sc (c); low-pass filtered HAADF image recorded on TEAM 0.5 microscope (d) of the core/shell interface viewed along the [001] zone axis.

From a focal series recorded on the TEAM 0.5 instrument we reconstructed the exit-plane wave function of one of the precipitates. The phase of the exit wave in Figure 2a clearly resolves the Li columns and reveals the Al_3Li long range order. Data on Li partitioning obtained by detailed EFTEM spectrum imaging (see Figure 2b) are in excellent agreement with atom probe tomography results.

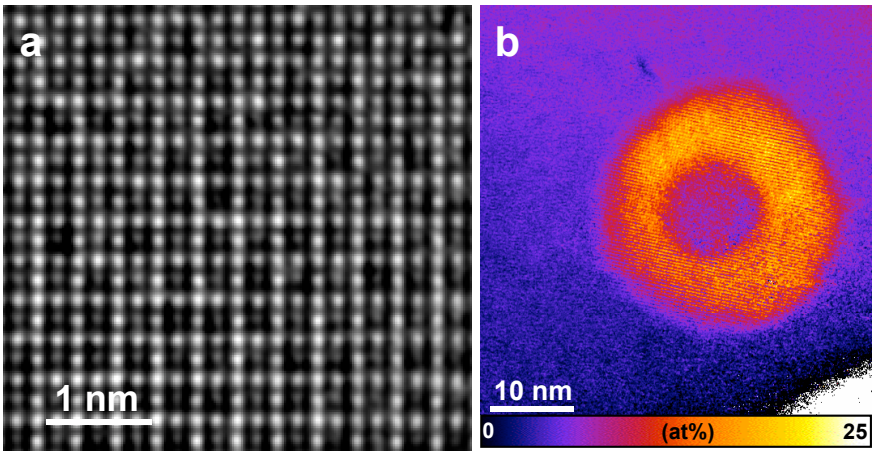

Figure 2: (a) exit wave reconstruction from 20 experimental images obtained at 300 kV showing Li columns at interface between core and shell; (b) Li concentration from EFTEM spectrum image mapping plasmon peak position using monochromated beam at 80kV.

This work shows that the Al_3(LiScZr) precipitates are based on Li-rich clusters that form by congruent ordering during spinodal decomposition after quenching. These Li-rich clusters serve as heterogeneous nucleation sites for the formation of Sc-rich precipitates during high-temperature aging. The Li-rich shell forms during subsequent low-temperature aging when Li atoms precipitate on the Sc-rich core. Our approach utilizes spinodal decomposition to generate uniformly distributed transient Li-rich clusters as transient nuclei for a two stage precipitation

sequence, which exploits the different mobilities of Li and Sc in Al. This approach to generating precipitate distributions can be applied to a range of alloys and could lead to new types of dispersion-strengthened materials.

Future Plans:

We will explore the mechanisms underlying the remarkable core-shell structures in Al-Li-Sc alloys by further detailed characterization of its microstructure and mechanical properties. The experimental characterization will be supported by a parallel computational effort in M. Asta's group to understand the energetics that underly the kinetic and thermodynamic behavior of these alloys. We also plan to modify the material with additions of other elements to enhance the alloy's strength.

A parallel collaboration with Asta's group will focus on interfaces between solid Al and liquid Pb and Pb alloys. This work will concentrate on the factors that control size-dependent behavior such as shape equilibration, Brownian motion, premelting, superheating and solubilities.

Our work on Al-Mo alloys will be extended to similar alloy systems and supplemented with a recently-built resonance frequency test device that can be operated in-situ during observation in an SEM.

Building on our collaboration with the Ramesh group on multiferroic perovskite/spinel films, we will test the possibility of growing mazed bicrystal oxide films with controlled morphology and crystallography.

Publication 2006-2008:

V. Radmilovic, A. Tolley, E.A. Marquis, M.D. Rossell, Z. Lee and U. Dahmen, "Monodisperse Al3(LiScZr) Core/Shell Precipitates in Al Alloys", Scripta Materialia 58, 529–532 (2008)

C.S. Roper, V. Radmilovic, R.T. Howe, and R. Maboudian, “Effects of annealing on residual stress and strain gradient of doped polycrystalline SiC thin films”, Elecrochemical and Solid State Letters, 11, D35-37 (2008)

S.I. Prokofjev, E. Johnson, V.M. Zhilin and U. Dahmen, "Dissolution Kinetics of Nanoscale Liquid Pb/Bi Inclusions at a Grain Boundary in Aluminum", Journal of Materials Science, 43, 3894-99 (2008)

E. Luber, R. Mohammadi, C. Ophus, Z. Lee, N. Nelson-Fitzpatrick, K. Westra, S. Evoy, U Dahmen, V. Radmilovic and D. Mitlin, "Tailoring the Microstructure and Surface Morphology of Metal Thin Films for Nano-Electro-Mechanical Systems Applications", Nanotechnology 19,125705 (2008)

C. Ophus, N. Nelson Fitzpatrick, Z. Lee, E. Luber, C. Harrower, K. Westra, U. Dahmen, V. Radmilovic, S. Evoy, and D. Mitlin, “Resonance properties and microstructure of ultracompliant metallic nanoelectromechanical systems resonators synthesized from Al–32 at. %Mo amorphous-nanocrystalline metallic composites”, Applied Physics Letters 92, 123108 (2008).

V. Radmilovic, U. Dahmen, D. Gao, C.R. Stoldt, C. Carraro and R. Maboudian "Formation of < 111 > fiber texture in beta-SiC films deposited on Si(100) substrates." Diamond and Related Materials 16, 74-80 (2007)

N. Nelson-Fitzpatrick, C. Ophus, E. Luber, L. Gervais, Z. Lee, V. Radmilovic, D. Mitlin, S. Evoy, “Synthesis and characterization of Au-Ta nanocomposites for nanomechanical cantilever devices”, Nanotechnology, 18 355303 (2007)

V. Radmilovic, C. Taylor, Z. Lee, A. Tolley, D. Mitlin and U. Dahmen "Nanoindentation properties and the microstructure of grain boundary precipitate-free zones (PFZs) in an AlCuSiGe alloy." Philosophical Magazine 87 3905-19 (2007)

E. Spiecker, V. Radmilovic and U. Dahmen "Quantitative TEM analysis of 3-D grain structure in CVD-grown SiC films using double-wedge geometry." Acta Materialia 55 3521-30 (2007)
S.I. Prokofjev, V.M Zhilin, E. Johnson and U. Dahmen, "Effect of Morphology on the Mobility of Nanosized Liquid Pb Inclusions in Solid Al", Diffusion and Defect Data 264, 55-61 (2007)
J. C. Hamilton, F. Leonard, E. Johnson and U. Dahmen, "Pb Nanoprecipitates in Al: Magic-Shape Effects due to Elastic Strain", Phys. Rev. Lett. 98, 236102 (2007)
M.D. Rossell, L.H. Zhang, and U. Dahmen, " Step Energy Analysis of Liquid Inclusions of Pb with Cd, In and Sn in Solid Al", Microsc. Microanal. 13, 1042 (2007)
U. Dahmen and T. Radetic, "Mazed Multicrystal Thin Films Grown on Single Crystal Templates", Proc. 1er Coll. 3M, Palaiseau 2007, ed, H. Hardouin Duparc, 39-45 (2007)
H. Zheng, Q. Zhan, F. Zavaliche, M. Sherburne, F. Straub, M.P. Cruz, L.Q. Chen, U. Dahmen and R. Ramesh, "Controlling Self-Assembled Perovskite-Spinel Nanostructures, Nano Letters 6, 1401 (2006)
H. Zheng, F. Straub, Q. Zhan, P.L. Yang, W.K. Hsieh, F. Zavaliche, Y.H. Chu, U. Dahmen and R. Ramesh, "Self-assembled Growth of BiFeO3-CoFe2O4 Nanostructures", Advanced Materials 18, 2747 (2006)
V. Radmilovic, M.K. Miller, D. Mitlin and U. Dahmen, "Strain-compensated nano-clusters in Al-Si-Ge alloys", Scripta Materialia, 54 (2006) 1973-78.
D. Mitlin, V. Radmilovic, T.-Y. Pan, Z. Feng, M. L. Santella, "Structure-Properties Relations in Spot Friction Welded (also known as Friction Stir Spot Welded) 6111 Aluminum", Materials Science and Engineering A, 441 (2006) 79-96.
E. Spiecker, V. Radmilovic and U. Dahmen, "Double-Wedge Technique for Quantitative Analysis of 3-D Structure in Thin Films", IMC16, 1325 (2006)
E. Johnson, S. Prokofjev and U. Dahmen, "In-Situ TEM Analysis of 1-D Brownian Motion of Liquid Pb Inclusions in Al", IMC16, 919 (2006)
E. Spiecker, A.K. Schmid, A.M. Minor, U. Dahmen, S. Hollensteiner and W. Jäger, "Self-Assembly of Linear Nanocavity Networks on Layered Crystal Surfaces" IMC16 (2006)
F. Dietz, E. Spiecker, H. Schroeder, U. Dahmen, and W. Jäger, "Nanowire Formation on Self-Assembled Nanofold Networks of Layered Crystal Surfaces", IMC16 1849 (2006)
E. Spiecker, A.K. Schmid, A.M. Minor, U. Dahmen, S. Hollensteiner, W. Jäger, "Nanocavity Networks by Folding Sheets of Layered Crystals", Microsc. Microanal. 12, 564 (2006)
S. I. Prokofjev, E. Johnson, V. M. Zhilin and U. Dahmen, "Influence of Elasticity of Dislocations on Thermal Motion of Trapped Liquid Pb Inclusions in Al", Advances in Science and Technology Vol. 46, 98-103 (2006)
Sugar, J.D., J.T. McKeown, A.M. Glaeser, R. Gronsky and V. Radmilovic "Spatially confined alloy single crystals for model studies of volumetrically constrained phase transformations." Applied Physics Letters 89, 17 (2006).
V. Radmilovic, C. Taylor, A. Tolley, D. Mitlin and U. Dahmen, "Nanoindentation Properties and the Microstructure of Grain Boundary Precipitate-Free-Zones (PFZs) in an AlCuSiGe Alloy", Philosophical Magazine, 87, 3905-19 (2007)
Z. Lee, C. Ophus, L. M. Fischer, N. Nelson-Fitzpatrick, K. L. Westra, S. Evoy, V. Radmilovic, U. Dahmen, and D. Mitlin, "Metallic NEMS Components Fabricated from Nanocomposite Al-Mo Films", Nanotechnology 17, 3063 (2006)
C.S. Roper, V. Radmilovic, R.T. Howe and R. Maboudian "Single-source chemical vapor deposition of SiC films in a large-scale low-pressure CVD growth, chemical, and mechanical characterization reactor." Journal of the Electrochemical Society 153, C562-66 (2006)
L. Gremillard, E. Saiz, V.R. Radmilovic and A.P. Tomsia "Role of titanium on the reactive spreading of lead-free solders on alumina." Journal of Materials Research 21, 3222-33 (2006)

The National Center for Electron Microscopy

U. Dahmen
National Center for Electron Microscopy
Lawrence Berkeley National Laboratory
Berkeley, Ca 94720
Email: UDahmen@lbl.gov

Program Scope

The National Center for Electron Microscopy at LBNL was established as a user facility and a forefront research center for electron-optical characterization of materials offering state-of-the-art instrumentation and expertise. Its purpose is to conduct fundamental research relating microstructural, microchemical and micromagnetic characteristics to materials properties and processing parameters; to develop advanced electron microscopy techniques and instrumentation; and to help educate future scientists in the theory and application of electron-optical microcharacterization.

The NCEM was officially dedicated in 1983 after the installation of two unique high voltage microscopes for high resolution and in-situ microscopy. The facility has been maintained at the state-of-the-art by continually updating its instrumentation with unique machines such as the One-Ångstrom Microscope, the Spin Polarized Low Energy Electron Microscope (SPLEEM), a Dual Beam FIB, two monochromated STEM/TEM instruments, an aberration-corrected dedicated STEM and most recently, the world's most advanced electron microscope, the TEAM 0.5 instrument.

NCEM provides scientific researchers with essential resources for electron beam micro-characterization of materials. Since its inception, the facility has played a key role in research efforts carried out by local and visiting national and international scientists. Center facilities are supported by a resident scientific and technical staff. In addition to providing guidance to visiting researchers, NCEM staff scientists actively conduct their own specialized research in materials science.

Recent Progress

The fundamental barrier to improving the electron microscope has been the presence of unavoidable aberrations in rotationally symmetric electromagnetic lenses. However, recent advances in aberration-correcting electron optics have led to increased resolution, sensitivity and signal to noise in atomic resolution microscopy. Building on these developments, the Transmission Electron Aberration-corrected Microscope (TEAM) project is a collaborative effort to redesign the electron microscope around aberration-corrected optics in order to extend the spatial resolution to 50 pm, improve contrast, stability, sensitivity, brightness and energy resolution [1].

The vision for the TEAM project is the idea of providing a sample space for electron scattering experiments in a tunable electron optical environment by removing some of the constraints that have limited electron microscopy until now. The resulting improvements in resolution, the increased space around the sample, and the possibility of exotic electron-optical settings will enable new types of experiments. The TEAM microscope will feature unique corrector elements for spherical and chromatic aberrations, a novel AFM-inspired specimen stage, a high-brightness gun and numerous other innovations that help extend resolution down to the half-Angstrom level.

The project is a collaboration of several DOE-funded efforts (LBNL, ANL, ORNL and FS-MRL) and two commercial partners (FEI and CEOS). Led by NCEM, the project pursues several key developments in parallel, with each partner responsible for a specific set of tasks. The machine is being implemented in two stages – TEAM 0.5 in 2008 and TEAM I in 2009.

The TEAM 0.5 instrument constructed under this project has recently demonstrated information transfer to below 50 pm in both STEM and TEM. The detection of GaN (555) and Au (660) image Fourier components in STEM images at 49 pm and 48 pm, respectively, and the extension of Young's fringes to below 50 pm in TEM mode, illustrated in figure 1, represent major improvements in instrumentation.

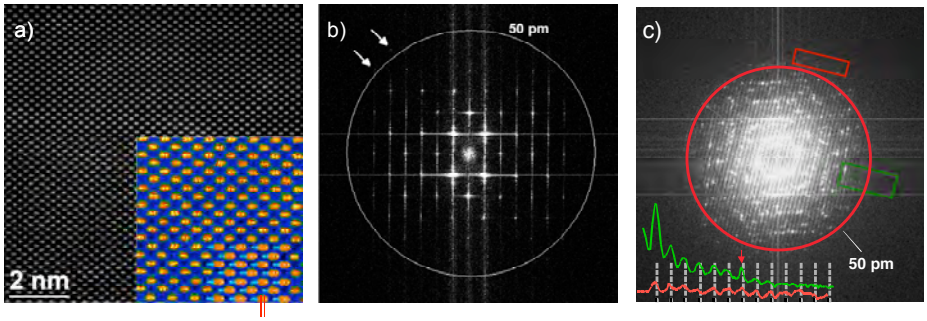

Figure 1. Performance of TEAM 0.5 microscope in STEM and TEM. Aberration-corrected high-resolution STEM image of GaN in [211] orientation (a), showing the 0.63Å distance between Ga dumbbells clearly resolved (see inset model). The corresponding diffractogram in (b) as well as the Fourier diffractogram from high resolution TEM images in (c) show Fourier components and Young's fringes extending beyond the 50 pm mark indicated by circles.

The TEAM 0.5 instrument is a double Cs-corrected microscope with a hexapole aberration corrector on the imaging side that fully corrects aberrations up to third order and partially up to fifth order, and an improved hexapole aberration corrector on the probe side that fully corrects aberrations up to fifth order with an information transfer to 0.05 nm. The machine is equipped with a specially developed high brightness gun and a Wien-type monochromator. A full description of the technical capabilities of TEAM 0.5 can be found at [2]. The instrument is available for user operations starting October 2008.

In the STEM mode, it is possible to exploit the small focal depth of a highly convergent aberration-corrected probe to retrieve detailed structural information from within the crystal volume [3]. Figure 2 shows an extended crystal defect - a buried Σ3 {112} grain boundary – that is visible only if the beam is focused into the crystal. In the TEM mode, high resolution images can be recorded with S/N=10, and single atom sensitivity, as shown for a Au bicrystal in d) [2].

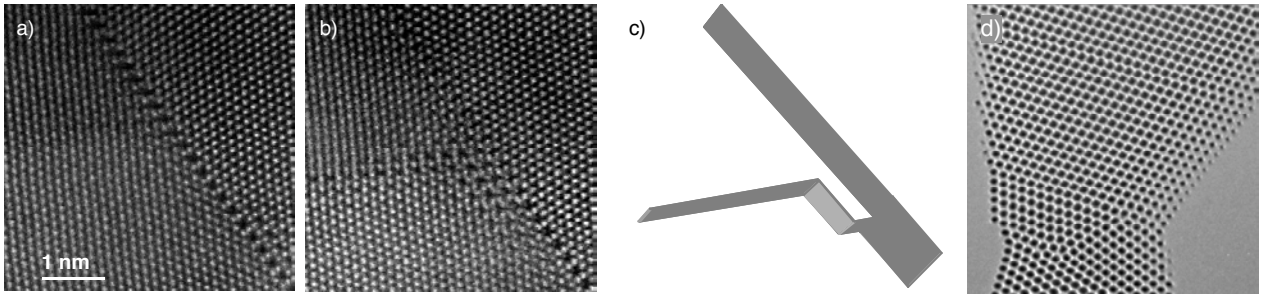

Figure 2a-c) HAADF STEM images of a faceted grain boundary in a Au bicrystal viewed along the [111] direction (a). A buried boundary segment becomes visible only when the probe is focused 6 nm into the sample (b). A schematic of the boundary geometry is shown in (c). The TEM lattice image in d) shows a nanoscale bridge containing a 90° <110> tilt grain boundary.

By operating the instrument at 80kV using the monochromated high-brightness gun, it was possible to maintain sub-Angstrom resolution and record lattice images of single-layer graphene sheets and their defects, such as those shown in Figure 3 [4].

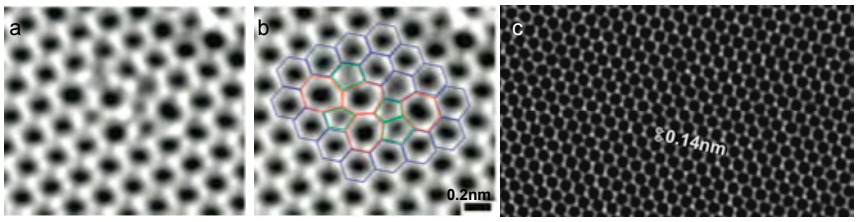

Figure 3 HRTEM images showing defect (a) and configuration (b) consisting of four pentagons (green) and heptagons (red). An exit wave reconstruction (c) shows single C atoms clearly resolved.

The combination of spatial and spectral resolution is critical to many materials properties that depend on localized electronic structure, as for example in nanoparticles or defects. The distribution of indium atoms in GaN was investigated by quantitative TEM imaging and spectroscopy. In suitably prepared samples it was found that spinodal decomposition causes phase separation with a wavelength of a few nanometers. Indium clusters can be present even in InN samples that exhibit spectroscopic features around 0.5-0.8 eV. The VEELS technique suggests a band gap of 1.7 – 2 eV for hexagonal InN [5,6].

Collaborative research between NCEM, Hysitron and GM Research and Development has led to direct observations of complete dislocation starvation in nanoscale Ni pillars using the NCEM quantitative in situ nanoindentation stage [7]. These observations help to explain the strong size effects seen in small volumes. Nanoindentation was also used to confirm superglide along a quasiperiodic grain boundary in gold. By using focused ion beam machining of nanopillars containing suitable grain boundaries in a bicrystalline thin film, it was possible to test specific well-defined grain boundaries and contrast them with other grain boundaries and single crystals. The observations were compared directly to atomistic simulations.

Sample preparation remains a major limitation for electron microscopy. A new double-wedge sample geometry has been developed which allows accurate statistical measurements of graded microstructures [8]. Applying this technique to the structure of CVD-grown polycrystalline cubic SiC films it was possible to characterize the grain size as a function of distance from the substrate. The data are well described by the van der Drift model of faceted film growth with a <111> texture that narrows with distance h from the substrate. It was found that the distribution of grain sizes d(h) is self-similar and the mean grain size follows a power law of the type $\langle d \rangle \sim h^n$. However, the measured exponent n = 0.68±0.1 is significantly larger than that previously predicted from mean field models and computer simulations of three-dimensional film growth (n=0.4). The accuracy of the experimental observations due to the new sample geometry reported here is sufficient to enable statistical tomography or provide guidelines for improved computer modeling [8].

The periodic shell structure and surface reconstruction of metallic FePt nanoparticles with icosahedral structure has been quantitatively studied by high-resolution transmission electron microscopy with focal series reconstruction at sub-angstrom resolution [9]. The icosahedral FePt nanoparticles fabricated by the gas phase condensation technique in vacuum have been found to be surprisingly oxidation resistant and stable under electron beam irradiation. The lattice spacing of (111) planes in the surface region were found to be size dependent and to expand by as much as 9% with respect to the bulk value of Fe52 Pt48. Controlled removal of the (111) surface layers

in situ results in a similar outward relaxation of the new surface layer. This unusually large layerwise outward relaxation is discussed in terms of preferential Pt segregation to the surface forming a Pt enriched shell around a Fe-rich FePt core.

Future Plans:

The recent development of aberration-corrected imaging and spectroscopy under the TEAM project has opened a door toward a new level of characterization, including single atom detection, depth sectioning tomography and atomic column spectroscopy. However, one of the greatest challenges for electron microscopy is 3D tomography at atomic resolution. The techniques currently applied for 3D reconstruction of nanoscale features suffer from artifacts due to projection effects. To overcome these artifacts it is necessary to develop zone axis tomography for a quantitative analysis of the internal atomic and external morphological structure of nanomaterials. This will require developments in stage control for accurate sample tilting, image analysis to linearize the relationship between image intensity and local thickness, and tomographic algorithms that admit external constraints. While this is a complex process, the rewards are great because such a development would fill the gap where current techniques fail, but where much of the scientifically significant processes take place, including facets, edges or corners in anisotropic materials such as catalytic particles. Coupled with new, single electron detectors currently under development, such techniques could also drastically reduce the electron exposure (and associated damage) for tomographic experiments of important energy-related materials such as zeolites or microporous composites.

A key strength of electron microscopy is its ability to observe individual nanoscale phases under constraint from a solid environment. This capability allows us to understand the influence of crystallographic and elastic constraints on the development of self-assembled structures and ensembles. To fully exploit this strength, it will be important to develop specialized sample geometries using synthesis techniques that are available in the nanoscience centers such as the Molecular Foundry. Examples of such sample geometries are layer-doped nanopillars, self-assembled arrays of aligned nanoparticles and atomically flat plane-parallel substrates like graphene or oxide-based crystals, and specialized supports such as single- or multiwall nanotubes and atomically flat substrates such as graphene sheets.

Further plans include the development microscopy techniques capable of imaging the interfaces between soft and hard matter, the development of novel sample preparation techniques, computer algorithms for quantification of data, and the combined use of electron scattering with other probes such as synchrotron scattering and atom probe tomography.

1. http://ncem.lbl.gov/TEAM-project/
2. Kisielowski et al., Microsc. Microanal. 14, 454 (2008)
3. Borisevic et al., J Electron Microsc 55, 7 (2006)
4. Meyer et al., Nano Lett (2008)
5. Kisielowski et al., Physica B 401, 639 (2007)
6. Erni et al., Ultramicroscopy 108, 84 (2008)
7. Minor et al., Nature Mater. 5, 697 (2006), Warren et al., Materials Today 10, 59 (2007)
8. Spiecker et al., IMC16, 1325 (2006), Acta Materialia 55, 3521 (2007)
9. Wang et al., Phys. Rev. Lett. 100, 017205 (2008)

Publication 2006-2008:

A searchable database of NCEM publications is available at http://ncem.lbl.gov/

Program Title: Statics and Dynamics of *Dimensionally* and *Spatially Constrained* Ceramic Oxides

Project Support: Department of Energy, Basic Energy Science Division, Materials Program:
Grant Number: DE-FG02-07ER46444

PI and contact Information: *Vinayak P. Dravid*
Professor, Materials Science & Engineering
Director, NU*ANCE* Center
2220 Campus Drive, Northwestern University
Evanston, IL 60208

E-mail: v-dravid@northwestern.edu

I. Program Scope, Research Approach and Scientific Objectives:

With the advent of sophisticated crystal growth approaches in the recent decade, it has become possible to synthesize complex oxide architectures with atomic and chemical precision comparable to that in semiconductor heterostructures. This promises a *renaissance* period for the traditional field of oxide ceramics, with exciting scientific and technological opportunities.

The natural evolution of functional oxide architecture calls for their *confinement* in *spatial* and *dimensional* modes. Here, *spatial confinement* refers to inevitable attachment of materials to a substrate or an overlayer, for example. *Dimensional* constraint arises from the ubiquitous need for materials to be confined to 0- (i.e., dots), 1- (lines) and 2- (i.e., films/membranes) dimensions to enhance aerial density and possible novel properties. Further, by juxtaposing two or more functional materials in close proximity, there are exciting new opportunities for *synergistic coupling* of disparate phenomena in hybrid confined materials systems.

The research scope and objectives revolve around the critical issues associated with patterning, characterization and functionality assessment of ceramic oxide systems under *spatial and dimensional constraints*, including their *dynamic* evolution and behavior.

A novel approach, based on combination of electron beam lithography and liquid precursor for patterning (positioning) ceramic oxides (i.e., soft-eBL) is being pursued (Fig. 1). The soft-eBL patterning approach synergistically combines the traditional *top-down* with emerging *bottom-up* method..

Both, *ex-situ* and *in-situ* dynamic studies (with TEM and synchrotron x-ray scattering) are undertaken which can provide high temporal and spatial resolution details of the dynamics of microstructure evolution of confined ceramic geometries, with plenty collaborative opportunities for rigorous modeling/simulations of confined ceramics.

The research addresses the following compelling issues in regards to nanopatterned ceramic oxides and heterostructures:

a) Fabrication strategies with exquisite control over size, shape, anisotropy, internal microstructure, for 3-D nanopatterned architecture,
b) Internal and external microstructure control of nanopatterned ceramics oxides,
c) *In-situ* and *ex-situ* monitoring of conversion of precursors to their solid-state form,
d) Atomic scale understanding of interfaces, to evaluate the influence of dimensional and spatial constraints,
e) Size, shape, anisotropy and substrate effects on localized properties and coupling phenomena.

Fig. 1: Schematic of "soft-eBL" approach, indicating its diverse attributes, for nanopatterning of ceramic oxides under *spatial* and *dimensional* constraints.

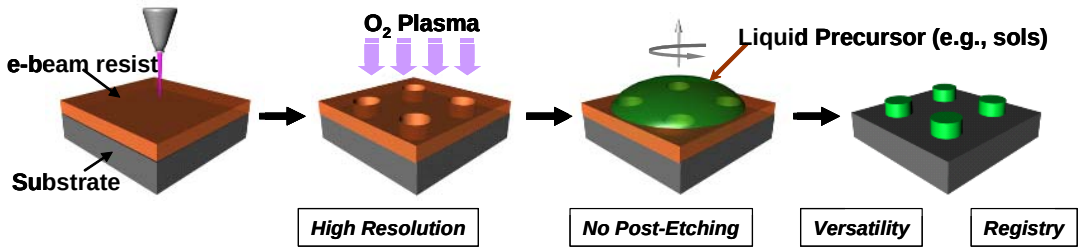

Embedded in the technical scope of the research are fundamental *scientific* questions, including:

1) How can one "*directly*" pattern "*refractory*" oxide ceramics, with size and shape-specificity at the nanoscale, without the recourse of etching or hard processing?
2) How does nucleation and growth from precursor to solid-state form, and the overall microstructure of oxide ceramics evolve under rigorous nanoscale spatial and dimensional constraints?
3) How do internal, external and heterostructure of *spatially and dimensionally* constrained ceramic oxides vary with thermal treatment? i.e., from nanoporous to epitaxial conversion? (e.g., see Fig. 2)

Fig. 2: Strategies to control "*internal*" microstructure of "*constrained*" oxide nanopatterns.

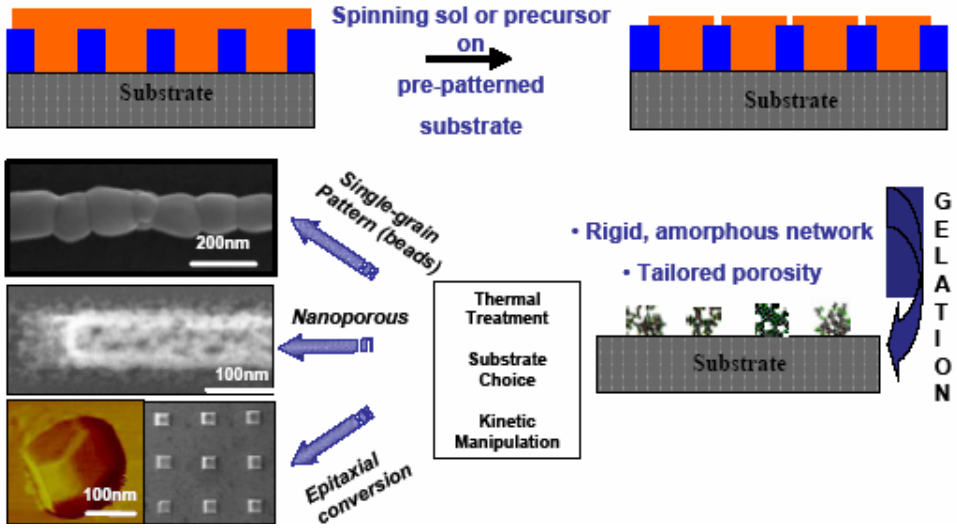

4) How do the "*functional*" characteristics of patterned ceramic oxides (e.g., capacitance, polarization, magnetization etc.) vary with spatial and dimensional constraints (e.g., pattern size, shape, substrate, orientation, strain)?
5) How to *characterize* and *validate* functional form of ceramic oxide patterns at the requisite nano- and atomic length-scales, and under *in-situ* dynamic conditions?

Thus, the combination of innovative patterning approaches for ceramic oxides and their extensive characterization may help open new vistas for fundamental understanding of *constrained* ceramic microstructures with significant implications for their technological applications in diverse energy-related applications.

II. Recent Research Progress:

In the Year-I of the project, we have continued to refine and advance soft-eBL as a versatile nanopatterning approach for complex oxides. We have further expanded the capabilities of soft-*e*BL into patterning diverse ceramics on a multitude of substrates at different dimensionalities, as well as tuning the microstructure and morphology of the nanopatterns by changing the patterning parameters. Finally, the conversion of sol-gel to solid state has been monitored by synchrotron x-ray scattering at ANL/APS, as well as localized strain measurements by nanoprobe diffraction.

The progress in Year-I covered the following themes:

II.1: Development of soft eBL as an enabling approach for spatial and dimensional confinement of ceramic oxide nanostructures: Here, we have developed analytical approaches to optimize eBL dosage for fabricating complex grid-bar nanopatterns (see Fig. 3), to explore the frustration of ferroelectric/ferromagnetic domain configuration in complex geometries.

II.2. Optimization of thermal conversion of sol-gel to enable internal "microstructure" control: Here we are developing thermal treatment and conversion strategies for sol-gel to various solid-state forms, from nanoporous to single-crystal epitaxial forms.

II.3: Implementation of tools and techniques to monitor conversion of sol-gel to solid state structures via electron, synchrotron radiation and scanning probe techniques: We are setting-up an *in-situ* heating stage at APS/ANL to enable real-time monitoring of sol-gel conversion to solid state form. Also, we are developing GISAXS, GIWAXS and nanodiffraction approaches for monitoring solid-state conversion, shape and porosity evolution and interfacial strain.

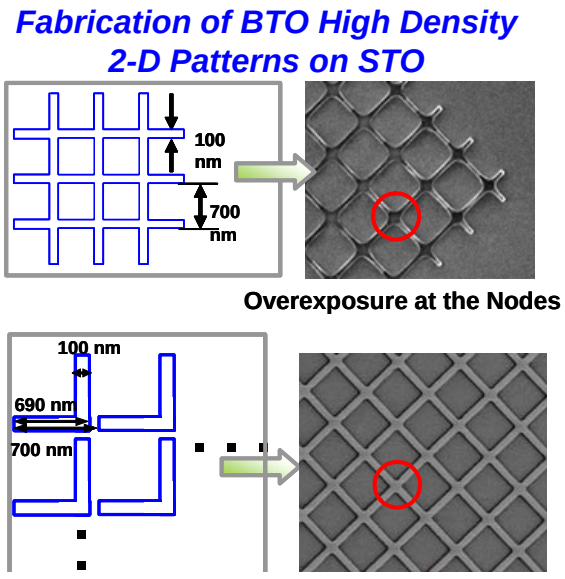

Figure 3: Comparison of traditional eBL approach for "cross" patterns, using traditional geometry and exposure (Top) and new analytical optimization. $BaTiO_3$ on $SrTiO_3$

IV. Planned activities for Year-II:

We will continue to combine innovative soft eBL experiments, coupled with more focused attention to the *in-situ* evolution of their microstructure, coupled with TEM/STEM and SPM measurements of strain and interfacial phenomena.

The specific planned activities include:

a) Soft eBL development for complex geometries and shapes such as grid bars, heterostructures and epitaxial nanopatterns,
b) Initiation of *in-situ* synchrotron and electron microscopy study of nucleation and growth of soft-eBL nanopatterns to their solid-state forms,
c) Interfacial strain measurements in nanopatterns via nanoprobe diffraction, CBED and related diffraction measurements.
d) Advanced TEM/STEM microscopy and SPM measurements of interfaces between nanopatterns and substrate; to understand the role of substrate orientation and interface strain on microstructure evolution.

These observations will be corroborated with S/TEM and SPM in the next period.

V. Publications/Inventions Related to DOE Project:

1. Pan Z, Li S, Wang Z, Yu MF, V.P. Dravid**,** ,"Patterning-controlled morphology of spatially and dimensionally constrained oxide nanostructures", *Applied Physics Letters* Vol: 91(14) 143105 (2007)

2. T. Sun, H. Hu, Z. Pan, X. Li, J. Wang and Vinayak P. Dravid, "In situ real-time investigation of kinetics of nucleation and growth of sol-gel-derived functional oxide thin films", Phys. Rev. B **77**, 205414 (2008)

3. S. Donthu, Z. Pan and V. P. Dravid, "Directed Fabrication of Ceramic Nanostructures on Fragile Substrates using Soft-electron Beam Lithography (soft-eBL)", *IEEE Trans. Nanotech*., in-press, April 2008.

4. T. Sun, S. Donthu, V.P. Dravid and J. Wang, "Effect of Pd doping on the microstructure and gas sensing performance of nanoporous SnO_2 thin films", submitted to *Phys. Rev., B*, July 2008.

5. Method of Making Nanopatterns And Nanostructures And Nanopatterned Functional Oxide Materials, *NU Invention Disclosure*, # 25069, Vinayak Dravid, Suresh Donthu, Zixiao Pan, 2007.

Single Atom and Molecule Manipulation and Its Application to Nanoscience and Nanotechnology
(DE-FG02-02ER46012)

Saw-Wai Hla, hla@ohio.edu, www.phy.ohiou.edu/~hla
Ohio University, Physics & Astronomy Department, OH-45701.

Program Scope

Atomic level understanding of materials properties is increasingly critical to develop power efficient and smart nanoscale devices. The scanning tunneling microscope (STM) manipulation combined with tunneling spectroscopy measurements is one of the most innovative and *unique* experimental techniques to investigate properties of individual atoms and molecules at the atomic limit[1-13]. Using STM tip as an analytical or engineering tool, individual atoms can be extracted from the nanoclusters one atom-at-a-time[-7], controlled excitation of molecules can be realized with single bond precision[4,5], and physical properties of nanoscale systems can be manipulated locally[1]. Thus, scientists now have a tool not only to '*see*' the individual atoms using conventional STM imaging, but also to '*touch*' and '*take*' the atoms or to '*hear*' their vibration by manipulating them with the STM tip[10].

In our research projects, we combine single atom/molecule manipulation schemes with a variety of tunneling spectroscopy measurements to investigate properties specific to the type of atoms or molecules on surfaces[1-13]. The innovative experiments in this project are tailored to address several critical issues covering both fundamental understanding, and development of novel atom/molecule based nanodevices. In particular, we investigate fundamental interactions between the STM tip and individual atoms and molecules, determine the magnitude of forces required to move individual atoms, demonstrate single molecule switches and devices, and explore charge transfer between the electron donor and acceptor molecules on surfaces.

Recent Progress

The atomic scale interaction is a fundamental problem of science. We have shown that just by approaching the STM tip over a silver cluster on a Ag(111) surface, the binding of the top cluster atom is greatly reduced due to the perturbation of the tip. By choosing a suitable tip-cluster distance, individual atoms from the silver cluster could be repeatedly and reproducibly extracted on a one-atom-at-a-time basis (Fig. 1)[7]. This process involves extraction of individual atoms from the cluster and a subsequent manipulation of atoms on the rough terrain of a three-dimensional cluster surface. Here, a mere tuning of the tip-cluster distance governs the atom extraction process. The experiment was conducted at low temperatures (4.6K) under an ultrahigh vacuum environment using a custom-built STM. Silver clusters used for the experiment were deposited on the Ag(111) surface by means of controlled tip-sample contact[11]. For a successful atom extraction from the cluster, the tip-cluster distance between the vdW edges of the atoms should be below 0.06 nm. Thus, this process further demonstrates the ability of controlling distances at a sub-atomic regime. The atom extraction process can be used to investigate the binding strength of atoms to form matter, and to quantitatively probe atomistic interactions on surfaces.

The basic laws of motion demand a force of an appropriate magnitude for the lateral movement of an object on a surface. This requirement extends to the nanoscale where moving individual atoms and molecules require a lateral force to overcome the surface forces against the movement. The ability to determine the lateral force strength at the atomic scale is vital for the development of molecular machines and nanoscale transport systems. We have developed a force measurement scheme by using STM atom manipulation procedure[6]. During manipulation of an atom on a surface, the atom follows the tip by hopping the surface lattice sites. In case of a pulling mode manipulation, the atom initially at rest is moved to the next surface site when the lateral component of attractive force between the tip and

manipulated atom over comes the surface forces[10]. The lateral force (F_{Lat}) is the vector component of the total force, F_{Tot}, and it can be generally described as:

$$F_{Lat} = F_{Tot}\cos\phi(r) = \frac{\Delta U}{\Delta r}\cos\phi(r)$$

where '*r*' is the tip-atom distance, '*U(r)*' is the tip-atom interaction at the distance '*r*', and 'ϕ *(r)*' is the angle between the total and the lateral force directions (Fig. 1). Since both '*r*' and '*cos* ϕ' are measurable quantities, the magnitude of lateral force to move the atoms, F_{Lat}, can be extracted if '*U(r)*' is known. Lateral manipulations of atoms with varying tip-atom distances reveal that the force vector angle between the total and lateral force directions linearly decreases with increasing tip-atom distances. This leads to determine the exponent of the attractive tip-atom potential experimentally, which is a direct measure of the force strength. This technique can be applied for the lateral force measurement of larger molecules including biological molecules on surfaces using a scanning tunneling microscope.

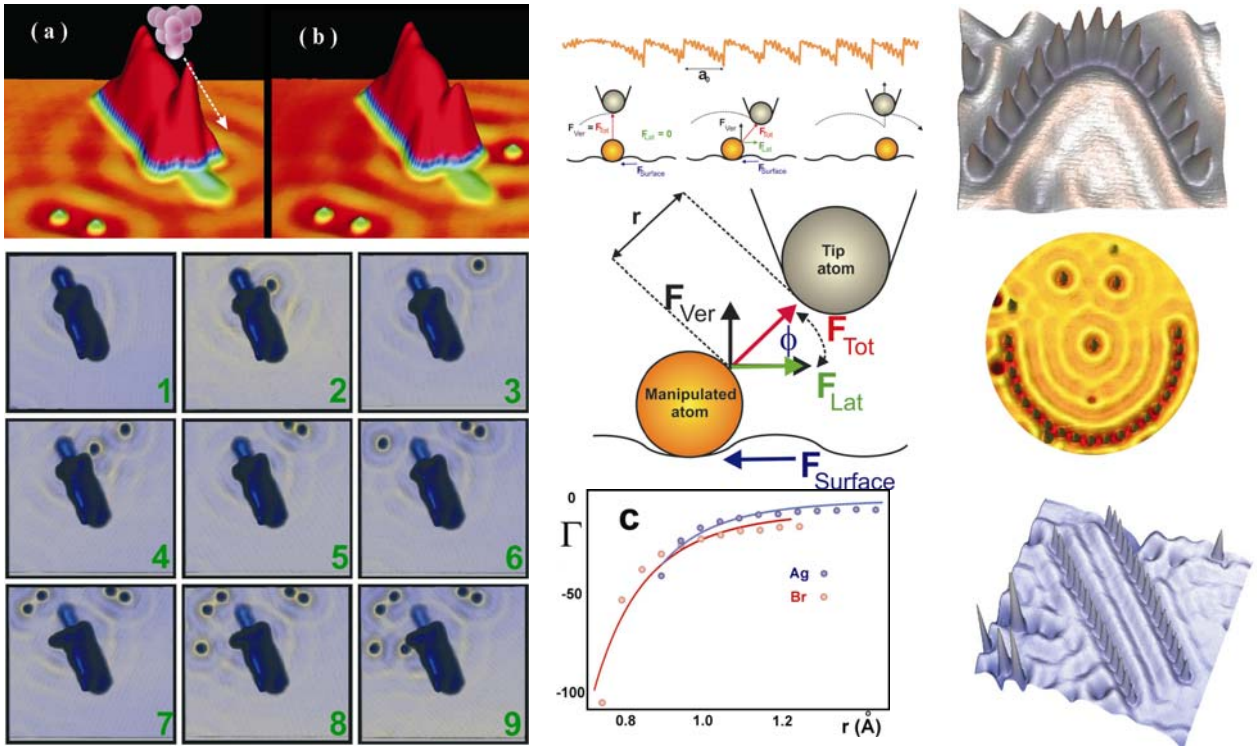

Fig. 1. (Left) (a) and (b). Individual atoms are extracted on an atom-by-atom basis from a silver cluster on a Ag(111) using STM manipulation. A sequence of STM images (1-9) showing repeated extraction of atoms from the cluster. (Right) Various atomic structures constructed by using the extracted atoms. (Middle) Lateral force measurement strategy. An STM tip-height signal shows single atomic site hopping of the atom. The drawings indicate the changes of vertical and lateral force (F_{Ver} & F_{Lat}) components during manipulation. (c) The measured tip-atom interaction potential curves for a silver and a bromine atom on a Ag(111) surface. (Right) Example quantum structures constructed by using extracted atoms from the native surface or from the nanoclusters using STM manipulation.

The interaction between a magnetic impurity and electrons from a nonmagnetic metal surface can give rise to a resonance near the Fermi level, known as the Kondo effect. Studying the changes in spin-electron coupling strength due to the formation of a two dimensional spin-network is important for the better understanding of the Kondo phenomenon, and for the development of spintronic devices[1,5]. We have systematically manipulated the Kondo resonance of Co-TBrPP molecular clusters on Cu(111) surface by using an STM tip (Fig. 2a and 2b). When a molecule is surrounded by other molecules, the surface state electrons are screened by the neighbor molecules resulting in a reduced spin-electron interaction. By removing the neighboring molecules one-at-a-time with the STM-tip, the Kondo effect of a center molecule inside the molecular assembly can be tuned in a controlled manner. This manipulation of the

two-dimensional molecular Kondo effect merges the spintronic research area to a rapidly evolving and most promising field of nanoscience, molecular self -assembly, and it thus opens novel routes for molecular spintronic applications.

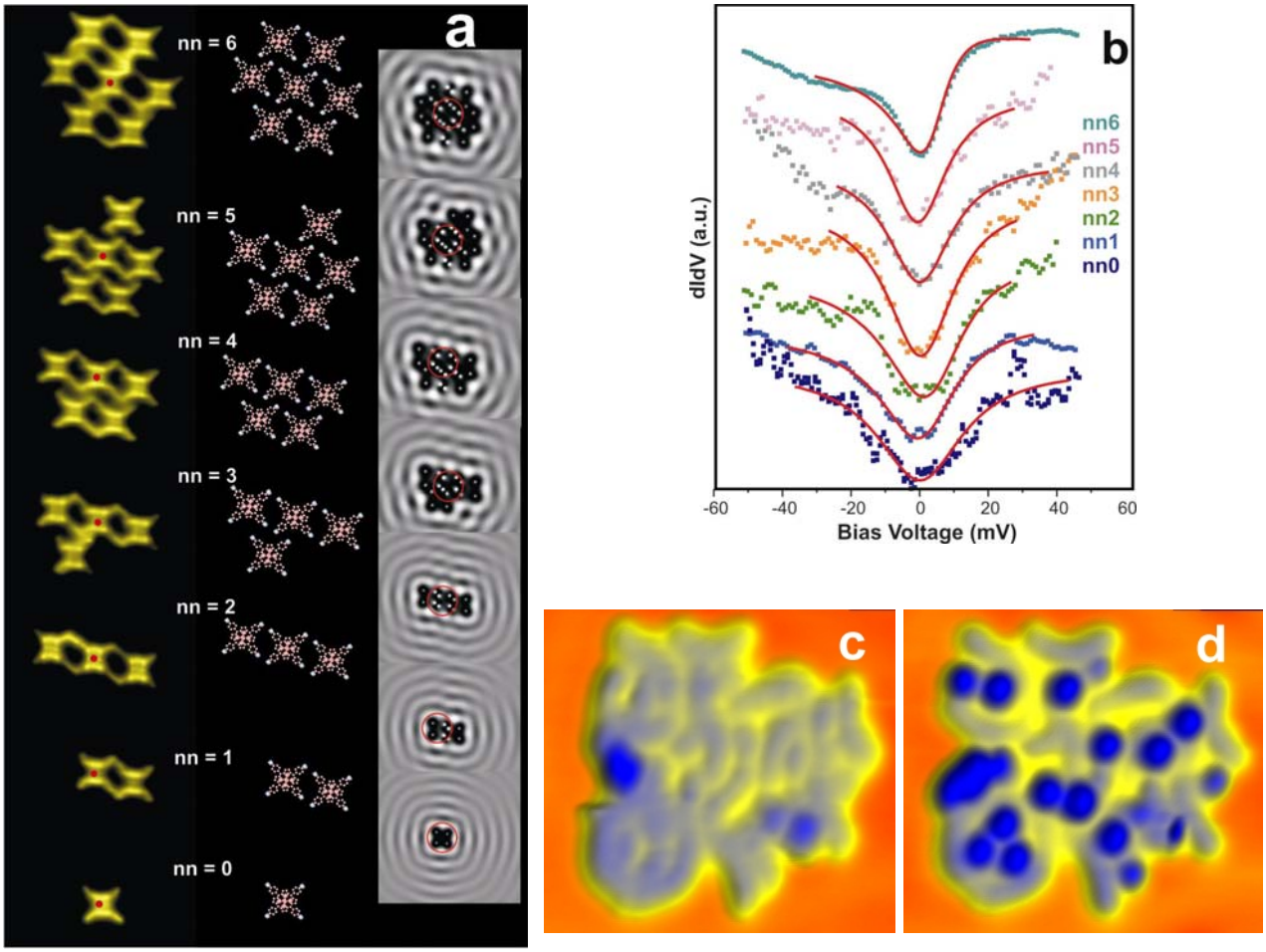

Fig. 2. (a) Individual TBrPP-Co molecules from a small molecular assembly are removed one at-a-time using STM tip. (b) The corresponding dI/dV-V Kondo resonance spectra are measured as a function of nearest neighbor molecule. (c) and (d): Molecular charge transfer switch. The 6T-F_4TCNQ complex imaged at 1.5 V (c). At -1.5 V, the F4TCNQ locations produce a bright contrast due to the charge transfer orbital (d). is realized by manipulating Co-TBrPP molecules with an STM tip (above).

When two types of molecules having opposite tendency to donate and accept electrons are put together, the transfer of electronic charge from one to another can take place. Recently molecular charge transfer complexes have emerged as a novel class of materials having potential applications in molecular magnets, non-linear optics, molecular electronics, and in energy storage devices. During this study, we have directly observed a hybrid molecular orbital formation in the electron donor sexithiophene (6T) and electron acceptor tetrafluoro-tetracyano-quinodimethane (F_4TCNQ) molecular charge transfer complex for the first time. The transfer of charge leads to realignment of molecular orbitals. This is demonstrated as a source for a voltage dependent switching (Fig. 2c and 2d), and it may find potential applications in molecular electronic devices.

Future Plan

We will continue to advance on the fundamental understanding of STM atom/molecule manipulation mechanisms as well as application of this technique in several critical research areas. Using a suitable

selection of STM manipulations and tunneling spectroscopy schemes, we are investigating 1) charge transfer between electron donor and acceptor molecules for molecular electronic and energy storage applications, 2) lateral forces to move individual atoms/molecules for the development of molecular machines, and 3) molecular switches and molecular based nanodevices.

References (DoE sponsored publications from 2006 to 2008)

Refereed Journals:

1. V. Iancu, A. Deshpande, & S.-W. Hla, '*Manipulation of Kondo Effect via Two Dimensional Molecular Assembly*', ***Phys. Rev. Lett.*** **97**, 266603 (2006). (Selected for online publication in Virtual Journal of Nanoscale Science & Technology 15 (2007)).

2. K.-F. Braun, V. Iancu, N. Pertaya, K.-H. Rieder, & S.-W. Hla, '*Decompositional, Incommensurate Growth of Ferrocene Molecules on a Au(111) Substrate*', ***Phys. Rev. Lett.*** **96**, 246102 (2006).

3. G. Newkome, P. Wang, C.N. Moorefield, T.J. Cho, P. Mohapatra, S. Li, S.-H Hwang, O. Lukoyanova, L. Echegoyen, J.A. Palagallo, V. Iancu, & S.-W. Hla, '*Nanoassembly of a Fractal Polymer: A Molecular Sierpinski Hexagonal Gasket*' ***Science*** **312**, 1782-1785 (2006).

4. V. Iancu, & S.-W. Hla, '*Realizing of a Four-Step Molecular Switch in Scanning Tunneling Microscope Manipulation of Single Chlorophyll-a Molecules*', ***Proc. Nat. Acad. Sci.*** **103**, 13718-13721 (2006).

5. V. Iancu, A. Deshpande, & S.-W. Hla, '*Manipulating Kondo Temperature via Single Molecule Switching*', ***Nano Lett.*** **6**, 820-823 (2006).

6. K.-F. Braun, & S.-W. Hla, '*Force Measurement with a Scanning Tunneling Microscope*. ***Phys. Rev. B*** **75**, 033406 (2007). (Selected for online publication in Virtual Journal of Nanoscale Science & Technology 15 (2007), and Virtual Journal of Biological Physics Research 13, Jan (2007).)

7. A. Deshpande, H. Yildirim, A. Kara, D.P. Acharya, J. Vaughn, T.S. Rahman, & S.-W. Hla, '*Atom-by-Atom Extraction using the Scanning Tunneling Microscope Tip-Cluster Interaction'*, ***Phys. Rev. Lett.*** **98**, 028304 (2007).

8. F. Jäckel, U.G.E. Perera, V. Iancu, K.-F. Braun, N. Koch, J.P. Rabe, & S.-W. Hla, '*Investigating Molecular Charge Transfer Complexes with a Low Temperature Scanning Tunneling Microscope*', ***Phys. Rev. Lett.*** **100**,126102 (2008).

9. K.-F. Braun, & S.-W. Hla, '*Charge Transfer in TCNQ-Sexithiophene Complex*', ***J. Chem. Phys.*** **129**, 064707 (2008).

10. S.-W. Hla, '*Scanning Tunneling Microscope Atom and Molecule Manipulations: Realizing Single Molecular Switches and Devices*', ***Jpn. J. Appl. Phys.*** **47**, 6063 (2008).

Refereed Proceedings:

11. V. Iancu, A. Deshpande, & S.-W. Hla, '*Controlling formation of nanodots and nanocavities using scanning tunneling microscope*'**, *IEEE Nano 2006 Proceedings***, 555-557 (2006).

12. A. Deshpande, K. Clark, D.P. Acharya, J. Vaughn, K.-F. Braun, & S.-W. Hla, '*Atomistic Constructions by using Scanning Tunneling Microscope Tip*', ***IEEE Nano 2006 Proceedings***, 562-564 (2006).

13. T. Skeini, J.-F. Steiner, & S.-W. Hla, '*Automated Atomic-Scale Construction*', ***IEEE Nano 2006 Proceedings***, 610-612 (2006).

Towards Atomistic Understanding of Kinetics and Thermodynamics of Phase Transitions and Energy Dissipation at a Single Defect Level by Scanning Probe Microscopy

S.V. Kalinin, S. Jesse, P. Maksymovych (Wigner fellow), A.P. Baddorf
(sergei2, sjesse, maksymovych, baddorfap)@ornl.gov

Postdocs and students: M. Nikiforov, B. Rodriguez,* K. Seal, O. Ovchinnikov (undergraduate)

Oak Ridge National Laboratory, Oak Ridge, TN 37831

Program scope

Kinetics and thermodynamics of phase transitions, order parameter dynamics, and electrochemical reactions alike are universally controlled by interfaces and structural defects. In this program, we aim to elucidate the atomistic mechanisms behind these transformations, bridging the extraordinary volume of phenomenological knowledge amassed in the last century and recent advances in atomic characterization by probe microscopy, STEM/EELS and density-functional theory. This goal is being accomplished through a synergistic effort involving (a) development of advanced Scanning Probe Microscopies capable of probing order parameter dynamics and energy transformation pathways on a single defect level, (b) capabilities for *in-situ* growth and characterization of atomically-controlled oxide surfaces, (c) systems with atomically engineered defect structures, and (d) integration of analytical, atomistic and mesoscopic theories and experimental multidimensional data using projection and clustering methods. Ferroelectric and ferromagnetic materials provide model systems for investigating the role of defects in phase transitions: systems in which bias-induced and field-induced phase transition between two equivalent polarization states is reversible and is not associated with diffusion, mass, or significant heat exchange and strain effects, allowing direct insight into atomistic mechanisms of bias-induced and field induced phase transformations on a single defect level.

Recent Progress

Microscopic and atomistic origins of interfacial functionality in complex oxides. Transition metal oxides exhibit an astonishing variety of intriguing and often useful mesoscopic behaviors that stem from the interplay of electric and magnetic dipoles and atomic structure linked through magnetoelectric, piezoelectric, and electron-phonon coupling. These properties can be induced, amplified, altered and thus controlled by introducing broken symmetry in the form of a surface or interface. Often, this coupling is mediated by a small number of structural defects. There is therefore an urgent need to develop a comprehensive picture of electronic and atomic structure of surfaces, interfaces, and defects in such materials. High-resolution electron microscopy yields this capability for bulk interfaces; however, surfaces and ultrathin films have long remained a challenge due to the intrinsic instabilities when in contact even with minute atmospheric contaminates.

A UHV based system referred to as the **Nanotransport system** combines atomically controlled growth (Pulsed Laser Deposition with RHEED control) and *in-situ* characterization of oxide thin films, incorporating facilities for electron spectroscopy (XPS and Auger), electron diffraction (LEED) and scanning probe microscopy (STM, AFM and NC-AFM). Fig. 1 presents an example of layer-by layer growth of $BaTiO_3/SrRuO_3$ layers. Disordered defects are observed in the atomically-resolved STM image of the $SrRuO_3$ (100) surface. Based on extensive DFT modeling, we believe these to be the result of ejection of SrO adpairs from the top layer to form rock-salt islands with simultaneous stabilization of the remaining RuO_2 surface by O_2 adsorption. Such unusual chemical disorder results in a (2x2) reconstruction of the surface seen by electron diffraction. Growth of $BaTiO_3$

* Currently Humboldt fellow at MPI Halle

on this structure maintains the reconstructed symmetry for 1-2 layers, but for thicker films returns to the expected (1x1) surface structure. This model is supported by STEM, which reveals the presence of interface intermixing in the form of 2 layer deep roughness. The intimate knowledge of the surface structure of $SrRuO_3$ is essential to address the polarization domain structure of ultrathin $BaTiO_3$ films grown on top; these have been experimentally shown to be uniformly polarized down to a thickness of 4 ML.

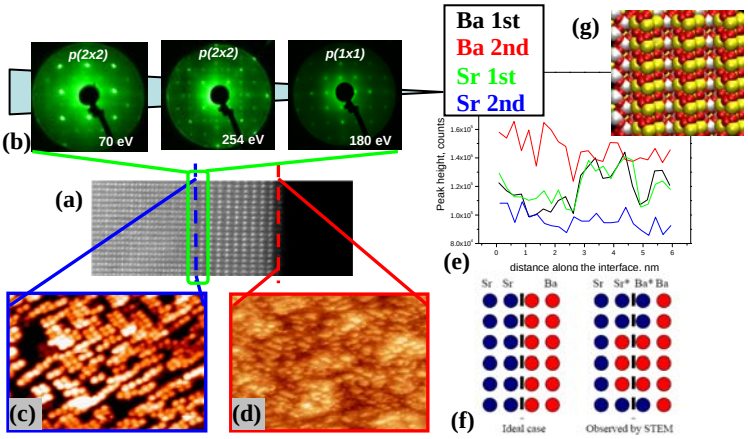

Figure 1. Schematics of atomically controlled materials growth. Shown are (a) STEM image, (b) evolution of LEED images from prostine SRO and after 1 and 10 ML BTO deposition, and atomically resolved images of (c) SRO surface before the deposition and (d) BTO surface after deposition. (e) STEM intensity profile along the interface, evidence for the formation of 2 unit cell deep islands (f) preexisting on the SRO surface. DFT modeling (g) explains the oxygen-induced stabilization of SrO advacancy islands. STEM: A. Borisevich and S. Pennycook, Modeling: V. Meunier (ORNL)

In the future we will apply the comprehensive toolkit of the Nanotransport system to unravel the role of the interface in the electronic and structural properties of oxide superlattices with a particular focus on unit-cell variations in the emergent behavior. This will be achieved through the synergy of *in-situ* growth capabilities with SPM techniques to address spatially resolved functional properties, including order parameter dynamics and energy dissipation, on the nanometer and ultimately atomic levels. Only this combination of environmental control and *in-situ* growth in the Nanotransport system and the nanoscale resolution of SPM will allow us to probe the functionality of surfaces and interfaces in-plane. This will open pathway to understanding antiferrodistortive and structure doubling reconstructions, defect dynamics, and other phenomena, complementing the capabilities of scattering and electron beam techniques.

Imaging local polarization dynamics and switching centers in ferroelectrics: Seminal work by Landauer[1] has demonstrated that the experimentally observed switching fields in ferroelectrics correspond to impossibly large (~10^3 - 10^5 kT) values of the nucleation activation energy. This Landauer paradox is representative of a universally-recognized role of defect centers in controlling the kinetic pathways of solid state and electrochemical reactions and phase transformations. We have developed a spectroscopic approach based on atomic force microscopy (AFM) to visualize and probe individual nucleation centers controlling polarization dynamics. The approach is based on acquisition of multiple local hysteresis loops on a closely spaced grid, providing a 3 order magnitude increase in data acquisition speed compared to the previous state-of-the-art. The probe concentrates an electric field to a nanoscale volume of material (~10 nm), as shown in Fig. 2 (a), and induces local domain formation. Simultaneously, the probe detects the onset of nucleation and the size of a forming domain via detection of the electromechanical response. The presence of defects lowers the nucleation energy or, equivalently, the voltage bias required for switching. Hence, a map of local nucleation voltages represents the spatial and energy distribution of switching centers.

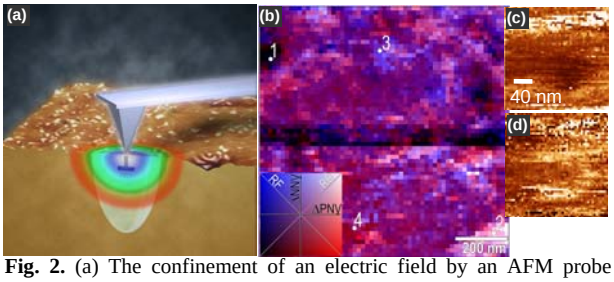

Fig. 2. (a) The confinement of an electric field by an AFM probe allows us to probe bias-induced phase transition within a defect free volume [2] or at a given separation from defects. The color map illustrates the RF and PB disorder potential in an epitaxial PZT film [3]. (c,d) A single defect in multiferroic $BiFeO_3$ [4]

Shown in Fig. 2 (b) is the nucleation voltage map of an epitaxial lead zirconate-titanate thin film. The dark spots on the image correspond to local nucleation centers, and

corresponding bias provides the information on local activation barrier on switching. The analysis of both positive and negative nucleation bias maps allows extracting the components of random bond (variation in depolarization energy of domain wall energy) and random field (built-in polarization) disorder components independently. This approach can be extended to map individual (unidentified) defects, as shown in Fig. 2 (c). This provides real space imaging of parameters that previously been accessible only in theoretical models, and are universal for all ferroic systems.

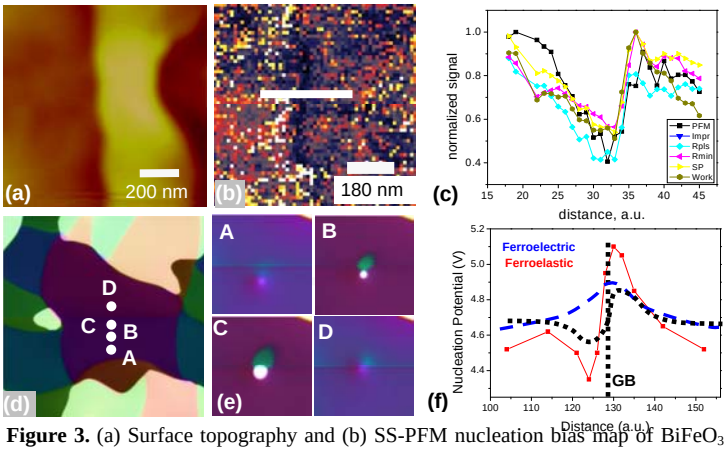

Figure 3. (a) Surface topography and (b) SS-PFM nucleation bias map of $BiFeO_3$ 24° (100) bicrystal grain boundary (GB). Each point in (b) is a hysteresis loop. (c) Ferroelectric switching properties across the interface. (d) Phase field modelling of domain structure. (e) Polarization distributions induced by the tip at 4.5 V bias for locations in (d). (f) Spatial distribution of nucleation voltage across the GB and schematic distribution of propensity for ferroelectric and ferroelastic switching across

The synergy of this spectroscopic imaging approach with systems with engineered defect structures (bicrystal grain boundaries) and phase-field modeling (with L.Q. Chen, Penn State University) opens a pathway for uncovering deterministic mesoscopic mechanisms behind defect-controlled order parameter dynamics and associated kinetic pathways (Fig. 2). In this case, the grain boundary impedes ferroelectric switching due to a built-in electric field. At the same time, in-plane breaking of rotational symmetry allows nucleation through the ferroelastic-ferroelectric twin localized at the grain boundary. The interplay between these two contributions yields *N*-shape variation of switching behavior across the interface in both experimental and modeling studies.

Understanding the switching behavior in ferroelectrics on the nanometer scale is directly relevant to the development and optimization of applications such as non-volatile random access memories, and high-density data storage. Beyond ferroelectrics, this approach can be extended to the role of defects on the thermodynamics and kinetics of other local reversible voltage-induced transitions, including phase-change materials and electrochemical reactions. This will provide a broad framework for studying the role of defects in nucleation and growth of new phases and in electrochemical reaction kinetics one defect at a time, opening a route to understanding the structure-property relationships of defect sites, and hence the optimization and control of these processes .

Energy dissipation measurements in Scanning Probe Microscopy. Energy transfer between the tip and the surface in SPM provides the fundamental information on local dissipative behavior. We have developed an approach based on an adaptive, digitally synthesized signal that excites a band of frequencies over a selected frequency range simultaneously (R&D100 2008).While in its infancy, we have demonstrated applicability of this band excitation approach for mapping energy dissipation in mechanical and electromechanical probes, including loss processes during ferroelectric domain formation, mapping viscoelastic behavior on surfaces, and evolution of dynamic behavior of the probes during force-distance curve acquisition. This capability adds a potential to probe not only conservative but also dissipative interactions in all SPMs.

Future plans:

Understanding of the fundamental physics of strongly-correlated oxide surfaces and interfaces necessitates a synergistic effort that involves (a) *in-situ* studies of grown or cleaved surfaces free of chemisorbed species, (b) development of stable ultrahigh vacuum platforms optimized for cross-coupled measurements [i.e. low cross-talk between driving and response signals] operating over broad

temperature and magnetic field ranges, (c) advanced software and hardware for fast data acquisition and processing beyond conventional force microscopy, and (d) integration with other spatially resolved probes, including STEM-SPM and SPM-focused X-ray methods. Our research effort specifically addresses first three of these directions, aimed at the following fundamental issues:

- **Ferroelectric behavior in low dimensional systems:** using a combination of ultra-high vacuum PFM, LEED-IV and NC-AFM to explore the coupling of ferroelectric and antiferrodistortive order parameters at surfaces and interfaces,[2] emergence of novel order ferroelectric phases such as the recently predicted toroidal polarization states,[3] and the role of surface chemistry in the polarization switching and domain structure,
- **Coupling between the lattice and tunneling transport**, including the effect of proper and improper ferroelectricity on electron transport through ultrathin films.
- **Nanoscale phase separation** and polarization dynamics in relaxor ferroelectrics and disordered materials imaged through acoustic and piezoresponse modes and fluctuation imaging
- **Coupling between magnetic and ferroelectric behavior** in multiferroic systems and interaction of these order parameters at surfaces, domain walls, etc.
- **Energy transformation** pathways, irreversible dynamics, and dissipation on the atomically defined defects and theory-experiment synergy using neural network based models.

Research supported by the U.S. Department of Energy Office of Basic Energy Sciences Division of Materials Sciences and Engineering and Division of Scientific User Facilities (SVK, SJ, BJR, and APB) and by the Laboratory Directed Research and Development program. The work is done in collaboration with L.Q. Chen (Penn State), R. Ramesh (UC Berkeley), M. Alexe (MPI Halle) and A. Morozovska (Ukrainian Academy of Science). The SS-PFM and Band Excitation SPM capabilities are available for user research at the CNMS.

DOE-sponsored publications 2004-2008 [In total, ~30 peer-reviewed papers (1 Nature Mat, 1 PNAS, 5 Phys. Rev. Lett., 3 patents and disclosures, 40 invited talks)]

1. B.J. RODRIGUEZ, S. JESSE, M. ALEXE, AND S.V. KALININ, *Spatially Resolved Mapping of Polarization Switching Behavior in Nanoscale Ferroelectrics*, Adv. Mat. **20**, 109 (2008).

2. S.V. KALININ, B.J. RODRIGUEZ, S. JESSE, Y.H. CHU, T. ZHAO, R. RAMESH, E.A. ELISEEV, AND A.N. MOROZOVSKA, *Intrinsic Single Domain Switching in Ferroelectric Materials on a Nearly-Ideal Surface*, PNAS **104**, 20204 (2007).

3. S. JESSE, B.J. RODRIGUEZ, A.P. BADDORF, I. VREJOIU, D. HESSE, M. ALEXE, E.A. ELISEEV, A.N. MOROZOVSKA, and S.V. KALININ, *Direct imaging of Spatial and Energy distribution of Nucleation Centers in Ferroelectric Materials*, Nature Materials **7**, 209 (2008).

4. S.V. KALININ, S. JESSE, B.J. RODRIGUEZ, Y.H. CHU, R. RAMESH, E.A. ELISEEV and A.N. MOROZOVSKA, *Probing the role of single defects on the thermodynamics of electric-field induced phase transitions*, Phys. Rev. Lett. **100**, 155703 (2008).

5. JUNSOO SHIN, V. B. NASCIMENTO, A.Y. BORISEVICH, E.W. PLUMMER, SERGEI V. KALININ, and A.P. BADDORF, *Polar distortion in ultra-thin* $BaTiO_3$ *films by in situ LEED-IV*, Phys. Rev. **B 77**, 245437 (2008)

6. P. MAKSYMOVYCH, S. JESSE, M. HUIJBEN, R. RAMESH, A. MOROZOVSKA, S. CHOUDHURY, L.Q. CHEN, A.P. BADDORF and SERGEI V. KALININ, *Intrinsic Nucleation Mechanism and Disorder in Polarization Switching on Ferroelectric Surfaces*, Phys. Rev. Lett., submitted

References

[1] R. Landauer, J. Appl. Phys. **28**, 227 (1957).

[2] A. Munkholm, S.K. Streiffer, M.V. Ramana Murty, J.A. Eastman, C. Thompson, O. Auciello, L. Thompson, J.F. Moore, and G.B. Stephenson, Phys. Rev. Lett. **88**, 016101 (2002).

[3] I.I. Naumov, L. Bellaiche L, and H.X. Fu, Nature **432**, 737 (2004).

Using Local Probes for the Study of Nano-scale Phenomena in Complex Materials

Principal Investigators: Aharon Kapitulnik - aharonk@stanford.edu
Hari Manoharan - manoharan@stanford.edu
Kathryn A. Moler - kmoler@stanford.edu
David Goldhaber-Gordon - goldhaber-gordon@stanford.edu

Mailing address: Stanford Institute for Materials and Energy Sciences (SIMES)
Geballe Laboratory for Advanced Materials
476 Lomita, McCullough Bldg.
Stanford, CA 94305-4045

PROGRAM SCOPE:

A collaborative research program focusing on the physics of nanoscale ordering phenomena in complex materials. The objectives of the program include: i) Deeper scientific understanding of correlated electron phenomena. By investigating model systems that address key physical effects found in many complex materials, including competing interactions, coexisting phases and their emergence from the nano-scale to bulk properties; ii) Study of new materials. The heart of this proposal is the collaboration with groups who develop new materials which may be used to answer critical scientific questions, or may be used for future applications; iii) Development of new tools for the study of correlated materials, with on the nano-scale. This approach is unique and involves state of the art facilities. New phenomena will lead to the invention of new ways to investigate them and vice versa. This program will therefore strengthen the wider DOE effort in nano-scale physics in the US; iv) Act as a national resource for the study of the development and characterization of novel materials using novel tools, and in training students and other technical personnel in these fields.

RECENT PROGRESS:

During FY2008, we have continued to concentrate our efforts on the materials synthesis issues associated with each of the projects. In each case, more precise characterization tools have been employed, and detailed structure-property relations are beginning to emerge. Progress in each of these areas is summarized below.

Magneto-optics Using a Sagnac Interferometer (Kapitulnik)

Ruthenates –We studied ultrathin films of $SrRuO_3$. We found that both, ferromagnetism and itineracy disappear at a critical thickness below 4 monolayers. The transition to a paramagnetic insulating phase is abrupt and is accompanied by a tendency towards perpendicular anisotropy in the ferromagnetic films. *High-T_C* – We continued our Polar Kerr-effect studies of $YBa_2Cu_3O_{6+x}$, observing non-zero Kerr rotations appearing near the pseudogap temperature T*, marking what appears to be a true phase transition. Anomalous magnetic-field training of the effect suggests that time reversal symmetry is already broken

above room temperature. *Proximity effect* – Using the Sagnac interferometer with the beam pointing at the superconductor we could verify that the magnetic order-parameter leaks from the ferromagnet into the superconductor in F/S bilayers with opposite sign and reduced intensity.

Virtual Scanning Tunneling Microscopy (Goldhaber-Gordon)

We have been developing a novel probe of electron organization in buried 2D electron systems, which serve as clean, tunable models for correlated electron behavior. This probe will also enable study of buried self-assembled structures such as ErAs quantum dots of interest for photovoltaics. We call the new probe a "Virtual STM", because it is based on tunneling into a buried semiconductor structure from a scannable virtual tip defined within the same semiconductor heterostructure. We have specified a custom cryostat in which to implement the Virtual STM. The cryostat will arrive in late FY09. By modeling and growth (Gossard, UCSB; Reno, Sandia) we have demonstrated the physical effect underlying our new probe: tuning tunneling between two electron layers in a semiconductor heterostructure by applying an external gate voltage.

STM and Atomic Manipulation (Manoharan)

Atomic manipulation with nuclear mass sensitivity – This year we have extended measurements to quantum-point-contact geometries. We observed that there is a small but detectable isotopic contribution to quantum transport past carbon nuclei. *Mapping of electron-boson interactions* – This year we extended these studies to map the complete non-local vibronic signature in optimized molecular geometries, including multi-walled quantum corrals. In Y-BSCCO (T_c = 96 K) we mapped "sideband" spectral features providing signatures of bosonic mode coupling. *Topological and spin effects in quantum materials* – In nanoassembled materials we have been mapping the effects of quantum mechanical phase in various forms. We began investigations on monolayer graphene as a prototype quantum material for Dirac fermion-based physics and topological effects. We discovered novel Dirac-Kondo ground state around magnetic impurities.

Magnetic Imaging and manipulation (Moler)

We set even stronger upper limits on spontaneous time-reversal-symmetry breaking (TRSB) edge currents and chiral domains in Sr_2RuO_4 and $PrOs_4Sb_{12}$. We demonstrated the power of MFM to manipulate vortices and probe vortex structure and dynamics in $YBa_2Cu_3O_{6.991}$ (YBCO), We published our discovery of kinked stacks of pancake vortices in $YBa_2Cu_3O_{6+x}$, and found that we can break a vortex into discrete parts. We used a phase-sensitive scanning SQUID technique to investigate various $RFeAsO_{1-x}F_y$ samples. A dense granular sample of $NdFeAsO_{1-x}F_y$ with T_c=48 K from Z.A. Ren and Z.X. Zhao in Beijing, with naturally occurring grain boundaries at many different angles, had well-coupled grains but none of the spontaneous magnetization that could arise from π junctions, constraining the order parameter of $NdFeAsO_{1-x}F_y$.

FUTURE PLANS:

Sagnac Interferometry – We will continue our general study of strongly correlated electron systems. The materials we plan to work on include $PrOs_4Sb_{12}$, URu_2Si_2, $Na_{0.33}CoO_2 1.4H_2O$,

UPt_3, as well as expand our study of high-T_C systems to the LBCO (in collaboration with M. Hucker at BNL), BSCCO and Hg-based compounds (in collaboration with M. Greven).

Virtual STM and Scanning Studies of Quantum Spin Hall Effect – Optimize the layer structure for VSTM, to achieve 100-fold gate-tunability of tunneling. Design and build a low-temperature scanning probe to use in Virtual STM (4K by end of FY2009, 100 mK 2010), with technical consultation from H. Manoharan. In parallel, with S.C. Zhang, study Quantum Spin Hall Effect in HgTe – insulating bulk behavior, but edges that propagate without scattering, at zero magnetic field. In particular, study nature of edge states using scanning probes.

Atom Manipulation STM/STS – We plan to investigate possible charge-Kondo physics in model molecular two-level systems. Work will continue on Y-BSCCO, and we will locally work with the group of M. Greven on other high-Tc systems. We plan to extend work on graphene to a collaboration with D. Goldhaber-Gordon to investigate graphene layers grown on semiconductors. This will help to seed a general shared scientific theme of topological insulators based on Dirac points in quantum materials, coupled also to the theory group.

Magnetic Imaging and manipulation – During FY2009, we will continue to apply more precise characterization tools to the materials described above with the aim of better understanding their correlated electron behavior. Of greatest urgency is the investigation of vortex behavior in $NdFeAsO_{1-x}F_y$, where we plan to continue surveying various samples with scanning SQUID microscopy and to measure the critical current at a single vortex level. If resources permit, we will also pursue persistent currents in exotic electronic systems.

RELEVANT PUBLICATIONS:

[1] *STM Studies of Near-Optimal Doped $Bi_2Sr_2CaCu_2O_{8+d}$,* A. Kapitulnik, A. Fang, C. Howald, and M. Greven, J. Phys. Chem. Solids 67, 344-9 (2006).

[2] *Gap Inhomogeneity-Induced Electronic States in Superconducting $Bi_2Sr_2CaCu_2O_{8+d}$*, A. C. Fang, L. Capriotti, D.J. Scalapino, S.A. Kivelson, and A. Kapitulnik, Phys. Rev. Lett. 96, 017007 (2006).

[3] *Distinguishing Patterns of Charge Order: Stripes or Checkerboards*, J. A. Robertson, S. A. Kivelson, E. Fradkin, A. C. Fang, and A. Kapitulnik, Phys. Rev. B 74, 134507 (2006).

[4] *High Resolution Polar Kerr Effect Measurements of Sr_2RuO_4: Evidence for Broken Time Reversal Symmetry in the Superconducting State*, Jing Xia, Maeno Yoshiteru, Peter T. Beyersdorf, M. M. Fejer, Aharon Kapitulnik, Phys. Rev. Lett. 97, 167002 (2006).

[5] *Inferring effective interactions from the local density of states: Application to STM data from $Bi_2Sr_2CaCu_2O_{8+d}$*, R. Jamei, J. Robertson, E-A. Kim, A. Fang, A. Kapitulnik, and S.A. Kivelson, Phys. Rev. B 74, 174521 (2006).

[6] *STM Studies of $TbTe_3$: Evidence for a fully Incommensurate Charge Density Wave*, A. Fang, N. Ru, I. R. Fisher, and A. Kapitulnik, Phys. Rev. Lett. 99, 046401 (2007).

[7] *Polar Kerr effect measurements of the high temperature $YBa_2Cu_3O_{6+x}$ superconductor: Evidence for broken symmetry near the pseudogap temperature*, Jing Xia, Elizabeth R. Schemm, G. Deutscher, S.A. Kivelson, D.A. Bonn, W.N. Hardy, R. Liang, W. Siemons, G. Koster, M.M. Fejer, and A. Kapitulnik, Phys. Rev. Lett. 100, 127002 (2008).

[8] *Preparation and properties of amorphous MgB_2/MgO superstructures: Model disordered superconductor*, W. Siemons, M.A. Steiner, G. Koster, D.A.H. Blank, M.R. Beasley, and A. Kapitulnik, Phys. Rev. B 77, 174506 (2008).

[9] *Quantum phase extraction in isospectral electronic nanostructures,* C. R. Moon, B. K. Foster, L. S. Mattos, G. Zeltzer, W. Ko, and H. C. Manoharan, Science 319, 782-787 (2008).

[10] *Single-atom gating of quantum-state superpositions,* C. R. Moon, C. P. Lutz, and H. C. Manoharan, Nature Physics 4, 454-458 (2008).

[11] *Scanning optical homodyne detection of high-frequency picoscale resonances in cantilever and tuning fork sensors,* G. Zeltzer, J. C. Randel, A. K. Gupta, R. Bashir, S. H. Song, and H. C. Manoharan, Applied Physics Letters 91, 173124 (2007).

[12] *Observation of the Kondo ground state for massless two-dimensional Dirac fermions in graphene,* L. M. Mattos, C. R. Moon, J. C. Randel, M. W. Sprinkle, C. Berger, K. Sengupta, A. V. Balatsky, W. A. de Heer, and H. C. Manoharan, Nature, submitted (2008).

[13] *Scanning Hall probe imaging of $ErNi_2B_2C$*, Hendrik Bluhm, Suchitra E. Sebastian, Janice W. Guikema, I.R. Fisher, and Kathryn A. Moler, Physical Review B 73, 014514 (2006).

[14] *Noise characteristics of 100nm-scale $GaAs/Al_xGa_{1-x}As$ scanning Hall probes*, C.W. Hicks, L. Luan, K.A. Moler, E. Zeldov, H. Shtrikman, Applied Physics Letters 90, 13352 (2007).

[15] *Upper limit on spontaneous supercurrents in Sr_2RuO_4*, J.R. Kirtley, C. Kallin, C.W. Hicks, E.-A. Kim, Y. Liu, K.A. Moler, Y. Maeno, and K.D. Nelson, Physical Review B 76, 014526 (2007).

[16] *Magnetic Fields above the Surface of a Superconductor with Internal Magnetism*, H. Bluhm, Physical Review B 76, 144507 (2007).

[17] *Stability of half-quantum vorticies in p_x+ip_y superconductors*, Suk Bum Chung, H. Bluhm, and Eun-Ah Kim, Physical Review Letters 99, 197002 (2007).

[18] *Two-dimensional vortex behavior in highly underdoped $YBa_2Cu_3O_{6+x}$ observed by scanning Hall probe microscopy*, J.W. Guikema, Hendrik Bluhm, D.A. Bonn, Ruixing Liang, W.N. Hardy, and K.A. Moler, Physical Review B 77, 104515 (2008).

[19] *Limits on the superconducting order parameter in $NdFeAsO_{1-x}F_y$ from scanning SQUID microscopy*, C.W. Hicks, T.M. Lippman, K.A. Moler, M.E. Huber, Z.A. Ren, and Z.X. Zhao, Submitted to Nature Physics (2008).

Electron Mapping on the Nanoscale

Rolf Koenenkamp
Physics Department, Portland State University, 1719 SW 10th Avenue, Portland, OR 97201
rkoe@pdx.edu

Program Scope

This project seeks to finalize the construction of an aberration-corrected photoelectron emission microscope, optimize its performance, maximize its spatial resolution and explore a number of new applications in imaging solid surfaces and interfaces.

The microscope in use is a unique PEEM system with a Y-shaped beam line (Fig.1), which uses a hyperbolic mirror for simultaneous correction of spherical and chromatic aberration[1,2]. In essence, mirror potential and mirror aperture are used to adjust the correction strength for the two types of aberrations. A numerical simulation based on the actual microscope design is in use to support the instrument optimization and calculate aberration coefficients. The ultimate goal in this work is a spatial resolution of ~2 nm.

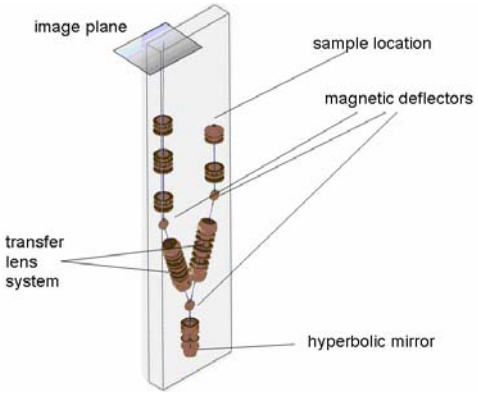

Fig. 1: Schematic diagram of the aberration-corrected PEEM

The goal of the experimentation part of the project is to demonstrate new applications for high-resolution PEEM, such as imaging of confined electron densities, electronic surface effects, local work-function variations[3], magnetic domain walls[4] and others[5].

Recent Progress

a) Electron optics: One of the early successes in the project was the experimental demonstration of aberration-correction within the microscope. Spherical aberration can be quantified from distortions in projection-images of simple geometrical structures[2]. For example, when a square mesh is placed close to the image point of the last lens in the microscope system, distortions become highly accentuated and the system aberration coefficients can easily be determined. For an aberration-free lens system the projection image will be distortion-free. These experiments are typically carried out in de-magnification, and accordingly the electron beam-direction in the microscope has to be reversed for these experiments. Fig. 2 shows representative results for this in-situ work. Distorted images resulting from negative or positive aberration coefficients are shown in part a) and b). Spherical aberration correction is demonstrated in part c).

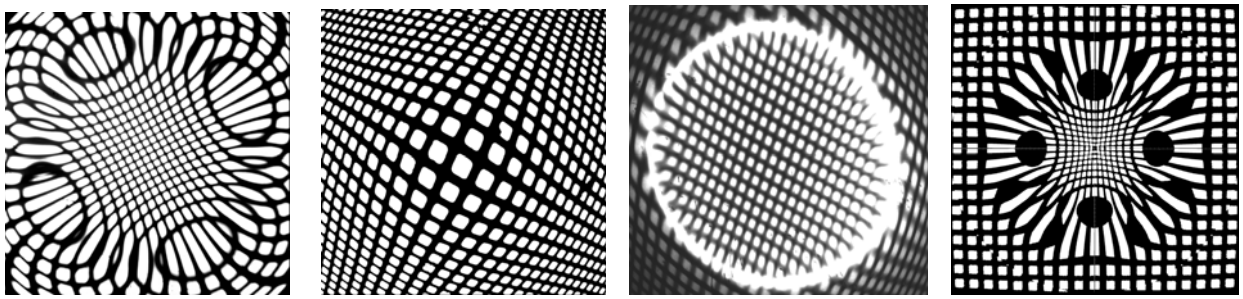

Figure 2: Results from projection images to study and quantify aberration coefficients in our PEEM. a: Distortion indicating a positive spherical aberration coefficient; b: neg. aberration coefficient; c: corrected aberration within 40mrad; d: simulated results for situation in a).

The correction strength is adjustable over a wide range, including regimes of under-correction andover-correction. The experimental findings are well corroborated by our numerical simulation (Fig. 1d). Correction of chromatic aberration is obtained when the projection images are unaffected by variations in electron energy. Simultaneous correction of chromatic and spherical correction is obtained when distortion-free and energy-stable images are observed. We were able to demonstrate these conditions. The estimated minimal system aberration is consistent with the envisioned resolution value of 2 nm[6,a1]. We believe these are the first in-situ experiments of this kind for mirror-based aberration correction.

Fig.3 shows in detail the dependence of the aberration coefficients on mirror voltage and the corresponding simulation results. These results can be used to determine the optimized instrument configuration. We were also able to demonstrate a magnification of ~10^5. At this magnification a 1 nm object feature is magnified to a 100 μm image feature which is easily resolved with the 2 μm phosphor grain size and the 3.7 μm CCD camera resolution. From its optical lay-out and configuration the microscope is thus capable of the envisioned 2nm resolution.

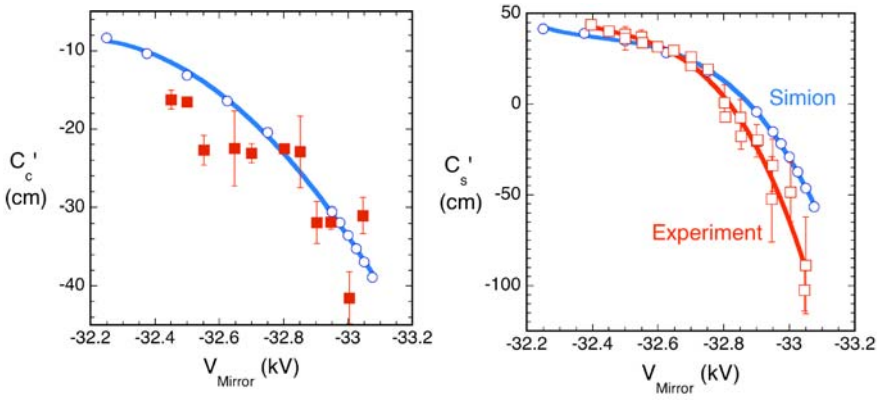

Figure 3: Experimental and simulated (SIMION) results for the dependence of the spherical and chromatic aberration coefficients on mirror potential; a: spherical, b: chromatic aberration coefficient.

a) b)

Fig. 4 shows examples for the resolution improvement obtained in the recent months. Size-calibrated nanoscale metallic samples were used to obtain high contrast images. A 2-dimensional Fourier-transform technique was applied for the resolution analysis. The resolution was improved from ~60 nm to a present best value of 9 nm.

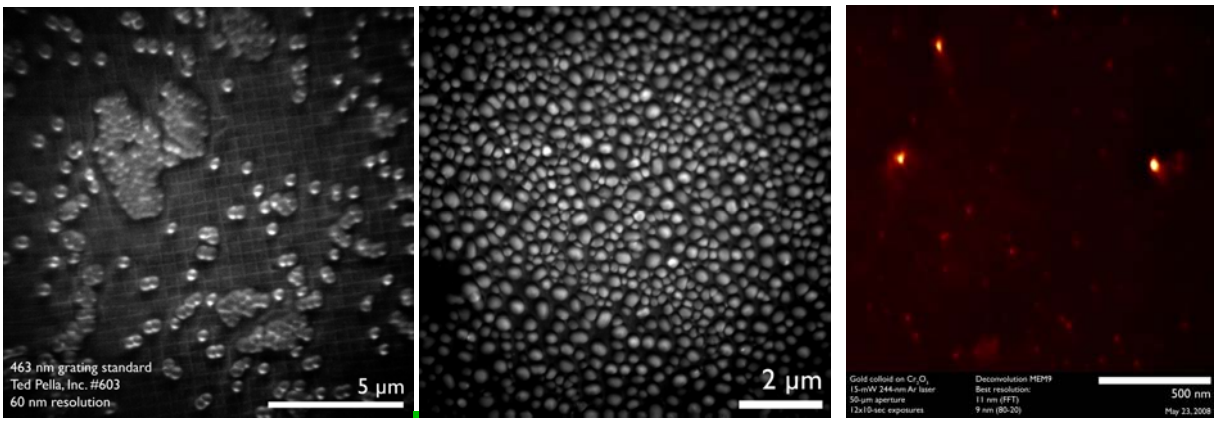

a) b) c)

Figure 4: PEEM images of Au islands on n-Si (a), polystyrene spheres on a TEM mesh (b), and Au colloids on Cr film (c).

Mechanical and electrical system stability as well as low noise levels in supply currents, voltages and radiation will need to be reduced to improve the resolution further.

b) Experimentation in the PEEM mode

Localized Ga implantation in n-Si: Work-function contrast is among the unique characteristics in PEEM. We began imaging experiments on Ga-implanted n-type Si wafers prepared with a 30 keV Ga^+ focused ion beam[7,8]. We could show that implantation densities $<10^{17}cm^{-3}$ are clearly visible in PEEM. For comparison, contrast between undoped and doped regions is lost at doping concentration of $\sim10^{18}cm^{-3}$ in a FEI Sirion XL30 field emission SEM.

Fig. 5 shows the enhancement of the photoemission in Ga-implanted regions of n-type Si, as the Ga-implanted regions appear brighter. A tentative explanation of these observations is that the larger workfunction in the p-Si areas leads to a downward surface band bending which allows tunneling emission of photoelectrons at sub-workfunction energies.

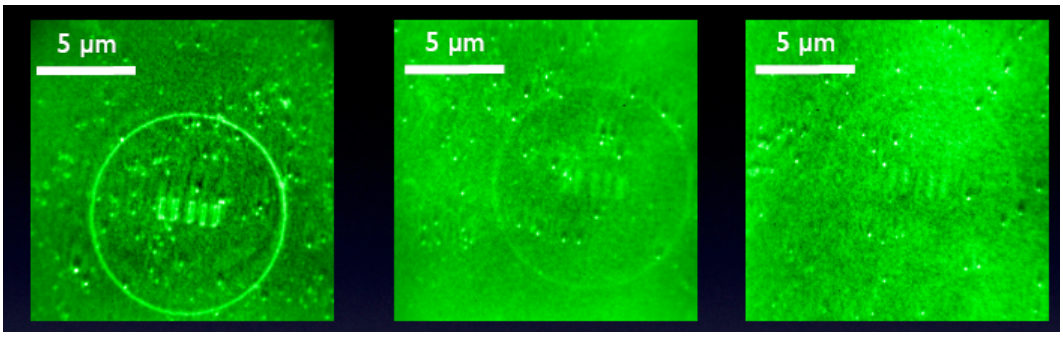

Figure 5: Line contrast images for 30kV Ga-implanted patterns in n-Si. The Ga concentrations decrease from left to right as 5 $x10^{19}$, 5 x 10^{18}, 5x $10^{17}cm^{-3}$. PEEM exposure time = 10s.

CdTe/MEH-PPV hybrid films were prepared by dispersing CdTe quantum dots in liquid polymers solutions and spin-casting the dispersion on glass substrates. The band line-up in these hybrid films is that of a staggered (type II) hetero-junction. Photoconductance spectroscopy shows a high degree of charge separation at the hybrid interface under photoexcitation. Essentially, photo-generated holes are transferred to the MEH-PPV, while photo-excited electrons are collected in the CdTe. We were able to show that the two carrier ensembles are separated beyond one Debye-length[a2]. It is expected that this charge separation will be observable in PEEM when high resolution is established. Changing quantum dot sizes and concentrations, illumination strength and bandgaps, should give rise to a variety of experimental situations with distinct appearance in PEEM.

First work on biological samples demonstrated very high contrast and low exposure damage in PEEM work as compared to SEM operation. The preliminary results indicate that due to the high sensitivity of PEEM, the exposure times on biological samples can be reduced to ~ 5ns when pulsed laser excitation is used.

Future Plans

For the immediate future the strongest challenge to the project remains the resolution. Improvements in vibration isolation, power supply stability and stray fields are currently being implemented.

The microscope itself will be extended to include a tunable pulsed laser system, a prep chamber, a magnetic compensator system, and a highly stable voltage divider to operate cathode, objective lenses and mirror from the same voltage source.

When the resolution approaches the 2 nm goal, more interesting experimental situations will be realized which will take advantage of the extraordinary resolution, sensitivity and brightness in an aberration-corrected PEEM. Self-assembled nanostructures will be used as an implantation mask to scale down doped areas in Si towards the ~5nm regime. In these samples depletion, accumulation and confinement effects will be studied.

Charge separation and confinement effects will also be studied in semiconductor/hybrid interfaces and in expitaxial semiconductor quantum-dot films.

Using magnetic garnet films we will try to establish an analysis technique that relies on the scattering of low-energy photoelectrons in magnetic surface fields. Since photoelectrons with energies only slightly above the workfunction have very low velocities, they are expected to be very sensitive to magnetic fields at the surface. Near domain boundaries the photoelectrons will be scattered due to the variation of the magnetization, and this scattering will result in optical image contrast.

References

1. G. F. Rempfer, J. Appl. Phys. 67, 6027 (1990)
2. G.F. Rempfer, D.M. Desloge, W.P. Skoczylas, and O.H. Griffith: Microscopy and Microanalysis 3, 14 (1997)
3. M. Giesen, R. J. Phaneuf, E. D. Williams, T. L. Einstein, H. Ibach, Appl. Phys. A 64, 423 (1997)
4. S. Anders, H. A. Padmore, R. M. Duarte, T. Renner, T. Stammler, A. Scholl, M. R. Scheinfein, J. Stöhr, L. Seve and B. Sinkovic, Rev. Sci. Inst. 70, 3973 (1999)
5. M. Cinchetti et al., Phys. Rev. Lett. 95, 047601 (2005)
6. J. Elstner, Thesis M.S. Physics, Portland State University, 2004
7. G. B. Thompson, M. K. Miller and H. L. Fraser, Ultramicroscopy 100, 25 (2004)
8. N. Mateescu, M. Ferry, W. Xu and J.M. Cairney, Materials Chemistry and Physics 106, 142 (2007)

DOE-sponsored publications from this work

a1. Image properties in an aberration-corrected photoemission electron microscope
R. Könenkamp, T. Jones, J. Elstner, R. Word, G. Rempfer, T. Dixon, L. Almaraz, W. Skoczylas, Physics Procedia 1, 505-511(2008)

a2. Unipolar transport and interface charge transfer in nanostructured CdTe/polymer hybrid films
Robert Meier, Robert C. Word, Athavan Nadarajah, and R. Könenkamp, Phys. Rev. B **77**, 195314 (2008)

Nanoscale Probes of Complex Materials with Atom Manipulation STM

Hari C. Manoharan

Department of Physics, Stanford University, Stanford, CA 94305
manoharan@stanford.edu • http://mota.stanford.edu

Program Scope

Our work on local probes of complex materials involves the full-time operation of two STM systems: (1) a variable-temperature UHV STM, and (2) an ultra-stable custom low-temperature UHV STM. The measurement techniques employed for the works described below cluster around scanning tunneling microscopy and spectroscopy, and include specializations on which we have concentrated in our lab: atomic manipulation, inelastic electron tunneling spectroscopy (IETS), and simultaneous measurements in a high magnetic field. The scientific work has been spread over three main thrusts: (1) development of new STM/STS instrumentation and techniques for application to complex ground states, (2) IETS-STM investigations of electron-boson interactions in nanostructures and superconductors, and (3) topological and spin effects in novel quantum materials.

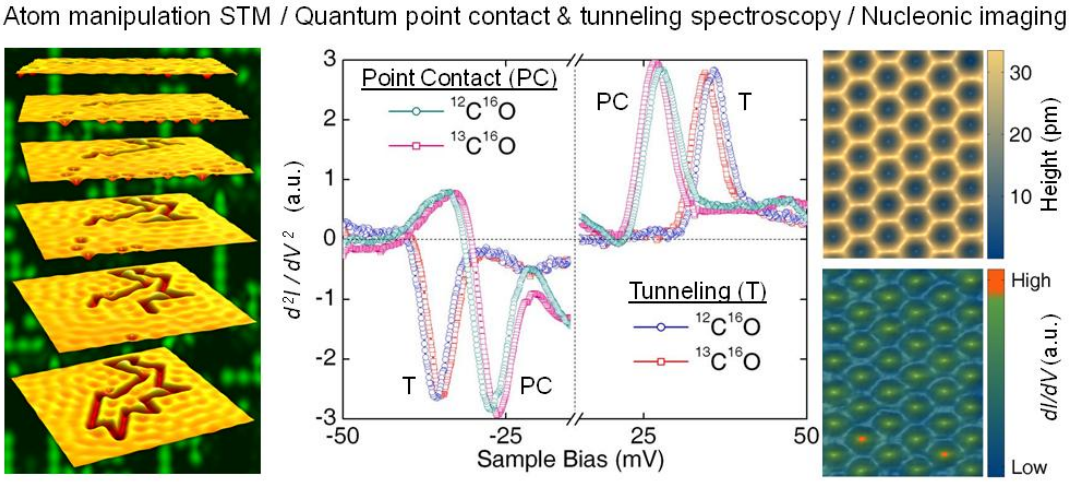

Fig. 1 State-of-the-art capabilities of our atom manipulation STM as demonstrated on carbon-based nanomaterials. (left) Topographs showing molecule-by-molecule assembly of quantum nanostructures and detection of electron wavefunctions on metal surfaces. (middle) Extension of elastic and inelastic electron spectroscopy from quantum tunneling to quantum point contact regimes. Additionally, high signal-to-noise allows distinction between nucleonic content through isotope information. (right) Simultaneous topograph and nucleonic scan allow individual carbon nuclei to be imaged (red dots correspond to carbon-13).

Recent Progress

Instrumentation capability: Atom manipulation STM / Quantum point contact & tunneling spectroscopy / Nucleonic imaging

In the initial stages of building our atomic manipulation STM and with DOE support, the system was additionally customized to study complex materials. Sample cleaving in UHV at room temperature and low temperature were developed along with changes to the sample preparation capabilities including an ultra-clean rf heating method. After initially demonstrating atomic manipulation, these abilities have been refined over the last three years to build increasingly complex nanostructures [Moon 2008a] [Foster 2008a] [Moon 2008b] and to serve as

a platform for high frequency measurements [Zeltzer 2007]. In addition, we have pushed down the noise floor on vibrational and electronic noise to achieve unprecedented sensitivity in our spectroscopy [Mattos 2008a]. The current state-of-the-art for this system is shown in Fig. 1, where examples of STM, STS, and nanoassembly are shown. Spectroscopy, through inelastic tunneling, is able to distinguish between isotopes in various molecules and within surfaces (here shown for carbon nuclei). This enables a unique scanning mode in which nucleonic information can be acquired simultaneous to topographic and electronic structure information. During this past year, we have made two major advances in capability: extending the IETS method all the way from quantum tunneling [Foster 2008a] to quantum point contact [Foster 2008b] while preserving nuclear mass discrimination (see Fig. 1), and extending measurement capability to high magnetic fields up to 6 T with no loss of resolution [Mattos 2008b]. We are now able to perform atom manipulation in these fields and also ramp the field during tunneling measurements with all zero-field abilities intact. These capabilities have enabled a new class of studies on materials, described below.

IETS-STM mapping of electron-boson interactions

We have extended molecular IETS STM studies [Stipe 1998] [Stipe 1999] [Foster 2008a] [Foster 2008b] to investigate collective modes and their coupling to electronic degrees of freedom in several materials. The physical phenomena range from molecular oscillators coupling to each other, localized vibrons coupling to quantized electrons, and phonon modes coupling to superconducting electrons.

We completed experiments in which we could control the interaction between localized bosonic modes (in the form of molecular oscillators) and a delocalized fermionic field (in the form of quantized 2D electron states). We realized this system by assembling molecular quantum corrals on Cu(111) and engineering the confined electron state to be resonant with measured molecular vibrons. Such a system has a curious duality with Dicke superradiance [Dicke 1954] in which a delocalized bosonic field (optical photons) interacts coherently with localized fermionic excitations (electrons in atomic orbitals, or more recently in quantum dots [Scheibner 2007]). Our measurements on the "dual-Dicke" geometry reveal a coherent interaction between the fermionic field and the localized bosonic modes, which was tuned by bringing the corral into and out of resonance through size adjustment. Since the electron wavelength was much longer than the spacing between molecules, collective excitations are possible and evidence for such modes was obtained by fitting the *e-v* (electron-vibron) coupling constant through a theory collaboration with Los Alamos [Fransson 2007]. These measurements demonstrate the importance of coherence in nanoscale electronic structure even in the presence of inelastic coupling. In collaboration with the materials synthesis groups of Martin Greven (Stanford) and Ian Fisher (Stanford), we investigated several novel superconductors. We performed STM imaging and spectroscopy of the high-temperature superconductor $Bi_2Sr_2Ca_{0.93}Y_{0.07}Cu_2O_{8+\delta}$ (Y-BSCCO), optimally doped with T_c = 96 K [Eisaki 2004]. In these materials we observe both sub-gap and super-gap features which are small or absent in the associated BSCCO-2212 crystal. An analysis of these features in dI/dV and d^2I/dV^2 are consistent with bosonic mode coupling. They allow an extraction of the coupling constant ($\lambda \sim 0.4$) and mode energies (~75 meV). Through a theory collaboration [Balatsky 2003] (also working locally with T. Devereaux and S. Kivelson), we have performed a spectral inversion process to quantitatively determine the electron-boson coupling constants and spatially map them [Mattos 2008a].

Topological and spin effects in novel quantum materials

The combination of natural or engineered electronic structure creating exact degeneracies due to geometry is a fertile area for robust topological effects in condensed matter. Not surprisingly, quantum mechanical phase often plays a role in the underlying ground states. In nanoassembled materials we have been mapping the effects of quantum mechanical phase in various forms, guided by ideas such as real-space and *k*-space exact degeneracies in band structure. Our atom manipulation and high resolution spectroscopy capabilities in magnetic fields up to 6 T were additionally used for sensitivity to Aharonov-Bohm phase, flux effects such as Landau level quantization, and coupling to the spin degree of freedom.

In the previous year we undertook quantum phase measurements of two kinds in nanoassembled structures. We demonstrated the measurement of the relative phase of two electronic states in a quantum superposition [Moon 2008b], as well as a method to map the internal phase of single quantum states [Moon 2008a], thus operating the STM as a versatile quantum phase meter. Both methods required the precise geometric tuning of topological degeneracies, also describable by supersymmetric quantum mechanics [Cooper 1995]. This year we began investigations on monolayer graphene (epitaxially grown on SiC through collaboration with W. de Heer [Berger 2006]) as a prototype quantum material for Dirac fermion-based physics and topological effects [Geim 2007]. Using FT-STS, we have mapped both pseudospin-flipping and chirality-reversing scattering processes on bare graphene [Rutter 2007], and then extended measurements to the investigation of magnetic adatoms (theory collaboration with A. Balatsky, K. Sengupta, S. Kivelson). We observed the Kondo ground state of Dirac fermions around local spin impurities, and we have mapped the spatial and magnetic-field dependence of this highly correlated state [Mattos 2008b]. We also performed the first atomic resolution imaging of the heavy-fermion compound USb_2 (collaboration with LANL).

Future Plans

Studies of *e-v* collective modes in nanostructures will be extended to optimized molecular geometries. Some of these have been calculated now and await creation by STM manipulation. Other planned experiments include a scaling analysis of the nonlocal vibronic signal vs. number of molecular oscillators, which provides a key signature of superradiance-type effects [Dicke 1954] [Scheibner 2007]. These studies will be performed in synergy with the molecular IETS experiments described in the previous section. We plan to investigate possible charge-Kondo physics in model molecular two-level systems, and extend work on graphene to investigate graphene layers grown on other semiconductors. Dirac material studies will include 2D graphene-based devices and extend to 3D materials such as topological insulators and other promising materials.

Literature cited

Publications attributed to previous work done under BES funding of this task

[Moon 2008a] *Quantum phase extraction in isospectral electronic nanostructures,* C. R. Moon, B. K. Foster, L. S. Mattos, G. Zeltzer, W. Ko, and H. C. Manoharan, *Science* **319**, 782-787 (2008a).

[Foster 2008a] *Carbon isotope coded molecular switch automata,* B. K. Foster, C. R. Moon, L. S. Mattos, G. Zeltzer, and H. C. Manoharan, submitted (2008a).

[Moon 2008b] *Single-atom gating of quantum-state superpositions,* C. R. Moon, C. P. Lutz, and H. C. Manoharan, *Nature Physics* **4**, 454-458 (2008b).

[Zeltzer 2007] *Scanning optical homodyne detection of high-frequency picoscale resonances in cantilever and tuning fork sensors,* G. Zeltzer, J. C. Randel, A. K. Gupta, R. Bashir, S. H. Song, and H. C. Manoharan, *Applied Physics Letters* **91**, 173124 (2007).

[Mattos 2008a] *Local signatures and spectral inversion of bosonic mode coupling in a high temperature superconductor,* L. S. Mattos, C. R. Moon, B. K. Foster, G. Zeltzer, M. Greven, A. V. Balatsky, and H. C. Manoharan, manuscript in preparation (2008a).

[Foster 2008b] *Nucleon-gated molecular conductance,* B. K. Foster, C. R. Moon, L. S. Mattos, G. Zeltzer, and H. C. Manoharan, manuscript in preparation (2008b).

[Mattos 2008b] *Observation of the Kondo ground state for massless two-dimensional Dirac fermions in graphene,* L. S. Mattos, C. R. Moon, J. C. Randel, M. W. Sprinkle, C. Berger, K. Sengupta, A. V. Balatsky, W. A. de Heer, and H. C. Manoharan, submitted (2008b).

Other references

[Stipe 1998] *Single-molecule vibrational spectroscopy and microscopy,* B. C. Stipe, M. A. Rezaei, and W. Ho, *Science* **280**, 1732-1735 (1998).

[Stipe 1999] *Localization of inelastic tunneling and the determination of atomic-scale structure with chemical specificity,* B. C. Stipe, H. A. Rezaei, and W. Ho, *Physical Review Letters* **82**, 1724-1727 (1999).

[Dicke 1954] *Coherence in spontaneous radiation processes,* R. H. Dicke, *Physical Review* **93**, 99-110 (1954).

[Scheibner 2007] *Superradiance of quantum dots,* M. Scheibner, T. Schmidt, L. Worschech, A. Forchel, G. Bacher, T. Passow, and D. Hommel, *Nature Physics* **3**, 106-110 (2007).

[Fransson 2007] *Surface imaging of inelastic Friedel oscillations,* J. Fransson and A. V. Balatsky, *Physical Review B* **75**, 195337-195331 (2007).

[Eisaki 2004] *Effect of chemical inhomogeneity in bismuth-based copper oxide superconductors,* H. Eisaki, N. Kaneko, D. L. Feng, A. Damascelli, P. K. Mang, K. M. Shen, Z. X. Shen, and M. Greven, *Physical Review B* **69**, 064512 (2004).

[Balatsky 2003] *Inelastic tunneling spectroscopy in a d-wave superconductor,* A. V. Balatsky, A. Abanov, and A. Jian-Xin Zhu, *Physical Review B* **68**, 214506-214501 (2003).

[Cooper 1995] *Supersymmetry and quantum mechanics,* F. Cooper, A. Khare, and U. Sukhatme, *Physics Reports* **251**, 267-385 (1995).

[Berger 2006] *Electronic confinement and coherence in patterned epitaxial graphene,* C. Berger, Z. Song, X. Li, X. Wu, N. Brown, C. Naud, D. Mayou, T. Li, J. Hass, A. N. Marchenkov, E. H. Conrad, P. N. First, and W. A. de Heer, *Science* **312**, 1191-1196 (2006).

[Geim 2007] *The rise of graphene,* A. K. Geim and K. S. Novoselov, *Nature Materials* **6**, 183-191 (2007).

[Rutter 2007] *Scattering and interference in epitaxial graphene,* G. M. Rutter, J. N. Crain, N. P. Guisinger, T. Li, P. N. First, and J. A. Stroscio, *Science* **317**, 219-222 (2007).

[Zhao 2006] *Crystal Growth and Characterization of the Model High-Temperature Superconductor HgBa2CuO4+delta,* X. Zhao, G. Yu, Y.-C. Cho, G. Chabot-Couture, N. Barisic, P. Bourges, N. Kaneko, Y. Li, L. Lu, E. M. Motoyama, O. P. Vajk, and M. Greven, *Advanced Materials* **18**, 3243-3247 (2006).

Ultrafast Dynamics at Nano-Interfaces

Chong-Yu Ruan
ruan@pa.msu.edu
Department of Physics and Astronomy, Michigan State University, MI 48824

Program Scope

The ability to sharpening our vision into the transformative nature of materials and macromolecules on the scale of 1-100 nm is perceived as essential to advancing nanoscience and nanotechnology. In particular, nanostructures, macromolecules, and interfaces can be used as the building blocks for advanced devices promising performance with high specificity and high speed at exceedingly high packing density in diverse areas, such as in electronics, optics, magnetism, catalysis, sensing, and quantum computing. Characterizing the underlying size- and shape-dependent processes, such as phase transition, transport, and chemistry, involving changes of atomic and electronic degrees of freedom on the sub-angstrom and femtosecond time scale [A,B], requires unprecedented combined space-time resolution. Initial phase of our project is dedicated to establish a new ultrafast diffraction camera with atomistic scale resolution (femtosecond-picometer) and molecular sensitivity (nm), capable of videographing the complex transient interactions at nanointerfaces. Its resolution and sensitivity were demonstrated in studying isolated nanoparticles and specially prepared surfaces with focused efforts in addressing the following important emerging properties on the nanometer length scale: (1) Ballistic versus diffusive phonon and charge transport in nanostructures: investigating the bottleneck for energy dissipation in a confined geometry; (2) Light-induced thermal versus nonthermal structural changes: exploring the pathways for all-optical material modification; (3) Correlation between the charge and atom within nanostructures: examining the co-evolution of atomic and electronic degree of freedoms, contrasting that to the bulk systems.

Recent Progress

Ultrafast electron nanocrystallography An ultrafast diffraction camera [1,2] has been constructed. The essential development is the capability of probing distributions of widely dispersed single nanoparticles using diffraction on the femtoseond to nanosecond timescale. By suppressing the substrate scattering background with a buffer ad-layer composed of self-assembled aminosilane molecules, superb signal-to-noise ratio for nanoparticles occupying less than 1% of the studied area is achieved. This is in contrast to X-ray and neutron diffraction approach in which the commonly required samples must have a high volume density and be μm to mm in size. The ability to study individual nanoparticles and interconnects on the atomic scale is essential to elucidate the elementary processes for nanoscale devices. This is achieved by incorporating a short-distance photogun with a proximity-coupled electron lens designed to alleviate the space-charge broadening and the effect of finite-size of the pump-probe overlap to achieve femtosecond diffraction for surface supported particles as small as 2nm, and a cryogenic sample manipulator capable of reaching sub-30 K to reduce the thermal background and increase the damaging threshold dosage.

We described pump-probe diffraction studies of photoinduced structural dynamics of nanophase gold [2] and silver particles [C] on self-assembled monolayers. By modeling the time-dependent Debye-Waller factor and refraction effect, the evolutions of the mean squared amplitude of vibration and the Coulomb potential of the particles were monitored in real time to determine heating, charging, and ensuing relaxation processes following femtosecond laser excitation.

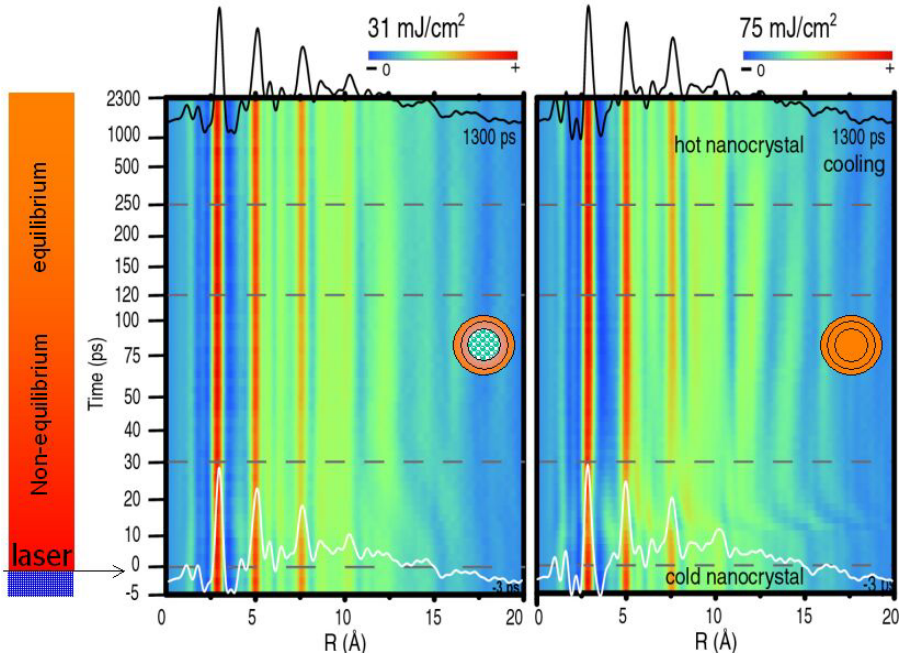

Fig. 1.

The melting dynamics of 2nm Au nanoparticles, constructed by stacking the pair distribution function of UEC patterns at a sequence of delays between –5ps and 2300 ps at irradiation fluence F=31 mJ/cm2 (left) and 75 mJ/cm2 (right) showing different degrees of structural changes. The edge-to-edge atom correlation (>1 nm) is significantly red-shifted compared to the nearest neighbor bonds, highlighting the strong inhomogeneity in the nanoscale structural disorders.

Surprising nonthermal heating mechamism has been found. By analyzing the transient Debye-Waller factor and the pair-correlation function, G(r) [D], lattice heating and local structural changes were deduced to reveal the size-dependent transport property of nanointerfaces and structural responses to optical and/or surface plasmon excitations for the surface-supported nanoparticles. The photoinduced structural modification was refined using a nano-cluster model employing Reverse Monte Carlo algorithm on the time-dependent G(r), showing formation of nanodomains surrounded by undercoordinated regions. The dynamics of interfacial charge transfer from the supporting substrate to the nanoparticle was also studied, in contrast to heat transport. By monitoring the collective shift of diffraction pattern emerging from the self-assembled monolayer, which acts as the molecular wires linking particle to the substrate, we directly observed the induced interfacial electric field from photo-assisted charge transfer into the nanoparticle. The characteristic charging time was found to be consistent with the product of the interfacial capacitance of nanoparticle and the resistance of the molecular wire, determined on the basis of tunneling through the molecular wires [3,C].

Material transformation far from equilibrium Extending the mode of material inquiry from the steady state to the excited state through selected photoexcitation allows the exploration of nonequilibrium material transformation on a complex energy landscape[B]. Observation of transient structures thus formed offers a glimpse into the transformation pathways connecting one structural state to another. Carbon, with its propensity to form a wide class of bonding networks (sp^2;sp^3 etc.) is ideal to study the dynamics of bond formation and breakage. In particular, the transformation between hexagonal graphite and cubic diamond is of considerable interest and is thought to occur via an intermediate state involving rhombohedral graphite. We reported the first direct structural determination of structural changes in graphite by a femtoseond laser pulse [4]. At moderate fluences of < 21 mJ/cm^2, after a short thermalization period of ~ 8ps, we attributed a temperature value to the graphitic layers and find the interlayer vibrational amplitudes to match those reported in X-ray and neutron scattering studies. At higher fluence values approaching the damage threshold (120 mJ/cm^2), we observed lattice vibration amplitudes to saturate. Following a

marked initial contraction of the interlayer spacing by 6%, graphite is driven nonthermally into a transient state with sp^3-like character, forming 1.9 Å long interlayer bonds, a first step of diamondization. *Ab initio* density functional theory (DFT) calculations attributed the cause to electronic structure changes induced by non-thermal heating of the electron gas, followed by a photo-induced charge separation causing a compressive Coulomb stress. Based on the potential rise sampled within the electron probed depth of 1 nm yields an internal field of E~1.2 V/Å. Based on that, we estimated a maximum energy density of 0.2 eV/atom, close to the 0.3 eV/atom value based on DFT for the activation barrier in the graphite-to-diamond transition.

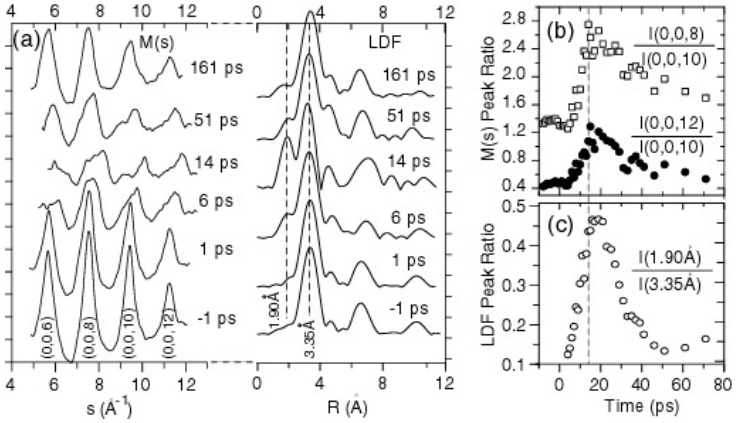

Fig. 2 *(a) Signature of sp3-like bonding in graphite. Structure factor M(s) and the corresponding LDF curves at selected time instances following strong photoexcitation. The transient peak at 1.9 Å in the LDF indicates formation of interlayer bond. (b) Ratio of peak intensities obtained from the diffraction patterns. The enhancement of the (0,0,12) with respect to (0,0,10) peak cannot be explained by thermal vibrations and indicates a transient structure consistent with sp3 bonding. (c) Ratio of peak intensity at R=1.9 Å and 3.35 Å in the LDF.*

<u>Transient photovoltage determination for nanointerface</u> Characterizing the rate of surface charging and recombination is essential for understanding the transient processes in surface photochemical reaction, photovoltaics, and single electron device [E]. We explored using electron diffraction as a potentiometer to determine the transient surface potential, which is directly related to the redistribution of charges at nanointerface and surface state charging. We studied the photoinduced surface potential changes on a Si(111) surface terminated with hydrophilic hydroxyl (OH) groups, a prototypical system for fabricating molecular electronic devices [5]. The femtosecond laser pulse was used to initiate carrier generation near the surface and in turn, the formation of a transient surface voltage (TSV), while a charge-sensitive electron pulse probed the ensuing carrier relaxation dynamics. A Coulomb refraction formalism was deduced to treat ultrafast diffraction data to determine the TSV. Using a low laser fluence, we found a band-flattening TSV of ~300 mV generated ~30 ps after the laser excitation. At moderate and high fluences, the TSV rise beyond the bandgap energy. This surprisingly large TSV (larger than band bending) is attributed to a modified space charge due to a nonequilibrium surface charge migration, induced by photoexcitation. We observed picosecond charge injection and relaxation dynamics with timescales similar to results obtained using ultrafast photoemission studies of surface carrier dynamics in a vacuum cleaved Si(111)-2×1 surface. This rapid recovery, which is an order of magnitude faster than the ambipolar diffusion of photoexcited carriers, can be understood based on a drift-diffusion model that couples surface carrier dynamics with transport in the space-charge layer. This also suggests that surface states at the hydroxylated silicon interface are highly rechargeable, making it an appropriate base electrode for molecular electronic transport study. This study demonstrates the joint charge and structure resolution of UED, extending its scope of application to include carrier dynamics, such as photovoltage generations,

catalysis, and transport at nanometer scale interfaces, beyond merely as an ultrafast structural probe.

Future Plans

Along the direction of studying nanoparticles, we will further elucidate their size-dependent transport characteristics by measuring their thermal and charge relaxation across the nanoparticle-substrate interface. Theoretic model will be further developed to account for various relaxation and transport processes under non-equilibrium conditions. We will also seek to understand the tunneling behavior across insulating layer leading to surface charging on the oxide surface. This will be achieved by consistently growing oxide layer on silicon substrate using PECVD or Ozone-oxidation techniques and ellipsometry to quantify the results. We will then determine the surface state charging and relaxation using ultrafast electron diffractive potentiometry technique developed here. Based on the rate of charging and recombination as a function of the oxide layer thickness, we should be able to determine the nature of the electron transport, and more importantly use it as a turning knob to control the physical and chemical properties of the nanoparticles. Along the direction of exploring nanoconfinement effects, we will continue to pursue joint determination of transient charge redistribution and structural changes using high-resolution ultrafast electron crystallography in a layered system to understand the correlation between the in-plane electronic excitation and the out-of-plane electronic and thermal relaxation. Especially by consistently thinning the graphite sample, we should be able to exploring the onset of the two-dimensional behavior caused by confinement effects. We can prepare the ultrathin graphite flasks using 'scotch-tape' method on thin oxide surface and study them with electron nanodiffraction method.

Reference

[A] H. Hakkinen, S. Abbet, A. Sanchez, U. Heix & U. Landman, *Angew. Chemie*, 42, 1297 (2003).

[B] K. Nasu, ed., "Photoinduced phase transition" (World Scientific, Hackensack, USA, 2004).

[C] R.K. Raman, R.A. Murdick, Y. Murooka, R. Worhatch, C.-Y. Ruan, "Molecular imaging of nanoscale fragmentation in Silver nanocrystals using ultrafast electron nanocrystallography", *Science* (submitted).

[D] C. Farrow, C.-Y. Ruan, S.J. Billinge, "Quantitative structural determination for ultrafast electron diffraction", *Phys. Rev. B* (submitted).

[E] L. Kronik and Y. Shapira, "Surface photovoltage phenomena: theory, experiment, and applications", *Surf. Sci. Rep.* 37, 1 (1999).

DOE Sponsored Publications in 2006-2008 (published)

[1] C-Y. Ruan, Y. Murooka, R.K. Raman, R. Murdick, and M.A. Khasawneh, "Towards ultrafast diffraction and spectroscopy of interfaces and nanomaterials using femtosecond focused electron pulses", *Microscopy and Microanalysis* 12 (Suppl.2), 150 (2006).

[2] C.-Y. Ruan, Y. Murooka, R.K. Raman, R.A. Murdick, "Dynamics of Size-Selected Gold Nanoparticles Studied by Ultrafast Electron Nanocrystallography", *Nano Lett.* 7, 1290 (2007).

[3] C.-Y. Ruan, Y. Murooka, R.K. Raman, R.A. Murdick, R. Worhatch, "Transient structural studies of nanoparticles using electron diffraction", *Microscopy and Microanalysis* 14 (Suppl.2), 30 (2008).

[4] R.K. Raman, Y. Murooka, C-Y. Ruan, T. Yang, S. Berber, D. Tomanek, "Direct observation of optically induced transient structures in graphite using ultrafast electron crystallography", *Phys. Rev. Lett.* 101, 077401 (2008).

[5] R.A. Murdick, R.K. Raman, Y. Murooka, C.-Y. Ruan, "Photovoltage dynamics of the hydroxylated Si(111) surface investigated by ultrafast electron diffraction", *Phys. Rev. B* 77, 245329 (2008).

Control of nanostructure growth at low temperatures

M. C. Tringides, M. Hupalo J. Chen and S. Binz
tringides @ameslab.gov, hupalo@ameslab.gov, chnjzh@iastate.edu, smbinz@iastate.edu Ames Laboratory and Iowa State University

I. Program scope

The growth of low dimensional structures (ultrathin films, islands , wires, etc.) with atomic scale control of their dimensions can result in novel properties as a result of confinement and/or lower atom coordination. If such control is achievable it would be possible to "tune" the structure electronic properties to specific technological applications (chemical reactivity, nanomagnetism etc.) , because their electronic structure (i.e. the confined electron energy levels) depends on their size. Two complementary techniques, Scanning Tunneling Microscopy (STM) and High Resolution SPA-LEED are used for structure characterization. In collaboration with theoretical groups worldwide we aim to attain a better understanding of the structure energetic stability and the controlling kinetic barriers.

I.Recent progress

Ia. QSE and crystallographic phase transition on In/Si(111)

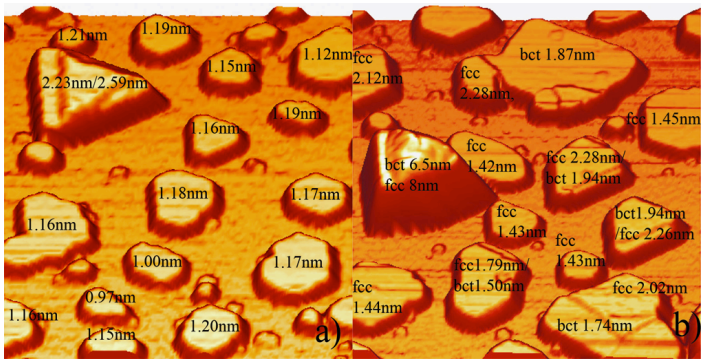

Fig.1 Growth of In on Si(111)-Pb- α√3x√3 at T=200K (a) 200x200nm^2 θ=2.5ML with fcc(111) islands . (b) 280x280nm^2 θ=5ML with fcc(111), bct(110) and mixed islands. The mixed island grew by 18ML although only 2.5ML has been deposited.

Since the previous meeting in 2006 one of our goals was to discover other metals besides Pb/Si(111)[1] with high degree of self organization as a result of Quantum Size Effects(QSE). Indium grown on one specific substrate (Si(111)-Pb-α-√3x√3) has resulted in uniform height fcc(111) flat top 4-layer islands[2], However the observed fcc(111) orientation (of triangular shapes) is different from the expected bct In bulk structure. The transition to bct(110) islands (of rectangular shapes) is observed at higher temperatures T>250K and coverages θ>6ML. These results have been confirmed both with SPA LEED and STM. Fig.1 shows the growth outcome of In on Si(111)-Pb-α√3x√3 at T=200K with islands of different crystallographic orientations. These results suggest the competition between two effects ,i.e., QSE stabilize uniform height fcc(111) and surface energy favors bct(110) structures for high T and θ. This opens the possibility of manipulating not only the island geometry (as in our previous Pb/Si(111) work) but the crystal structure itself. The coarsening kinetics of the crystallographic transition are very unusual because the available In atoms almost exclusively move to the bct than fcc islands. The bct islands very quickly grow to very large heights 30-40 layers even with the addition of a small In amount Δθ~1-2ML.

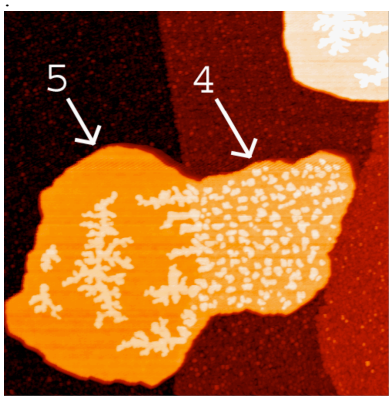

Fig. 2. 200 x 200 nm^2. An island that spans a single step with the left part of the island 5 and the right part 4 layers high. The 4-layer part has higher density of small compact islands while the 5-layer part has lower density of bigger fractal islands proving the strong dependence of bonding on QSE.

IIb Height dependent nucleation in QSE systems

QSE provide a very fast way for island height selection as shown in Pb/Si(111)[3]. Since the electronic structure of the islands depends on height this opens up the possibility to control the adatom bonding and reactivity by choosing islands of different height. A dramatic dependence of the second layer island morphology on island height was found[4]. The second layer nucleation after depositing a small amount of Pb at 40K shows dramatically different morphology: growth on a stable height results in low density fractal-like islands but growth on an unstable height results in

high density of smaller islands. Remarkably, this difference in morphology is observed on a single mixed island grown over a substrate step as shown in fig.2: the stable 5-layer part of the island has 60 times lower island density than the unstable 4-layer part. This indicates that the QSE stability condition normal to the surface is completely decoupled from the lateral degrees of freedom of the confined electrons. The two island parts are acting independently as if they were not connected. Extending this kind of experiments to heteroepitaxy or for the adsorption of gases will tests how well reactivity can be controlled with QSE.

These 40K experiments have answered an older question about the origin of low temperature diffraction intensity oscillations and in particular why for Pb/Pb(111) the oscillations were found to improve with decreasing temperature as low as 16K[5]. With STM we have directly observed ideal layer by layer Pb/Pb(111) growth, as a result of the fractal like second layer morphology.

IIc. Diffusion in systems with long range interactions

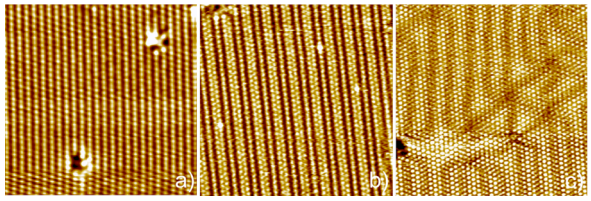

Fig.3.25x25nm^2 area showing initially the √7x√3 phase with θ=1.2ML (left) transforming into the (2,1) phase with θ=1.235ML (middle) followed by the (3,1) phase with θ=1.28ML after deposition of Δθ~0.04ML at 135K.

The realization of the numerous phases predicted by "Devil's Staircase" (DS_ in systems with long range repulsive interactions was recently found in Pb/Si(111)[6,7]. Surprisingly these numerous phases can be grown at low temperatures ~40K over macroscopic distances. Fig.3 shows a deposition experiment at 135K where a small amount Δθ~0.04ML is added causing the whole surface to transform from one well ordered phase to the next in the DS hierarchy[8]. This unusual observation can be explained from theoretical calculations of the collective diffusion coefficient D_c in systems with long range repulsive interactions. Instead of a gradual dependence of D_c on coverage, it was found that D_c has sharp maxima at low temperatures for every stable phase (i.e. for every rational value of the coverage θ=p/q) in agreement with the experiment.

IId. Unusually fast and collective diffusion of the Pb wetting layer

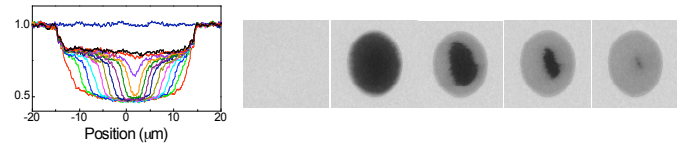

Fig.4 LEEM diffusion experiments in collaboration with Altman (Hong Kong) showing an unusual fast diffusion of the Pb wetting layer that can explain the fast QSE growth. The 5 panels to the right show the refilling of the initial hole(dark) generated by laser pulse at T=300K. The 1-d profiles to the left show the refilling with constant velocity, at regular time intervals Δt~0.2sec.

In collaboration with Altman(Hong Kong) we have used LEEM to study the evolution of coverage profiles in the Pb wetting layer on Si(111). The initial coverage step profile that is produced by laser induced desorption propagates rapidly from the edge of the circular desorption region at constant velocity and with unperturbed shape. This time dependence does not fit classical diffusion where the profile shape should becomes flatter. A critical dependence on coverage is observed where for $\theta<\theta_c=4/3$ML the refilling time increases dramatically. This novel mass transport is responsible for the remarkably efficient self-organization of uniform height Pb islands on the Si(111) surface[9].

II. Future work

IIa. Island chemical reactivity and QSE

An effect related to QSE and of potential practical importance is the increased electron density of states whenever an energy level crosses E_F[1]. Stronger bonding of adsorbates and higher chemical reactivity is expected. Since the energy level separation from E_F oscillates with island height, one expects higher reactivity for unstable vs stable height Pb islands.

Recent examples in the literature are the oxidation rate of Mg which was found to depend on film thickness [10] and CO adsorption on Cu films grown on Fe/Cu(100) epitaxial system[11]. The first

experiment monitored the thickness of the Mg oxide in XPEEM spectra. In the second experiment thermal programmed desorption spectra of CO were shifted by 10K to higher temperature indicating stronger CO adsorption for unstable heights.

Experiments will be carried out to understand hydrogen and oxygen adsorption first on the Pb islands. Similar adsorption will be carried out on Mg films grown on Si(111). QSE confining levels have been seen with photoemission[12]which suggests the existence or preferred heights in the correct T and θ "window". An atomic gas source already installed in the STM chamber will allow low temperature deposition so the Pb island height distribution will remain intact. We will monitor the adsorption as a function of island height and size. We would first test for in situ morphological changes on the island top with STM and STS. These local nanoscale experiments will be complemented with macroscopic experiments with programmed thermal desorption in the SPA-LEED chamber similar to the ones in [11].

If QSE films can be grown that are stable under reaction conditions and have height dependent yields, this can become important in heterogeneous catalysis. However an open question is the magnitude of the effect since in the experiments on continuous films[10,11], the difference in the adsorbed amount with thickness was less than 20%. This variation in reactivity will be enhanced by studying gas adsorption on individual Pb islands than continuous films. The Pb/Pb(111) second layer nucleation experiments described before[4] are very promising since a huge difference (60:1) in the density of adsorbed islands was found.

IIb. QSE and magnetic systems

QSE have also been observed in magnetic systems. In these systems the single level $E(k_z)$ is split into two separate levels differing by $\Delta E(k_z)$ due to the spin exchange interaction J. Spin-dependent reflectivity plays a major role in the giant magnetoresistance effect in ferromagnetic/nonmagnetic/ferromagnetic trilayers, with important application in computer technology. Oscillations in the reflectivity of spin-polarized electrons on energy were observed with Spin Polarized LEEM in Fe film on W(110) from the splitting of the levels and the different intensities for the majority and minority spins [14].

We plan to carry out spin-resolved STM and STS measurements with polarized STM tips to detect different magnetic signals on ferromagnetic films as a function of film thickness. Polarized tips will be prepared by depositing on a normal W tip ferromagnetic (Fe) or antiferromagnetic material(Cr)]. A polarized tip is more sensitive to electrons in the sample with the same spin so regions of different polarizations will have different signals. These can be seen in topographic and STS images as in [14]. Since the energy level position depends on height it is possible to observe both preferred heights and preferred polarization if QSE selection operates.

We plan to focus our studies of magnetic QSE on rare earth metals starting with Dy because there are already promising results in the literature that QSE are observable and because of the historic expertise in Ames lab to grow and characterize rare earth elements . Although Dy is reactive with Si and forms silicides at ~550C [15] the silicide is highly inert and most likely the smooth surface enhances diffusion so growth at low temperatures is possible. An indication that QSE can operate is the observation of a corrugation on top of the Dy islands grown on W(100) [15] reminiscent of the corrugation observed on Pb/Si(111).

Besides Si graphene layers grown epitaxialy on SiC substrates by thermal annealing will be used as substrates. We have initiated SiC experiments and discover a novel method to produce large (more then150nm) domains of single or bilayer graphene. An additional benefit of the weak interaction between graphene and the deposited metal is that it will be easier to predict the selected height by theory since the free standing approximation for grown films is applicable.

The ferromagnetic exchange interaction results in the splitting of the QSE levels between 0.5-1.0eV observable easily with STS. Furthermore if growth is carried out in the presence of a strong magnetic field B it is possible to control λ_F for each spin orientation and tune both the grown island height and its magnetization at sufficiently low temperature.

References

1. M. C. Tringides, M. Jalochowski and E. Bauer invited feature article in *Physics Today* April (2007)
2. J. Chen , M. Hupalo , M. Ji, C. Z. Wang, K.M. Ho and M. C. Tringides *Phys. Rev. B* 77 233302 (2008)
3. K. Budde et al. *Phys. Rev. Rap. Com.* ***B*** **61**, 10602 (2000).
4. S. M. Binz, M. Hupalo. M. C. Tringides *Phys. Rev.B* (submitted)
5. M. Jalochowski et al *Phys. Rev.* **B 51**, 7231 (1995).

6. M.Hupalo , J. Schmalian and M.C.Tringides *Phys Rev Lett. Phys Rev Lett.*, **90**, 216106 (2003).
7. M. Yakes, V. Yeh ,M.Hupalo and M. C. Tringides *Phys. Rev. B B* 69 224103 (2004)
8. M. Hupalo, M. Yakes, M. Zaluska-Kotur, Z. Gortel and M. C. Tringides *Phys. Rev. Let.* 98 135504 (2007).
9. K.L. Man, M.C. Tringides, M.M.T. Loy, M.S. Altman *Phys. Rev. Lett.* (submitted)
10. L. Aballe , A. Barinov , A. Locatelli , S.Heun and M. Kiskinova *Phys. Rev. Lett.* 93 196103 (2004)
11. A. G. Danese, F. G. Curti and R. A. Bartynski Phys. Rev. B 70 165420 (2004).
12. L. Aballe , C. Rogero K. Horn Phys. Rev. B 65 125319 (2002)
13. R. Zdyb and E. Bauer *Phys. Rev. Lett.* 88 166403 (2003)
14. M.Bode *Rep. Prog. Phys.* 66 523 2003)
15. N. Moslemzadeh, S.D. Barrett, J. Ledieu, E. Cox , *Surface Science* 539 (2003) 49–53 (2003)

Publications (since 2006)

1. "Self-Organization and Geometry Control of Pb Islands Grown on Anisotropic Substrates" M. Hupalo and M.C.Tringides *Phys. Rev B Rapid Comm* 75 041405 R 2006
2. "The dense α-√3x√3 Pb/Si(111) phase: a comprehensive STM and SPA-LEED study of ordering, phase transitions and interactions" S. Stepanovsky*, M. Yakes, V. Yeh**, M. Hupalo and M. C. Tringides *Surface Science 600 1417 (2006)*
3. "Impact of Interface Relaxation on the Nanoscale Corrugation in Pb/Si(111) Islands" T.L. Chan, C.Z. Wang, M. Hupalo, M.C. Tringides, W.C. Lu, and K.M. Ho *Surf. Sci. Lett.* 600 179 (2006)
4. "Quantum size effect on the diffusion barrier and growth morphology on Pb/Si(111)" TL.Chan , C. Z. Wang, M. Hupalo M.C. Tringides and K-M. Ho *Phys. Rev. Let.* 96 226102 (2006)
5. "Novel nucleation mechanisms driven by Quantum Size Effects" R. Feng, E.H. Conrad, M.C. Tringides, M Hupalo, P. Ryan, C. Kim, P.F. Miceli *Phys. Rev. Let.* 96 106105 (2006
6."Non-classical kinetics processes and morphologies in QSE driven growth in Pb/Si(111)" Z. Kuntova, M. Hupalo, Z. Chvoj and M. C. Tringides *Surf. Sci.* 600 4765 (2006)
7. "The Growth of Pb Nanocrystals on Si(111)7x7: Quantum Size Effects" C. A. Jeffrey, R. Feng, E. H. Conrad, P. F. Miceli, C. Kim, M. Hupalo, M. C. Tringides and P. J. Ryan *Superlattices and Microstructures* 41 168 (2007)
8. "Low temperature ultra fast mobility in systems with long range repulsive interactions: Pb/Si(111) M. Hupalo, M. Yakes, M. Zaluska-Kotur, Z. Gortel and M. C. Tringides *Phys. Rev. Let.* 98 135504 (2007)
9."Bilayer ring second layer nucleation morphology in Pb/Si(111)-7x7" Z. Kuntova, M. Hupalo, Z. Chvoj and M. C. Tringides *Phys. Rev. B* 75 205436 (2007)
10. "Unusual thermal stability of QSE Pb islands grown on Si(111)-In(4x1) " M. Yakes, J. Chen, M. Hupalo, and M.C. Tringides *Appl. Phys. Lett.* 90 163117(2007*)*
11. "Ultrafast kinetics in Pb/Si(111) from the collective spreading of the wetting layer" M. Hupalo and M. C. Tringides *Phys. Rev. B* 75 235443 (2007)
12. "Quantum Size Effects in metallic nanostructures" M. C. Tringides, M. Jalochowski and E. Bauer invited feature article in *Physics Today* April (2007)
15. "Interplay Between Indirect Interaction and Charge Density Wave in Pb adsorbed In(4x1)-Si(111)". M. Hupalo, T.-L. Chan, C. Z. Wang, K.-M. Ho, and M. C. Tringides *Phys. Rev. B* 76 045415 (2007)
16. "Strongly-driven coarsening of height selected Pb islands on Si(111)" M. Li , J.W. Evans, C. Z. Wang, M. Hupalo, M.C. Tringides, T.L. Chan and K.M. Ho *Surf. Sci. Lett.* 601 140 (2007)
17. "Quantum Modulation of Island Nucleation on Top of a Metal Nanomesa" Y. Han M. Hupalo, M.C. Tringides, Feng Liu *Surf. Sci. Lett.* 602 62 (2008)
18. "Diffusion from equilibrium diffraction fluctuations in ordered phases" E. Arapaki, P. Argyrakis, M.C. Tringides *Surf. Sci* 602 2162 (2008)
19. J. Chen , M. Hupalo , M. Ji, C. Z. Wang, K.M. Ho and M. C. Tringides *Phys. Rev. B* 77 233302 (2008)
20. Z.Kuntová Z. Chvoj M. C. Tringides M. Yakes *The Eur.n Phys. Jour. B 64 61 (2008)*

(submitted)

21. Z.Kuntová M. C. Tringides Z. Chvoj *Phys. Rev, B* (submitted)
22. S. M. Binz, M. Hupalo. M. C. Tringides *Phys. Rev.B* (submitted)
23. K.L. Man, M.C. Tringides, M.M.T. Loy, M.S. Altman *Phys. Rev. Lett.* (submitted)

Invited Talk:

Thomas F. Kelly
Imago Scientific Instruments

ATOMIC-SCALE TOMOGRAPHY OF MATERIALS

THOMAS F. KELLY
Imago Scientific Instruments Corporation
5500 Nobel Drive
Madison, WI 53711
tkelly@imago.com
www.imago.com

Atom-probe tomography (APT) provides three-dimensional structural and compositional analysis of materials at the atomic scale. In this talk, examples will be given of how APT is having impact on a wide variety of materials including metals, semiconductors, ceramics, and even synthetic organics and polymers. Recent specimen fabrication techniques using focused-ion beam instruments with in-situ manipulation have made it routine now to extract and analyze specimens from nanoscale structures including advanced alloys, device wafers and even finished components.

Other characterization techniques such as transmission electron microscopy (TEM) also provide information of this nature. An evaluation of these techniques' strengths and limitations shows that they are complementary. Furthermore, neither technique can truly deliver atomic-scale tomography (AST) information alone. However, by combining information from both techniques, synergies may be realized that will result in superior results and approach the ideal of AST. The prospects for AST by combining images will be explored.

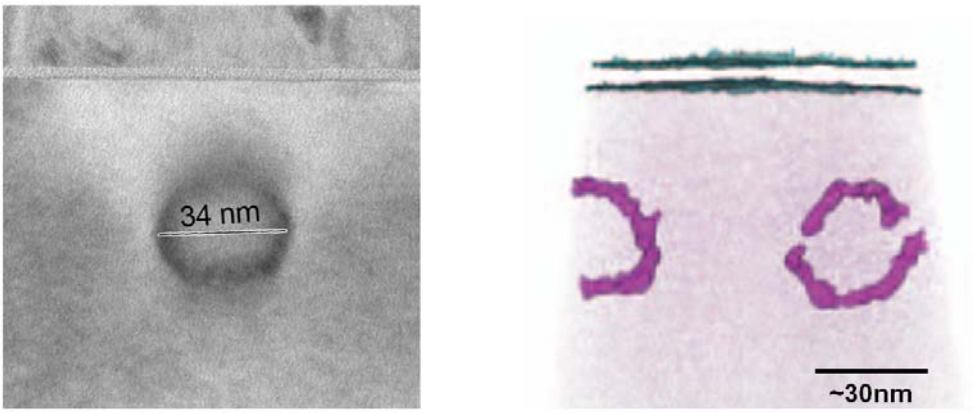

(Left) Bright-field TEM image of a vacancy dislocation loop resulting from arsenic implantation followed by after rapid thermal anneal at 600°C and drive-in anneal at 1000°C.
(Right) APT image of arsenic dopants (purple) implanted in silicon. Purple isoconcentration surfaces are shown for arsenic at 2 at%. Blue feature is an isoconcentration surface for oxygen which delineates the native oxide.
From: K. Thompson, Philip L. Flaitz, Paul Ronsheim, David J. Larson, and Thomas F. Kelly, Science 317 (2007) 1370.

Author Index

Participant List

Sarah Allendorf
Sandia National Laboratories

Mark Alper
Lawrence Berkeley National Laboratory

Ian Appelbaum
University of Delaware

Mark Asta
University of California, Davis

Nitash Balsara
Lawrence Berkeley National Laboratory

Norman Bartelt
Sandia National Laboratories

Jesse Berezovsky
Harvard University

Dawn Bonnell
University of Pennsylvania

Kit Bowen
Johns Hopkins University

Nigel Browning
Lawrence Livermore National Laboratory
University of California, Davis

Raffi Budakian
University of Illinois, Urbana-Champaign

Geoffrey Campbell
Lawrence Livermore National Laboratory

Venkat Chandrasekhar
Northwestern University

Y. Austin Chang
University of Wisconsin

Long-Qing Chen
Pennsylvania State University

Wai-Yim Ching
University of Missouri, Kansas City

Ulrich Dahmen
Lawrence Berkeley National Laboratory

J. C. Seamus Davis
Cornell University

Marc DeGraef
Carnegie Mellon University

James Dickerson
Vanderbilt University

Shen Dillon
University of Illinois, Urbana-Champaign

Vinayak Dravid
Northwestern University

Peter Flynn
University of Illinois, Urbana-Champaign

David Goldhaber-Gordon
Stanford University

Rachel Goldman
University of Michigan

P. Chris Hammel
Ohio State University

Patrick Han
Pennsylvania State University

Martin Harmer
Lehigh University

Saw-Wai Hla
Ohio University

Seungbum Hong
Argonne National Laboratory

James Horwitz
U. S. Department of Energy

Bernd Kabius
Argonne National Laboratory

Sergei Kalinin
Oak Ridge National Laboratory

Aharon Kapitulnik
Stanford University

Tom Kelly
Imago Scientific Instruments

Helen Kerch
U. S. Department of Energy

Rolf Koenenkamp
Portland State University

Thomas LaGrange
Lawrence Livermore National Laboratory

Francois Leonard
Sandia National Laboratories

Lian Li
University of Wisconsin, Milwaukee

Jian Luo
Clemson University

Margaret Lyday
Oak Ridge Institute for Science
and Education

Harindran Manoharan
Stanford University

Laurence Marks
Northwestern University

Martha McCartney
Arizona State University

Kevin McCarty
Sandia National Laboratories

Alan McGaughey
Carnegie Mellon University

Douglas Medlin
Sandia National Laboratories

Joanna Millunchick
University of Michigan

Andrew Minor
University of California, Berkeley
Lawrence Berkeley National Laboratory

Taisuke Ohta
Sandia National Laboratories

Xiaoqing Pan
University of Michigan

Joel Parks
Rowland Institute at Harvard University

Stephen Pennycook
Oak Ridge National Laboratory

Amanda Petford-Long
Argonne National Laboratory

Shashank Priya
Virginia Tech

Bryan Reed
Lawrence Livermore National Laboratory

Ian Robertson
University of Illinois
Chong-Yu Ruan
Michigan State University

Dilano Saldin
University of Wisconsin, Milwaukee

Miquel Salmeron
Lawrence Berkeley National Laboratory

Marvin Schofield
Brookhaven National Laboratory

Andrew Schwartz
U. S. Department of Energy

Renu Sharma
Arizona State University

Jerry Simmons
Sandia National Laboratories

John Spence
Arizona State University
Lawrence Berkeley National Laboratory

Susanne Stemmer
University of California, Santa Barbara

Peter Sutter
Brookhaven National Laboratory

Konrad Thuermer
Sandia National Laboratories

Peter Tortorelli
Oak Ridge National Laboratory

Michael Tringides
Ames Laboratory
Iowa State University

Maria Varela
Oak Ridge National Laboratory

John Vetrano
U. S. Department of Energy

Dwight Viehland
Virginia Tech

Vyacheslav Volkov
Brookhaven National Laboratory

Paul Voyles
University of Wisconsin, Madison

Michael Weinert
University of Wisconsin, Milwaukee

Paul Weiss
Pennsylvania State University

Robert Westervelt
Harvard University

Jorg Wiezorek
University of Pittsburgh

Judith Yang
University of Pittsburgh

Ali Yazdani
Princeton University

Alex Zettl
Lawrence Berkeley National Laboratory

Yimei Zhu
Brookhaven National Laboratory

Jane Zhu
U. S. Department of Energy

Jian-Min Zuo
University of Illinois, Urbana-Champaign